Vol. 101 No. 2 November 1, 1978
Completing Vol. 101

ISSN 0003-2670

ANALYTICA CHIMICA ACTA

International journal devoted to all branches of analytical chemistry

ELSEVIER SCIENTIFIC PUBLISHING COMPANY

ANALYTICA CHIMICA ACTA

International journal devoted to all branches of analytical chemistry
Revue internationale consacrée à tous les domaines de la chimie analytique
Internationale Zeitschrift für alle Gebiete der analytischen Chemie

PUBLICATION SCHEDULE FOR 1978 (incorporating the section on Computer Techniques and Optimization).

	J	F	M	A	M	J	J	A	S	O	N	D
Analytica Chimica Acta	96/1	96/2	97/1	97/2	98/1	98/2	99/1	99/2	100	101/1	101/2	102
Section on Computer Techniques and Optimization			103/1			103/2			103/3			103/4

Scope. *Analytica Chimica Acta* publishes original papers, short communications, and reviews dealing with every aspect of modern chemical analysis, both fundamental and applied. The section on *Computer Techniques and Optimization* is devoted to new developments in chemical analysis by the application of computer techniques and by interdisciplinary approaches, including statistics, systems theory and operation research. The section deals with the following topics: Computerized acquisition, processing and evaluation of data. Computerized methods for the interpretation of analytical data including chemometrics, cluster analysis, and pattern recognition. Storage and retrieval systems. Optimization procedures and their application. Automated analysis for industrial processes and quality control. Organizational problems.

Submission of Papers. Manuscripts (three copies) should be submitted to:
for *Analytica Chimica Acta:* Dr. A. M. G. Macdonald, Department of Chemistry, The University, P.O. Box 363; Birmingham B15 2TT, England;
for the section on *Computer Techniques and Optimization:* Dr. J. T. Clerc, Laboratorium für Organische Chemie, Swiss Federal Institute of Technology, Universitätstrasse 16, CH-8092 Zürich, Switzerland.

Information for Authors. Papers in English, French and German are published. There are no page charges. Manuscripts should conform in layout and style to the papers published in this Volume. Authors should consult Vol. 93, p. 379 for detailed information. Reprints of this information are available from the Editors or from: Elsevier Editorial Services Ltd., Mayfield House, 256 Banbury Road, Oxford OX2 7DE (Great Britain).

Reprints. Fifty reprints will be supplied free of charge. Additional reprints (minimum 100) can be ordered. An order form containing price quotations will be sent to the authors together with the proofs of their article.

Advertisements. Advertisement rates are available from the publisher.

Subscriptions. Subscriptions should be sent to: Elsevier Scientific Publishing Company, P.O. Box 211, 1000 AE Amsterdam, The Netherlands. The section on *Computer Techniques and Optimization* can be subscribed to separately.

Publication. *Analytica Chimica Acta* (including the section on *Computer Techniques and Optimization*) appears in 8 volumes in 1978. The subscription for 1978 (Vols. 96–103) is Dfl. 1000.00 plus Dfl. 120.00 (postage) (Total approx. U.S. $486.96). The subscription for the *Computer Techniques and Optimization* section only (Vol. 103) is Dfl. 125 plus Dfl. 15.00 (postage) (Total approx. U.S. $60.87). Journals are sent automatically by air mail to the U.S.A. and Canada at no extra cost and to Japan, Australia and New Zealand for a small additional postal charge. All earlier volumes (Vols. 1–95) except Vols. 23 and 28 are available at Dfl. 144.00 (U.S. $63.00), plus Dfl. 10.00 (U.S. $4.35) postage and handling, per volume.

Claims for issues not received should be made within three months of publication of the issue, otherwise they cannot be honoured free of charge.

Customers in the U.S.A. and Canada who wish to obtain additional bibliographic information on this and other Elsevier journals should contact our Journal Information Center, 52, Vanderbilt Avenue, New York, NY 10017. Tel: (212) 867-9040.

Statistical Treatment of Experimental Data

by J. R. GREEN, *Lecturer in Computational and Statistical Science, University of Liverpool, and* D. MARGERISON, *Senior Lecturer in Inorganic, Physical and Industrial Chemistry, University of Liverpool.*

Physical Sciences Data, Vol. 2

First published in 1977 and now reprinted with some minor revisions, this book is intended for researchers wishing to analyse experimental data using statistical methods. Statistical concepts and methods which may be employed, are explained, and the ideas and reasoning behind statistical methodology clarified. Formal results are illustrated by many numerical worked examples mainly taken from the laboratory. Concepts, practical methodology, and worked examples are integrated in the text.

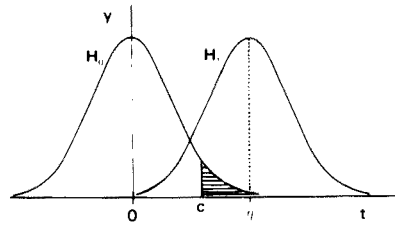

Consideration is given in this work to a large number of practical topics which are often omitted from standard texts. These include: obtaining an approximate confidence interval for a function of some unknown parameters; testing for outliers, stabilization of heterogeneous variances, and significant differences between means; estimation of parameters after performing tests; deciding what numbers of significant figures to quote for sample means and variances; straight-line and polynomial regression, through the origin or not, using weighted points, and testing the homogeneity of a set of such lines or curves.

The many examples provided throughout the text will serve as models for the various problems encountered by the readers when employing statistical methods to treat experimental data.

In addition to research workers in universities and industry, the book will be of use for first-year students of statistics, and will be especially suitable as the basis of a graduate course in experimental sciences.

CONTENTS: Chapters: 1. Introduction. 2. Probability. 3. Random Variables and Sampling Distributions. 4. Some Important Probability Distributions. 5. Estimation. 6. Confidence Intervals. 7. Hypothesis Testing. 8. Tests on Means. 9. Tests on Variances. 10. Goodness of Fit Tests. 11. Correlation. 12. The Straight Line Through the Origin or Through Some Other Fixed Point. 13. The Polynomial Through the Origin or Through Some Other Fixed Point. 14. The General Straight Line. 15. The General Polynomial. 16. A Brief Look at Multiple Regression. Appendices: 1. Drawing a Random Sample Using a Table of Random Numbers. 2. Orthogonal Polynomials in x. References. Index.

1977 1st revised reprint 1978 xiv + 382 pages US $39.25/Dfl. 90.00
ISBN 0-444-41725-7

ELSEVIER

P.O. Box 211, Amsterdam
The Netherlands
52 Vanderbilt Ave
New York, N.Y. 10017

The Dutch guilder price is definitive. US $ prices are subject to exchange rate fluctuations.

MERCK solvents – an imposing array

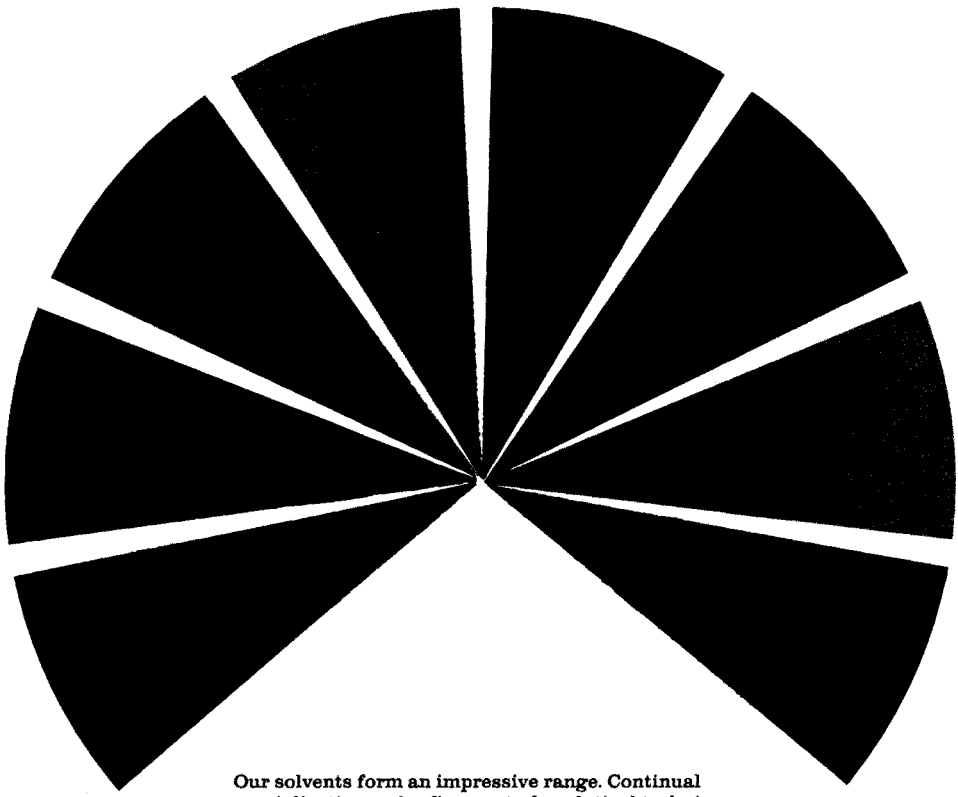

Our solvents form an impressive range. Continual specialisation and refinement of analytical techniques demand that the purity of MERCK solvents be specifically matched to the intended applications.

Our range includes:

401 d-Eü

pro analysi solvents
pro analysi solvents, dried (max. 0.01% H_2O)
solvents for extraction analysis
Uvasol® solvents for spectroscopy
Uvasol® solvents for fluorescence spectroscopy
solvents for scintillation measurements
solvents for chromatography LiChrosolv®
solvents for synthesis
The Merck box system enables you to save up to 22%.
Please send for our brochures.

Analytica Chimica Acta, 101 (1978) 231—238

POTENTIOMETRIC SELECTIVITY COEFFICIENTS OF LIQUID ION-EXCHANGE MEMBRANES FOR UNIVALENT AND DIVALENT IONS

RICHARD P. BUCK* and FREDERICK S. STOVER

William R. Kenan Jr. Laboratories of Chemistry, University of North Carolina, Chapel Hill, NC 27514 (U.S.A.)

(Received 30th March 1978)

SUMMARY

Digital simulation has been used to calculate potential—activity responses and concentration-dependent selectivity coefficients for membranes bathed in mixtures of univalent and divalent ions. For an ideal, dissociated, univalent-site liquid ion-exchange membrane, more accurate computations, based on Nernst—Planck equations, were possible than have been reported previously. Simulation results were used with four suggested equations for the membrane potential (including the IUPAC recommendation) to determine which equation gives best fit and most nearly constant selectivity coefficients. When concentration profiles found by digital simulation are employed, improved response equations are given which closely describe the dependence of surface concentrations on the mobility ratio for the bi-ionic case. From these equations a closed form solution to the diffusion equation yields an explicit expression relating the bi-ionic selectivity coefficient to membrane loading, single ion partition coefficients, and ion mobilities.

Analysis of the Nernst—Planck flux equations governing the responses of a mobile site, dissociated ion-exchange membrane to mixed univalent—divalent ion solutions is, at present, incomplete. Nevertheless, previous analysis [1] shows that: (a) computed cell potentials are not found as integrals of perfect derivatives; (b) computed cell voltages are not in the block logarithmic form of the Nicolski—Eisenman equation [2]; and (c) selectivity coefficients computed from experimental data assuming block logarithmic form will not be concentration-independent constants. Experimentally, ion-selective electrodes for divalent ion activity measurements are in wide use, often under conditions involving univalent interferences, e.g. in the determination of calcium in blood serum. Interpretation of responses of mixtures by using block logarithmic form equations with constant selectivity coefficients cannot give accurate representation of experimental data. Even approximate use of a constant coefficient over a narrow range of univalent interference concentration requires identification of selectivity coefficients appropriate for the precise calcium and sodium ion activities prevailing in the sample. Consequently, many selectivity coefficients for univalent ion interferences relative to divalent ion species have been reported [3—5], usually, but not always, for specific interference

levels. Unfortunately, these concentration-dependent selectivity coefficients have been determined for only one interference level by using the very limited mixed solution method or the bi-ionic potential technique (pure solution method) [6, 7].

In this paper, three premises are explored. One is that there is an optimum equation for calculation of mixture responses in which "optimum" means that the most nearly constant selectivity coefficient will be obtained. The second premise is that the optimum selectivity coefficient will depend only on the ratio of activities $(a_{Ca})^{\frac{1}{2}}/a_{Na}$. The third is that limiting selectivity coefficients at high interference (bi-ionic case) can be determined analytically, albeit approximately. As a first step, the extent of variation of the selectivity coefficient, as a function of the above activity ratio, is explored by using the three suggested response functions.

For a liquid cation-exchange membrane exposed to a test solution containing a monovalent cation and a divalent cation, the dependence of the potential on the external activities should be expressed as [6, 8]

$$\Delta\phi = \frac{RT}{2F} \ln\{[a_2' + \bar{k}_{21}^{pot} (a_1')^2]/[a_2'' + \bar{k}_{21}^{pot} (a_1'')^2]\} \quad (1)$$

where $\bar{k}_{21}^{pot}$ is the potentiometric selectivity coefficient, a_1 is the activity of the monovalent cation, a_2 is the activity of the divalent cation, and $\Delta\phi$ is the membrane potential; single primes indicate the test bathing solution, while double primes indicate the reference or internal solution. Theoretical analysis and experimental evidence [9] indicate that the potential can be expressed more exactly by

$$\Delta\phi = \frac{RT}{F} \ln\{[(a_2')^{\frac{1}{2}} + k_{21}^{pot} a_1']/[(a_2'')^{\frac{1}{2}} + k_{21}^{pot} a_1'']\} \quad (2)$$

In addition, the selectivity coefficient, k_{21}^{pot}, is a slowly varying function of $(a_2)^{\frac{1}{2}}/a_1$ while $\bar{k}_{21}^{pot}$ varies over many decades as response passes from control by a_2 to control by a_1. This result was found by Buck and Sandifer [1] who previously applied digital simulation to investigate the response of ion-exchange membranes to mixed valence solutions; they found that a single selectivity coefficient cannot be used to describe the membrane potential when neither cation dominates the response.

In the study described here digital simulation was applied to the same system to evaluate the ability of eqn. (2) to describe the potential response, to show how eqn. (1) can be modified to give almost equally good fit, and to show limitations on other suggested equations for membrane potentials. In particular, eqn. (1) can be modified by introducing the square root of $\bar{k}_{21}^{pot}$, namely $\bar{k}_{21}^{pot}$, which is more nearly constant in the equation

$$\Delta\phi = \frac{RT}{2F} \ln\{[a_2' + (\bar{k}_{21}^{pot} a_1')^2]/[a_2'' + (\bar{k}_{21}^{pot} a_1'')^2]\} \quad (3)$$

SIMULATION MODEL

The algorithm used to simulate membrane responses has been described [1, 10]. The diffusion potential is found by solving a system of equations

based on the dilute solution form of the Nernst—Planck flux equations

$$J_i = -u_i \left(RT \frac{\partial C_i}{\partial x} + z_i C_i F \frac{\partial \phi}{\partial x} \right) \tag{4}$$

the continuity equation,

$$\partial C_i / \partial t = -\partial J_i / \partial x \tag{5}$$

and an equation for the current density

$$I = F \Sigma z_i J_i \tag{6}$$

For the ith species, J_i is the flux, C_i is the concentration, u_i is the mobility and z_i is the valence; ϕ is the local electrical potential. Mobilities and activity coefficients are assumed to be independent of distance and concentration. The latter are assigned a value of one for all species. The reduced dielectric constant is set equal to zero, which eliminates the displacement current from eqn. (6) and eliminates regions of diffuse space charge from within the membrane. The segmented potential model is used, and the total membrane potential is computed by adding the diffusion potential to the two interfacial or Donnan potential differences. Calculated and reported values of electric fields, concentrations, mobilities and activities are reduced dimensionless quantities.

RESULTS

Figure 1 shows the digitally simulated potential response of a univalent cation-exchange membrane with mobile sites to varying activities of a divalent

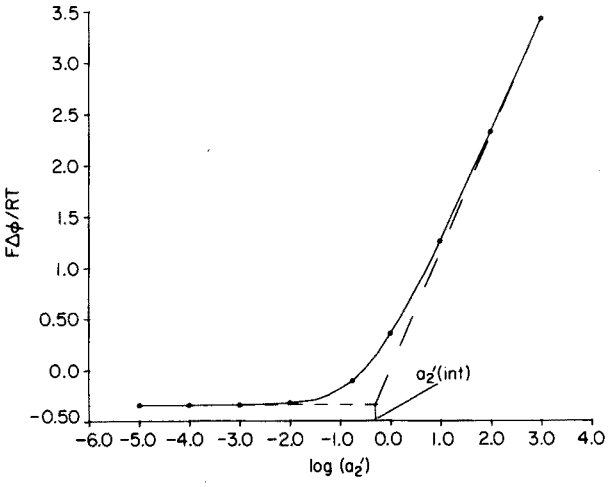

Fig. 1. Potential response to varying external activities of divalent ion 2 with constant activity of interferent univalent ion 1. $\bar{C}_s = 1$, $a_1'' = 0$, $a_2'' = 1$, $a_1' = 1$. Ionic mobilities are equal. Single ion extraction coefficients and activity coefficients are set equal to 1. Intersection of high-activity Nernstian response and low-activity interference response on the activity axis is indicated by a_2' (int).

ion. The reference solution contains only the divalent cation at a constant activity, $a_2'' = 1$. The test solution has a varying divalent activity, a_2', with a constant level of univalent interference, $a_1' = 1$. The single-ion extraction coefficients, k_i, have been given the value of unity to simplify the results. Mobilities of the divalent and univalent ions are equal. The total site concentration in the membrane is 1. The response shown in Fig. 1 cannot be exactly described by eqn. (1), (2) or (3). This can be verified by rearranging the equations to obtain expressions for the selectivity coefficient. From eqns. (1) and (3)

$$(\bar{k}_{21}^{\text{pot}})^2 = \bar{k}_{21}^{\text{pot}} = [a_2'' e^{(2F\Delta\phi/RT)} - a_2'] / [(a_1')^2 - (a_1'')^2 e^{(2F\Delta\phi/RT)}] \quad (7)$$

and from eqn. (2)

$$k_{21}^{\text{pot}} = [(a_2'')^{\frac{1}{2}} e^{(F\Delta\phi/RT)} - (a_2')^{\frac{1}{2}}] / [a_1' - a_1'' e^{(F\Delta\phi/RT)}] \quad (8)$$

These selectivity coefficients are plotted in Fig. 2 versus log $(a_2'^{\frac{1}{2}}/a_1')$.

The results show that none of the potential—activity expressions (eqns. 1—3) with a constant selectivity coefficient value can satisfy the digitally-simulated "experimental" data. The advantages of using eqn. (2) are emphasized, however; the selectivity coefficient incorporated in this equation changes far less with activity ratio than either that described in eqn. (1) or its modification, eqn. (3). In addition, at both low and high values of $a_2'^{\frac{1}{2}}/a_1'$, this selectivity coefficient is constant.

A third advantage of using k_{21}^{pot} of eqn. (2) is indicated by the fact that the selectivity coefficient decreases as the activity ratio moves further from the bi-ionic case (low $a_2'^{\frac{1}{2}}/a_1'$). Thus, the constant, bi-ionic selectivity coefficient is the lower limit for the selectivity of the membrane. In other words, the selectivity of the membrane towards divalent ions will always be better than, or equal to, that found in the extreme interference region.

The method recommended by IUPAC for determining selectivity coefficients is a version of the mixed solution method [3, 7]. An experiment is done to give results such as those in Fig. 1. The mono-ionic (high $a_2'^{\frac{1}{2}}/a_1'$) Nernstian response and the constant interference response segments are extrapolated until they intersect. The activity of the divalent ion in the test solution at this intersection, $a_2'(\text{int})$, is then found. A single value of this form of the selectivity coefficient is then computed from the intercept activity value and the activity of the univalent interference by

$$k_{21}^{\text{pot}} = (a_2'(\text{int}))^{\frac{1}{2}} / a_1' \quad (9)$$

for use in eqn. (2). From Fig. 1 and the known interference activity, this computed selectivity coefficient is 0.707 for the equal mobility case. But this value is simply the bi-ionic selectivity coefficient as shown in Fig. 2 at the left of the plot, and it is only an upper estimate of the working selectivity coefficient.

The mixed solution method can be better used to find the concentration-dependent working selectivity coefficients corresponding to k_{21}^{pot} in eqn. (2)

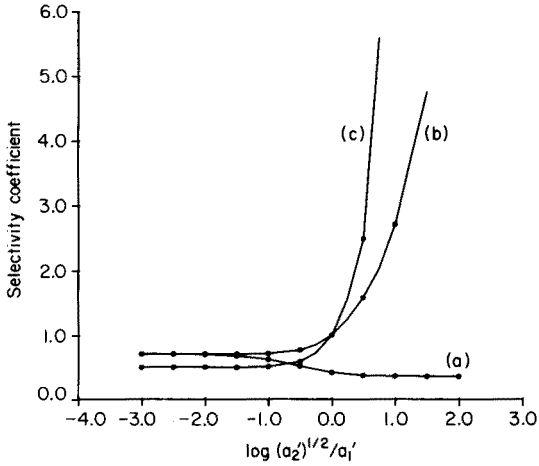

Fig. 2. Various potentiometric selectivity coefficients vs. univalent/divalent activity ratio in bathing solution. Membrane parameters are the same as in Fig. 1. Selectivity coefficients: (a) k_{21}^{pot} calculated from eqn. (8); (b) $\bar{k}_{21}^{pot}$ and (c) $\bar{k}_{21}^{pot}$ calculated from eqn. (7).

over a wide range of the ratio $a_2'^{\frac{1}{2}}/a_1'$. With the potential—activity data obtained from the above experiment, eqn. (8) can be used to give a whole family of k_{21}^{pot} values as a function of activity, not just the limiting bi-ionic value.

Selectivity as a function of mobility

For equal divalent and univalent mobilities, Fig. 3 shows that the selectivity coefficient of eqn. (2) is halved in going from the bi-ionic region to the mono-ionic, divalent region. Selectivity coefficients for eqn. (2), k_{21}^{pot}, are shown in Fig. 3 from simulated results based on various mobility ratios, u_1/u_2. As was shown earlier [1], the selectivity coefficient changes by more than a factor of 2 for $u_1/u_2 < 1$ and by less than a factor of 2 for $u_1/u_2 > 1$. The change in the selectivity coefficient with mobility ratio is qualitatively as expected. As u_2 increases, the selectivity coefficient at a given degree of interference decreases, and the selectivity toward the divalent ion improves.

An explicit solution relating univalent—divalent selectivities to external system parameters is not known. A partial solution to the combined Nernst—Planck and Donnan partition equations is

$$\Delta\phi = \frac{RT}{F} \ln \left[\frac{a_1' k_1 u_1 + 4u_2(k_2 a_2' C_2')^{\frac{1}{2}}}{a_1'' k_1 u_1 + 4u_2(k_2 a_2'' C_2'')^{\frac{1}{2}}}\right] + \frac{RT}{F} \int_0^{\delta} \frac{2u_2 dC_2}{4u_2 C_2 + u_1 C_1} \qquad (10)$$

where unit activity coefficients are assumed; k_i is the single-ion partition coefficient, C_i is the concentration of the counter-ions in the membrane, and δ is the membrane thickness. Earlier analysis [1], which assumed a linear steady-state site profile, yielded an approximate expression for the membrane selectivity coefficient:

$$k_{21}^{pot} = \frac{u_1 K_{12}}{2u_2(2\bar{C}_s)^{\frac{1}{2}}} \left[\frac{2\bar{C}_s}{4C_2' + u_1 C_1/u_2}\right] \left(\frac{\bar{C}_s - 2C_2'}{2\bar{C}_s - 4C_2' - u_1 C_1'/u_2}\right) \tag{11}$$

where $\bar{C}_s$ is the average site concentration and K_{12} is the ratio of single ion extraction coefficients, $K_{12} = k_1/(k_2)^{\frac{1}{2}}$. While eqn. (11) contains the unknown surface concentrations, digital simulation conveniently provides them. If these concentrations are used along with the other known input parameters, the accuracy of eqn. (11) can be checked against the selectivity coefficient computed by the simulation. The expression is exact for equal counter-ion mobilities (where it is known that the site profile is indeed linear), but is in error by 6% for mobility ratios of 5:1 in the bi-ionic case. A more exact, closed form expression for the bi-ionic selectivity coefficient is obviously desirable. Concentration profiles from digital simulations can be used to obtain it.

The bi-ionic activities are $a_1' = a_2'' = 1$ and $a_1'' = a_2' = 0$. Thus, for finite values of extraction coefficients, electroneutrality requires that $C_1' = C_s'$, and $C_2'' = C_s''/2$. A functional dependence of surface site concentration on mobility ratio is needed, and from the following observations, a guess at this functionality can be made:

(1) as $u_1/u_2 \to 0$, $C_s' \to 2\bar{C}_s$ and $C_s'' \to 0$;
(2) as $u_1/u_2 \to \infty$, $C_s' \to 0$ and $C_s'' \to 2\bar{C}_s$;
(3) when $u_1 = u_2$, $C_s' = C_s'' = \bar{C}_s$.

Of the various forms of $C_s' = f(u_1/u_2, \bar{C}_s)$ which agree with these conditions, the following functionality was found to correspond extremely well to the simulated results

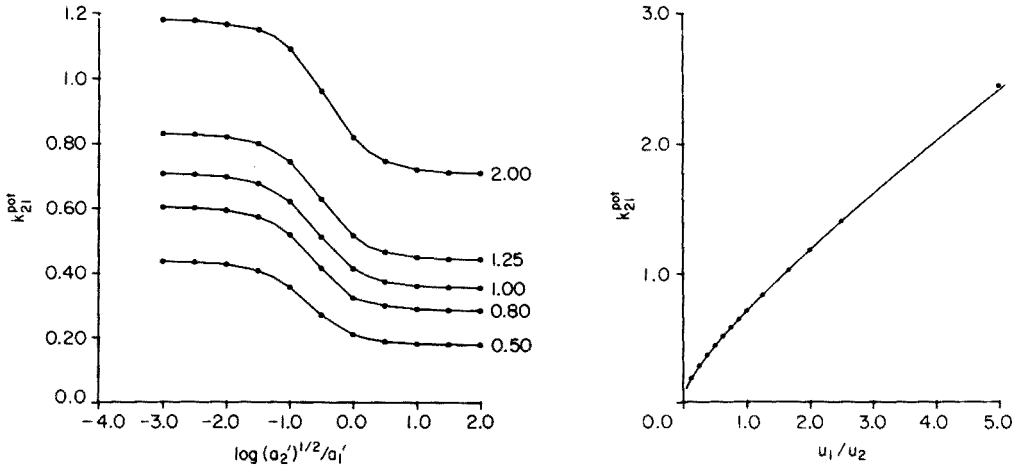

Fig. 3. Selectivity coefficient, k_{21}^{pot}, of eqn. (2) as calculated from eqn. (8) vs. activity ratio for various values of the mobility ratio, u_1/u_2 (shown on curves). Membrane parameters (except mobilities) are the same as in Fig. 1.

Fig. 4. Selectivity coefficient, k_{21}^{pot}, vs. mobility ratio. Points denote values computed by digital simulation. Solid line represents eqn. (18) for membrane parameters (except for mobility ratio) the same as in Fig. 1.

$$C'_s = 2\bar{C}_s\,[1/(1+r)] \tag{12}$$

where $r = (u_1/u_2)^{\frac{1}{2}}$. Site and counter-ion profiles are sufficiently linear to be approximated by

$$C''_s = 2\bar{C}_s[r/(1+r)] \tag{13}$$
$$C_1(x) \cong [2\bar{C}_s/(1+r)]\,[1 - x/\delta] \tag{14}$$
$$C_2(x) \cong [\bar{C}_s r/(1+r)](x/\delta) \tag{15}$$

where x is the distance through the membrane from the left (test) interface. Explicit distance-dependent ionic profiles make it possible to solve eqn. (10). Substituting $a''_1 = 0$, $a'_2 = 0$, $C'_2 = 0$ and the expressions for $C_1(x)$ and $C_2(x)$ into eqn. (10) gives two terms. The first is

$$\frac{RT}{F} \ln \left[r^2 k_1 a'_1 / 4 \left(\frac{k_2 a''_2 \bar{C}_s r}{1+r} \right)^{\frac{1}{2}} \right] \tag{16}$$

and the integral of the second term is found to be $[1/(2-r)]\ln(2/r)$. Combining this with the first term gives an analytical expression for the bi-ionic potential

$$\Delta\phi = \frac{RT}{F} \ln \left[a'_1 k_1 r^2 \left(\frac{2}{r} \right)^{\frac{1}{2-r}} \Big/ 4 \left(\frac{a''_2 k_2 \bar{C}_s r}{1+r} \right)^{\frac{1}{2}} \right] \tag{17}$$

which is the bi-ionic form of eqn. (2) with a selectivity coefficient of

$$k_{21}^{\text{pot}} = r^2 K_{12} \left(\frac{2}{r} \right)^{\frac{1}{2-r}} \Big/ 4 \left(\frac{\bar{C}_s r}{1+r} \right)^{\frac{1}{2}} \tag{18}$$

This expression, while an approximation, follows very closely the value of the computed bi-ionic selectivity coefficient as shown in Fig. 4. This is a higher-level approximation than the formula previously published [1], with the equation differing from the simulated result by less than 2% for a mobility ratio of 5:1. Examination of Fig. 4 shows that while eqn. (18) gives a rather complex, monotonic dependence of the selectivity coefficient on mobility ratio, this dependence is roughly linear with a slope of about 0.5 for mobility ratios greater than 1/4. The basis for the approximation is the related formulae for site concentrations as functions of mobility ratios (eqns. 12 and 13). These equations are exact for mixtures of two monovalent ions where, in the theory of Conti and Eisenman [11], the mobility ratio is raised to the power of $1/(1+\omega)$ with $\omega = 1$ for ions of univalent charge. In the present problem, the same exponent was used to avoid complications in integrating eqn. (10).

DISCUSSION AND CONCLUSION

By calculating membrane potentials for uni-negative mobile site (ideal and ionized) membranes bathed in mixtures of mono- and di-valent cations, it has been demonstrated that the data can be fitted by eqns. (1), (2) or (3). Each of these suggested equations is in block logarithmic form; the optimum

equation, as judged by most nearly constant selectivity coefficient, is eqn. (2). The generalized form of this equation, which is recommended for practical use, is

$$\Delta\phi = \frac{RT}{F} \ln\{[a'_A{}^{1/z_A} + (k^{pot}_{AB}\, a'_B)^{1/z_B}]/[a''_A{}^{1/z_A} + (k^{pot}_{AB}\, a''_B)^{1/z_B}]\} \quad (19)$$

The equation giving the least constant, most concentration-dependent selectivity coefficient is eqn. (1), which is recommended by IUPAC. Equation (3), an obvious modification of eqn. (1), is still not as suitable as eqn. (2).

A fourth equation for mixed di- and mono-valent ion responses has been given by Morf et al. [12]:

$$\Delta\phi = \Delta\phi_o + \frac{RT}{F} \ln\{\tfrac{1}{4} k^{pot}_{21}\, a'^2_1 + (a'_2 + \tfrac{1}{4} k^{pot}_{21}\, a'^2_1)^{\frac{1}{2}}\} \quad (20)$$

Analysis of this equation shows that it is just the sum of the interfacial potentials and is correct for the case when $u_1 = u_2$, i.e. when the diffusional potential is zero. In this case, the Morf equation fits the potential—activity data when a single, constant selectivity coefficient is used. One might speculate on how it could be modified to include situations where the ionic mobilities are unequal. Because of the form of the equation, however, it seems unlikely that modification would lead to a form with a constant selectivity coefficient.

Further analysis of eqn. (2) used digitally simulated concentration profiles for the derivation of a nearly exact expression for the bi-ionic selectivity coefficient in terms of known system parameters. This is a higher-order approximation than has been reported previously.

This work was supported by National Science Foundation Grant No. MPS75-00970.

REFERENCES

1 R. P. Buck and J. R. Sandifer, J. Phys. Chem., 77 (1973) 2122.
2 R. P. Buck, CRC Crit. Rev. Anal. Chem., 5 (1975) 323.
3 G. J. Moody, N. S. Nassory and J. D. R. Thomas, Hung. Sci. Instrum., 41 (1977) 23.
4 K. Srinivasan and G. A. Rechnitz, Anal. Chem., 41 (1969) 1203.
5 A. Hulanicki and Z. Augustowska, Anal. Chim. Acta., 78 (1975) 261.
6 I.U.P.A.C. Anal. Chem. Div. Pure Appl. Chem., 48 (1976) 127.
7 R. P. Buck, Anal. Chim. Acta, 73 (1974) 321.
8 J. R. Ross, in R. Durst (Ed.), Ion Selective Electrodes, National Bureau of Standards Special Publication No. 314, U.S. Government Printing Office, Washington, D.C., 1969, p. 57.
9 J. Bagg, O. Nicholson and R. Vinen, J. Phys. Chem., 75 (1971) 2138.
10 F. S. Stover and R. P. Buck, Biophys. J., 16 (1976) 753.
11 F. Conti and G. Eisenman, Biophys. J., 6 (1966) 227.
12 W. E. Morf, D. Ammann, E. Pretsch and W. Simon, Pure Appl. Chem., 36 (1973) 421.

Analytica Chimica Acta, 101 (1978) 239—245

ION-SELECTIVE FIELD EFFECT TRANSISTORS WITH POLYMERIC MEMBRANES

PAUL T. MCBRIDE, JIŘÍ JANATA*, PIERRE A. COMTE, STANLEY D. MOSS, and CURTIS C. JOHNSON†

Department of Bioengineering, University of Utah, Salt Lake City, Utah 84112 (U.S.A.)

(Received 25th May 1978)

SUMMARY

The construction and operation of ion-selective field effect transistors (ISFET) with polymeric membranes are described, and their electrical and chemical performance are discussed. The H^+, K^+, and Ca^{2+} ISFET's all show responses similar to those of the corresponding ion-selective electrodes, with $t_{95\%}$ response times of approximately 40 ms and accurate ion activity measurements for periods up to one month.

The concept of a transistor sensitive to different ions is quite simple: the gate metal of a conventional metal oxide semiconductor field-effect transistor (MOSFET) is replaced with a membrane which selectively interacts with one kind of ion in solution. The Nernst potential which develops at the membrane/solution interface, which is a function of the ion activity in solution, then modulates the drain current of the transistor. Transistors sensitive to hydrogen [1—3], sodium [2], potassium [3, 4] and calcium [4] ions have been reported and the theory of these devices has been discussed [5—9].

The common denominator of the three types of sensor based on ion-selective field effect transistors (ISFET) which are described in this paper is the mode of application of the ion-selective membrane: solvent casting. It has been pointed out before [3, 9] that the electrical integrity of ISFET's based on membranes is a necessary prerequisite for stable operation of these devices. The recently concluded study by Cohen et al. [10] has shown that properly prepared silicon nitride provides a stable gate insulator. The surface silanization process combined with an epoxy encapsulant then provides sufficient protection for the transistor chip against the aqueous electrolyte.

EXPERIMENTAL

Integrated circuit sensor fabrication

The integrated circuit (IC) chip [3] was eutectically die-attached to a

†Dr. Curtis C. Johnson was Chairman of the Department of Bioengineering until his recent death on March 25, 1978.

1.9 × 3.2-mm Kovar substrate coated with an approximately 0.80-μm layer of vacuum-deposited gold to provide an electrical connection of low resistance between the chip and substrate. This chip—substrate package was silanized with 3-aminopropyltriethoxysilane (Aldrich) for 12 h in a toluene (Fisher) reflux system, ultrasonically cleaned in toluene and dried in a desiccator. The chip—substrate package was then attached to a specially prepared dual-lumen 6-French PVC catheter (Edward's Labs — P/N 400317—5) with Eastman 910 adhesive, and electrical connections were made with an ultrasonic wire-bonder (Tempress EMB-1100) by means of 0.025 mm Al—1% Si wires. After the wire-bonding procedure, all the devices were checked for electrical characteristics and to establish the integrity of the sensor package. The devices were encapsulated with epoxy (EPON 825 [Shell] with J230 crosslinking agent [General Mills]) to provide electrical insulation for the bonding wires and exposed silicon regions of the chip, as well as to provide a suitable configuration around the chemically sensitive gate for casting membranes. The entire sensor package was finally cured at 60°C for 12—24 h.

Chemicals and membranes

Potassium and calcium ion-exchange membranes were cast from a 1 : 1 (v/v) mixture of tetrahydrofuran (Fisher) and cyclohexanone (Eastman) solution. The valinomycin-based K^+ membrane was prepared according to the formulation developed by Band et al. [11]. The calcium(II) membrane utilized t-HDOPP [*p*-(1,1,3,3-tetramethylbutylphenyl)phosphoric acid] as the electroactive material [12]. The pH membrane was cast from a chlorobenzene—dichloromethylene solution [13]. The membranes were applied to to CHEMFET gates by a process of 2—3 solution castings. All three types of membranes were allowed to cure for 8—12 h between membrane applications, and for approximately 24 h before solution testing was begun.

Solutions for K^+ and Ca^{2+} testing were prepared in two ways. Test solutions of concentration greater than 10^{-6} M were prepared from analytical-grade KCl (Mallinckrodt) or $CaCl_2 \cdot 2H_2O$ (MCB), dissolved in a 0.15 M NaCl solution to maintain ionic strength constant at low test ion concentrations. The stock 0.15 M NaCl solution was prepared from analytical-grade NaCl (J. T. Baker) and de-ionized—distilled water. This saline solution was found by regression analysis to contain a background concentration of approximately 10^{-6} M K^+ and Ca^{2+} ions, which necessitated the use of ion-complexing agents to provide low concentration solutions. Calcium solutions down to 2.5×10^{-9} M Ca^{2+} ions were prepared by using EDTA buffered at pH 7.26 with a background concentration of 200 mM KCl [12]. A suitable complexing system for K^+ ion is not available, and potassium testing was done only in diluted solutions of KCl in 0.15 M NaCl. Serum testing was done by using contacted rabbit plasma and expired human test serum to determine the stability and performance of the devices in contact with plasma proteins.

Hydrogen ion testing was done by using commercial pH buffers (Van-Lab,

Harleco) and by titration of a sodium acetate—sodium tetraborate buffer solution to obtain a full titration curve from pH 2—12. Activity coefficients for the test solutions were calculated from the formula $-\log f = 0.5115 z^2\mu^{\frac{1}{2}}/(1+\mu^{\frac{1}{2}})$.

Apparatus

A double-junction Ag/AgCl (saturated KCl) reference electrode with a 0.15 M NaCl salt bridge was used in parallel with a Ag/AgCl (0.15 M NaCl in 1% agar) reference electrode for all initial experiments [14]. The drain voltage (V_D) was set at + 2.00 V and supplied from a regulated power supply (PMC BP-20F). Drain current (I_{DS}) was measured with a PAR 170 (Princeton Applied Research) electrochemistry instrument, which also served as a variable gate voltage source (V_{GO}). The voltage was measured with a Keithley (Model 616) digital electrometer. Test solutions were stirred magnetically and contained in a temperature-regulated vessel. All measurements were made at either 25.0 or 37.0 ± 0.1°C except drain current—temperature studies.

For potassium and calcium titrations, stock solutions were added to sample volumes of 20.0 ml from an ultra-precision micrometer burette (Gilmont Inst., Model S 3100) accurate to ± 0.0001 ml. For pH titrations, 0.1 M HCl was added from an automatic burette system (Metrohm Inst., Dosimat E-412) and pH was simultaneously recorded with a glass pH electrode (Corning Model 476022). The experimental results were recorded with the PAR 170 system or a Linear Model 385 dual-channel chart recorder, with initial and final electrical calibration of the device to aid in analyzing the chemical response of the sensor.

RESULTS

pH ISFET

The pH response of the pH ISFET was tested by titrating a solution containing 0.1 M sodium acetate and 0.05 M sodium tetraborate with 0.1 M HCl. Because of the several dissociation equilibria, the pH changes gradually from approximately pH 12 to pH 2. The results of this measurement are shown in Fig. 1, from which it can be seen that the usable linear range is between pH 4 and pH 10 with a slope of 47 mV/pH. An average calibration slope between buffer solutions (pH 7 and pH 10) yields a value closer to 55 mV/pH, with no known reason to explain the discrepancy between the two methods. Bare gate pH sensors, utilizing the solid state Si_3N_4 gate insulator as a pH membrane, have also shown good response from pH 4 to pH 10; often with a greater slope than those obtained with the General Electric membrane. In agreement with LeBlanc et al. [13], the interference observed from phthalate ion prevents the use of commercial pH 4 buffer for calibration. This problem can be easily circumvented, however, by using a sodium acetate buffer which does not interfere.

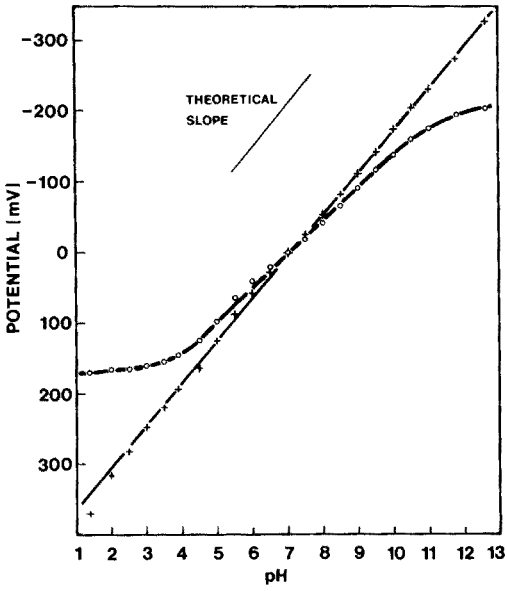

Fig. 1. Experimental titration curves showing both polymeric and solid-state (Si_3N_4) H^+ ISFET characteristics. (+) Si_3N_4; (0) General Electric pH membrane.

K^+ and Ca^{2+} ISFET's

Two types of test procedures were used for these sensors: either the sensor with an internal micro-reference electrode [14] was dipped into solutions of known concentrations of K^+ or Ca^{2+}, or a 1.0 M solution of KCl or $CaCl_2$ was added from a micrometer syringe to 20.0 ml of 0.15 M NaCl while the response of the sensor was continuously recorded. For values of Ca^{2+} below 10^{-6} M, calcium buffers were used [12]. The results of these tests are shown in Fig. 2, and the performance characteristics of the three ISFET's are summarized in Table 1. Potassium ISFET's were used continuously for more than 30 days without any detectable degradation of their performance. In the

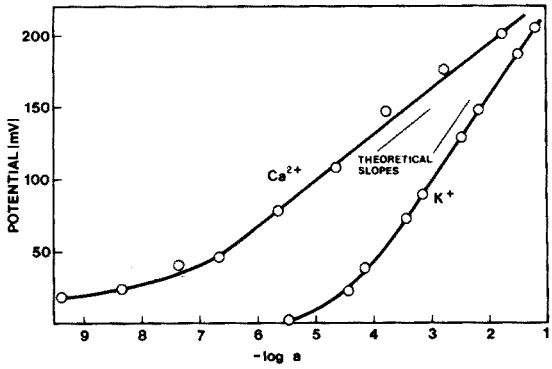

Fig. 2. Experimental response curves showing the characteristics of Ca^{2+} and K^+ ISFET's.

TABLE 1

Characteristics of the polymeric ISFET's

Membrane	Sensitivity (mV/decade)	Range	Stability ($mV\ h^{-1}$)	Lifetime (days)
pH	56 at 37°C	3—12 pH	1.0	10—20
K^+	57 at 25°C 59 at 37°C	$10^{-1} \rightarrow 10^{-5}$ M	0.1	> 20
Ca^{2+}	27 at 25°C 30 at 37°C	$10^{-1} \rightarrow 10^{-9}$ M	1.0	≤ 10

case of Ca^{2+} ISFET's, the membranes become opaque after approximately ten days of continuous exposure to solution with concurrent loss of response. Recovery of the sensors was observed after the catheter had been dried in a desiccator and a drop of cyclohexanone placed on the membrane itself. Following this recovery, the devices were usable for approximately five days.

On calcium and potassium sensors, the thickness of the membrane has an effect on the response of the device. Membranes thinner than about 40 μm sometimes produced a substantially lower slope (40 mV/pK^+ or less), and the same pattern was exhibited for calcium. This behavior is attributed to the existence of "pinholes" in the membrane which provide a solution path through the membrane shorting out the potential developed. With membranes 80—150-μm thick, this phenomena was not observed, and there was no deterioration of response over periods up to one month for K^+ sensors.

Time response

The dynamic response of these ISFET's with and without a membrane was tested. The response to a step change in the externally applied gate voltage is shown in Fig. 3(a), and the time response to a change in solution activity of the relevant ion is shown in Fig. 3(b). This experiment was performed by pointing the effluent jet from a syringe containing a higher or lower concentration solution against the active gate of the ISFET. The signal from the sensor was fed into a storage oscilloscope (Tektronix Model 7623 A), and photographed with a Polaroid oscilloscope camera.

It was interesting to observe that when a jet of solution of the same composition as the background electrolyte was applied against the Ca^{2+} or K^+ ISFET, very little change in drain current was observed. This indicates that these two types of ISFET's appear to be relatively insensitive to motion.

DISCUSSION

As was mentioned previously, a well behaved pH ISFET can be obtained by exposing the partially oxidized silicon nitride (Si_3N_4) surface of the gate insulator to solution. The main reason for the study of the membrane-based

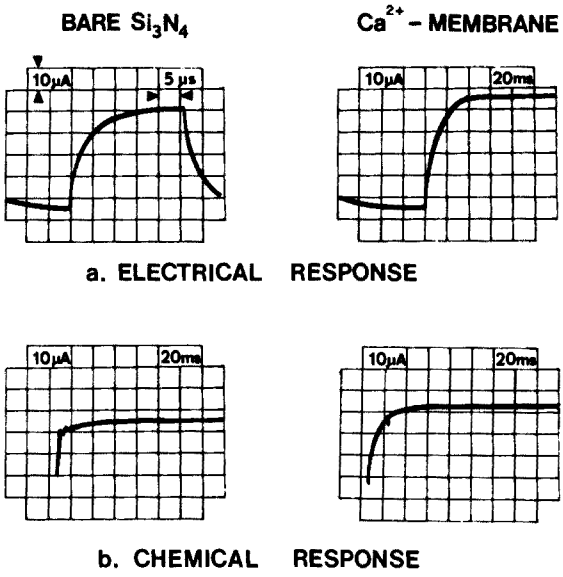

Fig. 3. Response of a solid-state membrane and a polymeric membrane to (a) a step change in external gate voltage; (b) a step change in concentration.

pH ISFET is the relatively high thrombogenicity of the silicon nitride surface. The linear range of both these types of devices, between pH 4 and 10, makes either type of device suitable for most biomedical applications.

The vastly improved stability of the K^+ and Ca^{2+} ISFET's reported here over those described previously [3, 4] is due to better membranes and encapsulation. While the progressive deterioration of the calcium membrane appears to be the limiting factor for the lifetime of this type of sensor, the ultimate lifetime of the pH and K^+ ISFET's is determined by the adhesion of the membrane to the surface of the chip and the ability of the encapsulants to protect the chip during long exposures to aqueous media. With the present encapsulation techniques, the average usable lifetime of the sensors (pH and K^+) is approximately 20 days. Similarly, the stability and temperature-sensitivity of the ISFET's are apparently determined by the transistor itself rather than by the ion-selective membrane.

It has been postulated [1, 9], that the in situ impedance transformation should shorten the response time of an ISFET compared to an equivalent ion-selective electrode. With a typical ISFET gate capacitance of 3 pF and the combined resistance of the reference electrode and membrane of 500 kΩ, the expected time constant would be 1.5 μs compared to the 25 μs observed here for the Si_3N_4 gate. The considerably longer time responses of the present membrane sensors — 40 ms to full response, as shown in Fig. 3 — indicates that the response-limiting factor is the formation of a diffusion layer at the membrane surface. The diffusion has been shown to be the

limiting factor in the response time for ion-selective electrodes [15, 16]. Thus it is unlikely that an ISFET can be a faster probe than the corresponding ion-selective electrodes. However, because of their small size localized rapid changes of activity can be registered much more easily.

Financial support for this work was provided by the NIGMS grant No. 22952. Financial assistance for Dr. P. A. Comte was kindly provided by Ebauches S. A. (Switzerland). We are grateful to Dr. J. D. Owens (Department of Physiology, University of Utah) for the gifts of the calcium(II) membranes and the calcium(II) buffer solutions, and to Dr. O. H. LeBlanc (General Electric, Research and Development, Schenectady, N.Y.) for the pH membrane.

REFERENCES

1 P. Bergveld, IEEE Trans. Biomed. Eng., BME-19 (1972) 342.
2 M. Esashi and T. Matsuo, IEEE Trans. Biomed. Eng., BME-25 (1978) 184.
3 S. D. Moss, J. Janata, and C. C. Johnson, Anal. Chem., 47 (1975) 2238.
4 S. D. Moss, J. Janata, and C. C. Johnson, IEEE Trans. Biomed. Eng., BME-25 (1978) 49.
5 R. P. Buck and E. D. Hackleman, Anal. Chem., 49 (1977) 2315.
6 J. M. Zemel, Anal. Chem., 47 (1975) 255A.
7 J. Janata, in P. Cheung (Ed.), Proceedings of Workshop on Theory, Design and Biomedical Applications of Solid State Chemical Sensors, March, 1977, Case Western Reserve University, CRC Press, Cleveland, Ohio, in press August 1977.
8 J. F. Schenck, J. Colloid Interface Sci., 61 (1977) 569.
9 J. Janata and S. D. Moss, BioMed. Eng., 11 (1976) 241.
10 R. M. Cohen, R. J. Huber, J. Janata, R. W. Ure, and S. D. Moss, Thin Solid Films, (1978) in print.
11 D. M. Band, J. Kratochvil, and T. Treasure, J. Physiol., 265 (1977) 5P.
12 H. M. Brown, J. P. Pemberton, and J. D. Owen, Anal. Chim. Acta, 85 (1976) 261.
13 O. H. LeBlanc, Jr., J. F. Brown, J. F. Klebe, L. W. Niedrach, G. M. J. Slusarezuk, and W. M. Stoddard, Jr,. J. Appl. Physiol., 40 (1976) 644.
14 S. D. Moss, J. B. Smith, P. A. Comte, C. C. Johnson, and L. Astle, J. Bioeng., 1 (1977) 11.
15 E. Lindner, K. Tóth, and E. Pungor, Anal. Chem., 48 (1976) 1071.
16 W. E. Morf, E. Lindner, and W. Simon, Anal. Chem., 47 (1975) 1596.

Analytica Chimica Acta, 101 (1978) 247—252

A FIELD EFFECT TRANSISTOR AS A SOLID-STATE REFERENCE ELECTRODE

PIERRE A. COMTE and JIŘÍ JANATA*

Department of Bioengineering, University of Utah, Salt Lake City, Utah 84112 (U.S.A.)

(Received 25th May 1978)

SUMMARY

The construction and performance of an integrated on-chip reference field-effect transistor is described. It is shown that excellent temperature and noise compensation can be obtained with this arrangement. The reference FET was used in conjunction with a pH ISFET and K^+ ISFET.

The theory of ion-sensitive field-effect transistors (ISFET) has been recently reviewed and the mode of operation of these devices has been compared with conventional ion-selective electrodes [1—3]. The principal advantages of ISFET's are their small size, the *in situ* impedance transformation, and the relatively easy possibility of manufacturing small, rugged multiprobes.

Like ion-selective electrodes, ISFET's require a reference electrode for a predictable operation. The quality of the measurement, therefore, depends on the performance of both half-cells. In addition, it makes sense to develop small, rugged ISFET's only if a reference electrode of the same size, or smaller, can be made. In order to provide a suitable reference electrode for ISFET's, two approaches have been used in the present work: in the first, a small Ag/AgCl reference electrode was incorporated in the upper lumen of the catheter [4] which was used as a support for the transistor chip. The reference electrode compartment was then connected with the sample by a free liquid junction. In the second approach, which is reported here, a pH ISFET was placed in a solution of constant pH which was then connected with the sample solution by a free liquid junction.

EXPERIMENTAL

Sensor preparation

The transistor chips have been described before [5]. They were mounted on the distal end of a dual-lumen PVC 6-French catheter (kindly provided by Edwards Laboratories Inc., Santa Ana, California) and encapsulated with

epoxy resin Epon 825. A small well (approximately 500 × 500 × 500 μm) was built around one ISFET gate and a pH-sensitive polymeric membrane was cast on both gates. Alternatively, bare silicon nitride gates were used. After curing the encapsulant, a 1% agarose (Bio-Rad Laboratory) gel prepared in a suitable buffer was packed into the reference gate well and a glass capillary (200-μm long; ca. 20-μm bore) was inserted into the gel. The reference electrode compartment was then closed with Epon 825. After some practice, the preparation of the reference gate takes 5—10 min. A schematic diagram of the gate and the measuring ISFET is shown in Fig. 1.

Equipment

The temperature was controlled by a circulating thermostated bath (Haake Model F4391). The measurement of pH was done with a Corning Model 10 pH meter. The drain current of both transistors was measured with a simple differential current follower (Fig. 2). The output of the two current followers or their difference was recorded on a dual-channel strip-chart recorder (Linear, Model 385). The titrations were done with a mechanical burette (Dosimat E412, Methrohm, Switzerland).

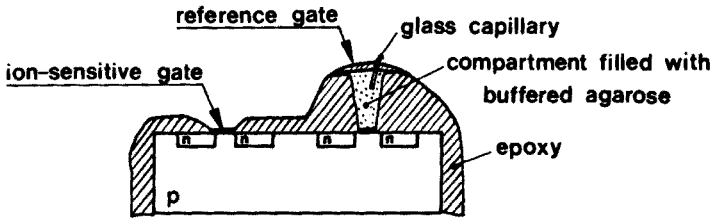

Fig. 1. A schematic diagram of a transistor chip with an ISFET and a reference gate.

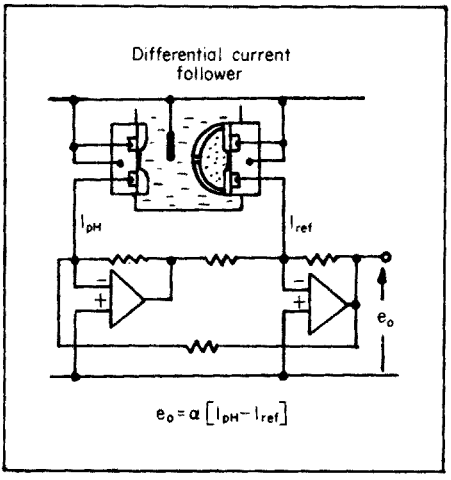

Fig. 2. A circuit diagram of a differential current meter.

Materials

Commercial buffers (Van-Lab) of pH 4.02, pH 6.98, pH 9.90 at 37°C were used for calibration for the titration. The standard 0.1 M HCl solution was prepared from a concentrate (Dilut-It, J. T. Baker Chemical Co.). All reagents were of analytical grade, and distilled de-ionized water was used for all experiments.

RESULTS AND DISCUSSION

The performance of the reference gate was evaluated according to the following criteria: pH response, lifetime, temperature, and noise sensitivity. Figure 3 shows the pH response of the pH-sensitive gate (H^+ - ISFET; curve a),

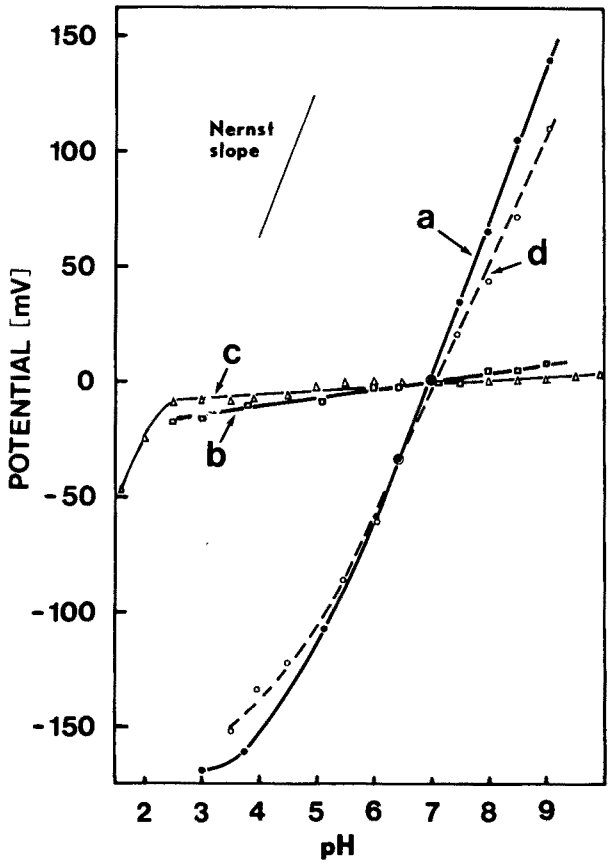

Fig. 3. The pH response of (a) H^+ ISFET; (b) reference gate with 0.1 M pH 7 buffer; (c) reference gate with 0.1 M pH 7 buffer and 4 M KCl; (d) difference between the reference gate and pH gate during titration of 0.05 M $Na_2B_4O_7$ with 0.1 M HCl at 37°C. A conventional double-junction Ag/AgCl reference electrode was used as the solution contact.

the reference gate (curve b, c) and the pH response of their difference (curve d). The usable range, pH 4—11, of the pH-sensitive gate is the same as that reported by LeBlanc et al. [6] for their polymeric pH electrodes. In agreement with LeBlanc et al. there is a strong interference of phthalate ion with the pH response of the pH membrane. This meant that commercial pH 4.0 buffers could not be used for calibration; instead 0.1 M acetate buffer of pH 4.0 was used. The transistor responds rapidly to change of pH and the long-term drift is good (0.02 pH/hour). In the linear range pH 5—10, the slope is 64 mV/pH at 37°C. The change of the reference gate potential with pH during the titration of 0.05 M sodium tetraborate with 0.1 M hydrochloric acid is linear, being 3 mV/pH for the internal reference with 0.1 M buffer and 1.5 mV/pH for the internal reference with 0.1 M buffer plus 4 M KCl solution. The small deviation of the reference gate current below pH 2.5 and above pH 10 (Fig. 3, curve c) is probably due to the presence of the capillary tip pH-potential [7].

The lifetime of the reference gate was tested by leaving the device continuously in solution and testing the pH response at various intervals. It was found that the performance of the reference gate did not deteriorate on storage in pH 7.0 buffer solution for at least four weeks.

Probably the most attractive feature of the reference gate is its ability to compensate for temperature changes and noise. Figure 4 shows the effect of changes of pH and temperature on the drain current of the pH ISFET (I_{pH} curve) and the difference of the drain currents of the pH and the reference gates ($I_{pH} - I_{REF}$ curve). When the solution contact is made via a proper reference electrode (such as Ag/AgCl, satd. KCl || sample . . .), the pH response of the pH gate and the difference are almost identical. However, as the temperature is changed from 37°C to 26°C, the drain current of the pH gate changes accordingly, while the difference remains practically unchanged. It can be shown that the change of the liquid junction potential with temperature is very small. Thus the small change (0.008 pH/°C) of the difference between the drain currents can be attributed, at least partially, to the difference between the change of the pH in the reference electrode compartment and the sample. Because of the similar temperature characteristics of the two sensors, the reference ISFET provides a temperature compensation of ±0.01 pH/°C with no need for an additional temperature calibration.

For the measurements which have been discussed up to this point, an ordinary stable reference electrode was used as a contact between the solution and the transistor substrate. However, this is not necessary if only the differences between the reference and the indicator gate have to be evaluated. Provided that an electrical contact is made between the substrate and the solution, the difference in drain currents is unaffected by the floating potential of this contact. Thus a bare silver wire, the exposed part of the silicon chip and even a paper clip have been used with no adverse effect on the drain current difference. This point is illustrated in Fig. 5, which shows the response of the drain current difference (lower curve) and the drain current of the pH gate when a noise was "injected" into the solution by touching the solution connection.

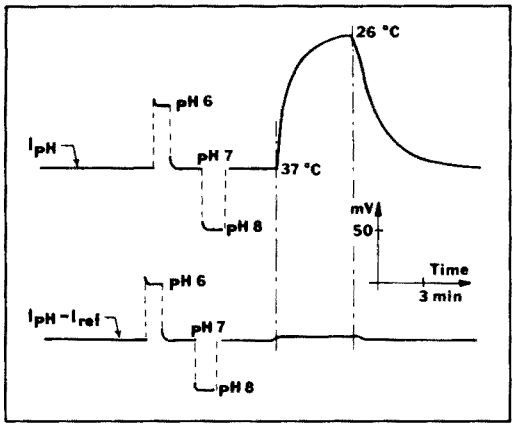

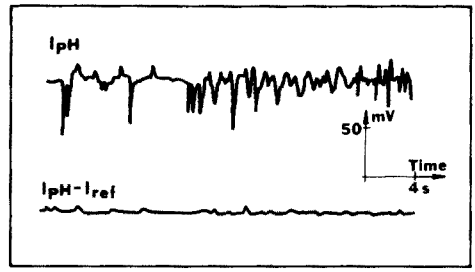

Fig. 4. A recording showing the response of the drain current of the uncompensated H^+ ISFET and the difference of the drain current of the H^+ ISFET and reference FET to temperature and pH.

Fig. 5. A recording showing the response of the drain current of the uncompensated H^+ ISFET and the difference of the drain current of H^+ ISFET and reference FET to common noise.

Circuits in which either the reference gate or the pH gate was operated in a feedback (constant current) mode were also studied. Because this is the preferred mode of operation for a single-gate measurement better results were expected than with the differential current follower. However, unless the characteristics of the two transistors are perfectly matched (which is rather difficult to achieve), the feedback operation offers no improvement over differential current measurement.

The general applicability of this approach was tested on the probe which incorporated a K^+ ISFET and the reference gate. The results obtained with this combination were equivalent to the case of the pH reference gate.

Conclusions

It has been demonstrated that the inherent advantages of a differential measurement, namely, temperature and noise compensation, can be obtained by using on-chip reference electrodes. As long as a suitable electrical contact to the solution is provided, the difference between the drain currents corresponds to the change of activity of the measured ion almost independently of the fluctuation of the potential of the solution contact.

Because of the small volume of the reference gate compartment, it is preferable to use a true buffer solution with high buffer capacity in this compartment rather than a solution of strong electrolyte such as KCl (as for a Ag/AgCl electrode). The high concentration of the neutral salt in the reference gate compartment reduces the liquid junction potential. The general applicability of this approach has been demonstrated by using it for the K^+ ISFET.

Because the reference gate can be made relatively easily, the only disadvantage of this arrangement is that one gate cannot be used for measurement of other ions. This is, however, a relatively small price to pay for the excellent temperature and noise compensation.

Financial support for this work was provided by NIGMS grant No. 22952. Financial assistance for one of us (P.A.C.) was kindly provided by Ebauches S.A. (Switzerland). The pH-sensitive membrane was kindly donated by Dr. O. H. LeBlanc (General Electric, Research and Development, Schenectady, N.Y.).

REFERENCES

1 J. Janata and S. D. Moss, BioMed. Eng., 11 (1976) 241.
2 R. G. Kelly, Electrochim. Acta, 22 (1977) 1.
3 R. P. Buck and D. E. Hackleman, Anal. Chem., 49 (1977) 2315.
4 S. D. Moss, J. B. Smith, P. A. Comte, C. C. Johnson, and L. Astle, J. Bioeng., 1 (1977) 11.
5 S. D. Moss, J. Janata, and C. C. Johnson, Anal. Chem., 47 (1975) 2238.
6 O. H. LeBlanc, Jr., J. F. Brown, J. F. Klebe, L. W. Niedrach, G. M. J. Slusarezuk, and W. M. Stoddard, Jr., J. Appl. Physiol., 40 (1976) 644.
7 M. Lavallee, O. F. Shanne, and N. C. Hebert (Eds.), Glass Microelectrodes, Wiley, New York, 1969.

Analytica Chimica Acta, 101 (1978) 253—259

ELECTROCHEMICAL FLOW-THROUGH DETECTOR FOR THE DETERMINATION OF CYSTINE AND RELATED COMPOUNDS

R. EGGLI*

Institute of Inorganic Chemistry, University of Zürich, CH-8001 Zürich (Switzerland)

R. ASPER

University Hospital of Zürich, CH-8091 Zürich (Switzerland)

(Received 24th April 1978)

SUMMARY

An electrochemical double cell for the detection of cystine in aqueous liquid streams is described. A column electrode of amalgamated silver powder is used to reduce cystine quantitatively to cysteine, which is detected amperometrically at a mercury electrode. The double cell is applied to the detection of cystine, cysteine and penicillamine in high-pressure liquid chromatography and to the selective determination of cystine and cysteine by flow-injection analysis.

Determinations of cystine are usually carried out by titrimetric [1], polarographic [2, 3] or colorimetric [4, 5] procedures which are based on the reactivity of the sulfhydryl group of cysteine which is formed by reduction of cystine. Thus, these methods respond to both disulfide and sulfhydryl species and a separation step is required when complex mixtures have to be analysed. Such a separation can easily be carried out by liquid chromatography [6], but no simple method for the flow-through detection of cystine or related disulfides has so far been published.

In this paper, an electrochemical dual-cell flow-through detector, sensitive to both disulfide and sulfhydryl compounds is described and applied to high-pressure liquid chromatography and to flow-injection analysis. The proposed procedure is based on standard principles of cystine analysis. The liquid stream is first passed through a column electrode of amalgamated silver grains at which cystine is quantitatively reduced to cysteine ($RSSR + 2H^+ + 2e \rightarrow 2RSH$) and oxygen is removed. The emerging cysteine is detected downstream amperometrically at a mercury electrode by means of the anodic reaction: $Hg + 2RSH \rightarrow Hg(RS)_2 + 2H^+ + 2e$ [7]. This amperometric method has recently been applied to the detection of sulfhydryl compounds in liquid chromatography [8] and to the determination of penicillamine disulfide which was first reduced to the respective sulfhydryl compound in a discontinuous procedure [9]. Grain-packed column electrodes, which enable rapid electrolysis of flowing solutions, have been used for electrochemical

separations [10] and for the coulometric detection of metal ions in liquid chromatography [11].

EXPERIMENTAL

Electrochemical apparatus

The arrangement of the two independent three-electrode cells is shown in Fig. 1. The column cell was made from a porous tube of silicon nitride (Degussit SN34, Degussa AG, length 32 mm, inner diam. 3 mm, outer diam. 6 mm), glued into a hollow cylinder of Plexiglas and packed with amalgamated silver powder (grain size 40—70 μm, mercury content 20%). The downstream end of the column was tightened by a Teflon washer containing a stainless steel frit. Contact to the working electrode bed was made by a silver wire of 0.5-mm diameter. The detector is a T-type mercury pool cell with 0.8-mm bores [8], machined from Plexiglas. A syringe (Hamilton 725) with its plunger attached to a spindle drive mechanism was used for delivery of mercury and for the precise control of the height of the mercury pool. The reduction cell was driven by a potentiostat (AMEL 549), and a polarograph (PAR 174) coupled to a strip chart recorder was used for the mercury pool cell.

The uncompensated resistances, measured in 0.025 M NaH_2PO_4—0.025 M Na_2HPO_4 with an a.c. Wheatstone bridge (Philips PR9500) at 50 Hz were, respectively, 250 Ω for the column cell and 6 kΩ for the mercury pool cell.

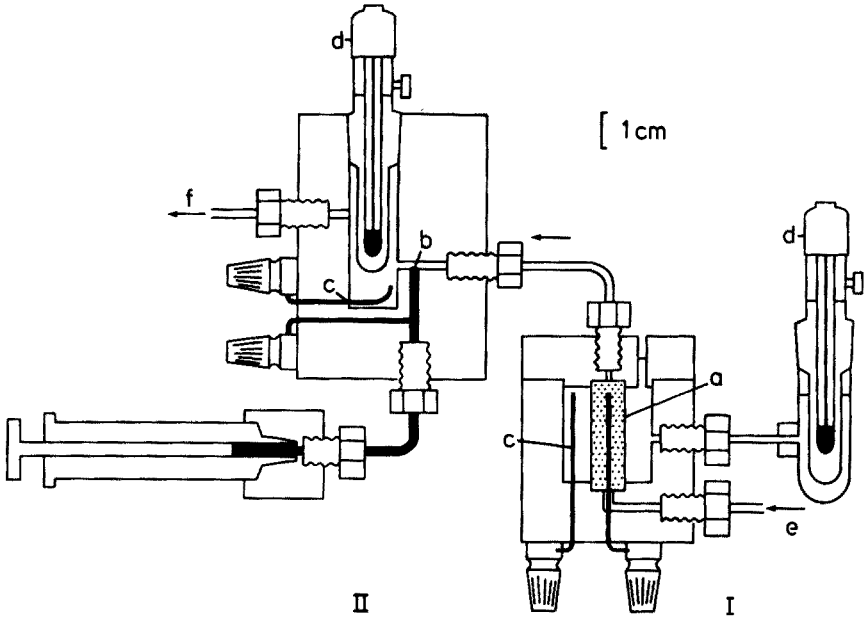

Fig. 1. Diagram of detection system. (I) Reduction cell; (II) detection cell; (a) column electrode; (b) mercury pool electrode; (c) platinum wire counter electrodes; (d) saturated calomel electrodes; (e) inlet; (f) outlet.

Flow apparatus

A reciprocating double-piston pump (ISMATEC PMP-50) connected to a 20-m coil of Teflon tubing (inner diam. 0.3 mm) was used for solvent delivery. Samples were injected through a Teflon valve (Rheodyne 50-20), fitted with a calibrated loop of a volume of 11.8 μl. A glass column (250 $\times$ 2 mm), packed with strong cation-exchange resin (Zipax SCX, DuPont), was used for chromatographic separations. All connections were made with Teflon tubes (0.8-mm i.d.) and standard Chromatronix fittings.

Chemicals

The buffers of pH 2.6 (0.090 M citric acid—0.022 M Na_2HPO_4) and of pH 7 (0.025 M NaH_2PO_4—0.025 M Na_2HPO_4) used as mobile phases were prepared from analytical-grade reagents and deionized water. Standard solutions of L-cystine, DL-cysteine and DL-penicillamine (Fluka, puriss.) were prepared daily with the buffer solution serving as mobile phase in the respective experiment.

General operating conditions

Both cells were driven at constant potentials. The mercury pool of the detector was adjusted so that it projected 0.2—0.3 mm into the liquid path. It was replaced after about 4 h of operation, regardless of the number of measurements performed within that time. Exclusion of oxygen was provided only when sulfhydryl compounds were selectively determined in the presence of related species. Then, the mobile phase and the sample solutions were purged with purified nitrogen and all Teflon lines, except the short connection between the reduction and the detection cell, were kept in a nitrogen atmosphere.

RESULTS AND DISCUSSION

The cathodic reduction of cystine to cysteine is a well known reaction at mercury [7, 12], but only limited information is available with respect to solid electrodes. Published results indicate that this reaction does not occur within the working potential ranges of platinum [13] and gold [14]. Preliminary experiments showed that the same applies to glassy carbon but that amalgamated silver behaved very much like mercury, as cystine can be reduced at potentials where no significant evolution of hydrogen occurs.

Characteristics of the column electrode

To determine the operating conditions of the reduction cell, the detector signals obtained from injections of 11.8-μl aliquots of 5×10^{-4} M solutions of cystine and of cysteine were measured as a function of the column electrode potential. The results obtained by using the phosphate—citrate buffer of pH 2.4 at a flow rate of 0.3 ml min^{-1} are given in Fig. 2. They show that cystine is reduced at potentials more negative than —0.5 V vs. SCE and that

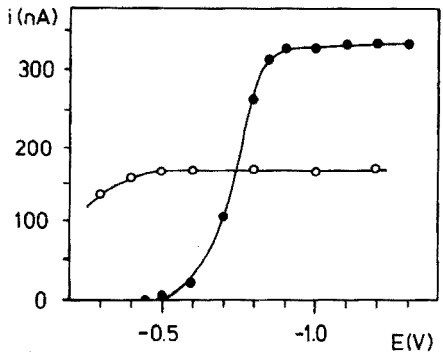

Fig. 2. Dependence of detector peak current I on column electrode potential E for cystine (•) and cysteine (○). Injected samples, 11.8 μl of 5 × 10^{-4} M solutions; mobile phase, phosphate—citrate buffer, pH 2.6; flow rate, 0.3 ml min^{-1}; detector potential, +50 mV vs. SCE.

a constant reduction yield is obtained between —0.9 and —1.3 V. Within this potential range, an average of 1.98 with a standard deviation of 0.06 was found for the ratio of the peak currents obtained when equimolar amounts of cystine and cysteine were injected. This ratio corresponds to a reduction yield of (99.0 ± 3)% as 2 mol of cysteine are formed by 1 mol of cystine.

The most precise results were obtained with column electrode potentials between —0.9 and —1.2 V. At more negative potentials, the response of the detector was affected by sharp current spikes caused by hydrogen bubbles evolved in the column electrode. The rate of hydrogen reduction increased rapidly with increasing flow rate and at a given column electrode potential, the highest flow rate compatible with useful operation of the double cell was determined by this interference and not by a decrease of the reduction yield. At a column electrode potential of —1.1 V, the average reduction yields, determined from four peak-current ratios at flow rates of 0.4 and 0.5 ml min^{-1} were 101 and 96.5% with standard deviations of 4 and 9% respectively.

The peak current—column electrode potential curves obtained when the phosphate buffer of pH 7 was used, were (within the limits of error) the same as those obtained with the acid buffer, but the effects of hydrogen evolution were considerably decreased. At —1.1 V, reduction yields of 99.5 and 98.1% with standard deviations of 2 and 5% were obtained at flow rates of 0.3 and 0.6 ml min^{-1}, respectively.

For practical work with both buffers, a flow rate of 0.3 ml min^{-1} and a column electrode potential of —1.1 V were used; this allowed quantitative reduction of cystine with negligible interference from hydrogen evolution (Fig. 3). Under these conditions, a steady-state reduction current of 0.7 mA was observed with undeaerated phosphate buffer of pH 7, which dropped to 0.3 mA when the buffer was deaerated and when all Teflon lines were kept in a nitrogen atmosphere. Thus the column electrode actually acts as an oxygen

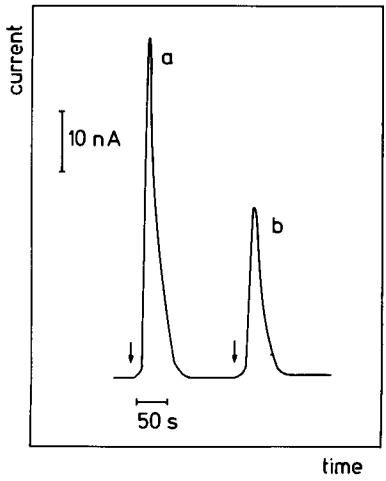

Fig. 3. Detector response to 11.8-μl injections of 5×10^{-5} M cystine (a) and cysteine (b). Injection points are marked by arrows. Column electrode potential —1.1 V; other conditions as noted in Fig. 2.

scavenger and injection of air-saturated supporting electrolyte produced no detector response.

Performance of the detector

As cystine is completely converted to cysteine in the column electrode, the performance of the double cell is governed by the performance of the mercury pool detector. Under the conditions used here (detector potential +50 mV vs. SCE, flow rate 0.3 ml min^{-1}), the detector had a peak-current sensitivity of 0.3 nA ng^{-1} of cystine and the coulometric yield was 0.9%. The limit of detection with respect to cystine, estimated from three times the standard deviation of the baseline current, was 0.1 ng. These values varied considerably with individually adjusted mercury pools, but the sensitivity for a given adjustment remained unchanged over hours of operation. The reproducibility of the detector signal was rather moderate: the peak current of an 11.8-μl injection of 5×10^{-5} M cystine had a relative standard deviation of 3%, estimated from 8 measurements at the same mercury pool in phosphate buffer of pH 7. Linear calibration curves (Fig. 4) were obtained for both cystine and cysteine in the range between 8.5 ng and 1.4 μg.

Analytical applications

Because of its low dead volume, the double cell can be used as a selective detector in h.p.l.c. This is illustrated by the ion-exchange chromatogram given in Fig. 5, where the double cell is used to detect cystine, cysteine and penicillamine.

Further, the flow injection technique can be used to analyse mixtures of cystine and cysteine selectively by exploitation of the operating characteristics

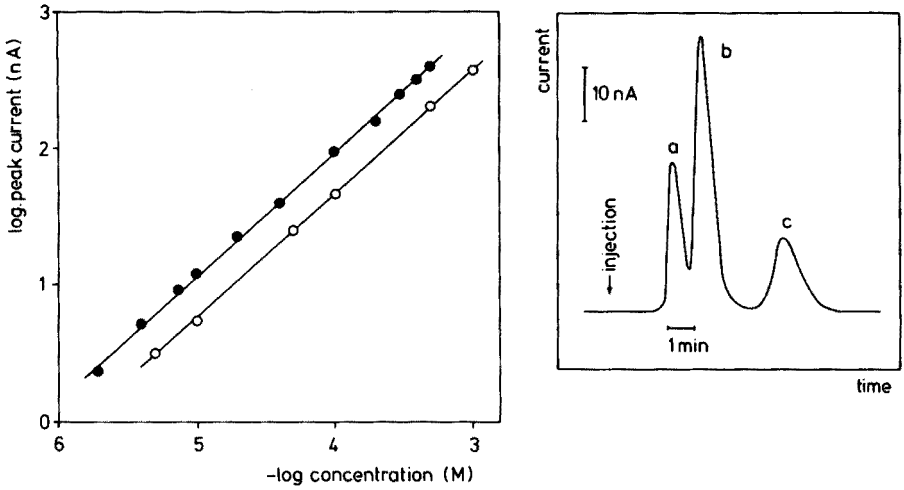

Fig. 4. Calibration curves of the dual cell for cystine (•) and cysteine (○) in phosphate buffer of pH 7. Volume of injected samples 11.8 μl; flow rate, 0.3 ml min^{-1}; column electrode potential, −1.1 V; detector potential, +50 mV.

Fig. 5. Liquid chromatogram of a mixture containing cysteine (a), cystine (b) and penicillamine (c), recorded with electrochemical dual cell. Stationary phase, Zipax SCX, 250 × 2 mm; mobile phase, phosphate—citrate buffer, pH 2.6; injected sample, 11.8 μl, 10^{-4} M of each component; other conditions as noted in Fig. 4.

of the reduction cell. The total amount of both compounds can be determined at a column electrode potential of −1.1 V, and cysteine alone can be detected at −0.45 V where cystine is not reduced. The amount of cystine can then be calculated from the difference between the signals. As the sensitivity with respect to mass is the same for both compounds, only a single calibration is needed. The performance of this method is illustrated by the results given in Table 1. The accuracy of the procedure depends on careful selection of the column electrode potential used for the selective determination of cysteine: at too negative potentials, cystine is reduced and the results for cysteine are too high; at potentials more positive than −0.45 V, a significant decrease of the cysteine signal is observed (Fig. 2), which is probably caused by the onset of anodic formation of mercury— and/or silver—sulfhydryl complexes. When the reduction cell was switched off, no signal was obtained, i.e. cysteine was completely trapped in the column electrode.

The main interferences are to be expected from species such as CN^-, SCN^-, SO_3^{2-}, I^-, Br^- and Cl^-, which give rise to anodic formation of mercury(I) compounds at the mercury pool detector. Of these ions, only SCN^-, Br^- and Cl^- can be tolerated in considerable amounts as their half-wave potentials are more positive than the detector potential. When flow-injection analyses were tested in phosphate buffer of pH 7 with a detector potential of +50 mV, accurate determinations of 10^{-4} M cystine were possible in the presence of

TABLE 1

Flow-injection analysis of mixtures containing cystine and cysteine (Sample volume, 11.8 μl; mobile phase, phosphate—citrate buffer, pH 2.6; flow rate, 0.3 ml min^{-1}; detector potential, +50 mV vs. SCE.)

Given		Found			
Sample composition		Peak currents (nA) at a column electrode potential of		Sample composition[a]	
Cystine (ng)	Cysteine (ng)	−1.1 V	−0.45 V	Cystine (ng)	Cysteine (ng)
0	142	44.9	43.7		142[a]
283	56.6	108	17.3	291	55.4
142	142	88.9	45.9	138	147
70.8	142	66.0	45.2	66.7	145

[a] Amounts of cystine and cysteine, calculated with a calibration constant of 0.312 nA ng^{-1}, obtained from the average of the two signals of the first sample.

up to 0.1 M chloride ($E_{1/2}$ = +0.25 V vs. SCE). With a detector potential of −10 mV, up to 0.2 M chloride could be tolerated, but the sensitivity with respect to cystine was slightly reduced.

REFERENCES

1 I. M. Kolthoff and W. Stricks, J. Am. Chem. Soc., 72 (1950) 1952.
2 M. Březina and P. Zuman, Die Polarographie in der Medizin, Biochemie und Pharmazie, Akad. Verlagsgesellschaft, Leipzig, 1956 p. 532.
3 K. Kužel, Clin. Chim. Acta, 48 (1973) 377.
4 P. Haux and S. Natelson, Clin. Chem., 16 (1970) 366.
5 R. A. Roesel and M. E. Coryell, Clin. Chim. Acta, 52 (1974) 343.
6 B. Fowler and A. J. Robins, J. Chromatogr., 72 (1972) 105.
7 M. T. Stankovich and A. J. Bard, J. Electroanal. Chem., 75 (1977) 487.
8 D. L. Rabenstein and R. Saetre, Anal. Chem., 49 (1977) 1036.
9 R. Saetre and D. L. Rabenstein, Anal. Chem., 50 (1978) 276.
10 T. Fujinaga and S. Kihara, CRC Crit. Rev. Anal. Chem., 6 (1977) 223.
11 D. C. Johnson and J. Larochelle, Talanta, 20 (1973) 959.
12 C. A. Mairesse-Ducarmois, G. J. Patriarche and J. L. Vandenbalck, Anal. Chim. Acta, 71 (1974) 165.
13 J. Pradáč and J. Koryta, J. Electroanal. Chem., 17 (1968) 167.
14 J. Koryta and J. Pradáč, J. Electroanal. Chem., 17 (1968) 177.

Analytica Chimica Acta, 101 (1978) 261—271

A NOVEL TITRATION TECHNIQUE FOR THE ANALYSIS OF STREAMED SAMPLES — THE TRIANGLE-PROGRAMMED TITRATION TECHNIQUE
Part 4. Automatic Evaluation of the Titration Curves obtained with Linear Signal Detectors

G. NAGY, Z. LENGYEL, Zs. FEHÉR, K. TÓTH and E. PUNGOR*

Institute for General and Analytical Chemistry, Technical University, Budapest (Hungary)

(Received 14th March 1978)

SUMMARY

An automatic evaluation technique is described for calculating the results obtained by the triangle-programmed titration technique, which is useful for carrying out titrations in flowing samples of small volume. A desk-top computer is employed with a relatively simple program for the evaluation. The properties of the program and its experimental applicability are described.

The principle of triangle-programmed titrations has already been described [1, 2]. The technique provides accurate titrimetric methods for measurements in streaming solutions. Titrations based on silver ion [3] and bromine [4] generated by current-programmed electrolysis have been reported. The triangle-programmed titration technique is suitable for the analysis of sample solutions of small volumes. In general, the technique combines the reliability of the titrimetric method with the advantages of analysis in flowing solutions. The promising results obtained suggested that the triangle-programmed technique could be useful for serial analysis on a routine scale. For serial analysis, it is of basic importance that the measuring technique should provide fast evaluation, display and storage of the results. The experimental work described here was designed to simplify the practice of triangle-programmed titrations by solving the problems involved in automatic evaluation of the results.

A simple universal solution of the problem is not easily achieved, because the evaluation involves location of two equivalence points on the complete titration curves. The location of the equivalence points and the determination of the time interval between their appearance can cause different problems for different titration reactions and detectors.

The present paper summarizes the results obtained for automatic evaluation of triangle-programmed titrations when the voltammetric detector used provides a linear electrical signal as a result of excess of reagent. This is valid if the sample is not electroactive under the conditions studied, which is often

the case in practice. Many different determinations with bromine, iodine, cerium(IV), etc., and appropriate voltammetric detectors are possible.

Evaluation of the results of the triangle-programmed titrations is as complicated as it is in the case of classical instrumental titrations, so automatic and highly reliable evaluation cannot be done with a simple mechanized method. Accordingly, a desk-top computer has been incorporated into the analyzer system to provide automatic evaluation.

EXPERIMENTAL

Instrumentation

The set-up used is a further development of the apparatus described earlier; a schematic design is shown in Fig. 1.

The flow-through electrolysis cell for generation of reagent contains two electrodes (1, 2) each of which is a platinum wire spiral. A current generator (Radelkis type OH-404A) is connected to the electrodes, the current being programmed with a signal generator (Philips type PM 5168) which gives a single-shot voltage signal in the form of an isosceles triangle. Details of the anodic (1) and cathodic (2) half-cells, separated by a dialysis membrane (3) have been reported earlier [4]. The reagent precursor solution (4) and the auxiliary solution (5) are passed, and the reaction at the anode, $2\,Br^- \xrightarrow{-2e} Br_2$, proceeds at a rate corresponding to the current program.

The generating and detecting parts of the flow-through channel are separated electrically by a drip vessel (6), into which the sample stream (7) is introduced. The solutions are streamed by peristaltic pumps [4] with buffer vessels (8, 9) to suppress oscillations.

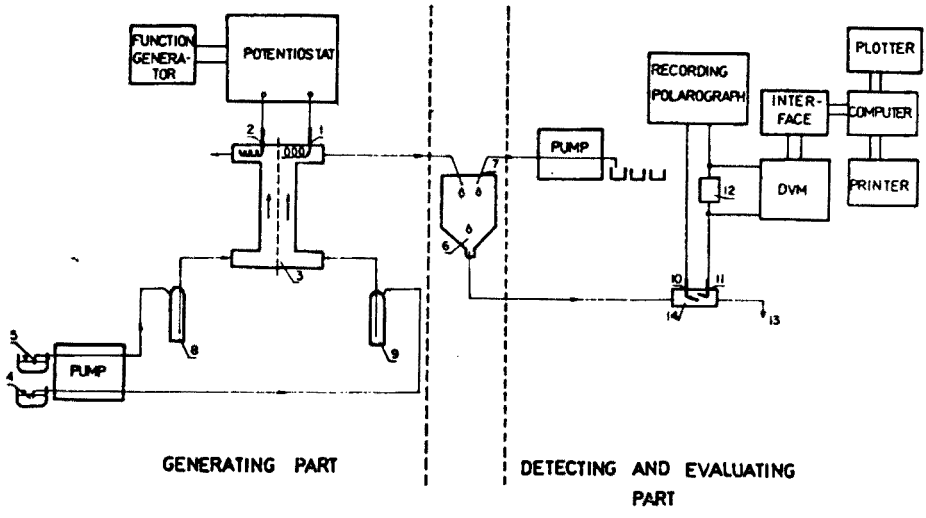

Fig. 1. Experimental set-up. For details, see text.

The detector comprises two platinum wire electrodes (10, 11) of equal size sealed into a glass tube (14), to which is applied a constant voltage of 0.3 V; the positively polarized electrode (10) acts as a quasi-reference electrode [4].

During the measurements, the voltammetric current—time dependence is recorded continuously. The current passes through a precision resistor (12; R = 100 Ω) which is connected to a digital voltmeter (13; DVM; EMG type 13—62/1), the voltage drop being measured every 40 ms. The data are fed into a desk-top computer (15; EMG type 666) through an interface (14) prepared in the laboratory. A plotter (16; EMG type 79813) and a printer (17; EMG type 893) complete the system.

The carrier stream finally passes to waste (13) as does the auxiliary solution (5).

Chemicals

The reagent-generating solution was 1 M sulphuric acid containing 0.5 M potassium bromide; 1 M sulphuric acid was employed as the auxiliary solution. Dilute arsenic (III) and sodium thiosulphate solutions were used as samples. All the chemicals employed were of analytical grade.

Some aspects of the system organization

In the triangle-programmed titrations considered here the excess of bromine reagent is detected biamperometrically. To carry out a measurement, the reagent-generating program is started by the signal generator [2—4]; the current passing through the generating electrodes increases linearly with time up to a certain time ($t = \tau$), after which it decreases up to time $t = 2\tau$. Accordingly, the mass flow of bromine increases up to time τ and decreases up to time 2τ. After the reagent stream and sample solution have mixed in the drip cell, the solution enters the detector cell, and the indicating electrode (cathode) at the cell voltage applied gives a current signal which is linearly related to the bromine concentration. The polarographic record is thus an almost perfect isosceles triangle. With manual evaluation, the two equivalence points are determined from the two intersections of the base line ($i_{vt} = i_{residual}$) and the extrapolated sides of the triangle.

For the Q value (the distance between the two equivalence points expressed as a time interval)

$$Q_c = 2\tau - 2\,(a/bn)\,cV \qquad (1)$$

which involves the duration of the reagent-addition program (2τ), the sample concentration (c), flow rate (V), the stoichiometric constants of the titration reaction (a and b), as well as another constant (n) characteristic of the reagent-addition program. The concentration of a sample can be determined either from eqn. (1), or from a suitable calibration curve, such as that shown in Fig. 2 for arsenic (III).

A triangle-programmed titration curve recorded for a sodium thiosulphate

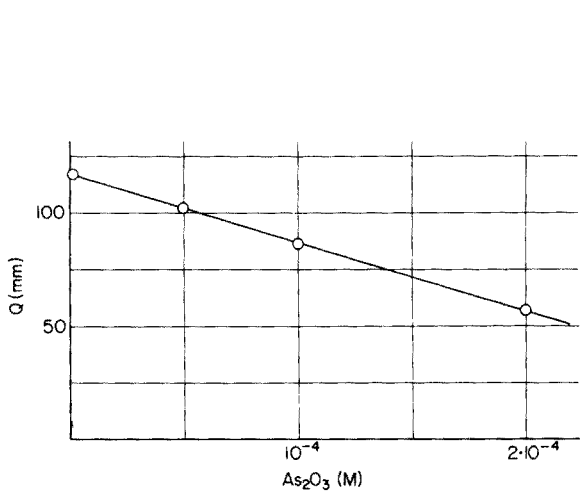

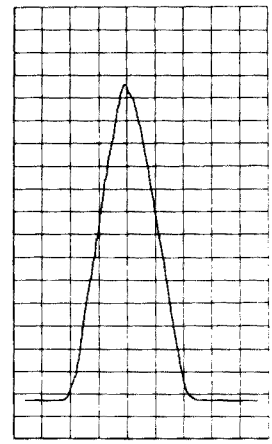

Fig. 2. Calibration curve for arsenic (III) i_{max} = 4.2 mA; 2τ = 200 s.

Fig. 3. Titration curve for 4 × 10^{-4} M thiosulphate solution. i_{max} = 8.46 mA; 2τ = 200 s.

sample is given in Fig. 3. As manual evaluation is tedious, an automatic method of evaluation was developed based on a small desk-top computer (storage capacity, 8K byte; data input channel speed 8K byte s^{-1}).

The following requirements must be satisfied by the computer program. First, the automatic evaluation must be consistent with the basic principles of the triangle-programmed technique, and must involve the Q value as the basis of evaluation. Several other promising automatic evaluation procedures appeared in the course of the work, but their application would make the results dependent on the detector sensitivity, which is not tolerable here. Secondly, the automatic evaluation must be accurate, precise and reproducible. Thirdly, the results must be printed out together with the important analytical parameters in a form appropriate for further data treatment. Fourthly, the evaluating program must have maximal flexibility to match the requirements of different types of titrations, and different samples and concentration ranges. Of course, the occurrence of errors caused by accidental irregularities must be minimized, the analysis time should not be increased appreciably, and, for economic reasons, the smallest computer capable of solving the problem should be used.

In order to determine the equivalence points, the system measures the detector signal successively at constant sampling intervals (T), and the time value relevant to each detector signal must be known. Remarkable storage capacity can be saved if the cycle generator of the A/D converter is used for the time-scale generation, instead of employing an external clock and storing the individual time data thus provided. In this case, if only the time parameter of the first detector signal is taken and stored, and the sampling

interval (T) is known from numbering the successively stored detector signals, their time data are readily obtained.

For the instrumentation and titrations considered here, the detector signal is directly proportional to the concentration of the reagent, but a very small residual current flows through the detector cell. Accordingly, the points where the residual current line is intersected by the sides of the triangular signal vs. time recording correspond to the two equivalence points. An oscillation — more or less periodic — can be observed in the current—time curve when the current is higher than the residual current. The amplitude of the oscillation depends on the momentary concentration (c_t) of the electroactive reagent in the solution in contact with the cathode. The oscillation is caused by the periodic change in the flow rate (V) of the solution. This is obvious when it is considered that the momentary intensity of the current (i_{vt}) can be described by the equation [5]

$$i_{vt} = i_R + (A + BV^{\frac{1}{2}})c_t \qquad (2)$$

where i_R is the residual current, and A and B are constants.

As a peristaltic pump, drip-vessel, and biamperometric detector are employed, the oscillation cannot easily be avoided. Therefore, the oscillating part of the titration curves must be replaced by two fitted lines to simplify location of the two equivalence points. The straight line fits are best done off-line by the method of least squares. Other curve-fitting methods were also examined and will be described elsewhere.

Because there is essentially no oscillation in the residual current ($c_t = 0$), the value used for location of equivalence points was simply taken from the meter. The residual current is generally very small, and significant errors are not caused in most cases if the $i = i_R$ line is replaced by the $i = 0$ line in the evaluation. Organizing the program in this way saves computer time and data storage capacity.

The shape of the triangle-programmed titration curve (Fig. 3) deviates from that of the theoretically expected isosceles triangle: the maximum does not show up as a sharp vertex, and the sides are slightly curved as they approach the base line, i.e. tailing is observed. This is definitely caused by mixing of the solution in the direction of the stream. The sections deviating from the overall triangle should not be used for the evaluation. Accordingly, a certain percentage of the i_t data taken and stored near the maximum is not used for the off-line curve-fitting step (window). To avoid the curved section caused by the tailing effect, a threshold current intensity is employed, and the i_t data are stored until their values exceed the value of the threshold. Obviously, both the window percentage and the threshold current level can easily be altered to fit the requirements of a particular measurement.

The measuring—evaluation program based on these considerations was prepared in keyboard language for the EMG 666 computer. The flow diagram is shown in Fig. 4. The program consists of three separate parts. The first part feeds the values of the different parameters required for the measurement and

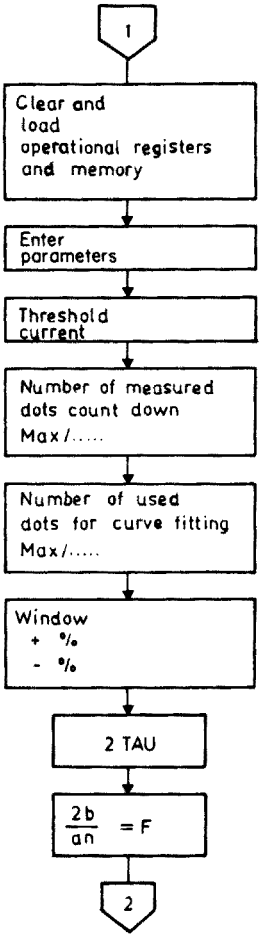

Fig. 4a.

evaluation into the computer. There are six manually given parameters: the storage of the measured (i_1) data is initiated together with the start of the time scale when the detector signal exceeds the preset threshold current; the measuring cycle stops when the detector signal falls below this value. However, if the fall happens quickly ($t < \tau/10$), the data collection is not interrupted. The disruptive effect of the detector signal oscillation in the rising section of the curve can thus be avoided.

In an early version of the program, the initiating effect of electrical noise was filtered out, but experience showed that this is not needed in the system used here. Given an appropriate threshold current determined from the residual current intensity and the extent of tailing, accidental initiation of

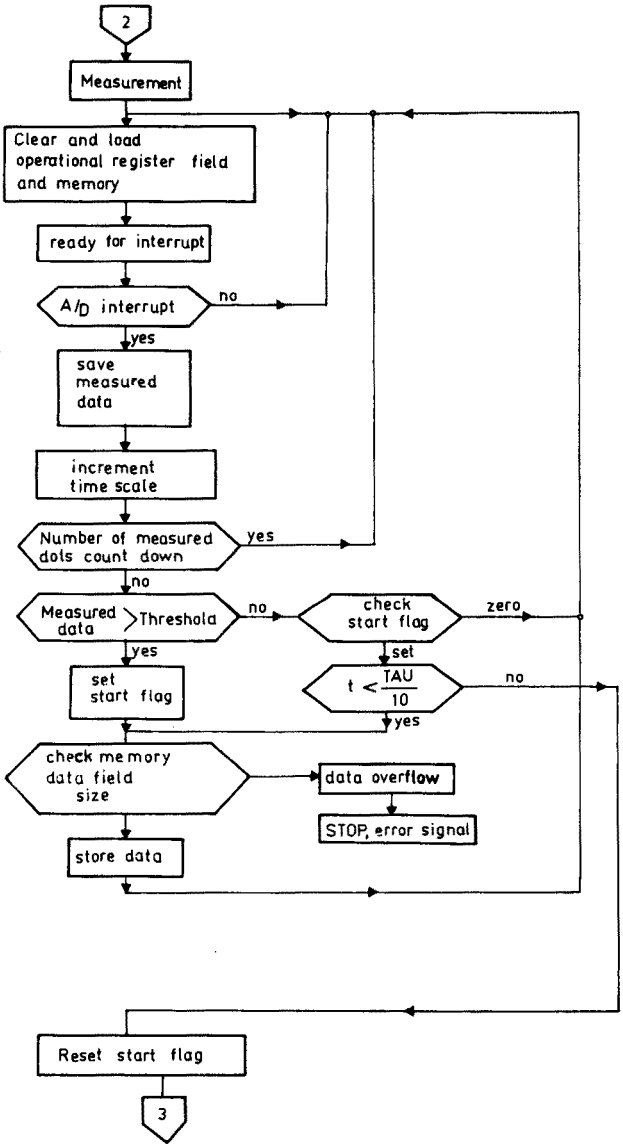

Fig. 4b.

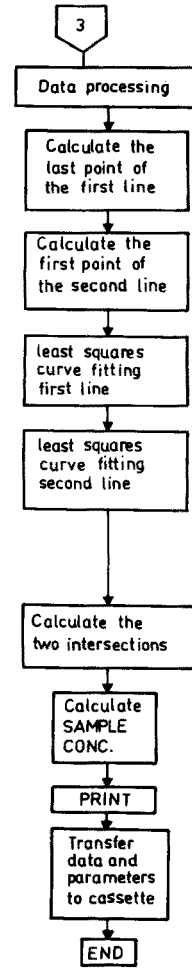

Fig. 4c.

Fig. 4. Flow diagram of the evaluation program used.

data collection will happen only in laboratories of extremely high electric noise level.

The value of NUMBER of DOTS, which is a single digit positive number, determines the portion of the data collected to be used for the curve-fitting. (When it is 1, every i_t value is used; when it is 2, every second i_t value is used, etc.)

The WINDOW shows the percentage by which the data used for curve-fitting are decreased in the vicinity of the maximum.

The value of 2 TAU means the entire length of the reagent-generating triangle program. It is advisable first to input the selected signal generator (2τ) value, which can later be slightly modified according to the results obtained in titrations of standard solutions. Occasional modification is needed if mixing in the direction of the flow becomes significant between the generator and the detector electrodes. In this case, if solutions of zero sample concentration are titrated, the time between the two equivalence points ($Q_{c=0}$) will be longer than the reagent generating cycle ($Q_{c=0} > 2\tau$).

The coefficient $2b/an$ in eqn. (1) can be fed into the computer as value F. Its value can be calculated from the parameters of the titration reaction, the reagent addition program and the sample flow. However, for better reliability, it is sometimes advisable to determine the F value from experimental Q_c values obtained by titrating standard solutions.

The second part of the computer program is the on-line measuring program, which provides the data collection and storage. The DVM measures a new value every 40 ms, and a certain (variable) part of these data are stored in the memory.

The third part of the program is off-line and does the evaluation. From the signal intensity—time data pairs of the two data fields the parameters of the two best-fit lines are calculated (slope and axial intersection). The time co-ordinates of the intersections of these lines with the zero signal line are determined (t_{E_1} and t_{E_2}). From the difference of these two values, which is equal to the Q_c value, and given the 2 TAU and F values, the computer calculates and prints out the unknown concentration.

RESULTS AND DISCUSSION

A few constant parameters must be given in the first interactive part of the computer program. These constants are established in two steps. First, a titration curve is recorded with the appropriate triangular reagent-addition program for a sample solution of zero concentration. On the basis of this recording, which is fairly close to an isosceles triangle, the values of THRESHOLD CURRENT and of the WINDOW are determined as indicated in Fig. 5.

It is advisable to select a THRESHOLD CURRENT value which is just above the curved section of the downward side of the triangular recording. The value of WINDOW is given by the extent (in percentage) of the curved

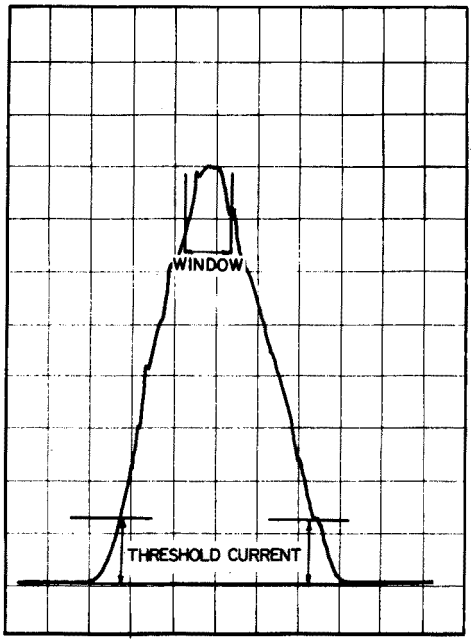

Fig. 5. Triangle-programmed titration curve marked with THRESHOLD CURRENT and WINDOW. i_{max} = 4.2 mA; 2τ = 400 s; $c = 2 \times 10^{-4}$ M.

section at the maximum. The titration curve also gives a rough value for 2 TAU, but this can also be taken from the frequency scale of the signal generator. In giving the NUMBER of DOTS value, a compromise must be made between the off-line computer time and the accuracy. The shorter the calculating time, i.e. the larger the value of this constant, the less accurate will be the curve-fitting.

As was mentioned earlier, to obtain improved accuracy, the $Q_{c=0}$ value should not be taken as 2 TAU, because the tailing effect is most significant at c = O.

It is expedient to determine the 2 TAU and F values simultaneously, by doing triangle-programmed titrations of two different standard solutions with concentrations bracketing the concentration range of the samples to be determined. Accordingly, the values F = 1 and 2 TAU equal to its approximate value are input, and two standard solutions of concentration c_1 and c_2 are titrated; on completion of the evaluation, two values α_1 and α_2 are output; here $\alpha_1 = 2\tau - Q_1$ and $\alpha_2 = 2\tau - Q_2$. An accurate value for 2 TAU under the given conditions and in the concentration range can then be obtained from

$$2\tau = (\alpha_1/\alpha_2)\,(Q_2-Q_1)/(\alpha_1/\alpha_2-1) \qquad (3)$$

Because $\alpha_1 = F\,c_1$ and $\alpha_2 = F\,c_2$ contain the accurate value for 2 TAU, the F constant can easily be determined (supposing that V is constant).

For preliminary checking of the evaluation program, isosceles triangular signals provided directly by the signal generator were fed into the computer through the DVM, and the Q value was evaluated. The scatter of the Q values was found to be 0.05%, which confirmed proper functioning of the program as well as the excellent stability of the signal generator used.

The effect of the NUMBER of DOTS value on the reproducibility of titrations of different samples was then examined. Given the periodic noise level, no significant improvement in reproducibility was obtained by increasing the number of data used for evaluation above 1000. However, to achieve a standard deviation of about 2% for the Q values, at least 400 data pairs are required for the curve-fitting step.

The effects of the THRESHOLD CURRENT value and of the WINDOW percentage on the scatter of the Q values were studied for titrations of 10^{-3} M arsenic (III). The results (Table 1) indicate that if the threshold current is too small, ($i_{Tn} < 5i_{max}/100$) the reproducibility becomes significantly worse. This is probably caused by the inclusion of points taken from curved sections of the titration curve among the data used for curve fitting. Obviously, however, any increase in the threshold current must be limited by the requirement of at least 400 data pairs for the evaluation. Much the same can be said about the WINDOW percentage. The triangular signal—time recording in very concentrated samples can be very small; thus if the originally given parameters are used, the number of i_t—t pairs available for evaluation may be too small to yield the required precision. The evaluation program makes it possible to repeat the complete off-line calculation any number of times; if necessary, the result can be recalculated to obtain better precision from more data. For this purpose, only the NUMBER of DOTS value must be decreased, if it is not already 1. Two values are printed out (or stored) after the evaluation: the

TABLE 1

Dependence of the Q_c scatter on the Threshold Current and on the Window

THRESHOLD CURRENT		WINDOW	
(%)[a]	Q_c scatter (%)	(%)[b]	Q_c scatter (%)
2.3	2.4	±5	4.0
4.5	1.2	±10	3.0
6.8	0.45	±20	1.5
9.09	0.13	±30	2.3
11.4	1	±50	3.6

[a]The THRESHOLD CURRENT is given as a percentage of the maximal detector signal.
[b]The WINDOW is given as a percentage of the number of data stored.

measured Q_c and the concentration calculated from it. Owing to the nature of the triangle-programmed method, the precision and accuracy which can be achieved depend strongly on conditions such as 2τ, flow rate and its stability, concentration range, reaction rate, etc. However, the reproducibility of the concentration values depends much more on the properties of the reagent-addition program than on the Q_c value (cf. eqn. 1).

For example, when two arsenic (III) samples with $c_1 = 10^{-5}$ M and $c_2 = 9 \times 10^{-5}$ M were titrated with a reagent-addition program of $2\tau = 84$ s, the relative errors of the Q_c values were found to be nearly equal: $\Delta\bar{Q}_1/\bar{Q}_1 = \Delta\bar{Q}_2/\bar{Q}_2 = 0.75\%$. However, the relative errors of the calculated concentrations were very different: $\Delta c_1/c_1 = 12.5\%$ and $\Delta c_2/c_2 = 0.7\%$. Obviously, such points must be considered in selecting the reagent-addition program. In the present measurements, the reproducibility of the results and the dependence of reproducibility on different parameters were studied by observing the reproducibility of the Q_c values.

The total computer time required comprises three different parts: (a) the execution of the first interactive part is input-limited; (b) the duration of the on-line measuring part is determined by the reagent-addition program; (c) the off-line evaluation step requires 3—30 s for calculation and print-out depending on the number of data pairs used for the curve-fitting.

The problems of automatic evaluation of the results obtained by triangle-programmed titrations in cases when a linear signal-transforming detector is employed to measure the excess of reagent, can be solved by employing a desk-top computer and a relatively simple program. Further studies are in progress to extend the automatic evaluation method to other cases of triangle-programmed titrations.

REFERENCES

1 G. Nagy, K. Tóth and E. Pungor, Anal. Chem., 47 (1975) 1460.
2 G. Nagy, Zs. Fehér, K. Tóth and E. Pungor, Anal. Chim. Acta, 91 (1977) 87.
3 G. Nagy, Zs. Fehér, K. Tóth and E. Pungor, Anal. Chim. Acta, 91 (1977) 97.
4 G. Nagy, Zs. Fehér, K. Tóth and E. Pungor, Anal. Chim. Acta, 100 (1978) 181.
5 G. Nagy, Zs. Fehér and E. Pungor, Anal. Chim. Açta, 52 (1970) 47.

Analytica Chimica Acta, 101 (1978) 273—281

A DUAL ION-SELECTIVE ELECTRODE DETECTOR FOR THE SIMULTANEOUS DETECTION OF BROMINE- AND CHLORINE-CONTAINING COMPOUNDS IN GAS CHROMATOGRAPHY

TSUGIO KOJIMA*, MITSUNOJO ICHISE, and YOSHIMITSU SEO

Department of Industrial Chemistry, Faculty of Engineering, Kyoto University, Yosida, Kyoto (Japan)

(Received 20th March 1978)

SUMMARY

A dual ion-selective electrode gas chromatographic detector which allows the simultaneous detection of chlorine- and bromine-containing compounds through two-channel operation is described. Components eluted from the g.c. column are hydrogenated, the hydrogen chloride and hydrogen bromide produced being absorbed in a standard solution of halide; the ion concentrations in the resulting solution are monitored by chloride- and bromide-selective electrodes. The dual electrode detector gives two chromatograms simultaneously, one selective for chlorine- and bromine-containing compounds and the other for bromine-containing compounds. The response ratio, i.e., the peak area of the readout from the chloride channel divided by that from the bromide channel for the same compound, gives valuable information. The Cl/Br ratio in an eluted molecule can be determined accurately from the response ratio if a standard reference compound is injected simultaneously.

The selective detection of compounds containing heteroatoms such as nitrogen, sulfur, and halogen in gas chromatographic eluates is important in obtaining information on unknown components of complex mixtures. A number of element-specific detectors are available, such as the flame photometric detector for sulfur and phosphorus, the electron-capture detector for halogen-containing compounds, and the alkali flame ionization detector for nitrogen and phosphorus compounds [1, 2]. Other selective detectors are based on post-column combustion or hydrogenolysis of organic compounds to produce small fragments, such as SO_2, H_2S, NO_2, NH_3, etc., which are then detected coulometrically or in an electrolytic conductivity cell [3—11].

Although many ion-selective electrodes have only limited selectivity, they can be applied for gas chromatographic (g.c.) detection after post-column treatment similar to that used in conjunction with coulometric and conductivity detectors [12]. The g.c. effluent is passed through a post-column reactor at 800—1000°C where the separated components undergo hydrogenolysis in the presence of a platinum or nickel catalyst. The gases are dissolved in a suitable absorption solution and the concentrations of ions produced from

simple inorganic gases are monitored continuously. Compounds containing chlorine, sulfur, nitrogen, and fluorine can be selectively detected [13—15]. The method can be used for determining 10^{-12} mol of sulfur compounds, 10^{-10} mol of chlorine compounds and 10^{-11} mol of fluorine compounds. If a dual detector equipped with two ion-selective electrodes is used, it is possible to detect fluorine and chlorine compounds simultaneously and selectively [15].

The construction of a dual electrode detector which allows the simultaneous and selective detection of chlorine- and bromine-containing compounds through two-channel operation is described in this paper. The calculation of the atomic ratio of the two elements to aid in the identification of unknown compounds is also discussed.

EXPERIMENTAL

A schematic diagram is shown in Fig. 1. Hydrogen at a flow rate of 25—40 ml min^{-1} from a cylinder (a) passes through the gas chromatograph (b, c). An electric furnace (d; 200-mm long) is operated at 900°C; a platinum tube (2-m long, 0.5-mm i.d.) serves as the hydrogenation tube (e). The carrier stream passes to a glass absorption tube (f) which has a gas—liquid contact area 0.8-mm i.d. and 25-mm high. The absorption solution (g) is pumped by a micro-pump (h) at a constant flow rate (0.6 ml min^{-1}) via a pulsation buffer tube (i) to the absorption tube where it absorbs hydrogen bromide and hydrogen chloride from the hydrogenated gases. Unabsorbed gases such as methane are separated, together with carrier gas, from the absorption solution in the gas—liquid separator and vented from the system.

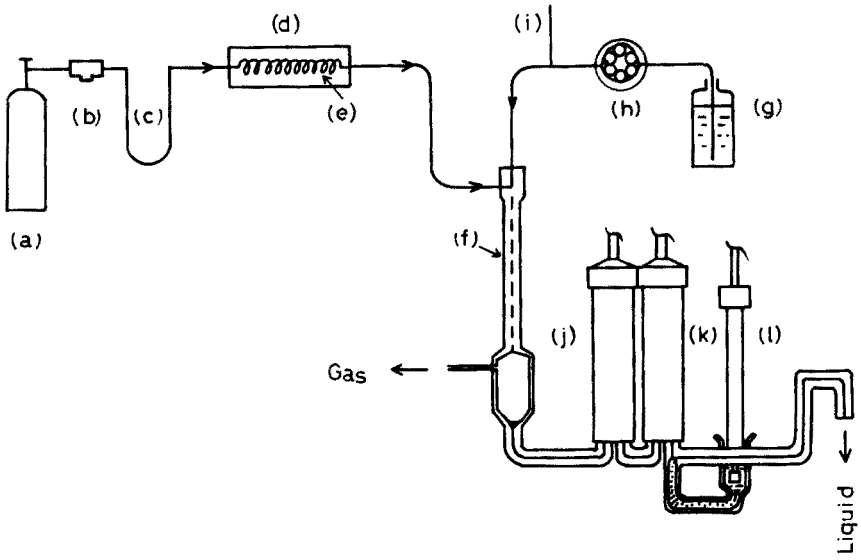

Fig. 1. Schematic diagram of the apparatus.

The emerging absorption solution is led through a measuring cell equipped with a chloride-selective electrode (j) and a bromide-selective electrode (k) and is then discarded. The absorption solution and the saturated calomel reference electrode (l) are connected by a saturated potassium nitrate solution-agar bridge. The measuring cell is shown in detail in Fig. 2.

The chloride- and bromide-selective electrodes used were an Orion Model 92-17 liquid membrane electrode and an Orion Model 94-35 solid-state electrode, respectively. Each electrode shows a potential for chloride or bromide ion activity in accordance with the near-Nernstian equations as follows:

$$E_{Cl} = E_{0(Cl)} - S_{Cl} \log (a_{Cl} + K_1 a_{Br}) \quad (1)$$

$$E_{Br} = E_{0(Br)} - S_{Br} \log (a_{Br} + K_2 a_{Cl}) \quad (2)$$

where K_1 is the chloride/bromide selectivity ratio for the chloride electrode, K_2 is the bromide/chloride selectivity ratio for the bromide electrode, and other symbols have their usual meanings. As K_2 is very small, eqn. (2) can be simplified to $E_{Br} = E_{0(Br)} - S_{Br} \log a_{Br}$. If the ionic strength of the absorption solution is kept constant, activities in eqns. (1) and (2) can be replaced by concentrations.

The difference in potential between the indicating electrode and the reference electrode is fed to an antilog converter circuit and a signal directly proportional to the halide concentration is recorded. The circuit for measuring the electrode potential (Fig. 3) comprises (a) a voltage follower with a QFT-2A amplifier (Philbrick/Nexus Research) as an impedance converter; (b) an adjustable-coefficient inverter (Philbrick PF-85AU inversion-type feedback

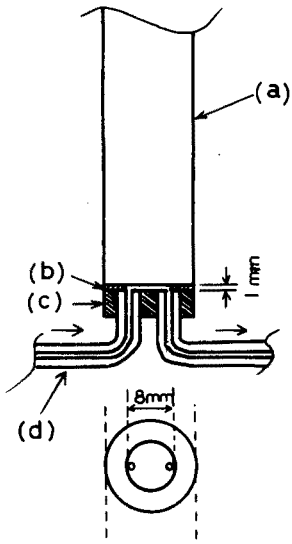

Fig. 2. Cell details. (a) Bromide-selective electrode body; (b) silicone rubber packing; (c) polyethylene plate; (d) glass capillary. The chloride-selective electrode was used by fitting a flow-through cap (Orion Research Inc.).

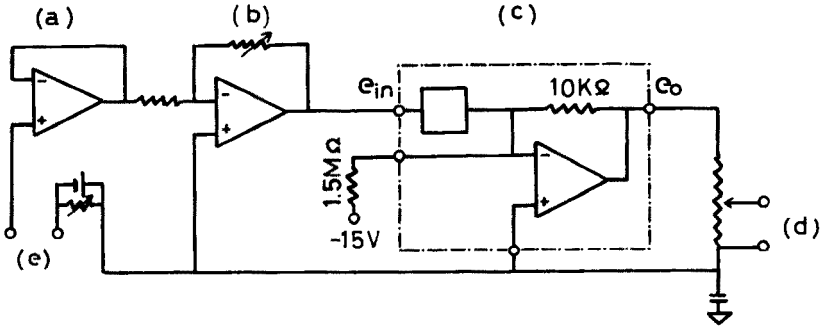

Fig. 3. Circuit for electrode detector.

coupling) as an adapter for (c), which is an antilog converter (Philbrick/Nexus Model 4351); (d) a 1-mV recorder; and (e) the signal input.

To use electrode in the Nernstian range, the absorption solution must contain about 10^{-3} M sodium bromide and about 5×10^{-3} M sodium chloride. When hydrogen bromide and hydrogen chloride are absorbed, so that the concentrations of the chloride and bromide are increased by ΔC_{Cl} and ΔC_{Br}, respectively, the changes in the potentials of the chloride- and bromide-selective electrodes are given by eqns. (3) and (4), respectively:

$$\Delta E_{Cl} = -S_{Cl} \log\left(1 + \frac{\Delta C_{Cl} + K_1 \Delta C_{Br}}{5 \times 10^{-3} + K_1 \times 10^{-3}}\right) \quad (3)$$

$$\Delta E_{Br} = -S_{Br} \log (1 + \Delta C_{Br}/1 \times 10^{-3}) \quad (4)$$

The antilog converter used has the following conversion characteristics: $e_0 = -(1/10)\, 10^{0.5 e_{in}}$. The change in potential, ΔE, enters as input e_{in} to the antilog converter after undergoing conversion and is then amplified A times in the inverter (see Fig. 3). Hence $e_{in} = -A\, \Delta E$. If gain A in the inverter is adjusted so as to make $A = 1/0.5\, S_{Cl}$, and if 0.1 V is added to each e_0 value, the converter provides a signal e'_0 to the recorder which is linear with respect to ΔC. Appropriate substitution in eqns. (3) and (4) then gives

$$e'_{0(Cl)} = -\frac{1}{10}\left(\frac{\Delta C_{Cl} + K_1 \Delta C_{Br}}{5 \times 10^{-3} + K_1 \times 10^{-3}}\right) \quad (5)$$

$$e'_{0(Br)} = -\frac{1}{10}\left(\frac{\Delta C_{Br}}{1 \times 10^{-3}}\right) \quad (6)$$

which are the equations valid for the chloride and bromide channels, respectively.

RESULTS AND DISCUSSION

Evaluation of the selectivity ratio with respect to bromide for the chloride-selective electrode

Figure 4 shows the plots of the final e'_0 outputs of the antilog converters vs. the halide concentrations. The rectilinear graphs show that the conversion of the signal from the ion-selective electrode is in accord with the results expected from eqns. (5) and (6).

Figure 5 shows typical plots for the evaluation of the selectivity ratio, K_1, for bromide with the chloride-selective electrode based on eqn. (5). For the plots shown in Fig. 5, the potential e'_0 was first measured in a known volume of the absorption solution containing 5×10^{-3} M NaCl and 1×10^{-3} M NaBr and known volumes of a stock solution containing chloride and bromide at a molar ratio of 1:1 or 1:0.5 were added successively, the potential $e'_{0(Cl)}$ being measured after each addition. The rectilinear plots obtained were used to estimate a value of K_1. The K_1 value found was 3.5 over the range of total halide concentration 6×10^{-3}—3×10^{-2} M.

Element-selective detection

An artificial mixture of organic compounds containing chlorine and/or bromine with a hydrocarbon added as standard, was run through the system to illustrate the selectivity. Figure 6 shows a comparison of the chromatograms obtained with the chloride-selective electrode, the bromide-selective electrode, and a flame ionization device as detector. The selectivity of the electrode detectors is excellent. Methane, water and ammonia which are produced from compounds containing C, H, O and N give little or no response. Hydrogen sulfide, which is produced from compounds containing sulfur, can be removed by a nickel catalyst in the furnace tube; the response to hydrogen sulfide then

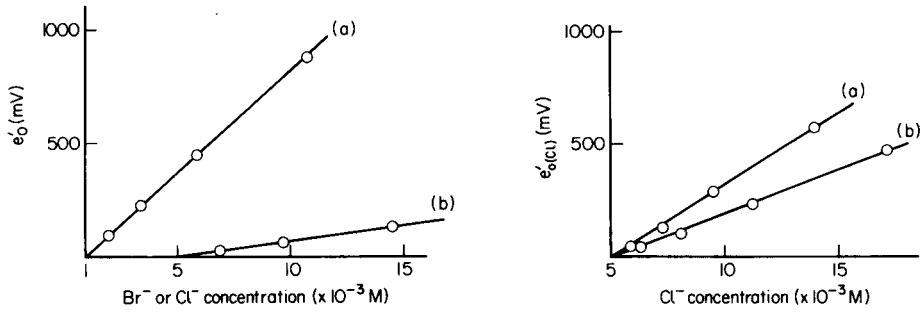

Fig. 4. Plots of output of antilog converter vs. concentration of halide ion. (a) Response of bromide-selective electrode to bromide ion; (b) Response of chloride-selective electrode to chloride ion.

Fig. 5. Plots for evaluation of the Cl/Br selectivity ratio with the chloride-selective electrode. For method, see text. Molar concentration ratio of Cl^- to Br^- in the stock solution: (a) 1:1; (b) 1:0.5.

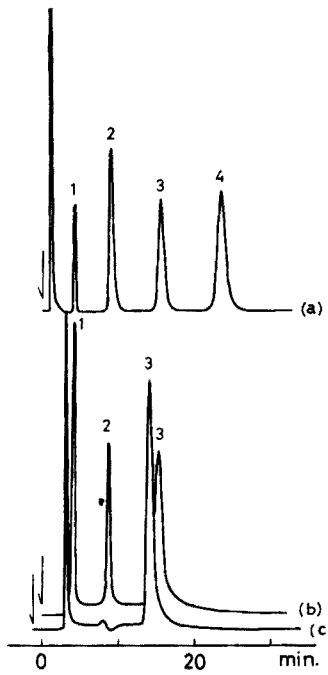

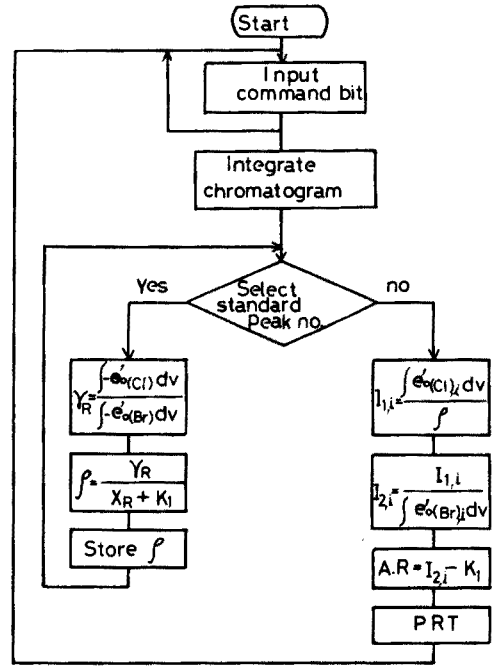

Fig. 6. Chromatogram of a mixture containing chlorine and/or bromine compounds. (1) Bromochloromethane; (2) 1-chloropentane; (3) 1-bromopentane; (4) n-nonane. (a) Flame ionization detector; (b) chloride-selective electrode detector; (c) bromide-selective electrode detector. The injections (1 μl) were of a solution containing 10^{-4} mol of bromochloromethane, 10^{-4} mol of 1-chloropentane, 10^{-4} mol of 1-bromopentane and 10^{-4} mol of n-nonane in 0.5 ml of pentane.

Fig. 7. Flow chart of the computer program to obtain atomic ratios.

becomes negligible. The minimum detectable amounts are of the order of 4×10^{-9} g Cl s^{-1} and 7×10^{-10} g Br s^{-1}. The linear range of the detector covers about three orders of magnitude.

Use of the electrode detector to obtain the atomic ratio

An ion-selective electrode detector has been reported for the simultaneous analysis of the column eluate for chlorine- and fluorine-containing compounds [15]. Since the atomic ratio is characteristic for many compounds, applications of these detectors would permit the identification of unknown compounds containing halogen atoms.

In the case of the dual detector equipped with the chloride- and bromide-selective electrodes, the atomic ratio (Cl/Br) can be determined from the response ratio if an appropriate correction is made. The peak area A_{Cl} for a compound containing chlorine and bromine on the chromatogram of the chloride channel can be represented as

$$A_{Cl} = \int -e'_{0(Cl)}\, dV \tag{7}$$

where dV is the differential of V, the volume of the flowing absorption solution. From eqn. (5), eqn. (7) can be written in the form

$$A_{Cl} = \frac{1}{10(5 \times 10^{-3} + K_1 \times 10^{-3})} \int (\Delta C_{Cl} + K_1\, \Delta C_{Br})\, dV \tag{8}$$

Here $1/10(5 \times 10^{-3} + K_1 \times 10^{-3})$ is the slope of the calibration plot of Fig. 4. If this slope is indicated by the symbol S'_{Cl}, then

$$A_{Cl} = S'_{Cl} \int (\Delta C_{Cl} + K_1\, \Delta C_{Br})\, dV = S'_{Cl}\, (m_{Cl} + K_1 m_{Br}) \tag{9}$$

where m_{Cl} and m_{Br} are the number of moles of hydrogen chloride and hydrogen bromide, respectively, dissolved in the absorption solution.

Similarly, the peak area A_{Br} for the same compound on the chromatogram of the bromide channel can be represented as

$$A_{Br} = \int -e'_{0(Br)}\, dV \tag{10}$$

Development analogous to the above equations, but based on eqn. (6) with $1/10(1 \times 10^{-3})$, i.e. the slope of the calibration plot of Fig. 4, indicated by S'_{Br}, leads to the equation

$$A_{Br} = S'_{Br} \int \Delta C_{Br}\, dV = S'_{Br}\, m_{Br} \tag{11}$$

As the detector monitors the same eluate simultaneously, the response ratio, γ, defined as the peak area on the chromatogram of the chloride channel divided by that of the bromide channel for the same compound, can be precisely determined:

$$\gamma = \frac{S'_{Cl}\, (m_{Cl} + K_1 m_{Br})}{S'_{Br}\, m_{Br}} = \frac{S'_{Cl}}{S'_{Br}} \left(\frac{m_{Cl}}{m_{Br}} + K_1 \right) \tag{12}$$

If the response ratio γ_R is measured for any reference compound containing chlorine and bromine at a known atomic ratio X_R, the slope ratio ρ can be calculated, because K_1 is known to have the value 3.5. Thus

$$\rho = \gamma_R/(X_R + K_1) = S'_{Cl}/S'_{Br} \tag{13}$$

Once the ρ value has been determined in this way, the atomic ratio (Cl/Br) for an unknown compound i can be obtained as follows. An $I_{1,i}$ value is obtained by dividing the peak area for unknown compound i on the chloride channel by ρ:

$$I_{1,i} = (\int -e'_{0(Cl),i}\, dV)/\rho = S'_{Br}(m_{Cl,i} + K_1 m_{Br,i}) \tag{14}$$

where suffix i denotes the unknown compound. By dividing $I_{1,i}$ by the peak area for the same compound on the bromide channel, $I_{2,i}$ can be obtained:

$$I_{2,i} = I_{1,i}/(\int -e'_{0(Br),i}\, dV) = (m_{Cl,i}/m_{Br,i}) + K_1 \tag{15}$$

Subtraction of K_1 from $I_{2,i}$ gives the atomic ratio, AR(Cl/Br), for the unknown compound:

$$AR = I_{2,i} - K_1 = m_{Cl,i}/m_{Br,i} \quad (16)$$

An Intel 8008 microcomputer system (or DEC microcomputer system LSI-11) was used for the calculation. A customised system would require only a microprocessor, a read-only memory of 1.5 K words, a read-write memory of 1 K words and digital input—output. The microprocessor is programmed to calculate the peak areas, to store the peak-area readings, and then calculate the atomic ratio for the unknown compound after all peaks are recorded. The flow chart is shown in Fig. 7.

The program, written in ASSEMBLY language, was prepared in two sections: calculation of peak areas, and calculation of atomic ratios with print-out. The computer cannot select the peak of the reference compound injected simultaneously; accordingly, the reference peak must be input in the first step of the second section. The program uses the peak area of the reference compound to calculate γ and ρ, and then calculates I_1 and I_2 values from the peak area of the unknown compound. Finally, the atomic ratio of the unknown compound is generated.

Bromodichloromethane, bromotrichloromethane, 1,2-dibromo-1-chloropropane, 1,2-dibromo-1,1,2-trichloroethane, 1,4-dibromobutane, and 1,2-dibromo-1-chloro-1,1,2-trifluoroethane were chosen as test compounds. A sample containing 10^{-2} mol each of these compounds was prepared and diluted 30-fold with n-pentane. After addition of a suitable reference compound, 1 μl was injected into a column (Durapak-Carbowax 400/Porasil C, 100-120 mesh, 1 m) and chromatographed. Table 1 shows the atomic ratio results obtained for the test compounds. For seven bromochloroalkanes, excellent agreement was found between the theoretical and found values.

For highest precision, the selection of the reference compound is critical. The reference compound peak should be eluted as close as possible to the compound to be measured. Optimal results are obtained when the concentration of the compound is adjusted so that the peak-area ratio is approximately unity.

TABLE 1

Chlorine—bromine atomic ratios found in halogen compounds

Sample	$CHBrCl_2$	$CBrCl_3$	$C_3H_5Br_2Cl$	$C_2HBr_2Cl_3$	$C_2H_2Br_2Cl_2$	$C_4H_8Br_2$	$C_2Br_2ClF_3$
Reference compound[a]	I	II	III	IV	IV	IV	II
AR found ($\bar{x}$)[b]	2.06	3.09	0.53	1.59	1.05	−0.27	0.52
S.d.	0.099	0.111	0.065	0.051	0.079	0.063	0.088
AR theor.	2	3	0.5	1.5	1	0	0.5
Deviation	0.06	0.09	0.03	0.09	0.05	−0.27	0.02

[a] I, bromochloromethane; II, 1-bromo-2-chloromethane; III, 1-bromo-3-chloropropane; IV, 1-bromo-4-chlorobenzene. [b] Average of 7 analyses.

REFERENCES

1 D. F. S. Natusch and T. M. Thorpe, Anal. Chem., 45 (1973) 1185A.
2 R. Pigliucci, W. Averill, J. E. Purcell and L. S. Ettre, Chromatographia, 8 (1975) 165.
3 D. M. Coulson and L. A. Cavanagh, Anal. Chem., 32 (1960) 1245.
4 R. L. Martin and J. L. Grant, Anal. Chem., 37 (1965) 644.
5 H. V. Drushel, Anal. Chem., 41 (1969) 569.
6 P. J. Klaas, Anal. Chem., 33 (1961) 1851.
7 R. L. Martin, Anal. Chem., 38 (1966) 1209.
8 O. Piringer, M. Pascalau, J. Chromatogr., 8 (1962) 410.
9 O. Piringer, E. Tataru and M. Pascalau, J. Gas Chromatogr., 2 (1964) 104.
10 D. M. Coulson, J. Gas Chromatogr., 3 (1965) 134; 4 (1966) 285.
11 R. C. Hall, J. Chromatogr. Sci., 12 (1974) 152.
12 T. Kojima, M. Ichise and Y. Seo, Bunseki Kagaku, 20 (1971) 20.
13 T. Kojima, M. Ichise and Y. Seo, Talanta, 19 (1972) 539; Bunseki Kagaku, 22 (1973) 208.
14 T. Kojima, Y. Seo and J. Sato, Bunseki Kagaku, 23 (1974) 1389; 24 (1975) 772.
15 T. Kojima, M. Ichise and Y. Seo, Bunseki Kagaku, 24 (1975) 7.

Analytica Chimica Acta, 101 (1978) 283—307

HIGH-PERFORMANCE PULSE AND DIFFERENTIAL PULSE POLAROGRAPHY
Part 2. Instrumental Considerations

W. P. van BENNEKOM

Department of Pharmaceutical Analysis and Analytical Chemistry, Subfaculty of Pharmacy, State University, Gorlaeus Laboratories, Wassenaarseweg 76, Leiden (The Netherlands)

(Received 12th September 1977)

SUMMARY

For high-performance normal and differential pulse polarography (h.p.n.p.p. and h.p.d.p.p.), the capacitance currents caused by drop growth and pulse application and the faradaic current caused by pulse application are considered in detail. The faradaic current phenomenon is discussed critically for both h.p.d.p.p. and conventional d.p.p. By considering both the capacitance and faradaic current caused by pulse application, the optimal position of the first current sampling can be calculated from charge-density data. The position of the second sampling can be optimized by considering the faradaic current caused by pulse application. The influence of practical sampling width (20 ms for European countries) on the results is evaluated and the implications are incorporated in the theory. When this sampling width is used, the influence of the capacitance current caused by drop growth on the results can be eliminated completely if the second current sampling is multiplied by an instrumentally determined factor, before it is subtracted from the first sampling. Thus for practical polarographic instrumentation, the signal-to-noise ratio can be improved greatly. From theoretical considerations, other instrumental requirements are discussed; the optimal characteristics for potentiostat and current-amplifier are evaluated. Requirements for optimal performance in h.p.n.p.p. and h.p.d.p.p. are reported.

The influence of the capacitance current caused by drop growth on the results in normal and differential pulse polarography (n.p.p. and d.p.p.) can be reduced remarkably by application of high-performance normal and differential pulse polarography (h.p.n.p.p. and h.p.d.p.p.), as was discussed in Part 1 of this series [1]. The required optimal wave-forms for h.p.n.p.p. and h.p.d.p.p., together with the timing and sampling sequence, are given in Fig. 1. In both modified methods, a potential pulse is applied at a fixed time τ in the final stages of drop life. At essentially constant potential E_2, the current is sampled twice, at delay times δ_1 and δ_2. The second current sampling is subtracted from the first, and the difference is recorded. Although the faradaic response is reduced with respect to conventional n.p.p. and d.p.p., the signal-to-noise ratio is improved greatly, resulting in a lower limit of detection. (The term "noise" is used for the remaining capacitance current, i_c, which can be measured by recording a polarogram without any electroactive substance in the solution.)

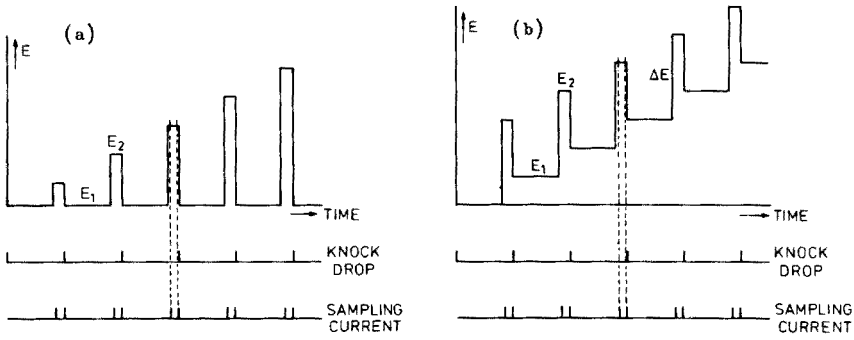

Fig. 1. High-performance normal (a) and differential (b) pulse polarography with the optimal waveforms with timing and sampling sequence.

For a totally reversible electrochemical reaction, h.p.n.p.p. gives the best sensitivity, but when sensitivity is considered together with wave resolution power, better performance will be achieved with h.p.d.p.p. [1]. Theoretically, in both modified methods, the influence of the capacitance current caused by drop growth on the results can be made exactly zero by multiplying the second current sampling, before subtracting it from the first one, by a factor containing only instrumentally determined parameters [1].

In the present paper, the proper choice of the delay times δ_1 and δ_2, which are the most important parameters in both h.p.n.p.p. and h.p.d.p.p., will be discussed in detail with respect to: (a) the capacitance current caused by drop growth; (b) the capacitance current caused by pulse application; (c) the faradaic current caused by pulse application; and (d) the faradaic d.c. current in the d.p.p. modes. The influence of practical sampling width on the results is evaluated, and the requirements for optimal performance in h.p.n.p.p. and h.p.d.p.p. are discussed.

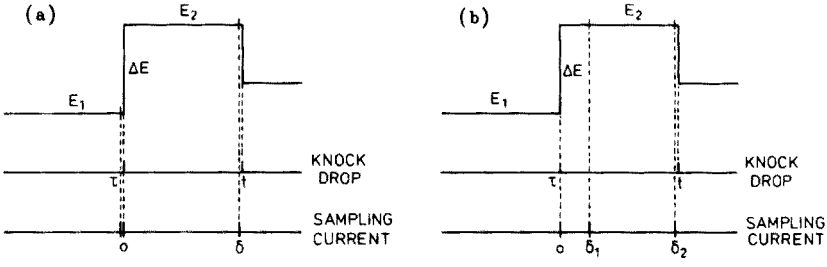

Fig. 2. Detailed timing and sampling sequence of conventional (a) and high-performance (b) d.p.p. for zero sampling width.

THE CAPACITANCE CURRENT CAUSED BY DROP GROWTH

Capacitance current caused by drop growth in d.p.p. and h.p.d.p.p.

In conventional d.p.p. (Fig. 2a), the capacitance current caused by drop growth, i_c, just before application of the modulation pulse can be described, if zero sampling width is assumed, by the d.c. polarographic capacitance current

$$i_{c,dc}(E_1, \tau) = -2/3\, km^{2/3}\, Q(E_1)\, \tau^{-1/3} \tag{1}$$

where $k = 0.008515\ m^2kg^{-2/3}$, m is the flow rate of mercury through the capillary in kg s^{-1} and $Q(E_1)$ is the charge density (in C m^{-2}) on the electrode surface at potential E_1. At τ second in drop lifetime, the potential is pulsed from E_1 to E_2, and thermodynamically the charge density is forced to change from $Q(E_1)$ to $Q(E_2)$, where $Q(E_2)$ is the charge density at potential E_2. After the time required to recharge the double layer, the capacitance current caused by drop growth during pulse application can be described by

$$i_{c,dc}(E_2, \tau + \delta) = -2/3\, km^{2/3}\, Q(E_2)\, (\tau + \delta)^{-1/3} \tag{2}$$

where δ is the delay time after pulse application.

The difference between eqns. (1) and (2) is the remaining capacitance current in conventional d.p.p., as was pointed out by Christie and Osteryoung [2]:

$$i_{c,dpp}(E, t) = -2/3\, km^{2/3} \left[\frac{Q(E_1)}{\tau^{1/3}} - \frac{Q(E_2)}{(\tau + \delta)^{1/3}} \right] \tag{3}$$

(Note that the second current sampling is subtracted from the first.)
In h.p.d.p.p. (Fig. 2b) the current is sampled twice, at δ_1 and δ_2 after pulse application. As these samplings are taken at essentially constant potential E_2, the remaining capacitance current can be written as

$$i_{c,hpdpp}(E_2, t) = -2/3\, km^{2/3}\, Q(E_2)\, [(\tau + \delta_1)^{-1/3} - (\tau + \delta_2)^{-1/3}] \tag{4}$$

The influence of this capacitance current on the results can be eliminated completely if the second current sampling is multiplied by the factor

$$[(\tau + \delta_2)/(\tau + \delta_1)]^{1/3} \tag{5}$$

which contains only instrumentally determined parameters, before it is subtracted from the first sampling [1]. For calculations, numerical information is required, and precise charge density data of a 0.1 M KCl solution [3] were used (Fig. 3). The theoretical backgrounds calculated for the d.p.p. modes are plotted in Fig. 4.

The capacitance current caused by drop growth in n.p.p. and h.p.n.p.p.

In n.p.p. at τ second in drop lifetime, the potential is pulsed from E_1 to E_2. In this method the current is measured only once, at the end of pulse application at essentially constant potential E_2 (Fig. 5a), and the capacitance current

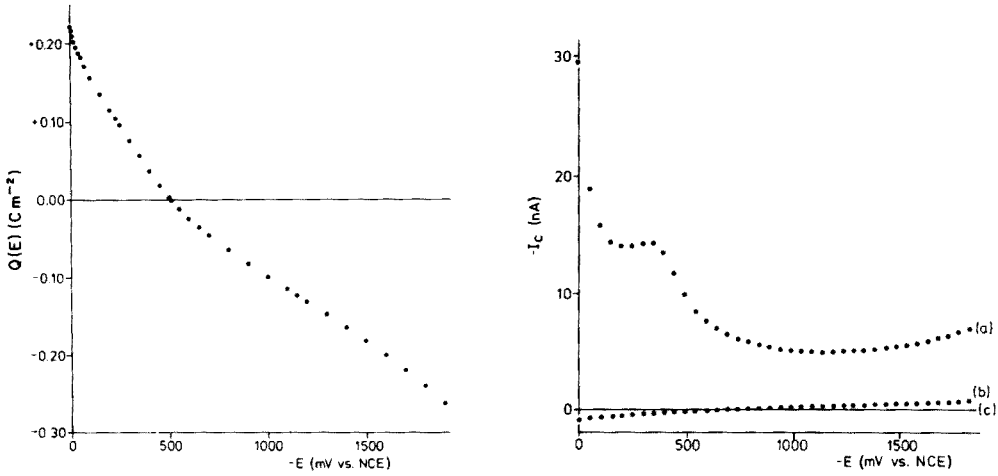

Fig. 3. Charge-density data for 0.1 M KCl [3].

Fig. 4. Theoretical d.p.p. polarograms of 0.1 M KCl. Modulation amplitude ΔE −50 mV (d.p.p. and h.p.d.p.p.); $m = 2 \times 10^{-6}$ kg s^{-1} (zero sampling width). (a) Conventional d.p.p., $\tau = 2.0000$ s and $\delta = 0.0400$ s (eqn. 3). (b) H.p.d.p.p., $\tau = 2.0000$ s and $\delta_1 = 0.0100$ s and $\delta_2 = 0.0400$ s (eqn. 4). (c) H.p.d.p.p. with multiplication of the second sampling by factor (5) before subtraction.

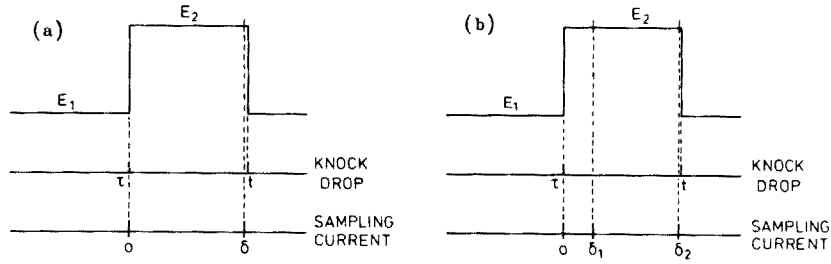

Fig. 5. Detailed timing and sampling sequence of conventional (a) and high-performance (b) n.p.p. for zero sampling width.

caused by drop growth, $i_{c,npp}$, can be described by an equation identical with eqn. (2).

In h.p.n.p.p., which involves taking two samplings during pulse application (Fig. 5b), the remaining capacitance current, $i_{c,hpnpp}$, can be described by an equation identical with eqn. (4). Accordingly, the influence of the remaining capacitance current on the results can be completely eliminated, as in the case of h.p.d.p.p., if the second current sampling is multiplied by factor (5) before the samplings are subtracted. For the n.p.p. modes, the theoretical backgrounds calculated for a 0.1 M KCl solution are plotted in Fig. 6.

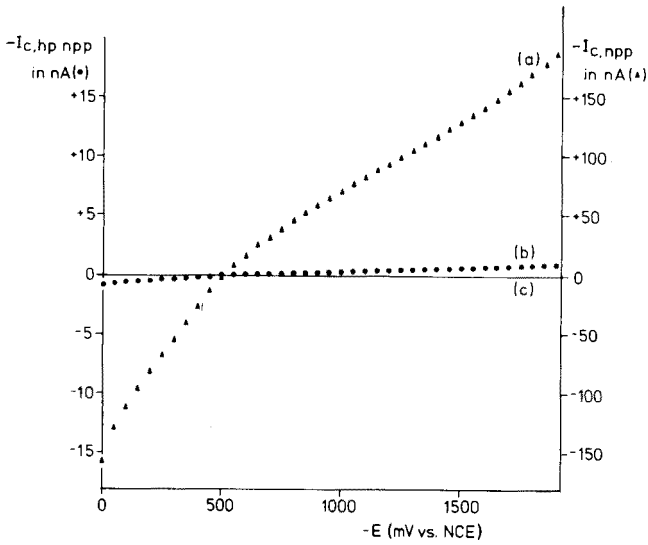

Fig. 6. Theoretical n.p.p. polarograms for 0.1 M KCl. E_1 = 0 mV vs. NCE; $m = 2.10^{-6}$ kg s^{-1} (zero sampling width). (a) Conventional n.p.p., τ = 2.0000 s and δ = 0.0400 s. (b) H.p.n.p.p., τ = 2.0000 s and δ_1 = 0.0100 s and δ_2 = 0.0400 s. (c) H.p.n.p.p. with multiplication of the second sampling by factor (5) before subtraction.

The influence of the sampling width on the measurements of the capacitance current caused by drop growth

As described above, the instantaneous values of the capacitance current caused by drop growth were calculated on the assumption of zero sampling width, although the sampling width obviously has a finite value. In polarographic instrumentation this sampling width must be 20 ms. The line frequency in European countries is 50 Hz, and any line frequency noise superimposed on a signal varying linearly with time will be cancelled because the integral over one sine wave of that frequency (or harmonic) will be exactly zero in the sampling time [4]. The influence of this 20-ms sampling width on the measurements of the capacitance current caused by drop growth is outlined below.

The capacitance current after pulse application in d.p.p. and n.p.p. can be described, according to eqn. (2), by

$$i_c\,(E_2, \tau + \delta) = -2/3\; km^{2/3}\, Q(E_2)\,(r + \delta)^{-1/3} \qquad (6)$$

when δ is made larger than the relaxation time of the cell—potentiostat system. In practical polarographic instrumentation, the current sampling is initiated at $(\tau + \delta)$ and stopped at $(\tau + \delta + \Delta)$ s in the drop lifetime, where Δ is the sampling width (Fig. 7). The mean value of the capacitance current, $\bar{i}_c$, during the sampling period can be calculated as

$$\bar{i}_c = (1/\Delta) \int_{\tau+\delta}^{\tau+\delta+\Delta} i_c \mathrm{d}\delta \qquad (7)$$

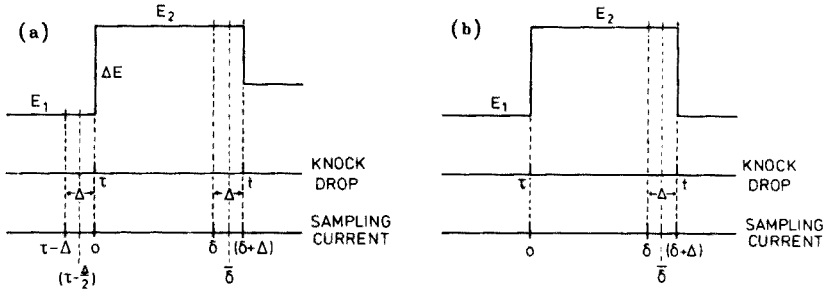

Fig. 7. Detailed timing and sampling sequence of conventional differential (a) and normal (b) pulse polarography for finite sampling width (20.0 ms).

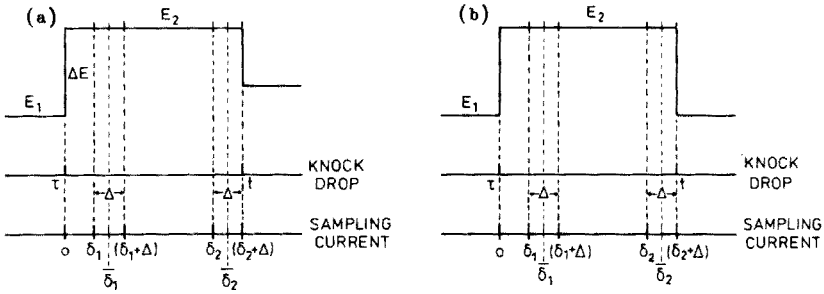

Fig. 8. Detailed timing and sampling sequence of high-performance differential (a) and normal (b) pulse polarography for finite sampling width (20.0 ms).

In h.p.d.p.p. and h.p.n.p.p. the first sampling is started at $(\tau + \delta_1)$ and finished at $(\tau + \delta_1 + \Delta)$ s, while the second sampling begins at $(\tau + \delta_2)$ and stops at $(\tau + \delta_2 + \Delta)$ s in the drop lifetime (Fig. 8).

Introduction of δ_1 in eqn. 6, substitution of eqn. (6) in eqn. (7) and subsequent integration, yields for the first current sampling

$$\bar{i}_c \text{ (1st sampling)} = -2/3\, km^{2/3}\, Q(E_2) \left[\frac{3}{2} \cdot \frac{1}{\Delta} \{(\tau + \delta_1 + \Delta)^{2/3} - (\tau + \delta_1)^{2/3}\}\right] \tag{8}$$

and for the second sampling $(\delta \rightarrow \delta_2)$

$$\bar{i}_c \text{ (2nd sampling)} = -2/3\, km^{2/3}\, Q(E_2) \left[\frac{3}{2} \cdot \frac{1}{\Delta} \{(\tau + \delta_2 + \Delta)^{2/3} - (\tau + \delta_2)^{2/3}\}\right] \tag{9}$$

The instantaneous capacitance currents caused by drop growth were calculated for three typical values of τ: $\tau_1 = 0.5000$, $\tau_2 = 1.0000$, $\tau_3 = 2.0000$ s for delay times from 0.0 to 60.0 ms. For reasons of simplicity, only the relevant time-dependent part of eqn. (6), $(\tau + \delta)^{-1/3}$, was computed. The results are plotted in Fig. 9.

As an example, the following conditions were adopted in both high-performance techniques: the first sampling was started at $(\tau + 0.0100)$ s and stopped at $(\tau + 0.0300)$ s, so that the sampling width was 20.0 ms. The

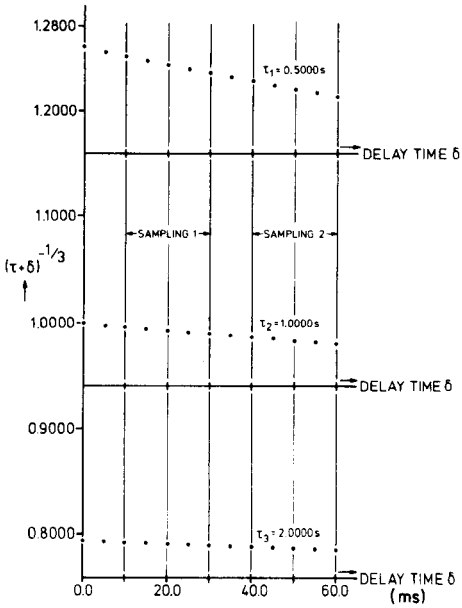

Fig. 9. Time-dependent part of eqn. (6) of the capacitance current caused by drop growth for typical τ-times, and the position of both current samplings for Δ = 20.0 ms (see text).

TABLE 1

Mean and instantaneous capacitance "currents" caused by drop growth in h.p.d.p.p. and h.p.n.p.p.

	δ (s)	i_c	τ = 0.5000 s	τ = 1.0000 s	τ = 2.0000 s
A	δ_1 = 0.0100 $\delta_1 + \Delta$ = 0.0300	$\bar{i}_c$ (1st sampling)	1.243590657	0.9934279350	0.7910737951
	δ_2 = 0.0400 $\delta_2 + \Delta$ = 0.0600	$\bar{i}_c$ (2nd sampling)	1.220552338	0.9838747581	0.7871958783
		$\Delta \bar{i}_c$ (Δ = 20.0 ms)	0.023038319	0.0095531769	0.0038779168
B	$\bar{\delta}_1$ = 0.0200 $\bar{\delta}_2$ = 0.0500	i_c ($\bar{\delta}_1$) i_c ($\bar{\delta}_2$) Δi_c (instantaneous)	1.243556587 1.220522444 0.023034143	0.9934208622 0.9838681468 0.0095527154	0.7910723593 0.7871944914 0.0038778679
C		Multiplication factor (A)	1.018875322	1.009709749	1.004926241
D		Multiplication factor (B)	1.018872363	1.009709345	1.004926188

second sampling was started at (τ + 0.0400) s and stopped at (τ + 0.0600) s in the drop lifetime (Fig. 9). The mean values of the capacitance current during the sampling period (the terms between brackets in eqns. 8 and 9) were calculated as well as the differences (Table 1A). These results are

compared with the instantaneous values in the middle of the sampling period, at $\bar{\delta}_1 = 0.0200$ s and at $\bar{\delta}_2 = 0.0500$ s after pulse application (Table 1 B).

It can be concluded that the mean value of the capacitance current for the required 20-ms sampling width is very nearly the same as the instantaneous value in the middle of the sampling (for all typical values of τ). This is also valid for the differences. Therefore the capacitance current caused by drop growth can be considered as a signal varying linearly with time. Thus, when a sampling width of 20 ms is used, the influence of line frequency noise will be cancelled completely, if there is no faradaic reaction.

To eliminate completely the influence of the capacitance current on the results (for instantaneous current values), the second sampling must be multiplied by factor (5). For the 20-ms sampling width, this factor must be rewritten:

$$[(\tau + \delta_1 + \Delta)^{2/3} - (\tau + \delta_1)^{2/3}]/[(\tau + \delta_2 + \Delta)^{2/3} - (\tau + \delta_2)^{2/3}] \qquad (10)$$

which is the quotient of eqns. (8) and (9). The results are given in Table 1C. Because the mean value can be approximated very well by the instantaneous value in the middle of the sampling period, factor (10) can be rewritten to $[(\tau + \delta_1 + \Delta/2)/(\tau + \delta_2 + \Delta/2)]^{-1/3}$. Introduction of $\delta_2 + \Delta/2 = \bar{\delta}_2$ and $\delta_1 + \Delta/2 = \bar{\delta}_1$ yields the multiplication factor $[(\tau + \bar{\delta}_1)/(\tau + \bar{\delta}_2)]^{1/3}$, where $\bar{\delta}_1$ and $\bar{\delta}_2$ are the delay times after pulse application in the middle of the sampling period, i.e. the mean delay times (Table 1D). It can be concluded from the results of Table 1 (C and D) that the multiplication factor, based on a sampling width of 20 ms, can be approximated very well by introduction of the mean delay times in the factor resulting from the zero sampling width case (for all typical values of τ).

In theory and in practice, the capacitance current caused by drop growth can be eliminated completely in both high-performance pulse polarographic techniques by multiplying the second current sampling by an instrumentally determined factor before the subtraction. The results and conclusions concerning the sampling width can be extended easily to conventional d.p.p. and n.p.p.

Conclusions

For practical polarographic instrumentation, the multiplication factor can be calculated exactly from the quotient of eqns. (8) and (9), resulting in the factor (10). However, a very good approximation of the theoretical multiplication factor can be achieved when the mean delay times after pulse application $\bar{\delta}_1$ and $\bar{\delta}_2$ are introduced. To achieve complete elimination of the effect of capacitance current on the results, an electronic circuit producing a multiplication factor depending on τ-time and delay times should be added to the polarograph. In order to cover the whole range of possibilities, the multiplication should be variable between 1.0 and 1.1.

THE CAPACITANCE CURRENT CAUSED BY PULSE APPLICATION

Considerations for a proper choice of δ_1 in h.p.d.p.p. and h.p.n.p.p. with respect to the capacitance current caused by pulse application

In view of the faradaic current caused by pulse application (see below), it is desirable to position the first current sampling as soon as possible in the pulse, i.e. directly after the relaxation time of the cell—potentiostat system. This relaxation time can be determined experimentally or calculated from charge-density data. Once the relaxation times are known, the position of the first current sampling can be optimized for the whole polarographic run. The given considerations will be valid for d.p.p. as well as n.p.p. wave-forms and are independent of the sampling process or sequence.

At the moment of pulse application in the d.p.p. and n.p.p. modes (at τ second in drop lifetime), the area A of the mercury drop is given by $A = km^{2/3}\tau^{2/3}$. The charge Q_1 (in coulomb) at the mercury—electrolyte interface at that moment can be calculated as $Q_1 = Q(E_1)\, km^{2/3}\tau^{2/3}$. Because of the thermodynamically required change in charge density from $Q(E_1)$ to $Q(E_2)$, assuming that the potential is pulsed from E_1 to E_2 instantaneously, the charge of the interface must become $Q_2 = Q(E_2)\, km^{2/3}\tau^{2/3}$. The excess charge ($Q_{excess}$), i.e. the difference between Q_1 and Q_2, is

$$Q_{excess} = km^{2/3}\tau^{2/3}\,[Q(E_1) - Q(E_2)] \tag{11}$$

While being transported, this excess charge causes the capacitance current from the pulse application ($i_{c,pulse}$):

$$Q_{excess} = \int_0^\infty i_{c,pulse}\, d\delta \tag{12}$$

The drop area can be considered constant during the process, because recharging is very fast (typically some milliseconds). It is assumed that $i_{c,pulse}$ can be described by some logarithmically decaying relationship [5—8]:

$$i_{c,pulse} = [(E_1 - E_2)/R_\Omega]\, \exp\,[-\delta/R_\Omega CA] \tag{13}$$

where $(E_1 - E_2)$ is the applied pulse height, which is constant for each drop in the d.p.p. modes, i.e. the modulation amplitude ΔE, and different for each drop in the n.p.p. modes; R_Ω* is the "three-electrode" resistance of cell and potentiostat, which can be very small when positive feed-back is applied; δ is the delay time after pulse application; and C is the capacity of the double layer (in F m^{-2}). During the recharge, depending on the completeness of the process, C also varies, which means that exact solution of the integral of eqn. (12) will be difficult. However, if C is considered to be constant during the recharging process over the potential range $(E_1 - E_2)$, an equivalent double-layer capacity C_{eq} can be determined from charge-density data.

*When an electroactive substance is reduced or oxidized, there will be a contribution of the faradaic current i_f to R_Ω (Warburg impedance).

Introduction of eqn. (13) into eqn. (12) and subsequent integration results in $Q_{excess} = -(E_1 - E_2)\, C_{eq}\, km^{2/3}\tau^{2/3}$. Combination of this relationship with eqn. (11) gives the constant equivalent capacity of the double layer during recharging:

$$C_{eq} = [Q(E_1) - Q(E_2)]/[E_1 - E_2] = \Delta Q(E)/\Delta E = |\Delta Q(E)/\Delta E| \qquad (14)$$

As $R_\Omega C_{eq} A$ is the time constant of the system, this term must be positive in all cases, so that C_{eq} must be positive, and this is possible by assuming an absolute value of C_{eq}. Where the differences are small, e.g. if a small modulation amplitude is used in the d.p.p. modes, the equivalent capacity will become equal to the differential capacity $[dQ(E)/dE]$.

For calculations, the charge-density data for a 0.1 M KCl solution [3] were used and the equivalent capacity (eqn. 14) was introduced into eqn. (13). For 0.1 M KCl solution, the resistance R_Ω is about 170 Ω; typical R_Ω values are 60 Ω for 1.0 M KCl, 170 Ω for 0.1 M KCl, and 1190 Ω for 0.01 M KCl [9]. Assuming positive feed-back by which the effective resistance R_Ω is reduced to 100 Ω, for the d.p.p. as well as the n.p.p. modes as a function of potential, the times required for $i_{c,pulse}$ to decay to the 1-nA level were calculated (Fig. 10). To illustrate the influence of R_Ω on the results, the relaxation times for the KCl solution were also calculated for an imaginary R_Ω of 1000 Ω (Fig. 10). The calculated curves have the form of a distorted differential capacity. For comparison, the differential capacity curve for the 0.1 M KCl solution [3] is given in Fig. 11.

In the n.p.p. modes, the relaxation times decrease as $|E_1 - E_2|$ increases when an ideal potentiostat is used. This phenomenon can be explained by noting that the equivalent capacity of the KCl solution decreases as $|E_1 - E_2|$ increases. Thus the time constant of the system ($R_\Omega C_{eq} A$) will become

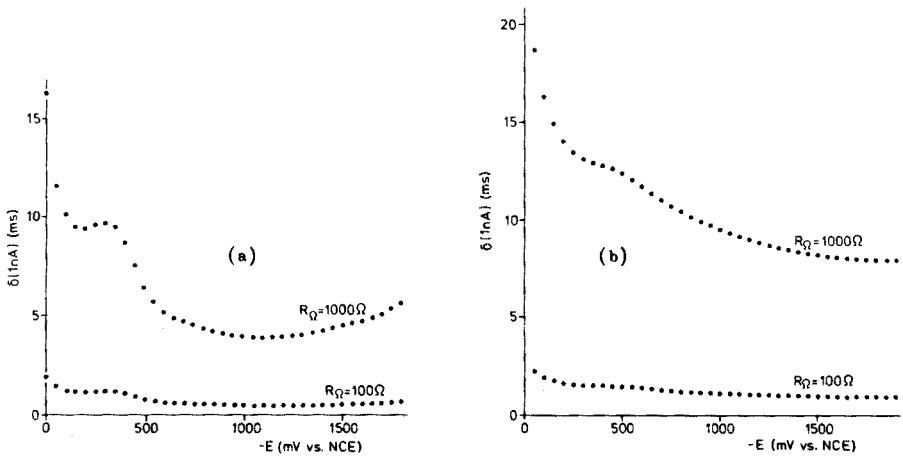

Fig. 10. The calculated relaxation times of a 0.1 M KCl solution from charge-density data [3] by applying the optimal waveforms of d.p.p. (a) and n.p.p. (b) for resistances of 100 Ω and 1000 Ω when $i_{c,pulse}$ = 1 nA (eqns. 13 and 14). The modulation amplitude ΔE = −100 mV (d.p.p. modes); E_1 = 0 mV vs. NCE (n.p.p. modes); $m = 2 \times 10^{-6}$ kg s^{-1}; τ = 2.0000 s.

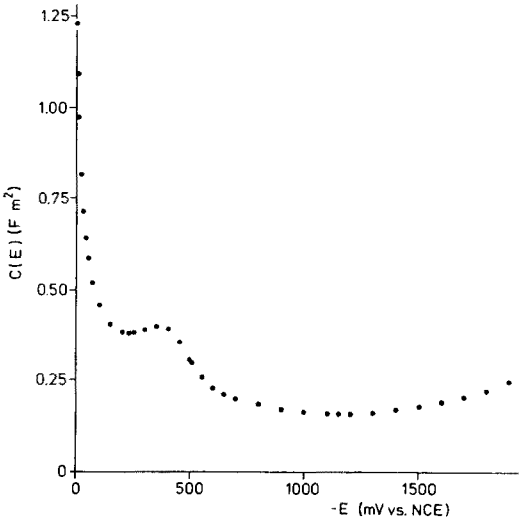

Fig. 11. Differential capacity data for 0.1 M KCl solution [3].

smaller and the decay will become faster. Moreover, if R_Ω is assumed constant, then at $\delta = 0$ s, $i_{c,pulse}$ increases linearly with $|E_1 - E_2|$, which gives rise to a faster cancellation of the charge deficiency. Thus, although Q_{excess} becomes larger as $|E_1 - E_2|$ increases, both the effects mentioned result in smaller relaxation times of the system. This conclusion is valid only when an ideal potentiostat is used and the approximations assumed are correct.

In practical polarographic instrumentation, there are only non-ideal potentiostats. The potentiostat cannot realize the required potential switch from E_1 to E_2 instantaneously because of the limited bandwidth. Moreover, the potentiostat may generate relatively high currents, e.g. the capacitance current caused by pulse application at $\delta = 0.0$ ms in the n.p.p. experiments can be as high as 19.0 mA, as $R_\Omega = 100\ \Omega$ and $|E_1 - E_2| = 1900$ mV. Therefore, because of the limited capability of the potentiostat, the relaxation time will be longer than the (approximate) calculated value.

When low concentrations have to be determined, the current amplifier should be very sensitive because very small current differences (in the nA range) must be recorded. Normally the current amplifier is saturated in the first stage of pulse application and this part of the instrument requires some recovery time to return to the linear dynamic range; thus the current amplifier can also contribute to a relaxation time larger than that calculated. Because of this recovery time, the position of the first current sampling can be delayed to some extent, especially if the first delay time should be very small. When digital equipment is used, the overload problem can be solved [10]; the current amplifier must have a wide linear dynamic range *and* a fast recovery time.

For a polarographic run, the first sampling must be positioned just after the time required for recharging the double layer, with the most unfavourable value in the potential range of interest (δ_1 s after pulse application). After that time, the contribution arising from pulse application can be considered as zero, and the capacitance current can be described completely in terms of drop growth (eqn. 6). Therefore, in the high-performance techniques, the influence of the capacitance current caused by drop growth on the results can be eliminated completely in all cases, regardless of the positions of δ_1 and δ_2.

Conclusions

If the best conditions in pulse polarography are used, it is possible to achieve almost complete elimination ($\leqslant$1 nA) of the capacitance current caused by pulse application within some milliseconds. However, in organic polarographic analysis, solvents involving much higher resistance and higher capacitance must often be used, with inherently longer relaxation times of the cell—potentiostat system. To achieve optimal sensitivity and complete elimination of the capacitance current caused by drop growth for those systems, the position of the first current sampling should be variable between 0 and 50 ms after pulse application.

To obtain smaller relaxation times of the cell—potentiostat system, the following features are required: (a) high-power potentiostat with an infinite band-width; (b) current amplifier with a very wide linear dynamic range and a fast recovery time; (c) small R_Ω values realized with a 3-electrode system, by applying positive feed-back and by using high concentrations of supporting electrolyte.

THE FARADAIC CURRENT CAUSED BY PULSE APPLICATION

The surface concentration of an electroactive substance at the electrode

An expression for the surface concentration $\bar{C}$ of the electroactive substance as a function of potential and bulk concentration is easily derived. The faradaic currents caused by pulse application in the d.p.p. and n.p.p. modes are then evaluated readily. From Faraday's law $dm/dt = i_f/nF$, and from Fick's first law $dm/dt = -DA(\partial C/\partial x)_{x=0}$, thus

$$i_f = -nFDA(\partial C/\partial x)_{x=0} \qquad (15)$$

where $(\partial C/\partial x)_{x=0}$ is the concentration gradient at the surface of the electrode and the other symbols have their usual meaning. If a totally reversible electrochemical reaction is assumed, with only the reduced form present in solution, and if the Nernstian model of linear diffusion to the electrode is accepted, ∂x can be replaced by d (the thickness of the diffusion layer*) and ∂C by

*In most electrochemical papers, symbol δ is used for the thickness of the diffusion layer; to avoid confusion, the symbol d is used here for the thickness of the diffusion layer. In this paper, δ is used for the delay time after pulse application.

$(\bar{C} - C)$, which is the difference between the concentration at the surface of the electrode $(\bar{C})$ and in the bulk solution (C). Thus eqn. (15) becomes

$$i_f = nFDA\ [(C - \bar{C})/d] \tag{16}$$

For a dropping mercury electrode (DME), i.e. an expanding spherical electrode, the thickness of the diffusion layer in d.c. polarography is $d_{dc} = [(3/7)\pi Dt]^{1/2}$, and $A = km^{2/3}t^{2/3}$, where t is the drop-time. Introduction of these terms into eqn. (16) gives for the d.c. faradaic current,

$$i_{f,dc}\,(E, t) = (7/3\pi)^{1/2}\, nFkm^{2/3}D^{1/2}t^{1/6}\,[C - \bar{C}] \tag{17}$$

which is equivalent to the Heyrovský—Ilkovič equation [1, 10]

$$i_{f,dc}\,(E, t) = (7/3\pi)^{1/2}\, nFkm^{2/3}D^{1/2}t^{1/6}C\left[\frac{1}{1 + \epsilon}\right] \tag{18}$$

where

$$\epsilon = \exp\,[(nF/RT)(E - E^{r}_{1/2})] \tag{19}$$

From eqns. (17) and (18), the surface concentration $\bar{C}$ as a function of potential and bulk concentration C can be expressed as $\bar{C} = C\,(\epsilon/1 + \epsilon)$. Figure 12 shows $(1/1 + \epsilon)$ and $(\epsilon/1 + \epsilon)$ plotted as a function of potential. Three different regions can be distinguished. In region (a), no faradaic reaction occurs, thus $\epsilon \to \infty$ or $\bar{C} = C$ and $i_{f,dc} = 0$. In region (c), the d.c. faradaic current has a maximum value, thus $\epsilon = 0$ or $\bar{C} = 0$ and $i_{f,dc} = i_{f,lim}$, i.e. all electroactive species arriving at the electrode surface react immediately. The faradaic current is determined completely by the slope of the concentration gradient in the diffusion layer; in this case, the gradient has maximum slope, and so this gives the limiting faradaic current $i_{f,lim}$. In region (b) i_f increases so that $0 < i_f < i_{f,lim}$ and therefore $0 < \epsilon < \infty$ or $0 < \bar{C} < C$. In this part of the polarogram, there is an actual surface concentration, because not all of the species arriving at the surface react immediately. The concentration gradient in the diffusion layer is between the value of case (c) and zero. This is the region of interest in the d.p.p. modes.

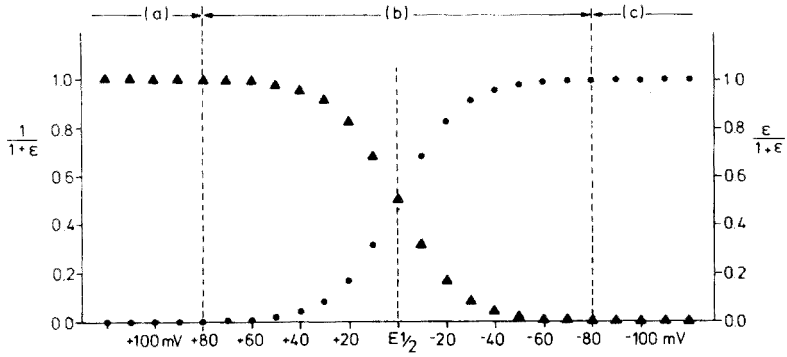

Fig. 12. Plots of $(1/1 + \epsilon)$ (•) and $(\epsilon/1 + \epsilon)$ (▲) as a function of potential for a totally reversible electrochemical reaction.

The faradaic current caused by pulse application in d.p.p.

In conventional d.p.p. at τ s in the drop lifetime, the potential is instantaneously pulsed from E_1 to E_2. The potential E_1 is so chosen that a d.c. faradaic reaction occurs, resulting in $i_{f,dc}(E_1, \tau)$. The surface concentration at potential E_1 ($\overline{C_{E_1}}$) will be (Fig. 13):

$$\overline{C_{E_1}} = C\,\epsilon_1/(1 + \epsilon_1) \tag{20}$$

where $\epsilon_1 = \exp[(nF/RT)(E_1 - E^r_{1/2})]$. Because of the pulse application (to potential E_2), the surface concentration is changed to $\overline{C_{E_2}} = C\,\epsilon_2/(1 + \epsilon_2)$, where ϵ_2 is defined analogously to ϵ_1. A new diffusion layer is thus formed, i.e. the diffusion layer caused by pulse application: d_{pulse} (Fig. 13). If a stationary spherical electrode is assumed (the duration of pulse application is relatively short), then $d_{pulse} = (\pi D\delta)^{1/2}$ *. Introduction of this relationship into eqn. (16), with substitution of $\overline{C_{E_1}}$ for C and $\overline{C_{E_2}}$ for $\bar{C}$, and expansion of A by $A = km^{2/3}(\tau + \delta)^{2/3}$ gives

$$i_{f,dpp}(E, t) = \frac{nFkm^{2/3}D^{1/2}}{\pi^{1/2}}\left[\overline{C_{E_1}} - \overline{C_{E_2}}\right]\frac{(\tau + \delta)^{2/3}}{\delta^{1/2}} \tag{21}$$

Introduction of the above terms for $\overline{C_{E_1}}$ and $\overline{C_{E_2}}$ gives

$$i_{f,dpp}(E, t) = \frac{nFkm^{2/3}D^{1/2}C}{\pi^{1/2}}\left[\frac{\epsilon_1}{1 + \epsilon_1} - \frac{\epsilon_2}{1 + \epsilon_2}\right]\frac{(\tau + \delta)^{2/3}}{\delta^{1/2}} \tag{22}$$

or

$$i_{f,dpp}(E, t) = \frac{nFkm^{2/3}D^{1/2}C}{\pi^{1/2}}\left[\frac{1}{1 + \epsilon_2} - \frac{1}{1 + \epsilon_1}\right]\frac{(\tau + \delta)^{2/3}}{\delta^{1/2}} \tag{23}$$

which result in a "first-derivative" curve.

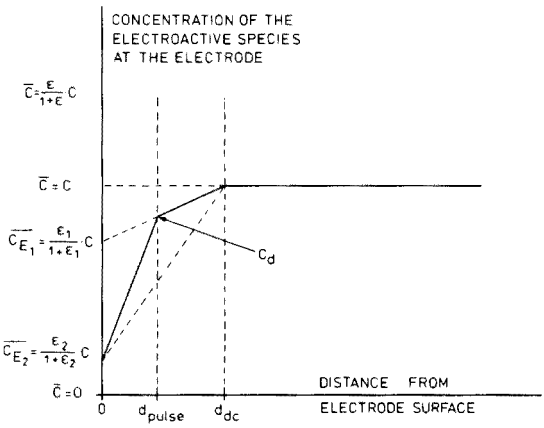

Fig. 13. Concentration profile of a reversible electroactive substance, assuming linear diffusion (Nernst) to the electrode in the d.p.p. modes. For explanation and calculation of C_d, see the section on The Faradaic Direct Current.

*$d_{pulse} = r_0(\pi D\delta)^{1/2}/[r_0 + (\pi D\delta)^{1/2}]$; for typical cases where $r_0 \gg (\pi D\delta)^{1/2}$, $d_{pulse} \to (\pi D\delta)^{1/2}$.

At τ s ($\delta = 0$), d_{pulse} is zero, and therefore the concentration gradient is infinitely great. The faradaic current caused by pulse application in d.p.p. is also infinitely great. Because of this current, the diffusion layer caused by pulse application extends into the solution, resulting in a smaller (pulse) concentration gradient and therefore in a smaller $i_{f,\text{dpp}}$; the slope in d_{dc} is assumed to be unaltered (Fig. 13).

In eqn. (23), the term in brackets has a maximum value which is dependent on potential E_1 and ΔE, because the maximum faradaic current caused by pulse application can be described [6] by

$$(i_{f,\text{dpp}})_{\max} = \frac{nFkm^{2/3}D^{1/2}C}{\pi^{1/2}} \left[\frac{\sigma - 1}{\sigma + 1}\right] \frac{(\tau + \delta)^{2/3}}{\delta^{1/2}} \tag{24}$$

where

$$\sigma = \exp\left[\frac{nF}{RT} \cdot \frac{(E_1 - E_2)}{2}\right] = \exp\left[\frac{nF}{RT} \cdot \frac{\Delta E}{2}\right]$$

When relatively large values of ΔE (>100 mV) are used, the diminution factor $(\sigma - 1)/(\sigma + 1)$ will be approximately one. In cases of small modulation amplitudes, i.e. small σ values, the value of $(i_{f,\text{dpp}})_{\max}$ and therefore the sensitivity of d.p.p. are reduced. The faradaic d.c. current is ignored, as is normal practice in conventional d.p.p.

The faradaic current caused by pulse application in n.p.p.

In conventional n.p.p., the potential is pulsed instantaneously from E_1 to E_2 at τ s in the drop lifetime. During the polarographic run, E_1 is kept constant and is usually selected so that no faradaic reaction occurs, i.e. before pulse application $C_{E_1} = C$ and $\epsilon \to \infty$ and therefore $i_f = 0$. The relationships $d_{\text{pulse}} = (\pi D\delta)^{1/2}$, which is the same for n.p.p. and d.p.p., and $A = km^{2/3}(\tau + \delta)^{2/3}$ can be introduced into eqn. (16), along with the expression $\overline{C_{E_2}} = C\,\epsilon_2/(1 + \epsilon_2)$, which describes the surface concentration after pulse application on the assumption of a faradaic reaction at potential E_2. This gives $i_{f,\text{npp}}$ as a function of potential and drop time:

$$i_{f,\text{npp}}(E_2, t) = \frac{nFkm^{2/3}D^{1/2}C}{\pi^{1/2}} \left[1 - \frac{\epsilon_2}{1 + \epsilon_2}\right] \frac{(\tau + \delta)^{2/3}}{\delta^{1/2}} \tag{25}$$

or

$$i_{f,\text{npp}}(E_2, t) = \frac{nFkm^{2/3}D^{1/2}C}{\pi^{1/2}} \left[\frac{1}{1 + \epsilon_2}\right] \frac{(\tau + \delta)^{2/3}}{\delta^{1/2}} \tag{26}$$

resulting in a sigmoidal curve. This current has its maximum value for $\epsilon_2 = 0$, i.e. the limiting faradaic current in n.p.p.; thus

$$(i_{f,\text{npp}})_{\max} = \frac{nFkm^{2/3}D^{1/2}C}{\pi^{1/2}} \frac{(\tau + \delta)^{2/3}}{\delta^{1/2}} \tag{27}$$

In the limiting case (ΔE is large, thus $\sigma \gg 1$), $(i_{f,\text{dpp}})_{\max}$ will become equal to $(i_{f,\text{npp}})_{\max}$ (eqn. 27).

In eqns. (24) and (27) the time-dependent term, i.e. $(\tau + \delta)^{2/3}/\delta^{1/2}$, is identical, and this term must be considered further. If all other quantities remain constant, the term indicates the sensitivity of both d.p.p. and n.p.p. The values calculated for three typical values of τ (0.5000, 1.0000 and 2.0000 s) and delay times δ from 0.0 to 200.0 ms are plotted in Fig. 14. These calculations show that it is desirable to choose large drop times and small delay times. In order to obtain maximum sensitivity, the current should be measured as soon as the capacitance current caused by pulse application has decayed to an adequately low level ($\leqslant$1 nA), i.e after some milliseconds.

The faradaic currents caused by pulse application in h.p.d.p.p. and h.p.n.p.p.

In h.p.d.p.p. and h.p.n.p.p., the current is sampled twice after pulse application and the difference is recorded, and so eqn. (24) must be rewritten as

$$(i_{f,hpdpp})_{max} = \frac{nFkm^{2/3}D^{1/2}C}{\pi^{1/2}} \left[\frac{\sigma - 1}{\sigma + 1}\right] \left[\frac{(\tau + \delta_1)^{2/3}}{\delta_1^{1/2}} - \frac{(\tau + \delta_2)^{2/3}}{\delta_2^{1/2}}\right] \quad (28)$$

and eqn. (27) as

$$(i_{f,hpnpp})_{max} = \frac{nFkm^{2/3}D^{1/2}C}{\pi^{1/2}} \left[\frac{(\tau + \delta_1)^{2/3}}{\delta_1^{1/2}} - \frac{(\tau + \delta_2)^{2/3}}{\delta_2^{1/2}}\right] \quad (29)$$

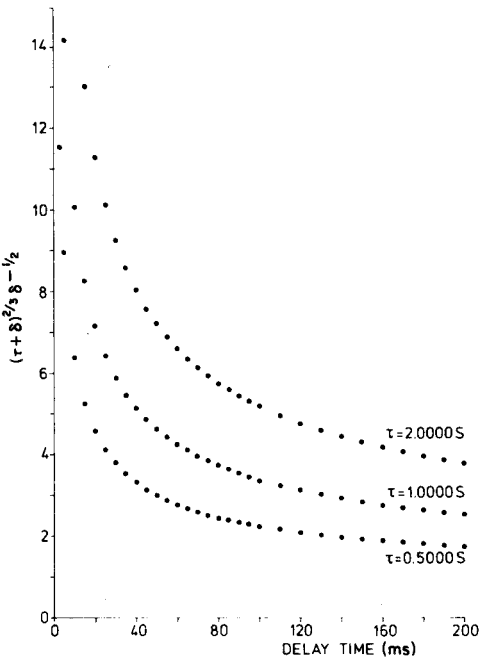

Fig. 14. The time-dependent term for typical τ- and δ-values in conventional d.p.p.

The time-dependent part of these relationships which indicates the sensitivity of the high-performance techniques, was calculated by applying for each of the three typical τ values, three typical values of δ_1 (5.0, 10.0 and 20.0 ms). The results are plotted in Fig. 15. From these calculations, it can be concluded that it is better to use small delay times δ_1 and large delay times δ_2; the drop time ($\tau + \delta$) s must be large.

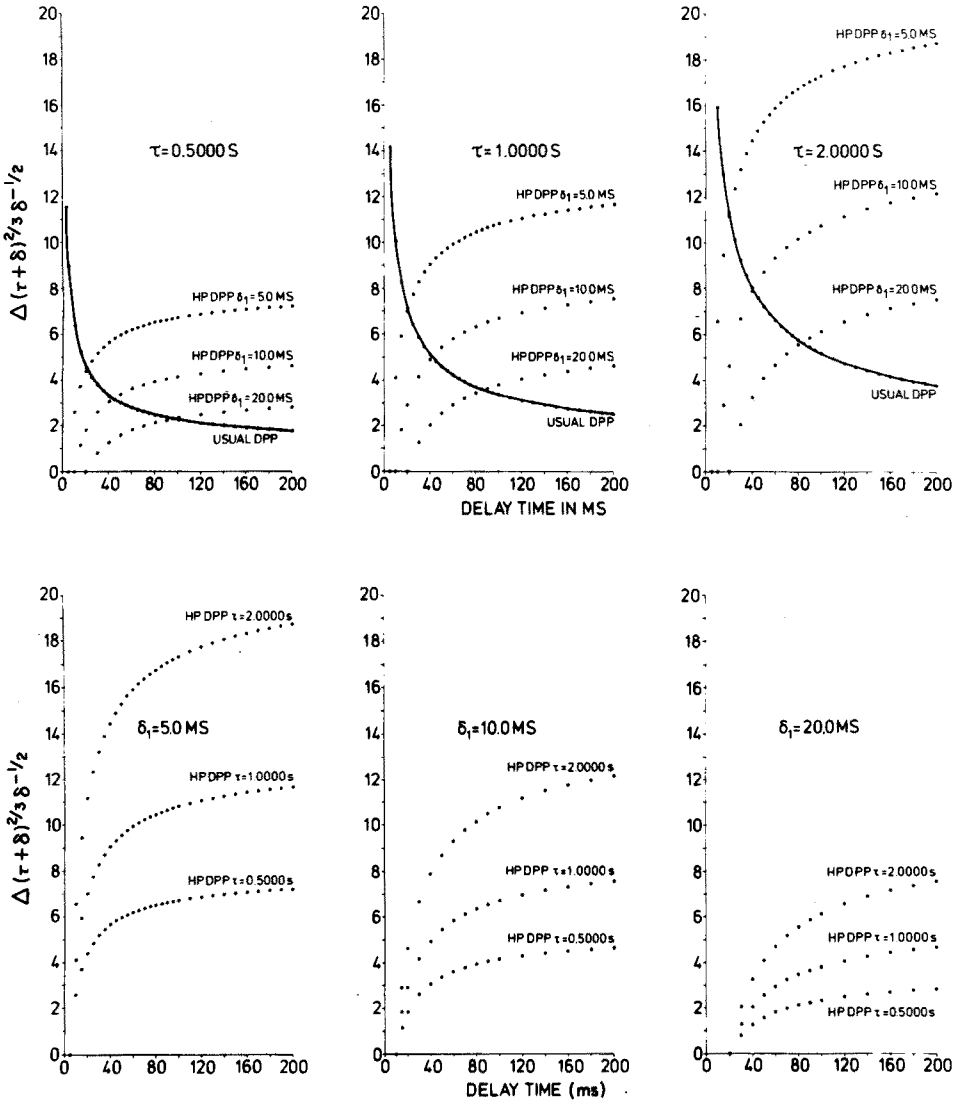

Fig. 15. The time-dependent term of eqns. (28) and (29) for typical τ- and δ-times.

The influence of the sampling width on the faradaic currents caused by pulse application

The sampling width must be 20 ms. However, to illustrate the influence of the sampling width on the sensitivity, the following conditions were adopted (as in the section on The capacitance Current Caused by Drop Growth); $\delta_1 = 10.0$ and $\delta_1 + \Delta = 30.0$ ms for the first sampling, and $\delta_2 = 40.0$ and $\delta_2 + \Delta = 60.0$ ms for the second one (Fig. 16). Mathematically, the mean value of the faradaic current during pulse application can be calculated as

$$\bar{i}_{f,pulse} = (1/\Delta) \int_{\tau+\delta}^{\tau+\delta+\Delta} i_f d\delta \tag{30}$$

The time-dependent part of the maximum values of $i_{f,dpp}$ and $i_{f,npp}$ has been calculated, so the integral

$$(1/\Delta) \int_{\tau+\delta}^{\tau+\delta+\Delta} [(\tau + \delta)^{2/3}/\delta^{1/2}] d\delta \tag{31}$$

can be determined.

The mean value of the first current sampling can be calculated by introducing δ_1 for δ and subsequent integration; the same procedure can be applied to the second sampling ($\delta \rightarrow \delta_2$). The values and the differences are given in Table 2 (A). The instantaneous values in the middle of the sampling period

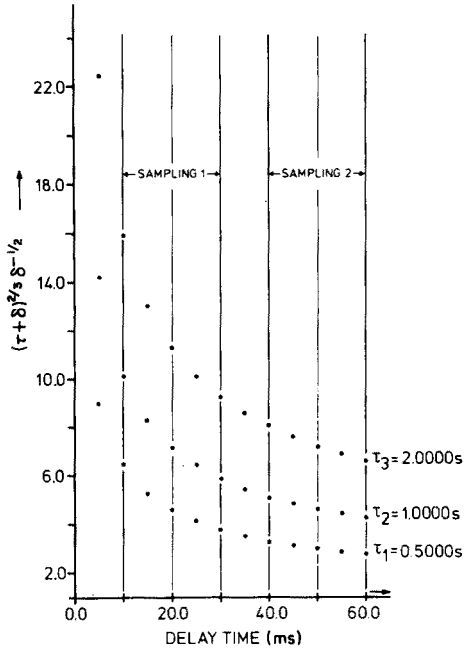

Fig. 16. The time-dependent term and the position of both current samplings for Δ = 20.0 ms (see text).

TABLE 2

Mean and instantaneous faradaic "currents" caused by pulse application in h.p.d.p.p. and h.p.n.p.p.

	δ (s)	$i_{f,pulse}$	τ = 0.5000 s	τ = 1.0000 s	τ = 2.0000 s
A	δ_1 = 0.0100 $\delta_1 + \Delta$ = 0.0300	$\Delta\bar{i}_{f,pulse}$ (1st sampling)	4.733019280	7.413434905	11.70328395
	δ_2 = 0.0400 $\delta_2 + \Delta$ = 0.0600	$\bar{i}_{f,pulse}$ (2nd sampling)	3.016098521	4.642497240	7.245819066
		$\bar{i}_{f,pulse}$ (Δ = 20.0 ms)	1.716920759	2.770937665	4.457464884
B	$\bar{\delta}_1$ = 0.0200	$i_{f,pulse}$ ($\bar{\delta}_1$)	4.572501935	7.165037208	11.29932712
	$\bar{\delta}_2$ = 0.0500	$i_{f,pulse}$ ($\bar{\delta}_2$)	3.002088269	4.619997200	7.216903616
		$\Delta i_{f,pulse}$ (instantaneous)	1.455376615	2.545040008	4.082423504
C	δ_1 = 0.0100	$i_{f,pulse}$ (δ_1)	6.383322464	10.06655605	15.92687989
	δ_2 = 0.0400	$i_{f,pulse}$ (δ_2)	3.315628349	5.132459888	8.042482341
		$\Delta i_{f,pulse}$ (instantaneous)	3.067694115	4.934096162	7.884397549
D		Multiplication factor[a]	1.018875322	1.009709749	1.004926241
E		$i_{f,pulse}$ (Δ = 20.0 ms and multiplication)	1.659990928	2.725860182	4.421770233

[a]Cf. Table 1, C.

are given in Table 2 (B). Since the values are not quite the same, it is not permissible to linearize, and so complete cancellation of the line frequency noise can never be achieved. The discrepancy is greater for the first current sampling than for the second, but is almost independent of the value of τ.

The moment of initiation of the first sampling is fixed previously. $I_{c,pulse}$ is assumed to be equal to, or smaller than, 1 nA at or before 10.0 ms. When an instrument is used with a sampling width of 20 ms, a dramatic reduction of $i_{f,pulse}$ is obtained compared to the instantaneous values of δ_1 = 0.0100 and δ_2 = 0.0400 s after pulse application (these delay times are also allowed for current sampling). The sensitivity is reduced to about 56% of the theoretically attainable value. Accordingly, it may be considered desirable to make the sampling width smaller. To avoid the problem of line frequency noise, another method of measuring is proposed.

If a sampling width of a few μs is used, the differences between the delay times must be a whole number of line cycles. Every sampling then contains some contribution from line frequency noise, but taking the difference cancels most of this contribution, and may cancel it completely in the case of a signal varying linearly with time. However, the faradaic current caused by pulse application cannot be considered to be linear during the sampling period (Table 2, A and B), and a small source of error will remain. (However, even in conventional d.p.p. and n.p.p. with 20-ms sampling widths, the line frequency noise can never be cancelled completely.) The decision between taking a sampling width of 20 ms or a much smaller width (to gain sensitivity)

depends on the type of analytical problem to be solved. In the following sections, a sampling width of 20 ms is used.

To eliminate completely the influence of the capacitance current caused by drop growth on the results, the second sampling must be multiplied by a factor containing only instrumentally determined parameters, before it is subtracted from the first sampling. This multiplication factor, calculated for the given conditions, is listed in Table 2 (D). The resulting sensitivity of the high-performance pulse polarographic techniques is given in Table 2 (E). It can be concluded that the reduction of faradaic sensitivity, caused by multiplication of the second current sampling before subtraction, is very small.

Conclusions

To gain faradaic sensitivity in both high-performance techniques, δ_1 should be made as small as possible, and δ_2 and τ as large as possible. To achieve better sensitivity, the sampling width can be made smaller than the desirable 20.0 ms; the difference between the first and the second current sampling must then be a whole number of line cycles.

THE FARADAIC DIRECT CURRENT IN D.P.P. AND H.P.D.P.P.

In conventional d.p.p., the output signal will contain some contribution of a faradaic current as a consequence of sampling at τ and $(\tau + \delta)$ s in the drop lifetime [2]. In h.p.d.p.p., therefore, there will be a similar contribution [1]. In both n.p.p. modes, potential E_1 is normally chosen so that there is no faradaic reaction before pulse application, hence the faradaic current phenomenon will be absent completely [2].

In conventional d.p.p., the faradaic current is sampled just before pulse application. For zero sampling width, $i_{f,dc}(E_1, \tau)$ can be described by

$$i_{f,dc}(E_1, \tau) = (7/3\pi)^{1/2} nFkm^{2/3}D^{1/2}C\,[1/(1 + \epsilon_1)]\tau^{1/6} \qquad (32)$$

After pulse application, the current is sampled again after a delay time δ. The faradaic current caused by pulse application is ignored for the moment. If $\overline{C_{E_1}}$ is assumed to be constant during pulse application, the faradaic current at $(\tau + \delta)$ s is given by

$$i_{f,dc}(E_2, \tau + \delta) = (7/3\pi)^{1/2} nFkm^{2/3}D^{1/2}C\,[1/(1 + \epsilon_1)](\tau + \delta)^{1/6} \qquad (33)$$

which seems to be the result of drop growth only. The difference between eqns. (32) and (33) is

$$(\Delta i_{f,dc})_{dpp} = (7/3\pi)^{1/2} nFkm^{2/3}D^{1/2}C\,[1/(1 + \epsilon_1)]\,[\tau^{1/6} - (\tau + \delta)^{1/6}] \qquad (34)$$

which is the contribution of the faradaic current to the output signal. As δ is typically rather small compared to τ, $(\Delta i_{f,dc})_{dpp}$ can be ignored, which is normal practice in conventional d.p.p.

In h.p.d.p.p. the contribution to the output signal of the difference in faradaic currents will become [1].

$$(\Delta i_{f,dc})_{hpdpp} = (7/3\pi)^{1/2}\, nFkm^{2/3}D^{1/2}C\, [1/(1+\epsilon_1)]\,[(\tau+\delta_1)^{1/6} - (\tau+\delta_2)^{1/6}] \tag{35}$$

For h.p.d.p.p., the difference between δ_1 and δ_2 must be large in order to increase faradaic sensitivity (see above). Moreover, to eliminate the capacitance current caused by drop growth, the second current sampling must be multiplied by the instrumentally determined factor, resulting in eqns. (34) and (35) of Part 1 [1]*. Both effects increase the difference obtained between the faradaic currents; thus the influence on the results cannot be ignored a priori and must be reconsidered. The use of relatively large delay times δ_2 has the implication that the "surface" concentration $\overline{C_{E_1}}$ cannot be considered constant, which was probably the assumption in the study of Christie and Osteryoung [2]. Accordingly, the remaining difference of the faradaic direct currents in both d.p.p. modes will be calculated more correctly, in order to evaluate the consequences for h.p.d.p.p. properly.

As was pointed out previously, the surface concentration of the electroactive species before pulse application can be described by $\overline{C_{E_1}} = C\,\epsilon_1/(1+\epsilon_1)$; during pulse application, the surface concentration will be $\overline{C_{E_2}} = C\,\epsilon_2/(1+\epsilon_2)$, and the diffusion layer caused by pulse application (d_{pulse}) is formed. A situation at $(\tau+\delta)$ s in drop lifetime will be considered for linear diffusion to the electrode (Fig. 13). To calculate the concentration gradient more correctly, the "surface" concentration $\overline{C_{E_1}}$ must be replaced by C_d, which is the concentration of the electroactive substance at the intersection of the d.c. and pulse diffusion layers. In the assumed model, C_d can be calculated as

$$C_d = C\left[\frac{\epsilon_1}{1+\epsilon_1} + \frac{d_{pulse}}{d_{dc}} \cdot \frac{1}{1+\epsilon_1}\right] \tag{36}$$

Introduction of the concentration gradient in the pulse diffusion layer (eqn. 16) gives the complete faradaic current after pulse application in the d.p.p. modes:

$$i_{f,dpp}\,(E_2, \tau+\delta) = \frac{nFkm^{2/3}(\tau+\delta)^{2/3}\,D\,C}{d_{pulse}}\left[\frac{\epsilon_1}{1+\epsilon_1} + \frac{d_{pulse}}{d_{dc}} \cdot \frac{1}{1+\epsilon_1} - \frac{\epsilon_2}{1+\epsilon_2}\right] \tag{37}$$

*From numerical calculations it can be concluded that, during the sampling period, the faradaic current can be considered as a signal varying linearly with time. For the required 20.0-ms sampling width, δ_1 and δ_2 in eqns. (34) and (35) of [1] should be replaced by $\bar{\delta}_1$ and $\bar{\delta}_2$, respectively.

or

$$i_{f,dpp}(E_2, \tau + \delta) = \frac{nFkm^{2/3}(\tau + \delta)^{2/3} D C}{d_{pulse}} \left[\frac{1}{1 + \epsilon_2} + \frac{d_{pulse}}{d_{dc}} \cdot \frac{1}{1 + \epsilon_1} - \frac{1}{1 + \epsilon_1}\right] \tag{38}$$

In h.p.d.p.p. this current is sampled at δ_1 and at δ_2 s after pulse application and the difference is recorded.

So far, d_{pulse} has been described simply by the relationship $d_{pulse} = (\pi D\delta)^{1/2}$. However, this relationship is not completely valid when large delay times are used (see p. 286). Brinkman and Los [11] and Fonds et al. [12] have formulated the condition for Cottrell behaviour of the DME with potential pulses. The expansion of the drop and its curvature can be neglected when $\delta/\tau < 0.01$. In the high-performance pulse polarographic techniques, the expression for d_{pulse} must therefore be modified: if a correction factor α (depending on δ and τ) is introduced, the expression for d_{pulse} can be written as

$$d_{pulse} = (\alpha\pi D\delta)^{1/2} \tag{39}$$

If $\delta/\tau < 0.01$, the correction factor will be $\alpha = 1$, i.e. Cottrell response. If δ is relatively large with respect to τ, d_{pulse} will approximate d_{dc}, thus $\delta \to (\tau + \delta)$ and $\alpha \to (3/7)$ (compare the conventional expression for the diffusion layer in d.c. polarography).

In h.p.d.p.p. the expressions for d_{pulse} for sampling 1 and sampling 2 can be written, respectively, as $d_{pulse}(\delta_1) = (\alpha_1\pi D\delta_1)^{1/2}$ and $d_{pulse}(\delta_2) = (\alpha_2\pi D\delta_2)^{1/2}$, where α_1 and α_2 are the correction factors at δ_1 and δ_2.

Introduction of these relationships into eqns. (37) and (38), and subtraction of the two current samplings, gives

$$\begin{aligned} i_{f,hpdpp}(E_2, t) = {} & \frac{nFkm^{2/3}D^{1/2}C}{\pi^{1/2}} \left[\frac{1}{1 + \epsilon_2} - \frac{1}{1 + \epsilon_1}\right] \left[\frac{(\tau + \delta_1)^{2/3}}{(\alpha_1\delta_1)^{1/2}} - \frac{(\tau + \delta_2)^{2/3}}{(\alpha_2\delta_2)^{1/2}}\right] \\ & + nFkm^{2/3}DC \left[\frac{1}{1 + \epsilon_1}\right] \left[\frac{(\tau + \delta_1)^{2/3}}{(\alpha_1\pi D\delta_1)^{1/2}} \cdot \frac{(\alpha_1\pi D\delta_1)^{1/2}}{[(3/7)\pi D(\tau + \delta_1)]^{1/2}}\right. \\ & \left. - \frac{(\tau + \delta_2)^{2/3}}{(\alpha_2\pi D\delta_2)^{1/2}} \cdot \frac{(\alpha_2\pi D\delta_2)^{1/2}}{[(3/7)\pi D(\tau + \delta_2)]^{1/2}}\right] \end{aligned} \tag{40}$$

or

$$\begin{aligned} i_{f,hpdpp}(E_2, t) = {} & \frac{nFkm^{2/3}D^{1/2}C}{\pi^{1/2}} \left[\frac{1}{1 + \epsilon_2} - \frac{1}{1 + \epsilon_1}\right] \left[\frac{(\tau + \delta_1)^{2/3}}{(\alpha_1\delta_1)^{1/2}} - \frac{(\tau + \delta_2)^{2/3}}{(\alpha_2\delta_2)^{1/2}}\right] \\ & + (7/3\pi)^{1/2} nFkm^{2/3}D^{1/2}C \left[\frac{1}{1 + \epsilon_1}\right] [(\tau + \delta_1)^{1/6} - (\tau + \delta_2)^{1/6}] \end{aligned} \tag{41}$$

It may be concluded that the main contribution to $i_{f,hpdpp}(E_2, t)$ results from "pure" faradaic currents caused by pulse application; only a minor part arises from the differences of the faradaic currents when no potential pulse is applied. Equation (41) can be written more concisely as

$$i_{f,hpdpp}(E_2, t) = i_{f,hpdpp}(\text{"pure pulse"}) + (\Delta i_{f,dc})_{hpdpp} \quad (42)$$

The contribution of the faradaic current to the output signal in the d.p.p. modes seems to be completely independent of d_{pulse} (without or with the correction factor α). For conventional d.p.p., this conclusion can be reached more directly from eqn. (37) or (38). The conclusions of Christie and Osteryoung [2] and Van Bennekom and Schute [1] concerning $(\Delta i_{f,dc})_{dpp}$ and $(\Delta i_{f,dc})_{hpdpp}$ still remain quite correct.

Because the faradaic current after pulse application can be considered as a signal which varies linearly with time during the required 20.0-ms sampling width, δ_1 and δ_2 can be replaced by the mean delay times $\bar{\delta}_1$ and $\bar{\delta}_2$. The last part of eqn. (41) can then be rewritten as

$$(\Delta i_{f,dc})_{hpdpp} = (7/3\pi)^{1/2} nFkm^{2/3}D^{1/2}C\,[1/(1+\epsilon_1)]\,[(\tau+\bar{\delta}_1)^{1/6} - (\tau+\bar{\delta}_2)^{1/6}] \quad (43)$$

In the "pure" faradaic current caused by pulse application with the 20.0-ms sampling width, $\bar{\delta}_1$ and $\bar{\delta}_2$ cannot be substituted for δ_1 and δ_2, because the signal cannot be considered as varying linearly with time. Moreover, α_1 and α_2 have to be replaced by

$$\bar{\alpha}_1 = (1/\Delta)\int_{\tau+\delta_1}^{\tau+\delta_1+\Delta} \alpha_1 d\delta \quad \text{and} \quad \bar{\alpha}_2 = (1/\Delta)\int_{\tau+\delta_2}^{\tau+\delta_2+\Delta} \alpha_2 d\delta$$

i.e. the mean correction factors for Cottrell description during the sampling period Δ, which cause deviations in the simplified theory.

From calculations, it may be concluded that when Δ = 20.0 ms, $\bar{\delta}_1$ = 20.0 ms and $\bar{\delta}_2$ = 200.0 ms and the second current sampling is multiplied by the required factor before subtraction, the influence of $(\Delta i_{f,dc})_{hpdpp}$ at E_{peak} can still be ignored. However, the contribution is larger than in conventional d.p.p. when $\bar{\delta}$ = 50.0 ms and Δ = 20.0 ms are used.

If zero sampling width zero is assumed and no multiplication is used, then $i_{f,hpnpp}$ can be written as

$$i_{f,hpnpp}(E_2, t) = \frac{nFkm^{2/3}D^{1/2}C}{\pi^{1/2}}\left[\frac{1}{1+\epsilon_2}\right]\left[\frac{(\tau+\delta_1)^{2/3}}{(\alpha_1\delta_1)^{1/2}} - \frac{(\tau+\delta_2)^{2/3}}{(\alpha_2\delta_2)^{1/2}}\right] \quad (44)$$

During a polarographic run α_1 and α_2 are constant, because τ, δ_1 and δ_2 are constant. Some deviation from the theoretical response will be obtained, but for practical polarography, the linear relationship between the recorded current and concentration C of the electroactive substance in the bulk solution will remain, which is the essential analytical condition.

REQUIREMENTS FOR OPTIMAL PERFORMANCE IN H.P.D.P.P. AND H.P.N.P.P. AND OVERALL CONCLUSIONS

The influence of the capacitance current caused by drop growth on the results can be eliminated completely in both h.p.d.p.p. and h.p.n.p.p., if the second current sampling is multiplied by an instrumentally determined factor, before the samplings are subtracted. The conclusion remains valid for the 20-ms sampling width because the capacitance current caused by drop growth can be considered as a signal varying linearly with time.

The d.p.p. modification described can become one of the most powerful analytical tools for both inorganic and organic systems with adequate sensitivity (sub-ppb determinations). The theoretical detection limit ($i_{f,hpdpp}$ = 1 nA) will be about 10^{-11} M for a reversible electrochemical reaction. It may be concluded from the theory developed that the limit of detection is fully determined by noise, i.e. electronic and capillary [13] noise. However, according to Sturrock and Carter [8] and Buchanan [14], capillary noise seems to be an artificial concept, probably caused by "classical electronic instrumentation". Recently, capillary response as a part of capillary noise has been discussed by Christie et al. [10, 15].

For high-performance polarography, as for alternate drop pulse polarography [10], noise remains the problem. Low-noise polarographic instrumentation has to be developed for sub-ppb determinations. The polarograph must be equipped with a (high) power potentiostat with an adequate bandwidth. The current amplifier must have a very large linear dynamic range and a fast recovery time. The first current sampling must be taken as soon as possible after pulse application, so that the relaxation time has to be small. This can be achieved by a three-electrode configuration, positive feed-back and high concentrations of supporting electrolyte. The second current sampling must be taken as late as possible, in order to gain faradaic sensitivity.

The faradaic current has been reconsidered and the conclusions reached previously are quite correct [1, 2]. Because of the use of relatively large delay times in both high-performance techniques, a (pragmatic) correction factor for Cottrell response is introduced. The influence of line frequency noise on $i_{f,pulse}$ can never be cancelled completely, even when a modified method of sampling is applied.

The author thanks Dr. H. J. de Jong and Drs. J. J. van der Lee for helpful advice and careful correction of the manuscript.

REFERENCES

1 W. P. van Bennekom and J. B. Schute, Anal. Chim. Acta, 89 (1977) 71.*
2 J. H. Christie and R. A. Osteryoung, J. Electroanal. Chem., 49 (1974) 301.
3 D. C. Grahame, J. Am. Chem. Soc., 71 (1949) 2975.
4 B. H. Vassos and R. A. Osteryoung, Chem. Instrum., 5 (1973–1974) 257.
5 H. Schmidt and M. von Stackelberg, J. Electroanal. Chem., 1 (1959/1960) 133.
6 E. P. Parry and R. A. Osteryoung, Anal. Chem., 37 (1965) 1634.
7 N. Klein and Ch. Yarnitzky, J. Electroanal. Chem., 61 (1975) 1.
8 P. E. Sturrock and R. J. Carter, CRC Crit. Rev. Anal. Chem., 5 (1975) 201.
9 C. P. M. Bongenaar and J. H. Sluyters, private communication.
10 J. H. Christie, L. L. Jackson and R. A. Osteryoung, Anal. Chem., 48 (1976) 242.
11 A. A. A. M. Brinkman and J. M. Los, J. Electroanal. Chem., 7 (1964) 171.
12 A. W. Fonds, A. A. A. M. Brinkman and J. M. Los, J. Electroanal. Chem., 14 (1967) 43.
13 G. C. Barker and A. W. Gardner, Fresenius Z. Anal. Chem., 173 (1960) 79.
14 E. B. Buchanan, Jr., private communication to [8].
15 J. H. Christie, L. L. Jackson and R. A. Osteryoung, Anal. Chem., 48 (1976) 561.

*Errata for ref. 1.
On p. 78, eqn. (31): for $\delta^{1/2}$, read $\delta_2{}^{1/2}$.
On p. 80, eqn. (41): for $\Delta(\Delta i_{f,npp})_{max}$, read $\Delta(\Delta i_{f,npp})$.

Analytica Chimica Acta, 101 (1978) 309—318

USE OF COMPUTERIZED INSTRUMENTATION FOR PSEUDO-DERIVATIVE DIRECT CURRENT AND NORMAL PULSE POLAROGRAPHY WITH CORRECTION FOR CHARGING CURRENT

A. M. BOND* and B. S. GRABARIC**

Department of Inorganic Chemistry, University of Melbourne, Parkville, Victoria, 3052 (Australia)

(Received 17th May 1978)

SUMMARY

The application of computerized instrumentation to pseudo-derivative d.c. and normal pulse polarography is described. Calculation of background current by means of a linear least-squares fit of data obtained prior to the rising part of the sigmoidal d.c. or pulse curve and extrapolation to other potentials enables close to the faradaic response to be obtained over wide concentration ranges. After subtraction of background current, least-squares fitting of the sigmoidal curve enables data smoothing to be undertaken and other calculations to be performed. Pseudo-derivative curves obtained by plotting current differences obtained from corrected and smoothed data provides limits of detection comparable to those of more sophisticated polarographic methods. The reduction of cadmium in 1 M NaCl is considered because it occurs at potentials near the electrocapillary maximum where charging current correction is most difficult. The limits of detection are 10^{-7} M for the pseudo-derivative d.c. method, and 10^{-8} M for the pulse method.

Conventional d.c. polarography suffers from several disadvantages compared with some of the more modern polarographic methods. For example, the sigmoidal curve obtained in the standard readout leads to poor resolution compared with the peaks associated with a.c. polarography and related techniques [1, 2]. Furthermore, d.c. polarography has a relatively unfavourable ratio of faradaic to charging current, which means that the sensitivity is less than for techniques which include methods of discriminating against the charging current. Normal pulse polarography, in which the potential is applied in a series of pulses of increasing amplitude rather than as the linear potential—time ramp used in d.c. polarography, has a considerably improved faradaic-to-charging current ratio and therefore a significantly lower limit of detection [2]. However, the disadvantages associated with a sigmoidal curve remain in normal pulse polarography and the charging current, even though reduced in magnitude, still provides the ultimate limitation to this technique.

**On leave from: Department of Inorganic Chemistry, Faculty of Technology, University of Zagreb, Zagreb, Yugoslavia.

In principle, taking the derivative of the sigmoidal d.c. or normal pulse polarograms should lead to substantially improved results, both in terms of resolution and minimization of the charging current problem [3]. However, the history of derivative d.c. polarography has been plagued by approaches that introduce undesirable instrumental artefacts and give non-theoretical responses [2].

The two successful approaches to recording derivative d.c. polarograms with analog circuitry have been based on taking the derivative after the data have been obtained in either the current-sampled [4—6] or time-averaged forms [4, 7]. In the current-sampled method, the difference in current obtained at the end of the mercury drop life between consecutive drops is plotted as a function of d.c. potential. This is therefore actually a difference or pseudo-derivative rather than true derivative method [3]. In the time-averaged method, efficient filtering of the signal fluctuations, time-averaging circuitry and time-derivative networks are used to obtain the derivative of average currents [7]. Both these methods virtually eliminate the oscillations resulting from the growth and fall of the mercury drop, and performance is extremely good, giving close to the theoretical response, high reproducibility and sensitivity significantly superior to d.c. polarography, [3, 7—9]. Thus, with advanced instrumentation and attention to experimental design, excellent derivative d.c. polarographic results can now be obtained and the technique challenges many of the more sophisticated methods of polarography [7—9].

The advent of the laboratory minicomputer has led to many significant innovations in electroanalytical chemistry [4, 10]. Because data can be stored in memory and subsequent mathematical operations readily performed with computerized instrumentation, filtering or smoothing techniques, charging current correction and a wide range of data manipulation procedures may be conveniently implemented very rapidly. Current-sampling procedures are an integral part of computerized instrumentation so that the pseudo-derivative d.c. and normal pulse techniques should be ideally suited to this kind of instrumentation. The present paper therefore describes the performance of these pseudo-derivative techniques when data treatment is performed on-line with a minicomputer. In particular, the possibility of applying extremely flexible and efficient approaches to charging current correction is examined as a means of providing performance which is substantially improved compared with results obtained solely by analog circuitry.

EXPERIMENTAL

All chemicals used were of analytical-grade purity. Solutions were thermostatted at (22 ± 1) °C and degassed with argon or nitrogen for a minimum of 15 min prior to recording a polarogram.

All polarograms were obtained by using a conventional three-electrode configuration. The reference electrode was Ag/AgCl (1 M NaCl) and the auxiliary electrode was platinum wire.

The electrochemical instrumentation consisted of a PAR Model 174 Polarographic Analyzer (Princeton Applied Research Corporation) interfaced to a PDP 11/10 minicomputer (Digital Equipment Corporation) used in conjunction with a CAPS-11 operating system. The computer was equipped with a DR-11 general-purpose interface which could be used to provide the logic and buffer register necessary for program-controlled parallel transfers of 16-bit data between the PDP-11 system and the polarographic analyzer. This interface also includes status and control bits that could be controlled by either the program or the external device for command, monitoring and interrupt functions. A TA-11 Cassette System Interface was used to load programs and for the input/output of data.

Sampling of the current output from the Analyzer was done with an AR-11 real-time analog subsystem which included a 16-channel, 10-bit A/D converter with sample and hold, a programmable real-time clock with one external input, and a display control with two 10-bit D/A converters. Sampled data as well as any transformed data were displayed on either a Tektronix D13 storage oscilloscope or on an X—Y recorder.

A program operating the Polarographic Analyzer, and acquiring, evaluating and displaying data was written in BASIC language with the system subroutines written in PAL 11 assembly language.

RESULTS AND DISCUSSION

The use of computerized instrumentation permits great flexibility in data treatment. Clearly, the initial feature that needs to be considered in developing data manipulation procedures for pseudo-derivative polarographic techniques is the nature of the d.c. and pulse polarogram themselves. A general equation for the description of polarographic waves is

$$E = E_{\frac{1}{2}} + K \ln (i_l - i)/i \qquad (1)$$

where i is the faradaic current, i_l the limiting faradaic current, E the potential, $E_{\frac{1}{2}}$ the half-wave potential when $i = i_l/2$, and K is a constant. This equation is normally applicable either rigorously or to an excellent approximation. Thus a least-squares fit to the observed polarogram based on the algorithm specified by eqn. (1) provides a convenient way of smoothing the data and statistically calculating i_l, $E_{\frac{1}{2}}$ and K for many electrode processes. In the present work an initial guess at $E_{\frac{1}{2}}$ is used and successive iterations are made until the variance is less than a predetermined level. A detailed description of a polarograph interfaced to a PDP-11 minicomputer for this kind of data manipulation has been presented by Bos [11] for conventional d.c. polarography and therefore needs no further discussion.

Equation (1) is valid only when purely faradaic currents are being measured. However, especially at low concentrations the background or charging current is significant. In analytical situations where the matrix is well defined, so that a blank is available, computerized instrumentation allows correction of charging

current simply by recording the blank, storing the result in memory and subsequently subtracting the background data from the sample curve. However, real samples frequently have unknown matrices and such a procedure is not possible. In this situation a mathematical approach can be used to correct for the background current. The charging current (i_c) in d.c. polarography is a non-linear function of potential. However, over a small potential range, except near the electrocapillary maximum or point of zero charge, the linear approximation is adequate [12].

At the foot of the i—E curve the faradaic current is essentially zero so that linear regression least-squares fit of the data points and extrapolation to cover the entire potential range of interest coupled with subtraction from the measured sigmoidal i—E curve is one simple approximate way of correcting for the background current. Such an approach also corrects for faradaic currents arising from electrode processes occurring at more positive potentials than the one under consideration. This method can readily be developed in an efficient manner with computerized instrumentation. The charging current in normal pulse polarography, whilst much smaller in magnitude, is still present [13] and can be treated in an analogous fashion.

Once the smoothed curve corrected for background current has been obtained, taking the difference between consecutive data points and producing a plot of Δi versus E is readily implemented under software control. Since ΔE is a constant, under the above conditions, a plot of Δi versus E is identical in shape to a $\Delta i/\Delta E$ versus E plot, and the simplified version of a pseudo-derivative plot can be used. In the present work, software sub-routines were developed for peak height and peak potential location including interpolation to obtain higher resolution than that indicated by ΔE. This is a parabolic least-squares fit of the data points near the peak. Sub-routines for eliminating bad drops and handling situations where values of ΔE or Δi may be numerically equivalent within the resolution of the A/D and D/A conversions and other cosmetic procedures have also been developed. Thus the final readout format routinely consists of smoothed and corrected curves displayed on an oscilloscope and on an X—Y recorder plus digital printout of $E_{\frac{1}{2}}$, i_1, and K for the sigmoidal d.c. and pulse curves and peak height and peak position of the pseudo-derivative plots. Further details of computer programs and instrumentation are available on request to the authors.

The fidelity of the procedure described above was tested on several systems, but to demonstrate most of the limitations and attractive features, the reduction of cadmium(II) in 1 M NaCl is considered in detail. This well-known electrode process is a reversible 2e amalgam-forming system: the $E_{\frac{1}{2}}$ value of around —0.64 V vs. Ag/AgCl is very close to the electrocapillary maximum or point of zero charge and therefore the assumption of a linear charging current correction is a "worst possible case" situation. Consequently, limitations in data treatment are clearly revealed in considering this example.

Figure 1 shows d.c. data obtained at a drop time of 0.5 s for reduction of 10^{-4} M cadmium(II) in 1 M NaCl. Curve (a) shows the raw data; at the

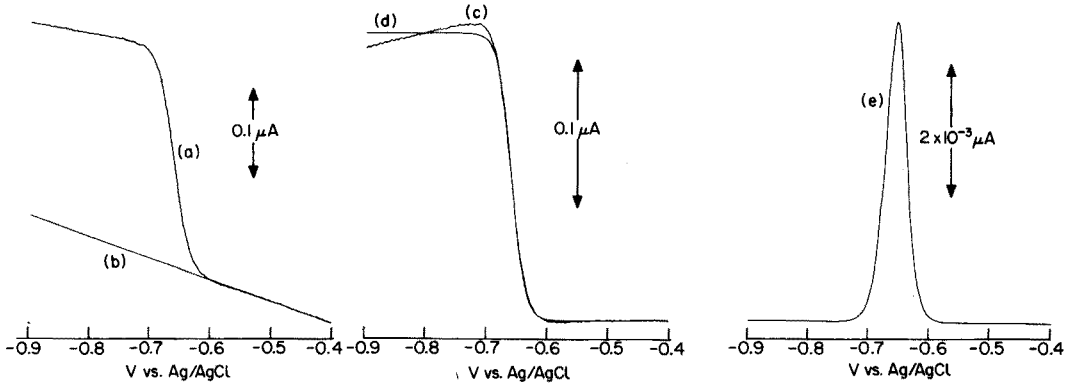

Fig. 1. Pseudo-derivative d.c. polarograms of 10^{-4} M cadmium(II) in 1 M NaCl, with 0.5-s drop time and 2 mV s^{-1} scan rate. (a) D.c. polarogram including background current; (b) linear extrapolation of background current; (c) d.c. polarogram after subtraction of background current; (d) smoothed d.c. polarogram; (e) pseudo-derivative d.c. polarogram.

relatively short drop time employed, the charging current is significant even with cadmium at the 10^{-4} M level so that the foot (least negative potential) and limiting current (most negative potential) regions of the curve are not parallel. Curve (b) shows the linear least-squares fit and extrapolation of the presumed background current data obtained from the foot of the wave. Clearly, the extrapolated straight line is not parallel to the limiting current region. This signifies that the linear approximation is not valid over the extended potential range. On subtraction of the extrapolated data, the resultant negative slope on the limiting current region of the corrected curve (curve c) reflects the breakdown of the linear assumption. With least-squares fitting and smoothing, the curve obtained is forced to have an exactly sigmoidal shape as defined by eqn. (1). Despite some discrepancies in the limiting current region of curves (c) and (d) the reproduction of the smoothing up to 90% of the wave height is accurate within the limit of experimental error. Consequently, despite the distortion in the limiting current region in the d.c. polarogram, the Δi vs. E data obtained in curve (e) are not significantly distorted at the peak position (ca. $E_{\frac{1}{2}}$) and the correct peak height is obtained at the 10^{-4} M concentration level. This was proved by comparing data obtained on a blank solution of 1 M NaCl and subtracting it from the raw data. Peak heights from the two methods agreed to better than 1% and peak positions to better than 1 mV. This result signifies that the linear extrapolation from the foot of the wave to $E_{\frac{1}{2}}$ is an excellent representation of the background current, and that the requirement of a much narrower extrapolation range than is needed in d.c. polarography means that background current correction is intrinsically more accurate than for d.c. polarography.

At the 10^{-4} M level with a drop time of 0.5 s, the reproducibility of peak positions of pseudo-derivative plots was ±0.3 mV and peak heights ±0.7% so that data of highly acceptable quality for analytical work are obtained.

At very low concentration levels in the 10^{-5}—10^{-6} M range where the magnitude of the charging current approaches that of the faradaic current with a drop time of 0.5 s under d.c. polarographic conditions, then the obvious tactic to improve the situation without resorting to the pulse method is to use longer drop times. Figure 2 shows a series of curves at the 10^{-6} M

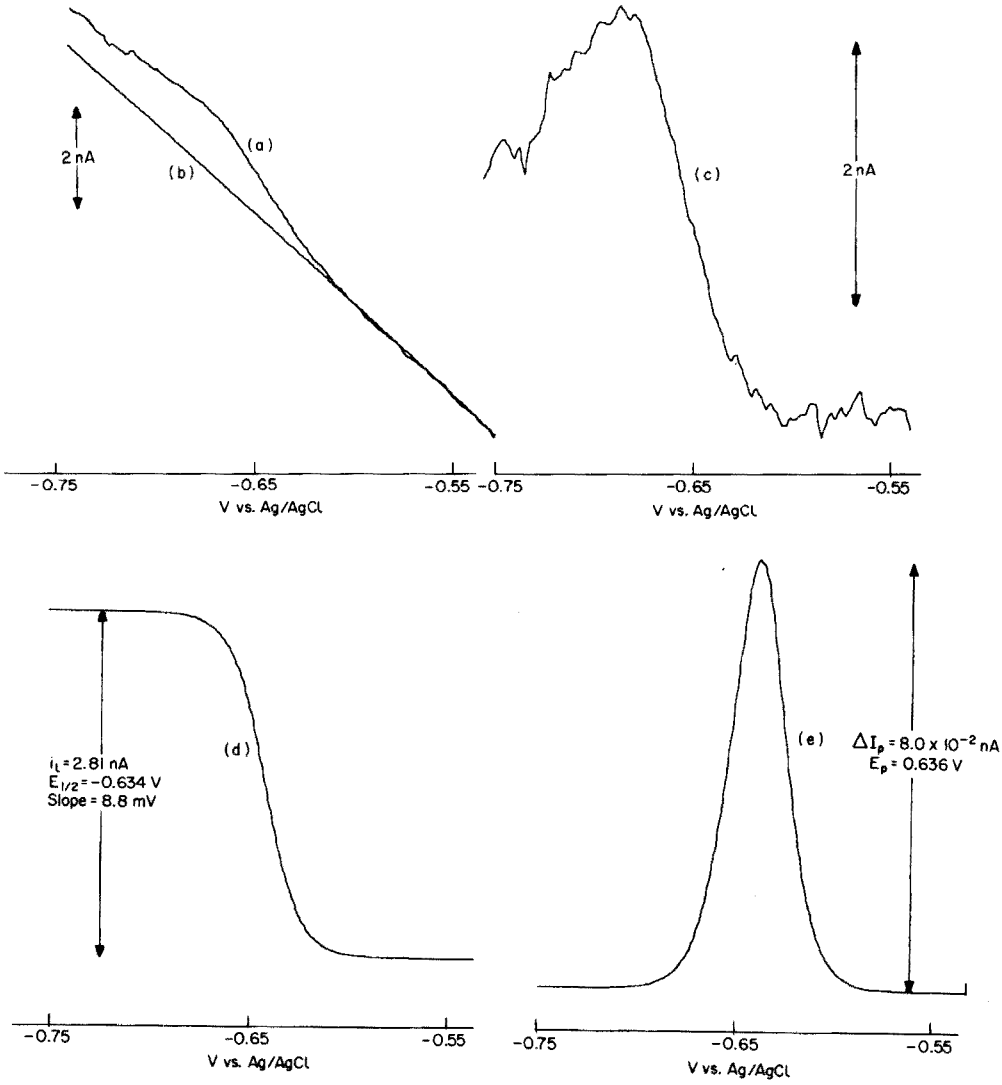

Fig. 2. Pseudo-derivative d.c. polarogram of 1 × 10^{-6} M cadmium(II) in 1 M NaCl, with 5.0-s drop time and 0.5 mV s^{-1} scan rate. (a) D.c. polarogram including background current; (b) linear extrapolation of background current; (c) d.c. polarogram after subtraction of background current; (d) smoothed d.c. polarogram based on all data points; (e) pseudo-derivative d.c. polarogram after all data points have been used in smoothing routine.

level for d.c. polarography with a drop time of 5.0 s. The raw data (curve a) show a poorly defined curve and the linear extrapolation (curve b) is far from adequate to define the limiting current accurately as shown in curve (c). Furthermore, the noise level after subtraction of the background current has increased substantially. At this concentration and for the d.c. polarograms, the smoothed curve obtained by least-squares fitting after correction of charging current is more dependent on which points are used to obtain the linear approximation to the charging current, as is shown by comparison of Figs. 2 and 3. Obviously, the best data are obtained when points are chosen as close to the foot of the wave as possible, but not so close that a significant faradaic component is present. Similarly, the best fit is obtained by including as few as possible data points on the limiting current region, i.e. the fit should be made over the smallest practical potential range so that the linear approximation is satisfied as exactly as possible. However, as Fig. 3 shows, the fit of the raw data and smoothed data to potentials at potentials far more negative than $E_{\frac{1}{2}}$ is still excellent. Pseudo-derivative plots are therefore still extremely well defined and reproducible at 10^{-6} M cadmium concentrations at a drop time of 5.0 s when a judicious choice of data points for the smoothing

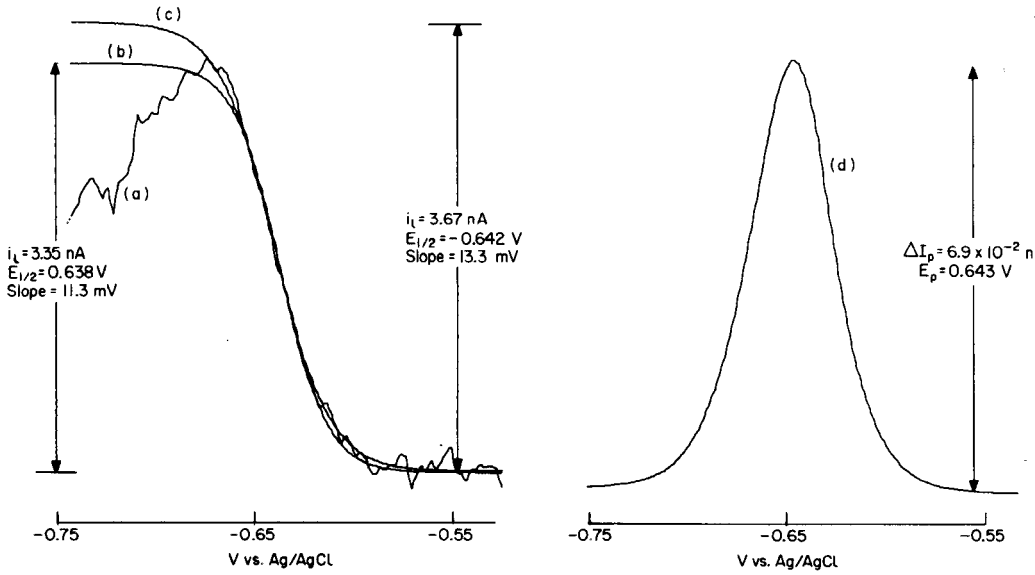

Fig. 3. Pseudo-derivative d.c. polarogram of 1 × 10^{-6} M cadmium(II) in 1 M NaCl based on fewer data points in the limiting current region compared with Fig. 2. The potential range, drop time and scan rate are as for Fig. 2. (a) D.c. polarogram after subtraction of background current with all data points used as in Fig. 2, curve c; (b) smoothed d.c. polarogram as in Fig. 2, curve d, but without using the last 20 data points on the limiting current region; (c) smoothed d.c. polarogram as in Fig. 2, curve d, but without using the last 35 data points on the limiting current region; (d) pseudo-derivative d.c. polarogram as in Fig. 2, curve e, but without using the last 35 data points on the limiting current region for smoothing the d.c. polarogram.

routine is made. Indeed, the transformation of the data shown in curve (a) to that in curve (d) of Fig. 2 clearly demonstrates the power of the computerized approach in electrochemistry. At the 10^{-6} M level and with a drop time of 5.0 s, the agreement of curves obtained by subtraction of charging current and calculation is still excellent, the peak potentials being within ±2 mV and peak heights ±3%.

At a drop time of 10 s, a limit of detection of 10^{-7} M for the determination of cadmium(II) in 1 M NaCl was obtained with d.c. techniques. At this concentration and condition, the charging current masked the faradaic current in the sense that the noise level became greater than the difference between faradaic and charging currents so that subtractive procedures had an unfavourable signal-to-noise ratio.

Clearly, because of the more favourable faradaic to charging current ratio associated with pulse polarography, superior data must be obtained with this method, and as Fig. 4 (curve a) shows, treatment of normal pulse curves at the 10^{-7} M level still gives extremely acceptable data. Peak potentials were reproducible to ±2 mV and peak heights to ±5% with a 5-s drop time at the 10^{-7} M level. The pseudo-derivative pulse method with a drop time of 10.0 s gave an improvement by an order of magnitude over the pseudo-derivative d.c. method, a detection limit of 10^{-8} M being found for cadmium in 1 M NaCl. For both the d.c. and normal pulse pseudo-derivative methods, peak heights were found to be a linear function of concentration over the range of 10^{-4} M to the limit of detection, and peak positions were independent of concentration within the limits of experimental error, as expected theoretically.

An interesting feature of the work was that the same detection limit applied whether the correction calculated by the linear least-squares method or the blank correction was used to subtract the background current. Whilst, in principle, it may appear that the use of a blank would be intrinsically easier and more reliable than the calculation method, the influence of trace amounts of oxygen and impurities is extreme when attempts are made to determine 10^{-7} M concentrations of cadmium. Obtaining matching test and blank solutions with respect to oxygen concentrations, etc. is not a trivial task. Complete removal of oxygen was found to require approximately 30 min, which is too time-consuming for routine application. The calculation method is more tolerant of traces of oxygen or impurities because the effects are simply incorporated into the background correction. In summary, therefore, the calculation method is superior in terms of convenience and reproducibility and is recommended as being applicable to most situations. When the pseudo-derivative techniques are used with computerized instrumentation, there seems no doubt that they are competitive with more sophisticated methods that are widely used and undoubtedly they would be superior in some instances.

For electrode processes having $E_{\frac{1}{2}}$ values at potentials well removed from the point of zero charge, e.g. at least 300 mV, the linear charging current approximation is considerably better than in the above example, as would be expected, and correction for charging current is therefore correspondingly more precise.

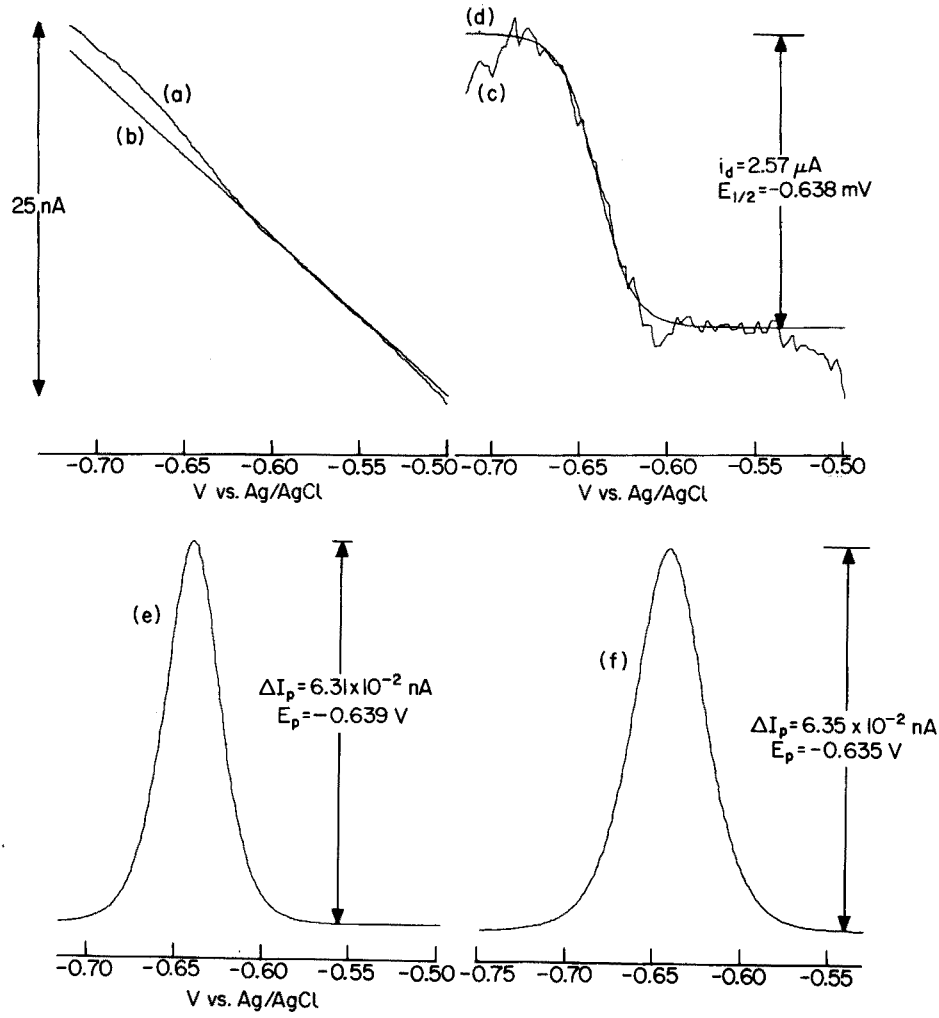

Fig. 4. Pseudo-derivative normal pulse polarograms of 10^{-7} M cadmium(II) in 1 M NaCl. Potential range, —0.50 to —0.75 V vs. Ag/AgCl; drop time and scan rate as for Fig. 2. (a) Normal pulse polarogram including background current; (b) linear extrapolation of background current; (c) normal pulse polarogram after subtraction of background current; (d) smoothed normal pulse polarogram; (e) pseudo-derivative normal pulse polarogram; (f) as for (e) but with initial potential of —0.53 V vs. Ag/AgCl.

REFERENCES

1 B. Breyer and H. H. Bauer, Alternating Current Polarography and Tensammetry, Interscience, New York, London, 1963.
2 H. Schmidt and M. von Stackelberg, Modern Polarographic Methods, Academic Press, New York, London, 1963.
3 A. M. Bond and R. J. O'Halloran, J. Electroanal. Chem., 68 (1976) 257.

4 A. M. Bond, Modern Polarographic Methods in Analytical Chemistry, Dekker, New York, in press.
5 J. Glickstein, S. Rankowitz, C. Auerbach and H. C. Finston, Adv. Polarogr., 1 (1961) 183.
6 C. Auerbach, H. L. Finston, G. Kissel and J. Glickstein, Anal. Chem., 33 (1961) 1480.
7 D. J. Fisher, W. L. Belew and M. T. Kelley, in G. J. Hills (Ed.), Polarography 1964, Macmillan, London, 1966, Vol. 1, pp. 89—134, 1966 and references cited therein.
8 H. C. Jones, W. L. Belew, R. W. Stelzner, T. R. Mueller and D. J. Fisher, Anal. Chem., 41 (1969) 772.
9 W. L. Belew, D. J. Fisher, H. C. Jones and M. T. Kelley, Anal. Chem., 41 (1969) 779.
10 Computers in Chemistry and Instrumentation, S. Mattson, H. D. Macdonald, Jr. and H. B. Mark, Jr. (Eds.), M. Dekker, New York, 1972.
11 M. Bos, Anal. Chim. Acta, 81 (1976) 21.
12 J. Heyrovsky and J. Kuta, Principles of Polarography, Academic Press, New York, London, 1966, pp. 53—60.
13 J. H. Christie and R. A. Osteryoung, J. Electroanal. Chem., 49 (1974) 301.

Analytica Chimica Acta, 101 (1978) 319—332

ROOM-TEMPERATURE PHOSPHORESCENCE CHARACTERISTICS AND LIMITS OF DETECTION OF SEVERAL PHARMACEUTICAL COMPOUNDS

ESTHER LUE YEN BOWER** and J. D. WINEFORDNER*
Department of Chemistry, University of Florida, Gainesville, FL 32611 (U.S.A.)
(Received 1st June 1978)

SUMMARY

The spectral characteristics and limits of detection for several pharmaceuticals obtained with room-temperature phosphorimetry are reported. The analyses were carried out under several different experimental conditions to observe the effect of changes in the environment and to arrive at the most suitable conditions for performing the measurements. Extreme selectivity of measurement was observed among the 28 pharmaceutical compounds studied.

Phosphorimetric analysis has been rarely used in biological and clinical applications because of unfamiliarity with the technique, solvent restrictions, and the necessity of working at low temperatures. However, analysis for drugs in biological fluids by conventional low-temperature phosphorescence has been shown to be a relatively sensitive and selective technique [1—4] and sometimes provides clarification of complex information obtained by other more popular techniques, such as fluorimetry. Low-temperature phosphorimetry has also been used in the measurement of pharmaceuticals containing antihistamines [5, 6], amphetamines and barbiturates [7], cocaine [8], vitamins [9], and sulfonamides [10]. O'Donnell and Winefordner [11] have reported recent advances in instrumentation and methodology in phosphorimetry which should facilitate the use of phosphorimetry for clinical analyses. Pulsed-source time-resolved phosphorimetry has been successfully applied in quantitative and qualitative analysis for drugs such as morphine, codeine, and cocaine [12].

Strong phosphorescence of organic molecules has until recently been observed only in rigid matrices, in the gas phase, or at very low temperatures. Phosphorescence at room temperature has been observed in a wide variety of compounds [13, 14] and its analytical utility has been demonstrated by Winefordner et al. [15, 16]. In the present paper, spectral data and limits of detection are reported for several pharmaceuticals under various experimental

**Present address: Department of Material Science and Engineering, University of Florida, Gainesville, FL 32611, U.S.A.

conditions by room-temperature phosphorimetry (r.t.p.). This method provides a simple, sensitive, selective, and rapid technique suitable for use in clinical applications. The use of the heavy atom effect has been shown to be extremely useful in further improving the sensitivity of this r.t.p. method [16, 17].

EXPERIMENTAL

Apparatus

A schematic block diagram of the instrumental system is shown in Fig. 1 and was previously described in detail [15]. Phosphorescence was measured with an Aminco-Bowman spectrophotofluorimeter with an Aminco-Keirs phosphoroscope attachment (American Instrument Co., Silver Spring, MD). Signals were detected with a 1P21 photomultiplier tube (Hamamatsu TV Co. Ltd.) with S-4 spectral response and PM voltage maintained at 700 V. Spectra were recorded on an X—Y recorder (MFE Corp., Salem, NH).

The sample holder was a modified version of that used earlier [15]. In order to reduce handling of the sample and sample support, individual replaceable sample holder tips were constructed (Fig. 2). Each tip consisted of a cylindrical block of aluminum (5/8 in. diameter, 1.25 in. long) with half of the lower 5/8 in. of the cylinder removed so that it was semicircular. This lower portion had a slit disc (5/8 in. × 5/8 in. and 5/128 in. thick) with a hole (0.25 in. diameter) in the center (sample illumination area) and was held in place by two screws arranged diagonally across the slit disc. This disc assisted in holding the sample support in position. A hole (0.25 in. diameter) was drilled in the top of the upper half of the aluminum block to accommodat the shaft of the sample holder. The entire assembly was painted black to reduce the scattered light from the shiny metal surfaces.

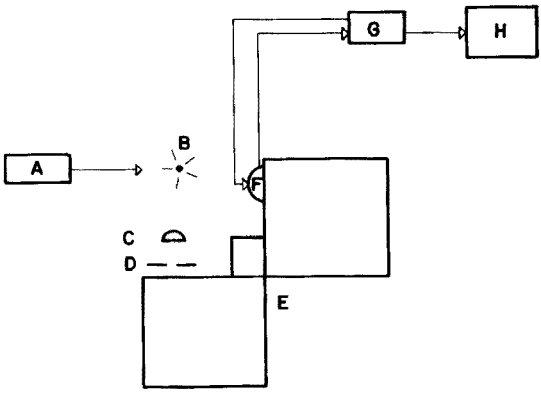

Fig. 1. Block diagram of instrumental system for room-temperature phosphorescence. (A) Aminco Xe lamp power supply; (B) 150-W xenon arc lamp; (C) quartz lens; (D) slit; (E) Aminco-Bowman spectrophotofluorimeter; (F) photomultiplier tube; (G) Aminco ratio photometer; (H) X-Y recorder.

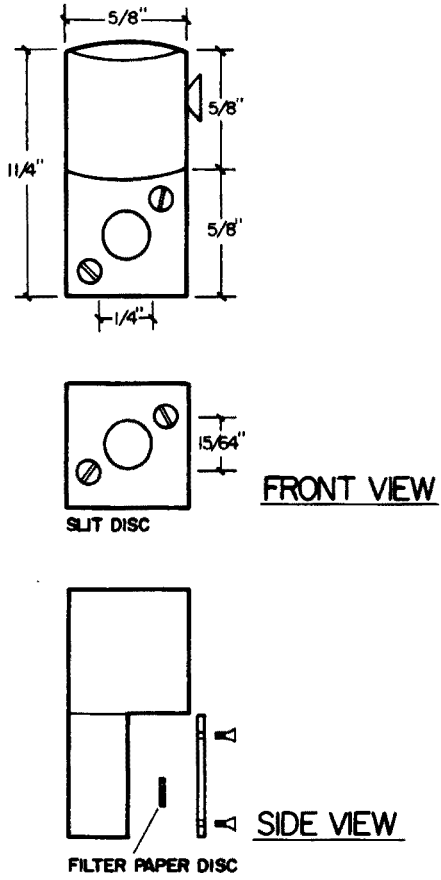

Fig. 2. Schematic diagram of new sample holder tip.

Materials

S and S 591-C filter paper (Schleicher and Schuell, Keene, NH) was used as the sample support for all the analyses. Sodium hydroxide (Fisher Scientific), sodium iodide (Alfa Products), silver nitrate (Mallinckrodt) and absolute ethanol (U.S. Industrial Chemicals Co., New York) were used to prepare the solvents. The pharmaceutical products listed in Table 1 were used as received.

Procedure

Filter paper circles (0.25 in. diameter) were made with a conventional paper puncher. A circle was placed on a clean sample holder tip with tweezers, making sure not to touch the surface to be measured with fingers. Each paper circle was then spotted with 3 μl of the solution to be measured, and 3 μl of any other solutions to be used, such as 0.2 M silver nitrate, 1 M sodium hydroxide, or 1 M sodium iodide solution.

TABLE 1

Spectral characteristics and limits of detection (LOD) of compounds of pharmaceutical interest by room-temperature phosphorescence

Compound	λ_{ex} (nm)	λ_{em} (nm)	Experimental conditions	LOD[a]
Antrenyl[b] 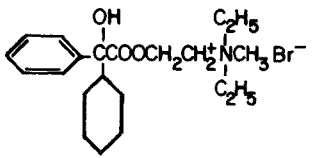	280	500	Aqueous solution	—[c]
	280	500	+1 M NaOH	—
	280	450, 490	+1 M NaOH + 1 M NaI	6.8 (20.4)
	280	500	+0.2 M $AgNO_3$	—
Anturane[b] 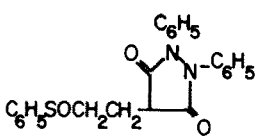	305	500	Ethanolic solution	—
	335	515	+1 M NaOH	—
	285	460	+1 M NaOH + 1 M NaI	1.8 (5.4)
	315	515	+0.2 M $AgNO_3$	—
Apresoline[b] 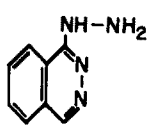	290	450	Aqueous solution	*[d]
	280	440	+1 M NaOH	2.7 (8.1)
	280	440	+1 M NaOH + 1 M NaI	0.9 (2.7)
	290	500	+0.2 M $AgNO_3$	—
Butazolidin[b] 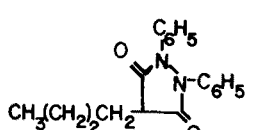	300	500	Ethanolic solution	—
	300	500	+1 M NaOH	—
	300	500	+1 M NaOH + 1 M NaI	—
	300	500	+0.2 M $AgNO_3$	—

Epinephrine[c]	280	500	130 ppm in 1 M NaOH	—
	280	500	+1 M NaI	—

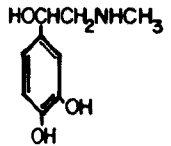

Esidrex[b]	290	490	Ethanolic solution	—
	275	440	+1 M NaOH	16.6 (49.8)
	275	440	+1 M NaOH + 1 M NaI	42.4 (127.2)
	275	500	+0.2 M $AgNO_3$	—

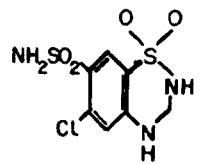

Forhistal[b]	290	500	Aqueous solution	—
	290	500	+1 M NaOH	—
	310	500	+1 M NaOH + 1 M NaI	—
	310	500	+0.2 M $AgNO_3$	—

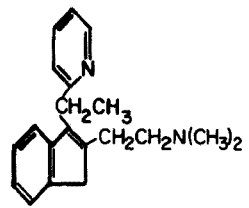

TABLE 1 (continued)

Compound	λ_{ex} (nm)	λ_{em} (nm)	Experimental conditions	LOD[a]
Locorten[b] 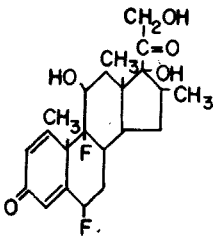	305	500	Ethanolic solution	—
	275	500	+1 M NaOH	—
	275	*455*, 490	+1 M NaOH + 1 M NaI	—
	275	515	+0.2 M $AgNO_3$	—
Metamphetamine hydrochloride[f]	250, 270	500	in 10% Ethanol	—
	250, 270	500	+1 M NaOH	—
	250, 270	500	+1 M NaOH + 1 M NaI	—
	250, 270	500	+0.2 M $AgNO_3$	—
Metandren[b] 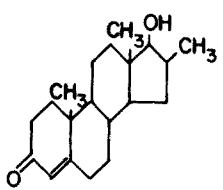	280	490	Ethanolic solution	—
	300	490	+1 M NaOH	—
	300	490	+1 M NaOH + 1 M NaI	—
	300	510	+0.2 M $AgNO_3$	—
Metopirone[b] 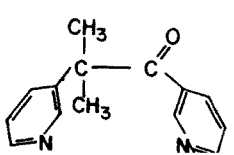	300	500	Ethanolic solution	—
	338	510	+1 M NaOH	—
	285	460	+1 M NaOH + 1 M NaI	1.5 (4.5)
	300	500	+0.2 M $AgNO_3$	—

Nupercaine hydrochloride[b]	295	445	Aqueous solution	1 (3)
	295	470	+1 M NaOH	—
	295	445	+1 M NaI	12.2 (36.6)
	260	450	+1 M NaOH + 1 M NaI	—
	295	515	+0.2 M $AgNO_3$	23.4 (70.2)
Otrivine[b]	275	490	Aqueous solution	—
	275	510	+1 M NaOH	—
	335	515	+1 M NaOH + 1 M NaI	—
	310	515	+0.2 M $AgNO_3$	—
Priscoline hydrochloride[b]	280	500	Aqueous solution	—
	280	*440*, 490	+1 M NaOH	—
	280	500	+1 M NaOH + 1 M NaI	16.5 (49.5)
	280	490	+1 M NaI	—
	280	500	+0.2 M $AgNO_3$	—
Privine hydrochloride[b]	280	*490*, 510	Aqueous solution	0.2 (0.6)
	280	435, *490*, 520	+1 M NaOH	0.2 (0.6)
	280	435, *490*, 520	+1 M NaOH + 1 M NaI	0.3 (0.9)
	280	435, *490*, 520	+1 M NaI	0.3 (0.9)
	280	515	+0.2 M $AgNO_3$	1.8 (5.4)

TABLE 1 (continued

Compound	λ_{ex} (nm)	λ_{em} (nm)	Experimental conditions	LOD[a]
Procaine hydrochloride[f]	305	445	Aqueous solution	0.5 (1.5)
	275	430	+1 M NaOH	0.6 (1.8)
	275	430	+1 M NaOH + 1 M NaI	0.3 (0.9)
	300	460	+0.2 M $AgNO_3$	26.6 (79.8)
Regitine hydrochloride[b]	310	500	Aqueous solution	—
	310	500	+1 M NaOH	—
	280	490, 515	+1 M NaOH + 1 M NaI	—
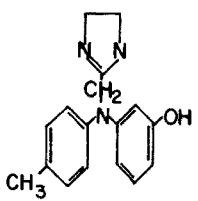	280	500	+0.2 M $AgNO_3$	—
Ritalin hydrochloride[b]	280	500	Aqueous solution	—
	332	515	+1 M NaOH	3.4 (10.2)
	282	*495*, 525	+1 M NaOH + 1 M NaI	0.5 (1.5)
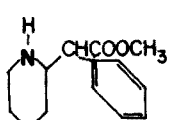	282	500	+1 M NaI	—
	300	510	+0.2 M $AgNO_3$	—

Serpasil[b] (Reserpine[g]) 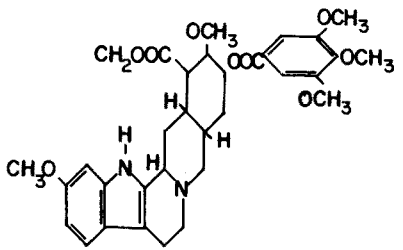	302	500	Ethanolic solution	—
	315	510	+1 M NaOH	—
	280	*495*, 520	+1 M NaOH + 1 M NaI	0.3 (0.9)
	280	500	+1 M NaI	—
	302	500	+0.2 M $AgNO_3$	—
Sintrom[b] 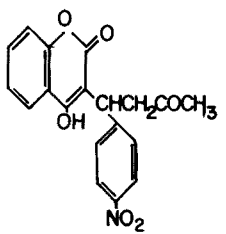	300	500	Ethanolic solution	—
	300	500	+1 M NaOH	—
	300	500	+1 M NaOH + 1 M NaI	—
	300	500	+0.2 M $AgNO_3$	—
Tandearil[b] 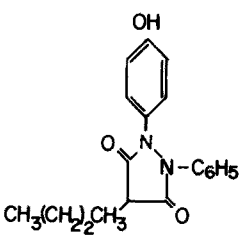	300	500	Ethanolic solution	—
	300	500	+1 M NaOH	—
	300	500	+1 M NaOH + 1 M NaI	—
	300	510	+0.2 M $AgNO_3$	—

TABLE 1 (continued)

Compound	λ_{ex} (nm)	λ_{em} (nm)	Experimental conditions	LOD[a]
Tegretol[b]	310	500	Ethanolic solution	—
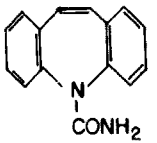	310	500	+1 M NaOH	—
	285	*495*, 520	+1 M NaOH + 1 M NaI	—
	310	515	+0.2 M $AgNO_3$	—
Thiopropazate dihydrochloride[h]	300	515	Aqueous solution	—
	300	520	+1 M NaOH	6.2 (18.6)
	275	*490*, 515	+1 M NaOH + 1 M NaI	2.3 (6.9)
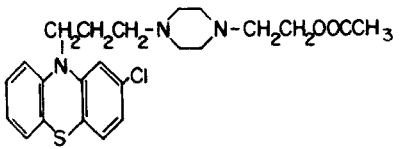	280	*490*, 515	+1 M NaI	—
	280	510	+0.2 M $AgNO_3$	6.7 (20.1)
Tofranil[b]	300	500	Aqueous solution	—
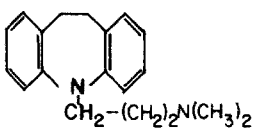	335	510	+1 M NaOH	—
	280	450	+1 M NaOH + 1 M NaI	—
	310	500	+0.2 M $AgNO_3$	—
Trasentine hydrochloride[b]	280	500	Aqueous solution	—
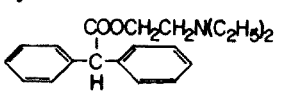	335	510	+1 M NaOH	—
	275	*490*, 520	+1 M NaOH + 1 M NaI	1.2 (3.6)
	300	*490*, 520	+1 M NaI	4.3 (12.9)
	300	515	+0.2 M $AgNO_3$	—

Vinblastine sulfate[g]	305	500	Aqueous solution	—
	278	*490*, 515	+1 M NaOH	2.1 (6.3)
	300	490	+1 M NaOH + 1 M NaI	—
	278	*490*, 515	+1 M NaI	0.9 (2.7)
	300	510	+0.2 M $AgNO_3$	—
Vioform[b]	300	500	Ethanolic solution	—
	300	500	+1 M NaOH	—
	300	510	+1 M NaOH + 1 M NaI	30.7 (92.1)
	300	510	+0.2 M $AgNO_3$	—
	288	500	+0.2 M $AgNO_3$ + 1 M HNO_3	—

[a]Limit of detection calculated for $S/N = 3$ and for 3-μl samples; 10 × LOD gives the lowest concentration or amount which can be reliably quantified. Values are given as ppm and as ng (in parentheses). [b]Ciba-Geigy Corp., Summit, N.J. [c]The dashes indicate that the signal is not analytically useful, being indistinguishable from background luminescence. [d]Asterisks indicate that the signal is not analytically useful but is distinguishable from background luminescence (e.g. Fig. 4). [e]Nutritional Biochemicals Corp., Cleveland, OH. [f]Applied Science Labs, Inc., State College, PA. [g]Eli Lilly, Indianapolis, IN. [h]Searle and Co., San Juan, PR.

The solutions used to prepare analytical calibration curves and to estimate limits of detection were prepared from stock solutions by serial dilutions. The compounds investigated were dissolved in deionized water, if they were water-soluble, and in ethanol if not readily soluble in water.

In applying the sample to the support, care had to be taken so that the tip of the syringe just touched the filter paper or else the solution would run up the outside walls of the syringe tip by capillary action. The sample holder tips were then placed under an infrared lamp for approximately 10 min to insure that the sample support was dry. The optimum drying time would, of course, be dependent on the solvent used. Drying was necessary because wet samples showed either low or undetectable phosphorescence signals. The temperature of the surface being dried was maintained at approximately 65°C by varying the distance between the i.r. lamp and the sample surface. Higher temperatures could be used but thermal decomposition must be avoided.

The sample holder tips were reproducibly replaced on the shaft of the sample holder by means of a set-screw on each tip and a notch on the shaft. This allowed simpler placement of the sample support in the sample holder, and involved less risk of scraping off the dried sample from the front surface of the support as was possible in the original design and procedure [15].

RESULTS AND DISCUSSION

Analytical figures of merit are listed in Table 1. The presence of sodium hydroxide was not necessary to observe phosphorescence at room temperature as was found previously by other workers [13—17]. Also, silver(I) ions appeared to have little or no effect as heavy atom perturbers, whereas sodium iodide usually led to increased signal intensities and lower (improved) limits of detection.

The correlation between molecular structure and phosphorescence characteristics at room temperature is not clear, for compounds with quite similar structures such as Anturane and Butazolidin, or Otrivine and Privine hydrochloride did not behave similarly. Anturane gave fairly intense emission at 460 nm with NaOH and NaI, while Butazolidin was not detectable. Likewise, Privine hydrochloride gave very intense phosphorescence emission under all conditions studied, while Otrivine did not emit under any condition tried. As observed with other compounds [14—17], the emission bands were broader and were slightly red-shifted from their emission peaks at 77 K as is depicted for Privine hydrochloride in Fig. 3. Limits of detection were estimated only for those compounds which gave a signal-to-background ratio of at least two and where the signals were thought to be analytically useful. In the case of Apresoline and others where the signal levels were distinguishable from the background only for fairly high concentrations of analyte (see Fig. 4), no limits of detection were calculated. The limit of detection is defined as that concentration of the analyte giving a signal-to-noise ratio of three.

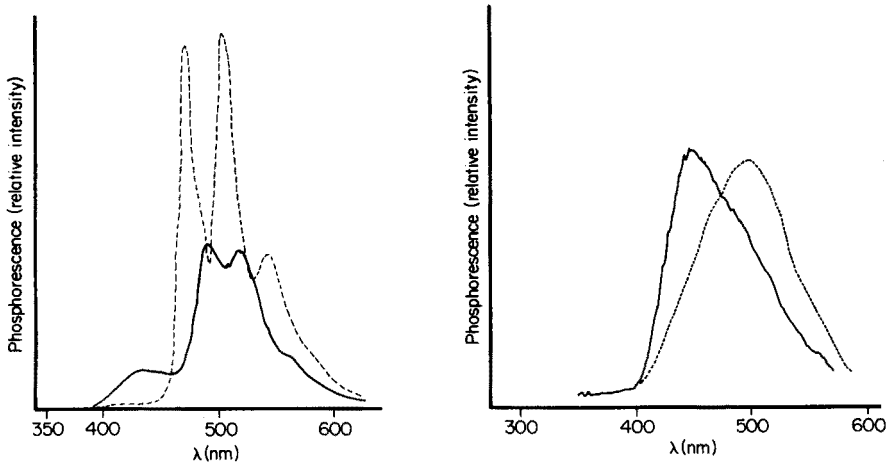

Fig. 3. Room-temperature phosphorescence and low-temperature phosphorescence of Privine hydrochloride. (---) Spectrum at 77 K; (—) spectrum at room temperature.

Fig. 4. Phosphorescence spectrum of Apresoline hydrochloride. (—) Analyte signal (250 ppm aqueous solution); (---) blank (paper with deionized water).

It was believed that thermal decomposition by the i.r. lamp might be the cause of lack of phosphorescence at room temperature for some of the compounds. Several of these compounds which gave no signal were therefore dried in a glove bag through which nitrogen at room temperature was passed, but room-temperature phosphorescence was still not produced.

The r.t.p. data obtained for the pharmaceutical preparations appear somewhat inconclusive; no definite statement can be made concerning the ability of a molecule to luminesce at room temperature based on its molecular structure. The results do serve, however, to extend the list of compounds which may be measured by phosphorescence at room temperature, where only minute quantities of sample are available, such as in clinical analysis. The results also show that very low limits of detection can be achieved with r.t.p., especially if a heavy atom perturber, such as sodium iodide is added to the samples. The technique is obviously a very simple and selective one and is quite suited to certain clinical analysis.

The authors thank the Ciba-Geigy Corp., Eli Lilly & Co., and Searle and Co., for their generous contributions of the pharmaceuticals studied. This work was supported by NIH GM-11373-15.

REFERENCES

1 S. Freed and W. Salmre, Science, 128 (1956) 1341.
2 J. D. Winefordner and H. W. Latz, Anal. Chem., 35 (1963) 1517.
3 J. D. Winefordner and M. Tin, Anal. Chim. Acta, 32 (1965) 64.

4 H. C. Hollifield and J. D. Winefordner, Talanta, 14 (1967) 103.
5 D. L. Wilson, D. R. Wirz and G. H. Schenk, Anal. Chem., 45 (1973) 1447.
6 D. R. Wirz, D. L. Wilson and G. H. Schenk, Anal. Chem., 46 (1974) 896.
7 C. I. Miles and G. H. Schenk, Anal. Chem., 45 (1973) 130.
8 V. I. Stenberg, S. P. Singh and N. K. Narain, Spectrosc. Lett., 8 (1977) 639.
9 J. J. Aaron and J. D. Winefordner, Talanta, 19 (1972) 21.
10 D. R. Venning, J. J. Mousa, R. J. Lukasiewicz and J. D. Winefordner, Anal. Chem., 44 (1972) 2387.
11 C. M. O'Donnell and J. D. Winefordner, Clin. Chem., 21 (1975) 285.
12 K. F. Harbaugh, C. M. O'Donnell and J. D. Winefordner, Anal. Chem., 46 (1974) 1207.
13 M. Roth, J. Chrom., 30 (1967) 276.
14 E. M. Schulman and C. Walling, Science, 178 (1972) 53.
15 S. L. Wellons, R. A. Paynter and J. D. Winefordner, Spectrochim. Acta, Part A, 30 (1974) 2133.
16 T. Vo-Dinh, E. Lue Yen and J. D. Winefordner, Anal. Chem., 48 (1976) 1186.
17 P. G. Seybold and W. White, Anal. Chem., 47 (1975) 1199.

Analytica Chimica Acta, 101 (1978) 333—338

DETERMINATION OF BENZO[a]PYRENE IN A FILTERED RETORT WATER SAMPLE BY SOLID-SURFACE FLUORESCENCE

R. J. HURTUBISE,* J. D. PHILLIP and G. T. SKAR

Department of Chemistry, The University of Wyoming, Laramie, Wyo. 82071 (U.S.A.)

(Received 30th March 1978)

SUMMARY

A method has been developed for determining benzo[a]pyrene in filtered retort water from an in situ oil shale process by employing liquid—liquid extraction, dry-column chromatography, thin-layer chromatography and fluorescence spectrometry. Benzo[a]-pyrene was identified and determined by detecting its fluorescence directly from chromato-plates. The accuracy and precision of the method are good; the limit of detection is ca. 0.08 ppb. Irreproducible results were obtained with unfiltered retort water samples.

Polynuclear aromatic hydrocarbons (PAH) have been investigated extensively in recent years mainly because they are carcinogenic to animals and probably to man [1]. Ershova and Mints [2] isolated PAH in petrochemical effluents, the stability of benzo[a]pyrene (BaP) in water was studied [3] and fluorimetric methods for PAH in natural water were developed [4]. Giger and Blumer [5] presented data for near-shore marine sediments which demonstrated the compositional complexity of a PAH fraction that was undocumented previously. McGinnes and Snoeyink [6] studied the fate of PAH in natural water systems; Harrison et al. [7] reviewed several aspects of PAH in raw, potable and waste waters. Fluorescence spectra, quantum yields, and concentration dependencies were reported for five PAH in water [8] and liquid—liquid extraction, thin-layer chromatography and fluorimetry were used [9] to determine benzo[a]pyrene in marine organisms and sediments. The extraction efficiency of PAH from water was investigated [10]. Flexible polyurethane foam was used to concentrate trace quantities of BaP from water by Saxena et al. [11]; open-pore polyurethane columns were used [12] for the collection and preconcentration of PAH from water and the aqueous solubility of PAH was found [13] by a coupled column liquid chromatographic technique. This report describes an inexpensive, rapid, sensitive, quantitative method for the determination of BaP in a filtered retort water sample obtained from an in situ oil shale process.

EXPERIMENTAL

Apparatus

The determination of BaP and the recording of fluorescence emission spectra have been described [14].

Materials

The dry column consisted of a 28-cm section of polyethylene tubing (0.25 in. i.d., Curtin Matheson Scientific, Inc.), 23 cm of which was packed with aluminum oxide, activity II to III according to Brockman (ICN Life Sciences Group, Cleveland, Ohio). The bottom of the column was plugged with glass wool. All solvents used were reagent grade. Distilled n-pentane was obtained from Burdick and Jackson Laboratories Inc., Muskegon, Michigan. Precoated, 20 × 20-cm 30%-acetylated cellulose chromatoplates were used for thin-layer chromatography (t.l.c.) work (Cel 300 AC/30-22 Brinkmann Instruments, Inc., Westbury, New York). The 99+% BaP was obtained from Aldrich Chemical Co., Milwaukee, Wis. A 10-μl Hamilton syringe was used in spotting the chromatoplates. A Selectasol chromatography chamber (Schleicher and Schuell, Inc., Keene, New Hampshire) was employed in determining the eluants to be used in the t.l.c. work.

The retort water samples were obtained from the Laramie Energy Research Center, Department of Energy, Laramie, Wyoming. Unfiltered and filtered (0.4 μm) retort water samples used in development of the analytical method were obtained from the Omega-9 collection (internal designation used by the Laramie Energy Research Center for process waters obtained during the in situ oil shale retorting experiment at Site 9 near Rock Springs, Wyoming, in 1976). The acquisition, process and storage of the Omega-9 retort water has been described [15]. The Omega-9 retort water collection and the samples used were maintained under refrigerated conditions. Chemical parameters indicative of the composition of the Omega-9 water used are: 3,470 ± 830 mg l^{-1} NH_4^+; 2,740 ± 730 mg l^{-1} $S_2O_3^{2-}$; 15,940 mg l^{-1} HCO_3^-; pH 8.6 ± 0.3; 1,030 ± 105 mg l^{-1} total organic carbon, and 14,510 ± 690 mg l^{-1} total dissolved solids [16].

Procedures

An accurately measured, filtered or unfiltered, retort water or distilled water sample was added to a 1-l separatory funnel. The sample was extracted four times with n-pentane, first with 100 ml for 10 min and then with three 50-ml portions for 5 min each. The n-pentane was pipetted from the separatory funnel after each extraction and the n-pentane layers were combined. In the filtered or unfiltered retort water samples, a third layer appeared during the extractions. This middle layer, which was more cloudy with unfiltered samples and appeared to be air and n-pentane trapped within the suspended material of the retort water, was eliminated partially by applying suction to the separatory funnel with a vacuum line. After removal of the

n-pentane layer for the last extraction, the middle layer was centrifuged and the resulting n-pentane layer was pipetted into the other n-pentane layers; the combined layers were evaporated to dryness at room temperature in an Erlenmeyer flask. For distilled water samples and filtered retort water samples, the evaporated residue was dissolved in 1 ml of n-hexane and transferred to a 1-ml volumetric flask where the n-hexane was evaporated to dryness. The Erlenmeyer flask was rinsed with n-hexane and the rinsings were added to the 1-ml volumetric flask. The volume was then diluted to 1 ml with n-hexane. For unfiltered retort water samples, the evaporated residue was dissolved in 1 ml of n-hexane, transferred to a 2-ml volumetric flask followed by the Erlenmeyer flask rinsings. The volume was then diluted to 2 ml with n-hexane. A 1-ml volume of n-hexane concentrate from either filtered or unfiltered samples was added to the aluminum oxide column, which was developed with 5 ml of n-hexane—ether (19:1). After development the column was observed with a u.v. handlamp and the purple fluorescent band was sliced with a razor blade from the column to give a 5-cm section. The migration distance to the center of the BaP band was 6.5 cm for BaP in distilled water, 8 cm for BaP in filtered retort water, and 8.5 cm for BaP in unfiltered retort water. To determine the exact migration distance for BaP from distilled water and retort water samples, a known amount of BaP was added to the samples and the spiked samples were carried through the extraction and column separation steps. The migration distances for the specific samples were very reproducible; after the migration distances had been determined, it was not necessary to run spiked samples. The aluminum oxide from the sliced section was stirred for 30 min with 20 ml of 1,2-dichloroethane. After the solvent had been decanted, the aluminum oxide was washed twice with 10-ml aliquots of 1,2-dichloroethane; the last wash was filtered rather than decanted. The combined extracts were evaporated to dryness under vacuum at room temperature and the residue was dissolved in 1 ml of n-hexane.

This solution (5 μl) was spotted in duplicate on a 30% acetylated cellulose chromatoplate. Standard solutions of BaP in n-hexane at concentrations of 2, 6, and 10 ng μl^{-1} were also spotted (5-μl amounts) in duplicate. The plate was developed to 10 cm with methanol—n-hexane—acetone (7:3:2) for distilled water and filtered retort water samples. For unfiltered retort water samples two developments were required because of a fluorescent impurity immediately above BaP on the chromatoplate. The first development was carried out with methanol—water—acetic acid—acetone (20:5:3:3) and the second with methanol—n-hexane—acetone (7:3:2). The chromatoplate was then air-dried and the fluorescence intensity was measured with the Kontes densitometer. Each spot was scanned perpendicular to the direction of development. Recorded peak heights, corresponding to fluorescence intensity of the standards, were plotted versus nanograms of BaP. The unknown amount of BaP on the chromatoplate was obtained from the calibration curve and calculated as nanograms of BaP per ml of retort water (ppb).

To identify BaP, the fluorescence emission spectra were measured directly from chromatoplates by the procedures described previously [17].

Distilled water and retort water samples were spiked with acetone solutions of BaP. Solutions of BaP in acetone (1 μg ml^{-1} and 2 μg ml^{-1}) were employed to prepare 5-ppb and 10-ppb spiked samples, respectively.

RESULTS AND DISCUSSION

Separation of BaP from retort water

n-Pentane was employed because it gives efficient extraction of PAH from water and evaporates readily [4]. The rationale for using dry-column chromatography and thin-layer chromatography to isolate BaP was discussed previously [14, 17].

Determination of BaP

Table 1 shows recovery data, sample size variation data and BaP content for spiked distilled water samples. For the unfiltered 250-ml samples, good recovery and reproducibility were obtained. With the 500-ml samples, good reproducibility was obtained but the recovery was somewhat low, indicating a sample-size dependency. When the spiked distilled water samples were filtered through Whatman No. 1 filter paper, the percentage recovery was very low (Table 1). Observation of the filter paper under u.v. radiation indicated the bright violet fluorescence of BaP; filter paper has a strong affinity for BaP, and samples should not be filtered through paper before analysis. Filter paper would be very effective for the removal of BaP from water; this is worthy of further investigation.

Table 2 shows recovery data, sample size variation data and BaP content for filtered and unfiltered retort water samples. Several filters (Millipore Corp.) were used in filtering the retort water samples by Laramie Energy

TABLE 1

Percentage recovery and reproducibility of the method for benzo[a]pyrene in distilled water samples

Sample (ml)	BaP added (ppb)	BaP found (ppb)	Recovery (%)
250	5.0	5.0	100
250	5.0	4.9	98.0
250	10.0	10.4	104
500	5.0	4.4	88.0
500	5.0	4.2	84.0
250[a]	5.0	1.6	32.0
250[a]	5.0	1.0	20.0

[a]Filtered through Whatman No. 1 filter paper.

TABLE 2

Percentage recovery and reproducibility of the method for benzo[a]pyrene in filtered and unfiltered retort water

	Sample (ml)	BaP (ppb)			Recovery (%)
		Present	Added	Found	
Filtered[a]	250	0	5.0	4.5	90.0
		0	5.0	5.1	102
		0	5.0	5.0	100
		0	5.0	5.0	100
		0	10.0	9.40	94.0
		0	10.0	8.64	86.4
	500	0	5.0	3.6	72.0
		0	5.0	3.6	72.0
		0	5.0	4.0	80.0
Unfiltered	250	15.3	10.0	18.8	35.0
		14.4	10.0	24.3	99.0
	500	18.7	—	—	—
		12.4	—	—	—
	250[b]	14.8[c]	10.0	2.6	26.0
			10.0	1.0	10.0

[a]Filtered as described earlier [15]. [b]Filtered through Whatman No. 1 filter paper. [c]Average of two determinations.

Research Center [15]. BaP was not detected in these samples (Table 2), and 100-μl sample extracts spotted on the chromatoplate showed no BaP. The recovery and reproducibility for BaP in the spiked Millipore filtered samples is good. As with the 500-ml distilled water samples, the 500-ml spiked Millipore filtered samples gave a low percentage recovery indicating a sample size dependency.

The unfiltered retort water samples contained suspended material and were more difficult to handle than the filtered samples. The results in Table 2 for the 250-ml unfiltered retort water samples show a wide variation in percentage recovery. Work with different unfiltered retort water samples gave similar results, and the results for the 500-ml unfiltered retort water samples showed a wide variation (Table 2). For two spiked unfiltered retort water samples, filtered through Whatman No. 1 filter paper, the percentage recovery was very low (Table 2). Observation of the filter paper under u.v. radiation showed the characteristic violet fluorescence of BaP.

The poor reproducibility for the unfiltered retort water samples is probably caused by adsorption of BaP on the suspended material in unfiltered retort water: no BaP was found in the filtered retort water samples. When 250-ml samples of unfiltered retort water were filtered through a medium-frit glass filter, BaP was not detected in the filtrate. 1,2-Dichloroethane was passed

over the residues in the glass filters, collected, and evaporated to dryness. The residue was dissolved in n-hexane and separated as described under "Procedures". BaP was detected visually on chromatoplates in both samples. Further work is needed to develop a method for determining the BaP adsorbed on suspended material; the limited number of samples available made it impossible to pursue this. Saxena et al. [11] suggested that part of the increased efficiency of retention of BaP on porous polyurethane foam, by heating tap water containing BaP, was related to the desorption of BaP from suspended particles in the water. Suspended material in water can have a pronounced effect [10] on the extraction efficiency of PAH from water. It is important to distinguish between dissolved BaP and BaP adsorbed on suspended material. The method developed in this work accurately determines dissolved BaP in water samples that are relatively free of suspended material.

Limit of detection

The limit of detection for BaP in filtered retort water extract, defined as described previously [14] was 0.9 ppb. When 100 μl of filtered retort water extract was spotted, the background signal was the same as that for 5 μl, and the limit of detection was 0.08 ppb, which could be decreased even more by spotting more sample on the chromatoplate.

This work was supported by the Department of Energy's Laramie Energy Research Center under Contract No. EY-77-C-04-3913 to the Rocky Mountain Institute of Energy and Environment.

REFERENCES

1 J. B. Andelman and J. E. Snodgrass, CRC Crit. Rev. Environ. Control, 4 (1974) 69.
2 K. P. Ershova and I. M. Mints, Hyg. Sanit., 33 (1968) 371.
3 A. P. Il'nitskii, K. P. Ershova, A. Ya. Khesina, L. G. Rozhkova, V. G. Klubkov and A. A. Korolev, Hyg. Sanit., 36 (1971) 9.
4 R. E. Keegan, Ph.D. Thesis, University of New Hampshire, Durham, New Hampshire, 1971.
5 W. Giger and M. Blumer, Anal. Chem., 46 (1974) 1663.
6 P. R. McGinnes and V. L. Snoeyink, Water Resources Center Report No. 80, University of Illinois, Urbana, Illinois, 1974.
7 R. M. Harrison, R. Perry and R. A. Wellings, Water Res., 9 (1975) 331.
8 F. P. Schwarz and S. P. Wasik, Anal. Chem., 48 (1976) 524.
9 B. P. Dunn, Environ. Sci. Technol., 10 (1976) 1018.
10 M. A. Acheson, R. M. Harrison, R. Perry and R. A. Wellings, Water Res. 10 (1976) 207.
11 J. Saxena, J. Kozuchowski and D. K. Basu, Environ. Sci. Technol., 11 (1977) 682.
12 J. D. Navratil, R. E. Sievers and H. F. Walton, Anal. Chem., 49 (1977) 2260.
13 W. E. May, S. P. Wasik and D. H. Freeman, Anal. Chem., 50 (1978) 175.
14 R. J. Hurtubise, G. T. Skar and R. E. Poulson, Anal. Chim. Acta, 97 (1978) 13.
15 D. S. Farrier, R. E. Poulson, Q. D. Skinner, J. C. Adams and J. P. Bower, Proceedings of The Second Pacific Chemical Engineering Congress, Denver, Colorado, Vol. 2, pp. 1031—1035, August, 1977.
16 D. S. Farrier, Laramie Energy Research Center, Personal communication.
17 R. J. Hurtubise, J. F. Schabron, J. D. Feaster, D. H. Therkildsen and R. E. Poulson, Anal. Chim. Acta, 89 (1977) 377.

Analytica Chimica Acta, 101 (1978) 339—357

THE USE OF ULTRAFILTRATION FOR THE SEPARATION AND FRACTIONATION OF ORGANIC LIGANDS IN FRESH WATERS

J. BUFFLE*, P. DELADOEY and W. HAERDI

Department of Inorganic and Analytical Chemistry, University of Geneva, 1211 Genève-4 (Switzerland)

(Received 2nd May 1978)

SUMMARY

The effects of various experimental conditions on the results obtained by using membrane filtration for the separation and fractionation of organic matter in fresh waters (mainly fulvic and humic substances) are described. The technique used (washing or concentration) and the initial concentration of the organic matter to be filtered are the most critical factors. The technique is used for the fractionation of eight water samples, one sample of peat interstitial water, five water extracts of soil and four water samples obtained by decomposition of leaves. The results are compared. A comparison is also made with results cited in the literature.

The complexing or adsorbing agents in natural waters may be classified, roughly, into four categories [1] according to their reactivity with inorganic ions:

(a) dissolved ligands, inorganic (e.g. Cl^-, SO_4^{2-}, HCO_3^-) or organic (e.g. amino acids, hydroxy acids), with low molecular weights ($M_w < 200$: fraction F1);

(b) dissolved compounds with surface-active properties and $200 < M_w < 10000$ (fraction F2), e.g. fulvic acids (FA), polyhydroxo complexes of metals such as Al(III) and Fe(III), and polysilicates;

(c) colloidal compounds, inorganic (silicates or metallic hydroxides or organic (humic acids (HA), polysaccharides, proteins) with $10^4 < M_w < 10^6$ (fraction F3);

(d) suspended particles, inorganic or organic, whose size is larger than 0.05 μm (fraction F4).

Although the division between these groups in not clear cut, each group has some characteristics physical properties. For example, F1 usually consists of soluble compounds; F2 of compounds with surface-active properties, F3 of hydrophilic colloids, and F4 of hydrophobic colloids. The groups are also characterized by different reactivities towards inorganic ions, with a decrease of complexation reactions and increase of adsorption or ion-exchange reactions in passing from F1 to F4. In the determination of the retention ability of a compound, the physical properties of the compound are important because they may affect the particular technique used, e.g. by adsorption on electrodes

[2—4] or by inducing secondary reactions such as coagulation of colloids. A method for the fractionation of the different kinds of ligands present in water is therefore needed, not only for measurements of the relative importance of the various ligands in complexation of a particular element (speciation studies) but also to facilitate the interpretation of the complexing properties of a particular category of ligands.

The choice of fractionation method should be made on the following criteria. It should be versatile, useful for any type of water, simple and sufficiently rapid. It should allow the separation of various groups with different molecular weights. It should, as far as possible, be insensitive to secondary effects such as adsorption or flocculation. Finally, dilution of samples should be minimal, and the addition of chemical reagents should be avoided because they may change the composition of the medium and act themselves as ligands.

These requirements greatly limit the possibilities of using methods such as precipitation, ion exchange, extraction, electrophoresis or isotachophoresis [5—10]. In this paper, the results obtained by centrifugation, ultracentrifugation, gel permeation chromatography and membrane filtration for the separation of organic matter (OM) from fresh waters are compared. The optimal conditions for ultrafiltration measurements were particularly studied.

EXPERIMENTAL

Apparatus

The ultracentrifugation experiments were done with a Spinco L5O ultracentrifuge. The Centriflo CF 25 filters (cut-off $M_w \approx 25000$ [11]) were Amicon products used with a classical centrifuge at 1800 rpm. Gel chromatographic measurements were done with Biogel P10 (fractionation limits, $1700 \leqslant M_w \leqslant 20000$) and Biogel P2 ($100 \leqslant M_w \leqslant 2000$) from Bio-Rad Laboratories.

Ultrafiltrations were done with the Amicon system (12-ml cell for Diaflo membrane; reservoir RA1). In addition, a cylindrical 70-ml cell having the same diameter as the 12-ml one was constructed with four stirring blades placed equidistantly on the stirring axis. The filters used were 8.0-μm, 0.2-μm, and 0.035-μm Schleicher and Schuell filters, and Amicon Diaflo PM10, DM5, UM2 and UM05 membranes.

Methods of determination

The concentrations of organic matter in the filtrates were determined as follows: (a) absorbances in the ultraviolet region (285 nm) were measured with a Beckman DB-G spectrophotometer; (b) fluorescence measurements with a Perkin-Elmer 204 spectrofluorimeter; (c) TOC with an Oceanographic International apparatus.

The metal ions (Pb(II), Cu(II), Zn(II), Ca(II), Fe(III) and Al(III)) in the fractionated samples were determined by atomic absorption spectrometry (a.a.s.), with a Pye Unicam SP 1900 spectrometer, or by using radioactive tracers (lead-210 and cadmium-115) and a Landy and Gyr apparatus.

The analytical methods for the compounds used in testing the UMO5 membrane were as follows: Ca^{2+} by a.a.s.; HCO_3^- by titration with sulfuric acid; dopamine, tiron and alizarin complexone by u.v. spectrophotometry at 300 nm; phenol red, bromothymol blue and bromophenol blue by spectrophotometry at 530, 650 and 630 nm, respectively; glycine by spectrophotometric analysis with 1,2-naphthoquinone-4-sulfonate [12]; glucose by spectrophotometric analysis with *o*-toluidine [13]; and citric acid by spectrophotometric analysis with pyridine and acetic anhydride [14]. Unless otherwise stated, reagents were analytical-grade Merck products.

Samples

Three types of waters were fractionated. Eight natural waters (Nos. 10—50) were initially concentrated by freezing concentration (7) to between 0.2 and 1.6 g l^{-1}; one of these was an interstitial water from peat (No. 41); waters 50a, 50b, 50c were sampled in the same area but were stored as concentrated solutions (ca. 0.9 g l^{-1}) for 3 months, 11 months and 3 years, respectively. Five aqueous extracts from soils (Nos. S0—S4) were tested, as well as four aqueous solutions produced by decomposition of leaves (Nos. F1—F4). The composition and stability of these solutions has been described in detail [15]. All these solutions were stored at 4°C in the dark. During the storage period, an initial decrease (maximum 30%) in the concentration of OM was observed in water samples filtered through 0.2-μm filters. However, after a few weeks, the concentration of OM stabilized and remained constant for more than twelve months. This decrease is attributed to flocculation of the high-molecular-weight compounds which are then retained on 0.2-μm membranes. As all the experiments described here were done with waters filtered through 0.2-μm filters more than one month after sampling, it is probable that the FA/HA ratio is slightly higher in these samples than in the initial fresh waters.

Unless otherwise stated, the samples were decarbonated before use by acidifying with $HClO_4$ to pH 4 and then reneutralizing the excess of acid with sodium hydroxide. Ultrafiltrations were done under nitrogen.

CENTRIFUGATION AND GEL PERMEATION CHROMATOGRAPHY

Centrifugation

Ultracentrifugation was used first to evaluate an order of magnitude of the molecular weight of the organic ligands of fresh water. Hydrogencarbonate was eliminated from sample No. 50b, the complexing properties of which are known [16]; the sample was then neutralized to pH 6.5, diluted to 30 mg l^{-1} of OM, and 10^{-6} M of radioactive Pb(II) or Cd(II) tracer was added. The solution was placed in a series of tubes (7 cm long) and ultracentrifuged at 40 000 rpm. A 1.0-ml sample (corresponding to the upper 6 mm of the solution in the tube) was withdrawn every hour, each time from a different tube, by means of a capillary tube without disturbing the whole solution. The decrease in radioactivity in the upper part of the solution is shown in Fig. 1.

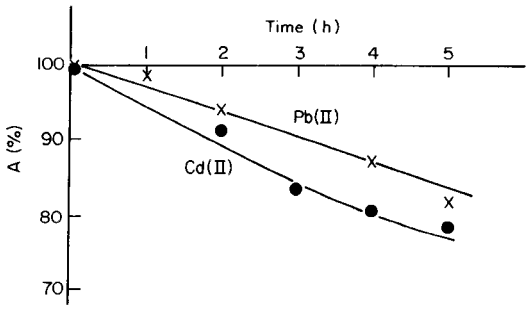

Fig. 1. Change (%) in the activity, A, of lead-210 and cadmium-115 in the upper part (ca. 6 mm) of the centrifugation tube, during ultracentrifugation of the complexes Pb—FA or Cd—FA; OM = 30 mg l^{-1} [Pb(II)] or [Cd(II)] = 10^{-6} M; pH 6.5; rotation speed 40 000 rpm; water No. 50b.

Although this decrease is small, the Svedberg equation made it possible to estimate the molecular weight of the complexes as less than 50 000.

This result was confirmed by the use of Amicon Centriflo filters for the filtration of complexes by normal centrifugation, with ^{210}Pb as tracer. More than 85% of the lead(II) passed through the filter, which indicates that most of the ligands have molecular weights smaller than 25 000.

Gel permeation chromatography

On the basis of these results, preliminary studies were made to fractionate the organic matter with Biogel P10 and P2. Water No. 50b was used without removal of carbonate and without electrolyte; the u.v. absorption of the fractions was measured at 285 nm.

The results obtained with Biogel P10 showed that 42% of the OM had $M_w \leqslant 2000$, whereas 58% was irreversibly adsorbed on the gel. The filtration on Biogel P2 gave two very broad bands which had maxima corresponding to $M_w \approx 1500$ (21%) and $M_w \leqslant 800$ (56%); 22% of OM was irreversibly adsorbed on the gel. These results roughly indicate that the M_w of most fulvic acid (FA) of fresh waters lies between a few hundred and a few thousand. They also indicate that the results are strongly influenced by adsorption phenomena.

It is probable that this effect, which has been mentioned by other authors [17, 18], could be decreased by eluting with an electrolyte solution. However, this would limit the use of the method, for the presence of an electrolyte in the fractions is not always desirable. Moreover, the pH range for the use of the gel is not always very large. Another limitation results from the fact, mentioned by several authors [19—22], that the results of gel permeation chromatography of FA and HA are not always reproducible and depend on the practical conditions used. Probably this is due, at least partly, to association of molecules [22, 23] but it hampers the use of the method.

ULTRAFILTRATION

Because of the broadness of the HA and FA bands in gel permeation chromatography [24], the selectivity of the method is not much better than that of ultrafiltration. However, the ratio of the area of the filtering material to the volume of solution is much lower for ultrafiltration, and so adsorption phenomena should be less important. Finally, gel permeation generally results in dilution of the sample, whereas, in ultrafiltration it is possible to choose operating conditions which result in either dilution or concentration. Moreover, these conditions are more easily controlled in the latter technique. Although ultrafiltration has already been used for the separation of HA and FA [18, 21, 22, 24–28], there is little information on the real influence of important parameters such as the concentrations of HA and electrolyte, the pH and pressure, or the reactivity of HA with "dissolved compounds", on the results of the separation. This paper describes some preliminary results in this field.

The results given above show that most HA and FA in fresh waters have $M_w < 25000$. Hence, the membranes suitable for fractionation are mainly those of the firm Amicon: PM 10, DM 5, UM2 and UM05 which have given cut-off limits of about 10000, 5000, 1000, and 500 respectively [12]. The first three are not charged whereas the fourth is negatively charged. This membrane was studied in detail because it would permit separation of "dissolved compounds" from surface-active or colloidal particles. The experiments were done with the Amicon 12-ml cell or with a 70-ml home-made cell. In the former case, the precision of the values given for the proportions of OM retained on the filter and in the filtrate is no better than 5–10%, because of the high dead volume (0.5–1.0 ml) compared to that of the cell and the difficulty of controlling the volume of the cell (variations ± 1–2 ml). In the following paragraphs, the terms membrane filtration and ultrafiltration, diafiltration and washing technique, retention factor and rejection coefficient, will be used equivalently [11].

The concentration technique

For reasons discussed later, this technique was used mainly with membranes PM10, DM5 and UM05. In this technique, the total volume (cell + filtrate) is kept constant. F_v is the fraction of the total volume in the filtrate, and F_{OM} is the fraction of OM in one of the fractions of the filtrate with respect to the total quantity of OM in the initial solution. F_{OM} is calculated from the absorbance at 285 nm.

The results described below and earlier [15] show that these F_{OM} values give a better idea of the proportions of HA and FA in the fractions than the overall quantity of OM obtained from TOC measurements.

$F_{OM} = f(F_v)$ *curves.* With the concentration technique, the $F_{OM} = f(F_v)$ curve should be a constant in the absence of secondary reactions. Two kinds of curves may be obtained (Fig. 2), depending on the conditions used.

(a) The initial value of Fig. 2a is too low, because of trapping, in the dead space of the cell, of the distilled water used for washing of system; this dilutes

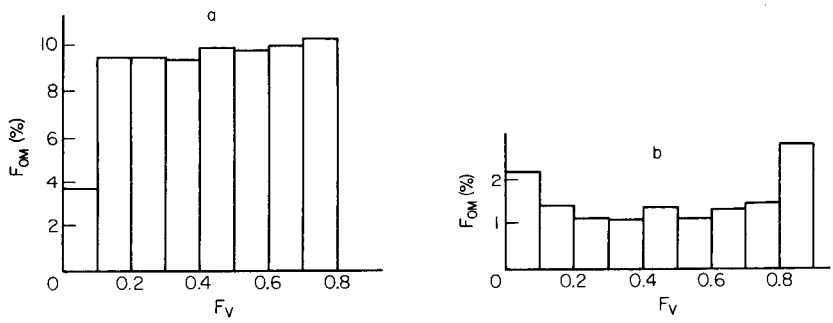

Fig. 2. Fraction of OM, F_{OM}, filtered through PM10 and UM2 as a function of F_V; decarbonated water No. 50c filtered through a 0.2-μm membrane; 12 ml cell; 0.1 M KNO_3. OM: (a) 100 mg l^{-1}; (b) 200 mg l^{-1}.

the first fraction. (b) In some cases, in particular with membranes of low porosit (UM2, Fig. 2b), the dilution effect may be masked by an initial decrease in F_{OM} caused by slow clogging of the filter. This effect is more pronounced when the solution contains a high concentration of high-molecular-weight species retained above the membrane, but can be minimized by using cascade filtration.

Finally, when $F_v > 0.8$, there is usually a sharp increase in F_{OM}, presumably because of the presence of a high concentration of OM in the cell towards the end of filtration. As a rule, it is preferable not to filter solutions containing more than a few g l^{-1} on PM10 and DM5 filters or a few hundred mg l^{-1} on UM2 membranes. For this reason, in the measurements made here, the filtration volume never exceeded 90% of the initial total volume. However, the proportion of OM in the filtrate (or in the cell) was calculated on the assumptions that all of it was filtered and that the OM content in the remaining 10% equalled the mean of the fractions found in the first 90%.

Influence of pressure and pH. Several experiments were performed with water sample No. 50a and the 12-ml cell. The carbonate-free water was filtered through a 0.2-μm filter, and then ultrafiltered through PM10 and UM2 membranes over pressure ranges of 0.5—3.5 atm. for PM10 and 3.0—5.0 atm. for UM2. These measurements were made with solutions containing an initial OM concentration of 0.31 g l^{-1} at two pH values (2.8 and 7.0).

The results showed that, within experimental errors, the pressure has no significant effect for a given pH and membrane. The same results were obtained with water sample No. 50c at pH 5.0 when these membranes were used. The mean values of the OM fractions which passed through the PM10 and UM2 membranes were respectively 67% and 22% at pH 2.8, and 77% and 24% at pH 7.0. A decrease in the fractions passing through the filter with decrease in pH was also observed by Ghassemi and Christman [29] in gel-permeation experiments. Although they interpreted this result by assuming an increase in the size of the molecule with decreasing pH, it might also be due to incipient coagulation at low pH (see below). Anyway, in the present case, this effect

is slight, and is probably insignificant because of the relatively large errors in the proportions (5—10%, see below), particularly in the pH range 4—9.

Influence of electrolyte. In general the presence of electrolyte may affect association of molecules and coagulation of colloids, as well as the electrostatic forces between the molecules to be filtered and the charged layer at the membrane surface caused by concentration polarization. However, the changes in the results for fractionation of water samples 50a and 50b in the presence and absence of KNO_3 (0.1 M) were always smaller than the errors in the proportions of OM in the fractions, irrespective of the membranes used. It should be noted that the initial ionic strength (I) of waters 50a and 50c was proportional to the concentration of OM, with $I = 1.9 \times 10^{-2}$ M for a total OM concentration of 0.1 g l^{-1}.

The washing technique

Evaluation of the retention factor. The cell volume was kept constant and the flushing solvent (distilled water) was adjusted to the same pH as the sample solution. For this type of experiment, eqn. (1) will hold for any compound [11]:

$$\ln (c_c/c_o) = -R\ (V/V_0) \qquad (1)$$

where c_0 and c_c are the sample concentrations in the cell before and after washing with a volume V; V_0 is the constant initial sample volume in the cell, and R is the retention factor which depends on the membrane used and on the structure of the filtered compound. R is representative of the rate of filtration of a given compound, approaching unity if the compound is not retained and zero if it is completely retained. Now $c_c V_0 = c_0 V_0 - \sum_i c_i V_i$, where c_i and V_i are the concentration and volume of the i^{th} fraction of the filtrate. Combining this with eqn. (1) gives

$$\ln(1 - \sum_i V_i c_i / V_0 c_0) = \ln(0.01\ F_c) = -R(V/V_0) \qquad (2)$$

where $V = \sum_i V_i$ and where F_c is the fraction of the compound left in the cell (in %) after washing with a volume V of solution. Hence, the retention factor R can be evaluated by plotting the left-hand term against V/V_0, and this allows quantitative comparison of the filtration properties of various compounds through a given membrane.

Several compounds with different molecular weights and structures were used in washing experiments to test eqns. (2), to estimate the cut-off level of molecular weight for UM05 membranes and to compare their behaviour with those of FA and HA. The concentrations of the compounds in the different filtered fractions were measured in each case and plotted against the volume V used for washing. These compounds were chosen because either they are present in natural waters or might have a structural resemblance to FA.

Measurements of R. Figure 3 shows that eqn. (2) is obeyed for pure solutions of citric acids and glycine. The same result was obtained with Ca^{2+}, HCO_3^- and glucose. The R values of these compounds are given in Table 1. Except for HCO_3^-, the R values decrease with increase in M_w. The curve in Fig. 3 shows

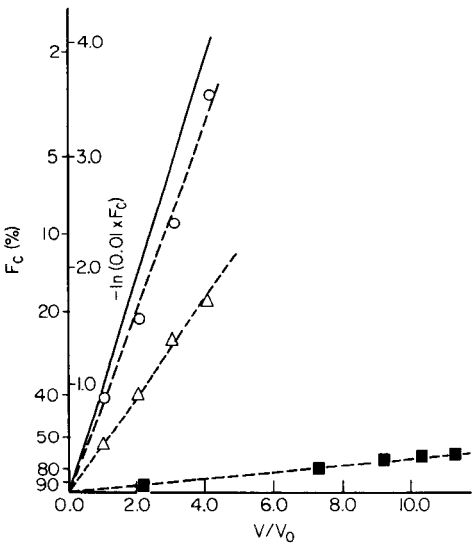

Fig. 3. Rate of filtration of various compounds on the membrane UMO5. Conditions of filtration: see Table 2. (——) Theoretical curve for R = 1. (○) Glycine; (△) citric acid; (■) FA. Water sample 50b; initial concentration, 0.19 g l^{-1}.

that fulvic acids also obey the relation given in eqn. (2) but the filtration rate is very slow compared to that for compounds of $M_w \leqslant 200$. For $V/V_0 = 4$, about 88% of FA remains in the cell which corresponds well to the mean value obtained in the next paragraph for the filtration of compounds with $M_w > 250$. The R values of the FA for a series of waters are given in Table 1. In comparing these values, it must be remembered that all the samples were previously filtered on 0.2 μm, 0.035 μm and PM10 filters. Hence these values of R are representative only of the low-molecular-weight fraction of the OM of these waters ($M_w < 10\,000$). The effect of the initial concentration on the filtration is discussed in the section dealing with the use of ultrafiltration for characterization. However, the results in Table 1 show that in all cases, these compounds behave as if their molecular weight were higher than 250.

Determination of the cut-off level of molecular weight for UMO5 membrane. Table 2 and Fig. 4 give the fraction F_c (%) of various compounds left in the cell after washing with a volume V of the solvent, where $V/V_0 = 4$ in most cases. Figure 4 shows quite clearly that regardless of the structure of the compound, the cut-off level (F_c = 50%) is about 210. This is in accordance with the value found by Ogura [26]; in Ogura's work, the cut-off level was less clear-cut than in the present work, probably because Ogura used the concentration technique which gives a higher value for the OM in the filtrate, particularly at the end of the filtration (see above). Table 2 also shows that pH has very little effect on the results, at least for compounds having molecular weights well above the cut-off limit.

TABLE 1

Values of R for different waters filtered on UMO5 membrane by the washing technique[a]

Compound filtered or water sample no.	R	Initial concentration of the filtered solution ($g\ l^{-1}$): c_0
Ca^{2+}	0.85	0.4
HCO_3^-	0.47	0.61
Glycine	0.85	0.73
Glucose	0.57	0.18
Citric acid	0.45	0.19
10	0.064	0.44
11	0.015	0.80
21	0.082	0.16
22	0.058	0.48
24	0.041	1.33
32	0.14	0.24
41	0.0076	1.95
50a	0.011	2.82
50a	0.055	0.57
50a	0.091	0.43
50b	0.064	0.19
S0	0.0015	5.65
S2	0.033	0.11
S3	0.052	0.105
S4	0.25	0.108
F3	0.093	0.12
F1	0.156	0.13

[a]A regression line may be drawn through the plot $\log R = f(\log c_0)$ obtained with the values of the samples 10—50 a,b, S0—S4, F1 and F3. The corresponding slope and correlation coefficient are -0.9 ± 0.3 and -0.88 respectively.

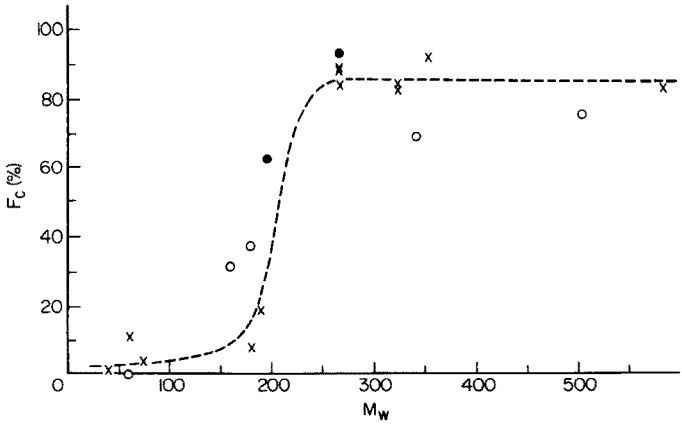

Fig. 4. Fractions of the compounds retained on UMO5 as a function of molecular weight. Conditions as for Table 2. Values obtained: (×) in this work by the "washing" technique; (•) in this work, by the "concentration" technique, (○) by Ogura [26].

TABLE 2

Determination of the cut-off level of the UMO5 membrane. (Unless otherwise stated, the washing technique with a 12-ml cell with a constant volume of solution of 5 ml was used for filtration.)

Compound	M_w	pH	Initial concn. (M)	Total washing volume (ml)	F_c (%)
Ca^{2+}	40	7.0	10^{-2}	20	1
Urea[a]	60	—	2.5×10^{-4}	—	0
HCO_3^-	61	8.0	10^{-2}	20	11
HCO_3^-	61	8.0	10^{-2}	25	3
Glycine	75	7.0	10^{-2}	20	4
Alloxan[a]	160	—	6.2×10^{-5}	—	32
Glucose	180	7.0	10^{-3}	20	8
Glucose[a]	180	—	4.2×10^{-5}	—	38
Citric acid	192	3.0	10^{-3}	20	19
Dopamine[b]	197	7.0	10^{-3}	—	63
Tiron[b]	268	3.0	10^{-3}	—	94
Tiron	268	7.0	10^{-3}	20	89
Tiron	268	9.0	10^{-3}	20	90
Tiron	268	13.0	10^{-3}	20	85
Alizarin complexone	325	3.0	10^{-4}	20	86
Alizarin complexone	325	7.0	10^{-4}	20	84
Sucrose[a]	342	—	2.1×10^{-5}	—	70
Phenol red[b]	354	9.0	10^{-4}	—	93
Raffinose[a]	504	—	1.4×10^{-5}	—	77
Bilirubin	585	7.0	10^{-5}	20	85
Bromothymol blue[b]	624	7.0	10^{-5}	—	77
Bromophenol blue[b]	670	7.0	10^{-5}	—	86

[a]Results of Fig. 3 of ref. 26: filtration by the concentration technique, 200-ml cell used.
[b]Filtration by the concentration technique.

Separation of FA and HA from the low-molecular-weight compounds of waters

The results described above, may be summarized as follows with regard to the separation of FA and HA from other constituents of waters. First, as u.v. absorbance at 285 nm seems to be relatively representative of FA and HA in unpolluted fresh waters [15], the results obtained above show that the molecular weights of these compounds always exceed 250. As the separation limit of the membrane UMO5 is ca. 210, this membrane is very useful for the separation of FA and HA from dissolved low-molecular-weight compounds (LMWC; $M_w < 200$). However, adsorption effects (see below) can be quite large if samples containing high-molecular-weight compounds are filtered directly through membranes with fine pores. In such cases, reproducible results can be obtained only by cascade filtration with several filters. Moreover, because of the possibility of adsorption, molecular association and/or coagulation phenomena during the filtration, the concentration technique is not recommended especially if the OM content retained in the cell is high (more than a few hundred milligrams). In contrast, factors such as pH, pressure and electrolyte concentrations seem to play a minor role.

Finally, for all the fresh waters studied by ultrafiltration in this paper, the following observations were made: (i) PM10 and DM5 membranes behave similarly; (ii) most of the FA and HA are retained between PM10 and UMO5; (iii) UM2 and UMO5 membranes behave similarly, as is also seen in Fig. 1 and ref. [24]; (iv) the reproducibility of the washing technique is always better than that of the concentration method.

Accordingly, the best and fastest method for separating HA and FA from LMWC seems to be to filter the water samples through 0.2 μm, 0.035 μm and PM10 filters arranged in cascade by means of the concentration technique and then to filter the filtrate of PM10 by the washing method with UMO5 membrane. In the latter step, the results obtained above for R show that for $V/V_0 = 5$, about 85% FA and 10% LMWC are retained, while for $V/V_0 = 10$, the percentages retained are 75 and 1%, respectively. Thus, depending on the aim of the work, a compromise has to be made as to which ratio should be chosen.

Separation of FA from inorganic ions. It must be borne in mind that these percentages are based on results obtained with pure solutions. To establish the efficiency of the separation, a detailed investigation must be made with systems containing mixtures of LMWC and FA. The association of FA with LMWC may modify completely the results obtained previously [30], as has indeed been reported for inorganic ions [21, 24, 27]. The same effect was observed here for Mg^{2+} ions; for some of the water samples listed in Table 1, magnesium was determined in the fractions of the filtrate obtained from UMO5 by the washing technique.

Plotting log (c_c/c_0) vs. V/V_0 [eqn. 1, with c_c and c_0 as the concentrations of Mg(II)] gave non-linear curves. The highest values of R were calculated from the slopes of the tangents to the curves at $V/V_0 \rightarrow 0$. However, these values of R were of the order of 0.2, which is much lower than that expected for compounds which are not retained (see Ca^{2+} in pure solution, Table 1).

In addition, it was not possible to separate FA from Fe(III), Al(III), Cu(II), Pb(II) and Zn(II), by washing (with distilled water) samples previously acidified to pH 2. In all cases, the ratios of metal to OM found in the cell were similar before and after the filtration; $V/V_0 = 5$ was used for these experiments.

In further tests, water sample 24 acidified to pH $\approx$ 2 with perchloric acid was filtered on 0.2 μm, 0.035 μm and PM10, and washed with 10^{-2} M $HClO_4$ on UMO5. Values of R calculated for Fe(III), Ca(II), and OM (from absorbance measurements) were found to be 0.39, 0.37, and 0.055, respectively, for $V/V_0 \leqslant 5$. The behaviour of Ca^{2+} was similar to that of Mg^{2+} in the experiments reported above. These results also showed that, after washing with a volume V corresponding to $V/V_0 = 10$, 90% of Ca(II) and Fe(III) were eliminated from the solution in the cell, and 27% of OM passed through the membrane.

These results indicate that separation of FA from metals is possible by washing the water with acid. However, the elimination of more than 80—90% of the metals seems to be difficult, because this would require a high value of V/V_0, which leads to a significant loss of FA. Moreover, washing takes a long time for high values of V/V_0: 16 h was necessary for $V/V_0 = 10$. In a further experiment, water 24 was filtered first on 0.2 μm, 0.035 μm and PM10

immediately after acidification to pH 2, and then filtered again on the same membranes 16 h later; 25% of OM was retained, mainly on PM10, in the second filtration. This was probably due to a slow flocculation process, which may cause additional adsorption problems, if it occurs during the filtration on UMO5.

It must be pointed out that the same considerations would perhaps apply to the separation of low-molecular-weight FA ($M_w < 10\,000$) from the higher-molecular-weight compounds, because FA may react with some of them.

USE OF ULTRAFILTRATION FOR CHARACTERIZATION OF ORGANIC MATTER IN WATER

The cascade system of ultrafiltration can be used as a means of characterizing the OM by measuring the proportion of OM retained between the various membranes. The above paragraphs indicate that the reproducibility is dependen on that of the membrane used, on the concentration of the solution and on the filtration technique.

Appraisal of the reproducibility of the results

To test the reproducibility of the membranes, six experiments were carried out with cascade filtration systems. The membranes used were successively: 8 μm, 0.2 μm, 0.1 μm, PM10 and UM2. Concentration techniques were used in all these cases and all the membranes were changed after each filtration, except for UM2 and PM10 which were changed after every three filtrations. To remove any OM which might have been adsorbed on the surface, these two membranes were soaked after each filtration and left to stand overnight in 5×10^{-3} M NaOH and then rinsed with distilled water. The 12-ml cell and water sample 50a containing 0.3 g OM l^{-1} were used with 0.1 M $NaNO_3$ as the electrolyte.

These results together with those obtained for the effect of pH and pressure with the PM10 and UM2 membranes and the results obtained with UMO5 membranes, showed that the reproducibility obtained by using the same membrane several times is similar to that obtained by changing the membranes, provided that the filtering layer is undisturbed. However, this layer may easily be wrecked during conditioning of the membrane for re-use. This is not always noticeable to the naked eye but it causes a very large increase in the OM found in the filtrate. Since there is no means of checking this effect when the compound is unknown, new filters should be used for each filtration.

From the results obtained above (see also Fig. 4 for UMO5), the error in evaluating the proportions of OM with PM10 and UM2 was estimated to be about 5% (absolute value) for low proportions of OM and 10% for high proportions of OM. This error includes the error made in volume measurements. As will be seen, the total error can be minimized by using low concentrations of OM, the washing technique and the cell with larger volume. However, since the membrane itself is the chief source of error, a really significant decrease in the overall error seems improbable.

Role of the concentration of OM and the filtration technique used.

The results of cascade filtration for water sample 50a under various conditions are given in Table 3. In all cases, the concentration technique was used for filtration except for the results given for UMO5 in column 4. In this case, $V/V_0 = 5$ was used and no electrolyte was added. All the values reported are

TABLE 3

Results of fractionation (%) of water No. 50a
(12-ml cell for columns 1, 2, 3; 70-ml cell for column 4. For columns 2 and 4, the mean values obtained, respectively, with 5 and 3 filtrations are reported. No electrolyte was added to the solution. For the filtration technique: see text.)

Column No.	1	2	3	4
Initial concentration (mg l^{-1})	20	300	900	900
Membrane		3		
8 μm	0			8
		5		
0.2 μm				
		8		
0.035 μm ($M_w \approx 10^6$)	0		19	10
		2		
PM10 ($M_w \approx 10^4$)				
	36	55	50	
UM2 ($M_w \approx 10^3$)				69
	19		29	
UMO5 ($M_w \approx 210$)		30		
	44		2	13

given as the ratio F(in %) of OM in a given fraction to the total concentration of OM present initially in the solution, and were measured by determining the absorbance at 285 nm. As the error in F is fairly large, only variations greater than 8—10% have real significance. With the exception of UMO5, all the molecular weight cut-off levels for different membranes were taken from the Amicon Catalogue [11]. Similar results were obtained for water samples 41 and 24.

Table 3 makes it possible to compare the influences of the initial concentration of OM in the solution (columns 1, 2 and 3) and of the filtration techniques (columns 3 and 4). For a given water sample and a given filtration technique, an increase in the initial OM concentration causes an increase in the high-molecular-weight fractions (HMWF) and a decrease in the low-molecular-weight fraction (LMWF) of the OM. The R values given in Table 1 support this statement. Although part of the variation in R observed for different waters may be due to different FA structures in these waters, the values in Table 1 (see footnote) indicate that R is almost inversely proportional to the initial concentration of FA in the filtrate. Furthermore, this is confirmed by the values of R obtained with the same water (50a) for three different initial concentrations of FA.

Results similar to those of Table 3 but obtained with other waters showed that the initial OM concentration always affects the results, but that the magnitude of the effect depends on the nature of the water. In any case, this factor has to be taken into account in order to obtain reproducible results.

A comparison of the results in columns 3 and 4 of Table 3 indicates that, under these conditions, the difference between the results obtained by the concentration and washing techniques is significant but not high. However, the results obtained for a wide range of waters have shown that the washing technique gives more reproducible results than the concentration method; probably because, with the former method, the concentration in the cell remains more or less constant, whereas with the latter method, the concentration increases up to ten times during the experiment.

After an experiment, the membranes were sometimes coloured, showing that part of the OM had been adsorbed. The values given in Table 3 were obtained from absorbance measurements of the filtrate and the initial solution. Hence, the values given for the unfiltered fractions include the OM fraction adsorbed on the membrane. The results obtained for the amount of OM adsorbed, as estimated from other results, indicated that adsorption occurs essentially on the UM2 and UMO5, up to 30% of the initial OM being adsorbed in some cases. The actual value seems to depend more on the nature of the water rather than on the initial concentration. For a normal fresh water, an average 15% of OM is adsorbed in UMO5.

Comparison of the fractionation of various types of water

The results obtained by the cascade ultrafiltration system for natural fresh waters (nos. 10—50 a: type I), interstitial peat water (no. 41: type III), water

extracts of soils (nos. S0—S3: type II) and aqueous solutions resulting from the decomposition of leaves (nos. F1—F4: type IV) are given in Tables 4 and 5. The concentration technique was applied in all cases except those indicated in the Tables by vertical double lines for which the washing technique was used. As before, the proportions of OM in each fraction were determined by absorbance measurements at 285 nm (Table 4). For each fraction, the ratios A/TOC and F/TOC are reported in Table 5, where A is the absorbance, TOC is total organic carbon and F is the maximum fluorescence intensity in arbitrary units; all fluorescence measurements were made at the maximum emission and excitation wavelengths (about 450 nm and 350 nm, respectively [15]).

The distribution of FA and HA in the different fractions (Table 4) shows that, on the whole, for the same type of water, the mean molecular weight of the organic matter is similar and decreases in the order: IV $\geqslant$ III > II $\simeq$ I. Indeed, the possible enrichment of FA compared to HA in water sample during the conservation period should be taken into account (see Experimental). The values for samples 10—24 and 50a can be corrected for this effect by using a mean value of 20% for the decrease in total OM [15] and by taking into account the fact that this decrease is probably mainly due to the disappearance of the high-molecular-weight compounds (M_w > 10 000).

The values obtained in this way for water samples and those for water extracts from soils are very close to each other, which suggests that an important fraction of FA in fresh waters may come from the leaching of the soils by rain water. The mean value of M_w for the OM of peat water is much higher,

TABLE 4

Proportions (%) of the OM retained in the various ultrafiltered fractions calculated from absorbance measurements at 285 nm.
(100% = OM ultrafiltered on 0.2 μm.)

Water	Proportions of OM in the fractions[a]			
	(0.2 μm)	(0.035 μm)	(PM10: $M_w \approx 10\,000$)	(UMO5: $M_w \approx 210$)
10	3.0		81.1	12.0
11	1.0		70.2	15.0
21	6.7		71.7	13.7
22	0.0		67.5	20.8
24	20.1		28.2	20.7
41	44.8	33.4	17.2	4.6
50a	10.9		75.0	14.1
S0	7.7		57.0	23.0
S1	18.8		56.5	9.9
S2	9.5		29.5	20.9
S3	17.2		46.0	18.2
F1	65.0	15.0	15.0	5.0
F2	55.0	0.0	3.0	
F3	60.0	10.0	10.0	5.0
F4	75.0	0.0	10.0	

[a]The nature of the membrane is given in brackets.

TABLE 5

Values of the A/TOC and F/TOC ratios for various ultrafiltered fractions (TOC in g l^{-1}; fluorescence intensity (F) in arbitrary units; A in absorbance units.)

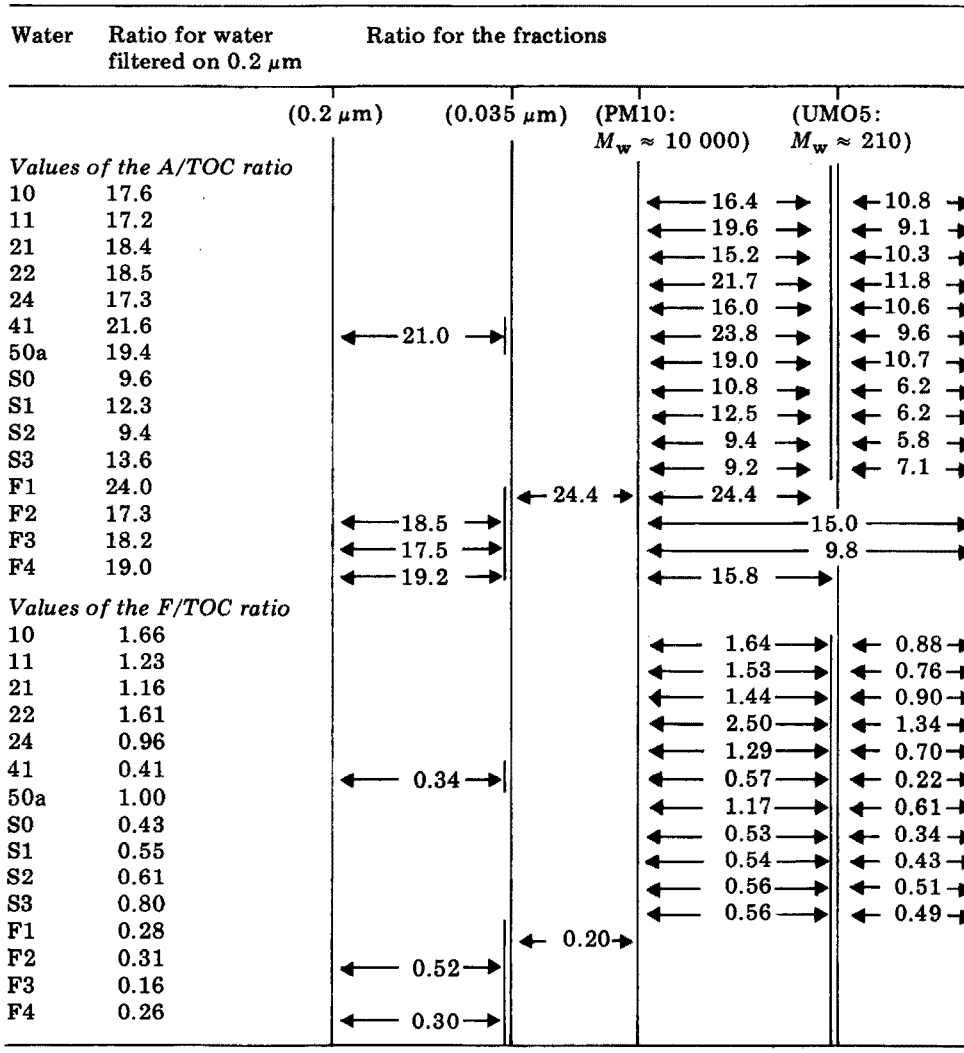

which shows that this kind of water is not a good model for HA and FA of "normal" surface waters.

Although the present results on surface waters are in agreement with those of Ghassemi and Christman [29], there is an important discrepancy with those of Schindler and Alberts [27], Allen [28] and Gjessing [21], who found that most of the OM of surface waters have $M_w > 10\,000$. This might be due to several causes. First, all these authors used UM10 membranes while PM10 membranes were used in the present work. Although the theoretical cut-off limit is 10 000 for both membranes, there is a large difference in the

OM retention from fresh waters (95% on UM10 and 36% on PM10 according to the results of Wilander [24]). Secondly, as the initial concentration of the sample and the filtration technique have significant effects on the final results, it is not possible to make a rigorous comparison when these factors are not known accurately. For example, the high values of M_w observed by Schindler and Alberts [27], compared with the present results, might be ascribed to the fact that they did not use cascade filtration. Finally, as discussed below, the results also depend on the type of water, which should be defined as accurately as possible.

From Tables 4 and 5 it can be seen that, for a given water, the A/TOC ratio is constant for $M_w > 210$, but decreases for the fraction for which $M_w < 210$. This indicates that phenolic compounds are retained while the small non-absorbing aliphatic compounds pass through the UMO5 membrane. The F/TOC ratio behaves similarly to the A/TOC ratio, which indicates that the fluorescence properties observed in waters rich in organic matter are really related to the fulvic or humic substances of these waters.

These results, along with those of other studies [15, 16], show that for similar type of waters or water extracts, the properties of the OM are similar. Thus it can be inferred that the results of detailed studies on one water will give not only the characteristics of that water, but also those of other waters of the same type. Thus waters 10—22 and 50 are typical eutrophic surface waters with high OM contents (3—15 mg C l^{-1} in the untreated waters) but not situated in a peaty region. Water 24 (10 mg C l^{-1}) was sampled in a very eutrophic pond located in a peaty region, and sample 41 was an interstitial water (ca. 45 mg C l^{-1}) from pure peat. It is clear that the mean M_w of the OM of these waters increases in this order. Hence, from the point of view of the properties of the organic compounds, such as their size or their complexing ability [15], the surface fresh waters could be divided, roughly, into three classes: non-eutrophic waters containing mainly debris of recently decomposed living organisms, eutrophic waters containing mainly fulvic and humic-like compounds, and peaty waters. The values of A/TOC, and F/TOC (Table 5) could be useful parameters for the determination of the type of an unknown water.

On this basis, if the type of water studied is specified, it seems to the authors that the difficulties encountered in attempts to characterize the properties of the OM of one type of water lie much more in the absence of careful and standardized use of analytical methods than in the diversity of waters used by the various workers.

CONCLUSION

The results described here indicate that the most useful membranes for ultrafiltration of organic matter in natural fresh waters are the Amicon membranes UMO5, UM2 and PM10 (or their equivalents). Factors such as the electrolyte concentration, the pressure and even the pH do not seem to have

any great effect on the ultrafiltration results provided that extreme conditions are not used.

However, the results depend greatly on the interactions of the organic matter:

(a) with other dissolved molecules or colloidal particles, making the separation more difficult;

(b) with the membrane, because of its adsorbent properties, thus modifying the filtration and causing losses in the separation step;

(c) with each other to form aggregates (or association products) as mentioned by other authors [6, 18, 22, 23]. This phenomenon also modifies the results of fractionation but seems to be reversible in freshly concentrated waters. This association process is supported by the fact that flocculation of concentrated solution of FA and HA (ca. 1 g l^{-1}) occurs after certain periods (often 8—12 months). Other results [2, 15] also seem to confirm this association process for solutions with concentrations greater than 80 mg l^{-1}. This might be one reason for the lack of reproducibility reported by some authors who used gel permeation chromatography for the separation [20].

In any case, the reactivity of HA and FA in the separation seems to be the most important factor in obtaining irreproducible results. The separation process invariably leads to a modification of chemical factors inside the cell which in turn may modify the reactivity and properties of the compounds under study. Thus a good method of separation can be developed only if the properties of these compounds are sufficiently known. As the converse is also true, the two problems must be studied in parallel.

We thank particularly J. Malleviall, J. Ph. Buffle and A. Devillers (Société Lyonnaise des Eaux et de L'Eclairage, Le Pecq, Paris) and their collaborators for providing water samples 50 abc and concentrating them and for their kind assistance in the concentration of other fresh waters. We also thank H. Häni (Station Fédérale de Recherches en Chimie agricole et sur l'Hygiène de l'Environnement, Liebefeld/Berne) and P. Blaser (Institut Fédéral de Recherches forestières, Birmensdorf/Zürich) for providing soil extracts and aqueous solution of decomposed leaves, respectively, and P. Burkard (Service des Eaux de Genève) for his kind assistance in TOC measurements. The financial assistance provided by the Swiss National Foundation for Scientific Research (project 2.587 - 0.76) is gratefully acknowledged.

REFERENCES

1 W. Stumm and P. A. Brauner, in J. P. Riley and G. D. Skirrow (Eds.), Chemical Oceanography 2 edn., Academic Press, London, 1973.
2 J. Buffle, Lecture at EUCHEM Conference, Lerum (Suède) (1977).
3 J. Buffle, A. Cominoli, F-L. Greter and W. Haerdi, Proc. Anal. Div. Chem. Soc., February 1978, 59.
4 P. L. Brezonik, P. Brauner and W. Stumm, Water Res., 10 (1976) 605.
5 E. S. K. Chian and F. B. De Walle, Environ. Sci. Technol., 11 (1977) 158.

6 M. Schnitzer and S. U. Khan, Humic Substances in the Environment, M. Dekker, New York, 1972.
7 J. Mallevialle, Les Agents Complexants Naturels des Eaux, Thèse No. 451. Université P. Sabatier de Toulouse, 1974.
8 J. M. Serra and G. T. Felbeck Jr., in D. Povoledo and H. L. Golterman (Eds.), Humic Substances, Their Structure and Function in the Biosphere, Centre for Agricultural Publishing and Documentation Wageningen, 1975, p. 311.
9 E. T. Gjessing, T. Gjerdahl in ref. [8], p. 43.
10 H. Morita, Geochim. Cosmochim. Acta, 37 (1973) 1587.
11 Amicon Ultrafiltration Publication Nos. 426V and 427.
12 N. H. Furman, G. H. Morrison and A. F. Wagner, Anal. Chem., 22 (1950) 1561.
13 E. Hultman, Nature, 183 (1959) 108.
14 J. R. Marier and M. Boulet, J. Dairy Sci., 41 (1958) 1683.
15 J. Buffle, P. Deladoey and W. Haerdi, (a) Etude de caracterisation et de comparaison des propriétés des matières humiques et fulviques de différentes eaux. (b) Application d'un systeme de titration automatique à la mesure de la complexation du cuivre par les substances fulviques et humiques et interpretation des résultats. Rapports sur le projet No. 2.587—0.76 du F.N.S.R.S.
16 J. Buffle, F. L. Greter and W. Haerdi, Anal. Chem., 49 (1977) 216.
17 W. Wildenhain and G. Henseke, Fresenius Z. Anal. Chem., 229 (1967) 271.
18 E. T. Gjessing, Physical and Chemical Characteristics of Aquatic Humus, Ann Arbor Science Publishers, Ann Arbor, 1976.
19 J. Ph. Buffle, Recherche, Dosage et Elimination des Matières Organiques Naturelles Contenues dans les Eaux Destinées à l'Alimentation", Rapport de la Société Lyonnaise des Eaux et de l'Eclairage, 1974.
20 H. Söchtig, in ref. [8], p. 321.
21 E. T. Gjessing, Schweiz. Z. Hydrol., 35 (1973) 286.
22 E. T. Gjessing, Schweiz. Z. Hydrol., 33 (2) (1971) 592.
23 D. S. Orlov, Y. M. Ammosova and G. I. Glebova, Geoderma, 13 (1975) 211.
24 A. Wilander, Schweiz, Z. Hydrol., 34 (1972) 190.
25 E. T. Gjessing, Environ. Sci. Technol., 4 (1970) 437.
26 N. Ogura, Mar. Biol., 24 (1974) 305.
27 J. E. Schindler and J. J. Alberts Arch. Hydrobiol., 74 (4) (1974) 429.
28 H. L. Allen, Oikos, 27 (1976) 64.
29 M. Ghassemi and R. F. Christman, Limnol. Oceanogr., 13 (1968) 583.
30 W. F. Blatt, S. M. Robinson and H. J. Bixler, Anal. Biochem., 26 (1968) 151.

Analytica Chimica Acta, 101 (1978) 359—365

THE DETERMINATION OF NITROFURANTOIN AND SOME STRUCTURALLY RELATED DRUGS IN BIOLOGICAL FLUIDS BY HIGH-PRESSURE LIQUID CHROMATOGRAPHY

H. ROSEBOOM* and H. A. KOSTER

Farmaceutisch Laboratorium der Rijksuniversiteit te Utrecht, Catharijnesingel 60, Utrecht (The Netherlands)

(Received 21st April 1978)

SUMMARY

A method for the determination of therapeutic concentrations of nitro-furantoin in plasma and urine is described; after extraction of the drug and the internal standard (2,6-dinitrophenol), the extract is concentrated and injected onto a reversed-phase chromatographic system. A blank chromatogram shows no interfering peaks when detection is carried out at 365 nm. The limit of detection (ca. 10 ng ml^{-1} for a 1-ml plasma sample) is about two orders of magnitude better than with existing methods. Some structurally related drugs can be extracted, chromatographed, and determined in the same way.

Since its introduction in 1952 nitrofurantoin has been widely used for the treatment of urinary tract infections. The bio-availability of this drug from different formulations has had to be evaluated from urinary excretion data because of the lack of sensitivity of the available analytical methods, e.g. the nitromethane—hyamine method, as described by Conklin and Hollifield [1] and modified by Mattock et al. [2], or the polarographic methods [3—6]. The limit of detection in these methods varies from 0.5 to 2 $\mu g\ ml,^{-1}$ which is about the maximum blood level after oral administration of therapeutic doses [2].

There is a need for a sensitive assay for nitrofurantoin in plasma to permit a better evaluation of the pharmacokinetics and pharmaceutical effects of this drug, as only 40% is excreted unchanged in urine [7]. Moreover, there is a significant risk of neuropathy in patients receiving nitrofurantoin [8] when their glomerular filtration rate is somewhat low. In those cases it is advisable to monitor the drug concentration in plasma and urine simultaneously. The biological half-lives of drugs, as determined from urinary excretion data, can differ significantly [9] from those obtained from plasma level data, and this might indicate a significant accumulation of drug in the renal tubular membrane resulting in interference by drug molecules in the integrity of the membrane structure.

The method described in this paper can measure nitrofurantoin concentrations down to 20 ng ml^{-1} in a 1-ml plasma sample and down to 2 $\mu g\ ml^{-1}$ in urine. The method can also be used to determine other antibacterial agents that are structurally related to nitrofurantoin.

EXPERIMENTAL

Reagents

The reagents used were: methanol, dimethylformamide, glacial acetic acid and nitrophenols (Merck, Darmstadt); dichloromethane (Lamers en Indemans, 's-Hertogenbosch); nitrofurantoin and nitrofurazone (Brocacef, Maarssen); furazolidone (Norwich Chemical Co., Utrecht); hydroxymethylnitrofurantoin (Inpharzam, Amsterdam). All solvents were of reagent grade; deionized water was used throughout.

Liquid chromatography

A Waters ALC/GPC 202 liquid chromatograph, equipped with a model 6000A solvent delivery system, U6K injector, and 440 u.v. absorbance detector was used.

The stainless steel column (30 cm) was packed with LiChrosorb 10 RP 18 (Chrompack, Middelburg). The solvent consisted of mixtures of methanol and water, containing 0.5% of glacial acetic acid; the flow rate was 2.5 ml min^{-1} and the detector was set at 365 nm.

For determination of the capacity factors, the drugs and the nitrophenols were dissolved in aqueous 5% (v/v) dimethylformamide to a concentration of 0.1 mg $ml.^{-1}$ Aliquots (25 μl) of these solutions were injected and chromatographed with various methanol concentrations. In the nitrofurantoin assay, the concentration of methanol in the solvent was 30%.

Extraction efficiency studies

Extraction efficiencies were determined spectrophotometrically with a Perkin-Elmer model 139 spectrophotometer. Known amounts of the compounds were dissolved in 0.5 M phosphate buffers of various pH values. These solutions were extracted with various solvents at various volume ratios. The absorbance of the solutions was measured before and after extraction at λ_{max} for each compound at the particular pH value. The extraction efficiency was calculated as the difference between the absorbances before and after extraction, divided by the absorbance before extraction.

Procedure for nitrofurantoin

To 1 ml of plasma in a centrifuge tube was added 20 μl of a solution of 2,6-dinitrophenol in water (125 $\mu g\ ml^{-1}$), 2 drops of 4 M HCl and 3 ml of a solution of dimethylformamide in dichloromethane (10%, v/v). After mixing on a vortex mixer for 30 s, the tube was centrifuged for 10 min at

3000 rpm and the organic phase was transferred to another tube by filtration through phase-separating paper. The solution was reduced to ca. 100 μl under nitrogen at 40°C in a metal heating block. Aliquots (25 μl) of this solution were injected into the liquid chromatograph. Quantification was carried out by measuring peak height and also peak area with an SP 4000 digital integrator (Spectra Physics, Schijndel).

The procedure was used for urine with minor modifications. Because the concentrations in urine are much higher than in plasma, the urine was diluted 10 times before analysis and the amount of internal standard added was increased to 200 μl.

Standard curves were obtained by adding known amounts of nitrofurantoin to blank plasma or urine and subjecting these samples to the above procedure.

RESULTS AND DISCUSSION

Liquid chromatography

The u.v. spectrum of nitrofurantoin shows two absorbance maxima at 265 nm and 370 nm with molar absorptivities of 17,300 and 13,100 l mol cm^{-1}, respectively. From this point of view the best wavelength for monitoring the eluate seems to be 254 nm. Extracts of blank plasma samples were chromatographed and the eluate was monitored simultaneously at 254 nm and 365 nm; Fig. 1 shows that 365 nm is the wavelength of choice because of the completely clean chromatogram. Consequently, the internal standard should also absorb at this wavelength, and the chromatographic properties of some nitrophenols and some drugs, structurally related to nitrofurantoin, were therefore compared with those of nitrofurantoin. Table 1 gives the capacity factors for these compounds at various methanol concentrations; the other nitrofurans are not well separated from nitrofurantoin and therefore cannot be used as an internal standard, whereas the nitrophenols have quite different capacity factors. The best internal standard for nitrofurantoin is 2,6-dinitrophenol, which is well separated from nitrofurantoin, while its retention time is not too long.

Extraction efficiencies

In order to find the optimal conditions for the extraction of nitrofurantoin from biological fluids, the extraction efficiencies with various solvents at different pH values were determined. The results are given in Table 2. The best result was obtained with ethyl acetate, but as nitrofurantoin was unstable in this solvent, the mixture of dichloromethane/dimethylformamide was chosen. The extraction efficiencies of the potential internal standards were also determined, with dimethylformamide in dichloromethane (10%, v/v) as a solvent (Table 3). At pH values below 6 the extraction efficiency with dimethylformamide in dichloromethane is quite good for the nitrofurans and the nitrophenols; in general, more than 95% is obtained in a single extraction with three times the volume of the aqueous phase.

TABLE 1

Capacity factors k' for some nitrofurans and nitrophenols at various methanol concentrations
(Column, LiChrosorb 10 RP 18; flow-rate, 2.5 ml min^{-1}; u.v. detector, 365 nm. In all cases 0.5% of glacial acetic acid was added to the mobile phase.)

Compound	k'				
	20%	25%	30%	35%	40%
Nitrofurantoin	2.95	1.88	1.23	0.81	0.65
Hydroxymethylnitrofurantoin	2.96	1.85	1.25	0.80	0.62
Furazolidone	3.54	2.25	1.54	1.00	0.79
Nitrofurazone	3.55	2.43	1.55	1.05	0.77
2-Nitrophenol	>10	>10	>10	8.03	5.88
4-Nitrophenol	>10	8.87	6.20	4.43	3.47
2,4-Dinitrophenol	>10	>10	8.12	5.45	4.20
2,5-Dinitrophenol	>10	>10	9.91	6.37	4.83
2,6-Dinitrophenol	8.96	6.48	4.60	3.23	2.50

TABLE 2

Extraction efficiency for nitrofurantoin from buffered solutions with various solvents at a volume ratio of 1 : 1

pH	% Extracted				
	Chloroform	Ether	Ethyl acetate	Chloroform/ isopropanol (95 + 5, v/v)	Dichloromethane/ dimethylformamide (90 + 10, v/v)
2	40	43	93	52	81
4	60	61	93	69	84
6	25	30	90	39	83
8	8	9	48	10	36
10	2	2	10	5	3

TABLE 3

Extraction efficiencies of nitrofurans and nitrophenols with dimethylformamide in dichloromethane (10%, v/v) at various pH values (volume ratio 3 : 1)

Compound	% extracted			
	pH 2	pH 4	pH 6	pH 8
Nitrofurantoin	95	96	95	67
Hydroxymethylnitrofurantoin	94	95	94	65
Furazolidone	98	99	97	98
Nitrofurazone	82	84	84	82
2-Nitrophenol	99	100	100	99
4-Nitrophenol	99	100	99	95
2,4-Dinitrophenol	98	100	81	19
2,5-Dinitrophenol	100	100	99	46
2,6-Dinitrophenol	100	99	60	10

Assay procedure

The addition of two drops of 4 M HCl to 1 ml of plasma or urine resulted in pH values below 4, which is sufficiently low for a good, constant recovery of the compounds from the fluids. The use of phase-separating paper permitted rapid, almost quantitative, transfer of the organic phase from one tube to the other. The blank chromatogram in Fig. 1 shows that this paper does not introduce interfering peaks. With evaporation of the organic phase in a metal heating block under nitrogen at 40°C, the extract cannot be evaporated to complete dryness because of the high boiling point of dimethylformamide. It is possible to evaporate the solvent completely by raising the temperature to 70 or 80°C, but this often resulted in significant degradation of the internal standard. When the temperature was maintained at 40°C, significant degradation of nitrofurantoin nor 2,6-dinitrophenol was never observed, even when the evaporation was continued for several hours. Solutions of nitrofurantoin had to be stored in darkness to prevent degradation of the compound, but solutions of 2,6-dinitrophenol could be stored in daylight for several weeks without degradation.

Figure 2 shows a chromatogram of a plasma sample, spiked with nitrofurantoin to a concentration of 0.5 $\mu g\ ml^{-1}$ and treated as described under Procedure. The symmetrical, well separated peaks and absence of interfering peaks, permit quantification from either peak height or peak area measurements.

The calibration curves for plasma (ranging from 0.02 to 2 $\mu g\ ml^{-1}$) and for urine (ranging from 2 to 200 $\mu g\ ml^{-1}$) were straight lines through the origin. The minimum detectable quantity was ca. 10 ng ml^{-1} of plasma. The standard

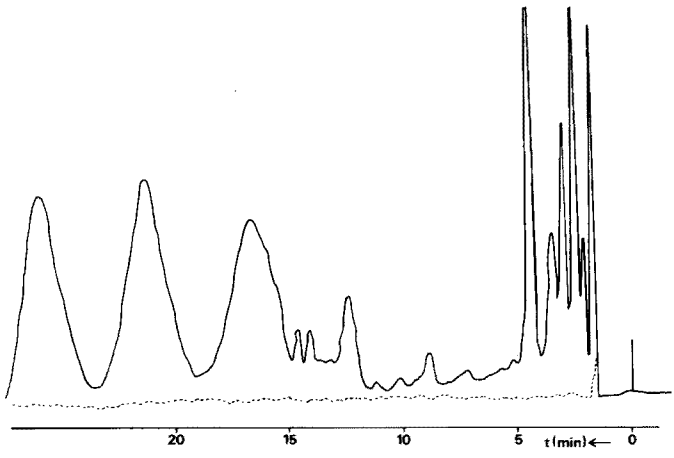

Fig. 1. Chromatogram of a blank plasma sample, treated as described under Procedure, without addition of internal standard. Detection at 254 nm, solid line; detection at 365 nm, broken line. Column, LiChrosorb 10RP18. Solvent, 30% methanol in water containing 0.5% glacial acetic acid; flow, 2.5 ml min^{-1}. Sensitivity, 0.005 AUFS.

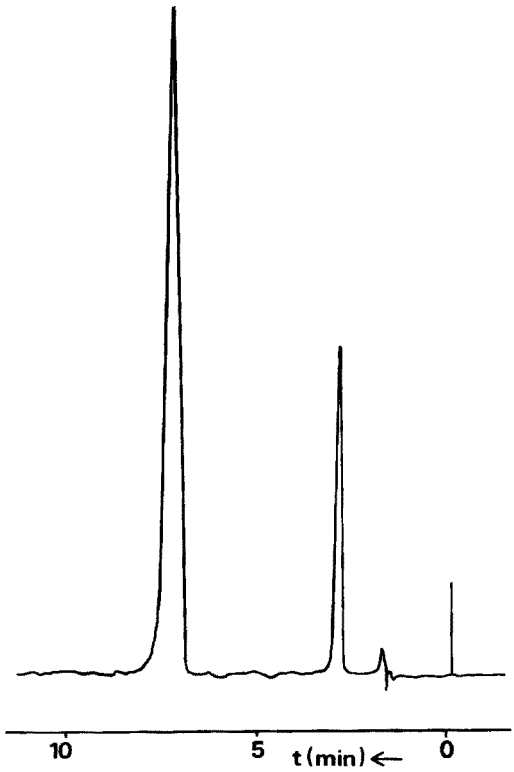

Fig. 2. Chromatogram of a blank plasma sample, spiked with nitrofurantoin to a concentration of 0.5 μg ml^{-1} and treated as described under Procedure. Column, solvent and flow as for Fig. 1. Detection, 365 nm. Sensitivity, 0.01 AUFS.

deviation for the plasma procedure was 8% at the lowest concentrations and 3% at concentrations of 0.1 μg ml^{-1} and higher. For urine, the standard deviation was 3% over the whole range; the day-to-day reproducibility of the slope of the calibration curve was within 5%.

Although only ca. 40% of an administered dose of nitrofurantoin is excreted unchanged, its metabolites have never been definitely identified although metabolism of nitrofurantoin involves reduction to the amino compound and cleavage of the furan ring [10], resulting in disappearance of the characteristic absorption maximum at 370 nm. This means that metabolites of nitrofurantoin do not interfere with the assay; although they may be extracted from acidic medium and have the same retention volume as the internal standard or the parent compound, they would not be detected at the wavelength used.

The chromatographic properties and extraction efficiencies of some other nitrofurans and nitrophenols (Tables 1 and 3) indicate that the procedure can also be used for the determination of these nitrofurans in biological fluids with one of the nitrophenols as an internal standard.

REFERENCES

1 J. D. Conklin and R. D. Hollifield, Clin. Chem., 11 (1965) 925.
2 G. L. Mattock, I. J. McGilveray and C. Charette, Clin. Chem., 16 (1970) 820.
3 H. P. Moore and C. R. Guertal, J. Ass. Offic. Agric. Chem., 43 (1960) 308.
4 B. M. Jones, R. J. M. Ratcliffe and S. G. E. Stevens, J. Pharm. Pharmacol., 17 (1965) 52 S.
5 J. S. Burmicz, W. F. Smyth and R. F. Palmer, Analyst, 101 (1976) 986.
6 W. D. Mason and B. Sandmann, J. Pharm. Sci., 65 (1976) 599.
7 H. K. Reckendorf, R. Castringius and H. Spingler, Med. Welt, 15 (1963) 816.
8 A. I. Jacknowitz, J. L. Le Frock, J. L. Prince and A. Randall, Am. J. Hosp. Pharm., 34 (1977) 759.
9 Y. M. Amin and J. B. Nagwekar, J. Pharm. Sci., 65 (1976) 1341.
10 H. Holmen-Christensen and H. O. Andersen, Acta Pharmacol., 25S4 (1967) 50.

Analytica Chimica Acta, 101 (1978) 367—374

SIMPLE MODE OF ZEEMAN SPLITTING OF ABSORPTION LINES IN ATOMIC ABSORPTION SPECTROMETRY

V. OTRUBA, J. JAMBOR, J. KOMÁREK, J. HORÁK and L. SOMMER*

Department of Analytical Chemistry, J. E. Purkyně University, 61137 Brno (Czechoslovakia)

(Received 30th March 1978)

SUMMARY

Simple equipment is described for exploiting the normal Zeeman splitting of atomic absorption lines in external alternating magnetic fields of various geometry which is suitable for flameless and flame techniques. High-level continuous or background absorption can be eliminated in this way. This is demonstrated for the determination of traces of copper and molybdenum with a carbon rod (Varian CRA 90).

Recently, the Zeeman splitting of atomic lines of selected elements in magnetic fields of various geometry has often been suggested for background elimination in atomic absorption spectrometry (a.a.s.) especially when electrothermal atomization is used [1—10]. In general, the effects of strong, constant and alternating magnetic fields with lines of force perpendicular or parallel to the light beam, on both the emission and absorption line profiles of particular atoms, can be exploited. The effects of the different polarization of the split components or atomic line profile modulation can be similarly applied for analytical purposes. The atomic line is split into three components (π and $\pm\sigma$) by a strong perpendicular magnetic field; the π-component (parallel polarization) does not change in wavelength, whereas the σ-components are polarized perpendicularly and their wavelength is changed in proportion to the field intensity.

Most authors have used the split emission line, measuring analyte absorption with the π-component and the background absorption with the σ-components if they were sufficiently separated [1—4]. The π- and σ-components can be separately monitored by means of rotating polarizers and a phase retardation plate. The splitting of the absorption line by the magnetic field has been less exploited [5—7, 9, 10]. The radiation from the source, chopped by a rotating polarizer, has been alternately absorbed by the differently polarized components of the absorption line under the influence of a steady perpendicular magnetic field. In this way, the vapour absorbs the incident radiation polarized parallel to the magnetic field, whereas the perpendicularly polarized radiation indicates only the background at the σ-component of the absorption line [5, 6, 10]. A Glan polarizing prism can also be used to separate perpendicularly

polarized light into two components after passage through the monochromator. These components are measured by two photomultipliers [10].

In this paper, selective modulation of the absorption line by various types of strong alternating magnetic field is reported. Readily available and home-made modules are used with a carbon rod or a conventional slot burner. The determinations of copper, molybdenum, iron and chromium were selected as models. A similar simple arrangement with a Méker burner and an acetylene—air flame has proved feasible for splitting selected absorption lines of a number of elements [7].

THEORY

An electromagnet fed by a 50-Hz alternating current causes a periodic alternating change in the absorption coefficient of an absorption line. In this way, the amplitude of the transmitted light is modulated by the changes in the magnetic field intensity, but the light emission from the hollow cathode remains constant. Figure 1 shows some schematic absorption profiles changed

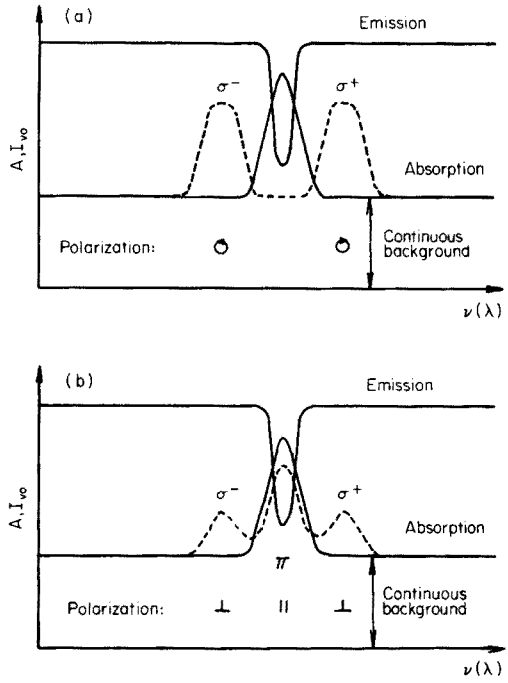

Fig. 1. Interaction schemes of the emission line profile with the modulated absorption line profile in magnetic fields of different geometry. (a) Magnetic field parallel to the light beam; (b) magnetic field perpendicular to the light beam. (——) Absorption profile without magnetic field; (----) absorption profile in magnetic field. A (absorption) relates to absorption mode, and $I_{\nu o}$ to the emission mode.

by magnetic fields perpendicular or parallel to the absorbed light beam. If the amplitude of the light modulation is measured against the concentration of absorbing atoms, the influence of continuous background, source and detector noise and the broad band absorbance of molecules is decreased considerably and the detection limit for particular elements is improved.

The intensity of the absorption line changes with time in a strong alternating magnetic field because its profile is changed by splitting. It is split into three components [$\pi(\Delta M = 0)$ and $\pm\sigma(\Delta M = \pm 1)$] if the magnetic field lines are perpendicular to the monochromatic beam from the hollow-cathode lamp, or into two components ($\pm\sigma$) if the magnetic field lines are parallel to the incident radiation. This is valid for singlet electron transitions in the atom; the transitions studied in this paper are shown in Table 1.

If the alternating photomultiplier output voltage is amplified by a suitable logarithmic amplifier and measured, eqn. (1) is valid:

$$\ln I_{\nu 2} - \ln I_{\nu 1} = (\mathcal{K}_2 - \mathcal{K}_1) N l \qquad (1)$$

where $\mathcal{K}_1$ and $\mathcal{K}_2$ are the atomic absorption coefficients in the medium without and with the magnetic field, N is the number of free atoms in 1 cm^3, l is the absorption path, and $I_{\nu 1}$ and $I_{\nu 2}$ are the intensities of transmitted radiation with and without the magnetic field, respectively; $\ln(I_{\nu 2}/I_{\nu 1})$ is independent of the continuum absorption in the $\nu_2 - \nu_1$ interval and of the incident intensity, $I_{\nu 0}$.

The suppression of inselective absorption and of source and detector instabilities depends on the quality of the logarithmic amplifier. In the present investigations $\Delta I_\nu = I_{\nu 1} - I_{\nu 2}$ was evaluated directly as an alternating component of the current by a selective amplifier tuned to the frequency change of the magnetic field:

$$\Delta I_\nu = I_{\nu 2} - I_{\nu 1} = I_{\nu 0} \exp[(-\mathcal{K}_2 N l) - \exp(-\mathcal{K}_1 N l)] \qquad (2)$$

In this case, the detector signal is no longer independent of the incident light intensity $I_{\nu 0}$, but the influence of inselective absorption is again greatly suppressed though not eliminated. Compared to the classical mode of a.a.s., the error from inselective absorption does not increase with decreasing concentration of analyte and can be further diminished by numerical corrections. A magnetic field parallel to the absorbed beam gives the largest effect on the

TABLE 1

Atomic lines used for Zeeman splitting

Element	Wavelength (nm)	Spectral terms
Chromium	359.35	$^7S_3 - {}^7P_3$
Iron	248.33	$^5D_4 - {}^5F_5$
Molybdenum	313.26	$^7S_3 - {}^7P_4$
Copper	324.75	$^2S_{\frac{1}{2}} - {}^2P_{\frac{3}{2}}$

absorption line [7]. A polarized incident light beam would further improve the separation of split components.

EXPERIMENTAL

Apparatus

Because of difficulties with the generation of an alternating magnetic field parallel to the incident beam, two different magnets were constructed. One with flat pole adapters positioned along the flame (field perpendicular to the beam) was used for flame studies. The other with a single pole had a scattered magnetic field in the middle of which the carbon rod was situated. It had a local field intensity of ca. 0.3 Tesla (cf. Fig. 2).

The equipment for the Varian CRA-90 carbon rod studies is shown schematically in Fig. 2. The unmodulated light beam from the hollow-cathode lamp was focused by a u.v. achromatic lens (f = 78.5 mm) into the orifice of the carbon rod mini-furnace over which the pole adapter of the electromagnet was situated and fed by 8 A a.c. at 220 V and 50 Hz. It produced an absorption line profile modulation at 100 Hz. The transmitted radiation was focused by a second identical lens onto the entrance slit of the SPM-2 monochromator (C. Zeiss, Jena, DDR) which has a grating (651.5 lines mm^{-1}) working in the second order. A photomultiplier (FVC 52A, C. Zeiss, Jena), magnetically-shielded, served as detector behind the exit slit of the monochromator, for which the voltage was taken from a 750-V dry plate anodic battery (Leclanché). The d.c. photocurrent was measured by a d.c. picoammeter (Tesla BM 483), and the alternating component by a selective nanovoltmeter (types 208 or 230, Unipan, Poland) as a voltage across a 1 MΩ loading resistance. A strip-chart recorder (Toschin Electron, Japan) was connected to the nanovoltmeter output.

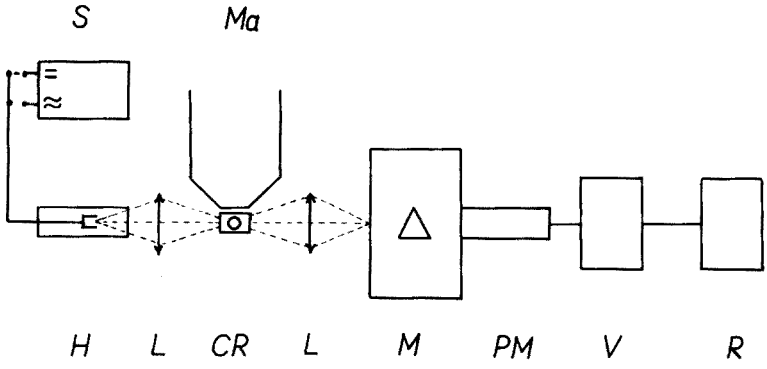

Fig. 2. Schematic diagram of the equipment used for the carbon rod in the magnetic field; S, power source; H, hollow-cathode lamp; L., u.v. achromatic lens; CR, carbon rod; Ma, single-pole electromagnet; M, monochromator; PM, photomultiplier; V, nanovoltmeter; R, recorder.

The hollow-cathode lamp was fed by d.c., i.e. without modulation, during the Zeeman splitting. The 100-Hz field modulation of the absorption line profile was measured only at the photomultiplier output. For checking responses in the conventional single beam mode, the lamp was fed by d.c. with 385-Hz sine modulation, with the peak current equal to the d.c. supplied to the lamp in the field modulation experiments. No magnetic field was used in this case.

The equipment for the flame studies was as follows. A single-slot, 10-cm burner was situated between the pole adapters on an electromagnet producing field lines perpendicular to the beam. The burner and nebulizer were from a Perkin-Elmer Model 306 spectrometer. The magnet was fed by 16 A at 380 V and 50 Hz, giving a peak magnetic field intensity of 0.6 Tesla between the poles. The electrical and optical arrangement was as described above, but with lenses of 150-mm focal length.

RESULTS

Determination of copper and molybdenum with the carbon rod

The optimal instrumental parameters are given in Table 2. Calibration plots for 2—60 μg Cu ml^{-1} were obtained for various media giving a strong continuum absorption, by both conventional and Zeeman splitting measurements. The absorption peaks obtained for samples 0.1 M in NaCl and 0.01 M in HNO_3 are compared in Fig. 3. The suppression of inselective absorption is very effective but a small negative signal appears in the presence of sodium chloride coming from the alternating component of the increase in continuum absorption as a result of the Fourier expansion. This can be compensated electronically but usually does not interfere because it is shifted in time with respect to the copper signal. As eqn. (2) was used for the evaluation of ΔI_v during the Zeeman splitting, the analyte sensitivity depends on the residual background level for solutions with a large continuum absorption. The value of the analyte signal can be corrected for the sensitivity change if the value

TABLE 2

Optimal instrumental parameters for the carbon rod experiments

Parameter	Element	
	Cu	Mo
Wavelength (nm)	324.75	313.26
Lamp current (mA)	10	30
N_2 flow rate (l min^{-1})	2	2
Drying	95°C/35 s	110°C/35 s
Ashing	900—1000°C/2.5 s	700°C/15 s
Atomization	2000°C/2 s	2500°C/2 s
Ramp	500°C s^{-1}	600°C s^{-1}
Analyte volume (μl)	10	10

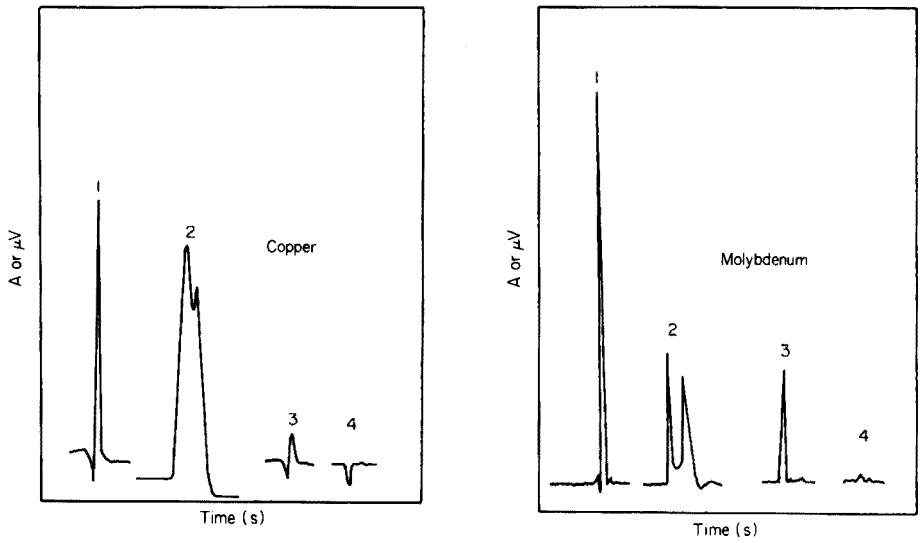

Fig. 3. Copper absorbance signals from carbon rod for solutions 0.1 M in NaCl and 0.01 M in HNO_3: (1) 20 ng Cu ml^{-1}, Zeeman splitting; (2) 20 ng Cu ml^{-1}, conventional mode; (3) 2 ng Cu ml^{-1} in water only, Zeeman splitting; (4) blank of (1) with Zeeman splitting. On the ordinate, A relates to the conventional absorption mode and μV to the Zeeman splitting mode.

Fig. 4. Molybdenum absorbance signals from carbon rod for solutions 0.1 M in NaCl: (1) 80 ng Mo ml^{-1}, Zeeman splitting; (2) 20 ng Mo ml^{-1}, conventional; (3) 20 ng Mo ml^{-1}, Zeeman splitting; (4) 0.1 M NaCl blank only. A and μV as for Fig. 3.

of this background level can be estimated at the instant of the copper atomization peak. The results are collected in Table 3. The improved performance with use of Zeeman splitting is clearly demonstrated. The decreased precision for copper determination in the presence of perchlorate comes from the considerable corrosion of the carbon. No signal is obtained in the presence of 0.5 M sodium chloride either because atomization of copper does not occur or because the absorption line profile is greatly deformed by the matrix and does not split in the magnetic field. Traces of copper can also be detected in an aqueous phase saturated by methyl isobutyl ketone, and 0.1 M or 0.5 M in potassium nitrate or 0.05 M in EDTA after the extraction of copper chelates with *N*-heterocyclic azo dyes. The use of a deuterium lamp background corrector failed to allow copper determination in these circumstances [8].

Atomization signals for molybdenum with and without Zeeman splitting are shown in Fig. 4. Calibration plots were measured for various media with 20—80 μg Mo ml^{-1} as ammonium molybdate. As with copper, inselective absorption is very effectively suppressed by using Zeeman splitting, but the residual inselective absorption influences the sensitivity in a similar way as for copper. The results are collected in Table 4.

TABLE 3

Determination of copper with the Varian CRA-90 carbon rod

Medium	Mode	Calibration slope[a]	Intercept[a]	R.s.d. (%)	Detection limit[b]	
					(ng ml^{-1})	(pg)
0.1 M HNO_3	Conventional	0.0059	0.012	3.5	2.6	26
	Zeeman	15.11	6.2	3.3	0.5	5
	Zeeman corr.[c]	15.11	1.2	3.3	0.5	5
0.01 M HNO_3 +	Conventional	0.0019	0.275	12	10	100
0.1 M NaCl	Zeeman	10.97	9.4	3.8	0.6	6
	Zeeman corr.	14.45	1.8	3.8	0.6	6
0.1 M HNO_3 +	Conventional	0.0	0.430	—	—	—
0.5 M NaCl	Zeeman	0.0	6.5	—	—	—
0.01 M HNO_3 +	Conventional	0.0048	0.021	4.0	3.9	39
0.1 M KNO_3	Zeeman	10.87	7.6	3.5	0.5	5
	Zeeman corr.	11.50	3.4	3.5	0.5	5
0.01 M HNO_3 +	Conventional	0.0017	0.190	16	14	140
0.5 M KNO_3	Zeeman	4.62	10	8.2	1.1	11
	Zeeman corr.	7.65	8.0	8.2	111	11
0.01 M HNO_3 +	Conventional	0.0024	0.180	11	9.8	98
0.05 M EDTA	Zeeman	12.47	14	3.6	0.7	7
	Zeeman corr.	15.27	11	3.8	0.7	7
Methyl isobutyl	Conventional	0.0061	0.047	3.4	2.8	28
ketone (sat.) +	Zeeman	14.88	7.0	3.8	0.5	5
0.01 M HNO_3	Zeeman corr.	15.19	2.0	3.8	0.5	5
0.01 M HNO_3 +	Conventional	0.0021	0.220	21	12	120
0.1 M $NaClO_4$	Zeeman	6.03	13	8.8	1.1	11

[a]The slopes correspond to absorbance/ng ml^{-1} for the conventional mode, and μV/ng ml^{-1} for the Zeeman mode. The intercepts correspond to the background and are given as absorbance (conventional) or μV (Zeeman).
[b]Metal concentration corresponding to three standard deviations of the blank.
[c]The correction term for the slope is slope $\times I_0/I$, where I_0 is the intensity of incident radiation, I is the intensity transmitted by the medium, and I/I_0 corresponds to the continuum light absorption of the blank measured conventionally at the instant when the metal atoms reach their maximum absorption.

Determination of chromium, molybdenum and iron with air—acetylene flames

The relevant parameters were: Cr, 357.87 nm with acetylene at 7 l min^{-1}; Mo, 313.3 nm with acetylene at 9 l min^{-1}; Fe, 248.33 nm with acetylene at 7 l min^{-1}. The air flow was 23 l min^{-1} in all cases. Calibration plots were linear up to 25 μg Mo ml^{-1}, 17 μg Cr ml^{-1} and 14 μg Fe ml^{-1}. The results are shown in Table 5. In these experiments, the splitting of the absorption lines was not strong enough because of the weaker magnetic field used, but nevertheless the detection limit was half of that for the mode without Zeeman splitting.

TABLE 4

Determination of molybdenum with the Varian CRA-90[a]

Medium	Mode	Calibration slope[a]	Intercept[a]	R.s.d. (%)	Detection limit[b]	
					(ng ml^{-1})	(pg)
H_2O	Conventional	0.0031	0.006	2.3	1.2	12
	Zeeman	21.9	18.5	1.9	0.6	9
	Zeeman corr.[c]	21.9	1.5	1.9	0.6	9
0.1 M NaCl	Conventional	0.0028	0.115	7.1	4.1	41
	Zeeman	17.3	28.7	2.1	1.0	10
	Zeeman corr.	20.3	4.8	2.1	1.0	10
0.1 M EDTA	Conventional	0.0029	0.130	12	13	130
	Zeeman	16.3	33	4.5	1.1	11
	Zeeman corr.	19.8	5.5	4.5	1.1	11

[a–c]Notes as for Table 3.

TABLE 5

Determination of Cr, Mo and Fe in acetylene—air flames

Element	Mode	Calibration slope[a]	Intercept	R.s.d. (%)	Detection limit (μg ml^{-1})[b]
Cr	Conventional	0.062	0.0	1.3	0.12
	Zeeman	89	13.1	1.5	0.07
Mo	Conventional	0.0125	0.01	1.9	0.19
	Zeeman	175	35	1.3	0.06
Fe	Conventional	0.058	0.0	2.1	0.21
	Zeeman	67.5	44	1.9	0.11

[a]The slopes correspond to absorbance/μg ml^{-1} for the conventional mode and μV/μg ml^{-1} for the Zeeman mode. Intercepts are given in absorbance or μV as for Table 3.
[b]Defined as for Table 3.

The authors wish cordially to thank Mr. Paul Grob, Varian AG., 6300 Zug, Switzerland for the loan of a CRA-90.

REFERENCES

1 T. Hadeishi and R. O. McLaughlin, Science, 174 (1971), 404; 187 (1975) 348; Anal. Chem., 48 (1976) 1009.
2 H. Koizumi and K. Yasuda, Anal. Chem., 47 (1975) 1679; 48 (1976) 1178; J. Spectrosc. Soc. Jpn., 23 (1974) 290; Spectrochim. Acta, Part B, 31 (1976) 237.
3 R. Stephens and D. E. Ryan, Talanta, 22 (1975) 655, 659.
4 D. E. Vernot and R. Stephens, Talanta, 23 (1976) 849.
5 J. B. Dawson, E. Grassam, D. J. Ellis and M. J. Keir, Analyst, 101 (1976) 315.
6 H. Koizumi, K. Yasuda and M. Katayama, Anal. Chem., 49 (1977) 1106.
7 V. Otruba, J. Jambor, J. Horák and L. Sommer, Scripta Fac. Sci. Nat. Univ. Brno, 6 (1976) 1.
8 J. Komárek, J. Havel and L. Sommer, Collect. Czech. Chem. Commun., in press.
9 Y. Uchida and S. Hattori, Oyo Butsuri, 44 (1975) 852.
10 E. Grassam, J. B. Dawson and D. J. Ellis, Analyst, 102 (1977) 804.

Analytica Chimica Acta, 101 (1978) 375—384

NON-DISPERSIVE ATOMIC FLUORESCENCE SPECTROMETRY OF NANOGRAM AMOUNTS OF ANTIMONY WITH A HYDRIDE GENERATION TECHNIQUE

TAKETOSHI NAKAHARA*, SYOJI KOBAYASHI and SÔICHIRÔ MUSHA

Department of Applied Chemistry, College of Engineering, University of Osaka Prefecture, Mozu-umemachi, Sakai 591 (Japan)

(Received 20th February 1978)

SUMMARY

Atomic fluoresence spectrometry (a.f.s.) with a non-dispersive system is combined with a hydride generation technique for the determination of antimony at the nanogram level. Fluorescence measurement is based on the reduction of antimony by either zinc or sodium borohydride, introduction of the stibine into the premixed argon (entrained air)—hydrogen flame, and excitation with an antimony electrodeless discharge lamp. The detection limits are 0.5 and 1.0 ng of antimony for zinc and sodium borohydride, respectively. The reagent blank for a 20-ml sample is ca. 5 ng of antimony for both reductants. Analytical working curves from peak-height or peak-area measurements are linear over ca. 4 orders of magnitude. Other hydride-forming elements and several metals, e.g. gold, nickel, palladium and platinum, interfere. The method gives satisfactory results for the determination of trace amounts of antimony in waste waters and lead.

In a.f.s. by direct nebulization of solutions into the flame, some authors [1—10] have reported detection limits of 0.04—20 ppm of antimony with measurement (dispersive system) mostly at 217.6 and 231.1 nm; others [5, 8] have obtained a detection limit of 0.04 ppm of antimony with a non-dispersive system. For both systems, hollow-cathode or electrodeless discharge lamps were used as excitation sources, and air—propane, air—hydrogen, air—acetylene or argon—hydrogen flames as atom reservoirs. A detection limit of 100—300 ppm of antimony was obtained [4, 11] with a xenon arc lamp continuum excitation source.

In atomic absorption spectrometry (a.a.s.) the sensitivity for antimony has been markedly improved with a technique based on the reduction of antimony and introduction of the stibine into an atom reservoir (flame, heated silica tube, or heated graphite furnace). Generally, reduction in acidic media is achieved with granular zinc [12, 13] or with sodium borohydride pellets or solution [13—21]. Pollock and West [22] used titanium trichloride and magnesium rod in acidic media for the generation of stibine.

Thompson [23] reported the determination of antimony, together with arsenic, selenium and tellurium, by a.f.s. with a hydride generation technique

and a dispersive measuring system at 231.1 nm; the detection limit was 0.1 ppb of antimony for 1-ml samples. Tsujii et al. [24] described a non-dispersive a.f.s. method with hydride generation and obtained a detection limit of 3 ng of antimony.

The performance of a newly-constructed a.f.s. instrument has been tested by measuring the fluorescence signals of mercury [25] and arsenic [26] with dispersive and non-dispersive systems. Dagnall et al. [1] and Kolihová and Sychra [9] reported the spectral characteristics of nine antimony lines which exhibit atomic fluorescence. Antimony, therefore, is one of the most suitable elements for non-dispersive a.f.s. From a preliminary study, under the same conditions of measurement, the non-dispersive atomic fluorescence sensitivity is at least one order of magnitude better than that obtained by the dispersive system with the 217.6-, 231.1- and 259.8-nm antimony lines, the relative sensitivities of which are 0.45, 1.00 and 0.39, respectively. The non-dispersive system has the advantage of higher throughput (larger solid angle, exit and input pupils, and higher transmission) and simultaneous measurement of all the fluorescence lines, but it is susceptible to increased flame background noise and sometimes to spectral interference. This paper describes the non-dispersive a.f.s. of antimony with a hydride generation technique and a premixed argon (entrained air)—hydrogen flame. A comprehensive, comparative study of the zinc and sodium borohydride reduction systems, and of the interference effects of acids and diverse elements on the fluorescence signal of antimony has been made.

EXPERIMENTAL

Reagents

All reagents were of analytical-reagent grade (Wako Pure Chemicals Ltd.) unless otherwise stated. The standard stock solution (1000 ppm), prepared by dissolving 1.000 g of high-purity antimony (99.999%, Mitsuwa Chemicals Ltd.) in 10 ml of nitric acid plus 5 ml of hydrochloric acid and diluting to 1 l with distilled water, was diluted, as required, immediately before use.

Zinc tablets were prepared by mixing 25 g of zinc powder (250 mesh) and 2 g of kaolin powder(Acid-washed American Standard, Fisher Scientific Co.) with ca. 5 ml of distilled water in a mortar. The paste obtained was molded into small tablets (10 mm diameter, 3 mm thick, ca. 0.6 g in weight) which were dried in an electric oven. For the $NaBH_4$ method, portions of sodium borohydride powder (0.03—0.1 g) were wrapped in thin rice paper (9 cm diameter, Kodomo-Odori Oblate Co. Ltd.) and stored in a desiccator.

Instrumentation

The components of the system are listed in Table 1 and shown schematically in Fig. 1. For a dispersive measuring system, the photomultiplier and its housing (10, Fig. 1) were replaced by a monochromator (0.3-m Ebert mounting, JE-30, Nippon Jarrell-Ash Co.) equipped with a photomultiplier (R-106 UH,

TABLE 1

Components of non-dispersive atomic fluorescence instrument

Item	Description (model no.) and supplier
Light source and power	
Lamp	Sb electrodeless discharge lamp, EMI
Power supply	Mictrotron 200, 2450 ± 25 MHz, Electro-Medical Supplies
Resonant cavity	Model 211 L, 3/4-wave resonant cavity, Electro-Medical Supplies
Light chopper	Laboratory-made
Lenses	30-mm diameter, 75-mm focal length, quartz
Burner	Laboratory-made
Photomultiplier	R-166, "solar-blind" type, Hamamatsu TV
High voltage power supply	412 B, John-Fluke
Preamplifier	JP 406, Nippon Jarrell-Ash
Power supply	± 15 V, laboratory-made
Lock-in amplifier	572 B, NF Circuit Design Block
Line-power stabilizer	A-133, NF Circuit Design Block
Oscilloscope	CS-1351, Trio
Pen recorder	QPD_{54}, Hitachi
Digital integrator	RD-01, Tokyo Kagaku
Stibine generating unit	ASD-1A, Nippon Jarrell-Ash

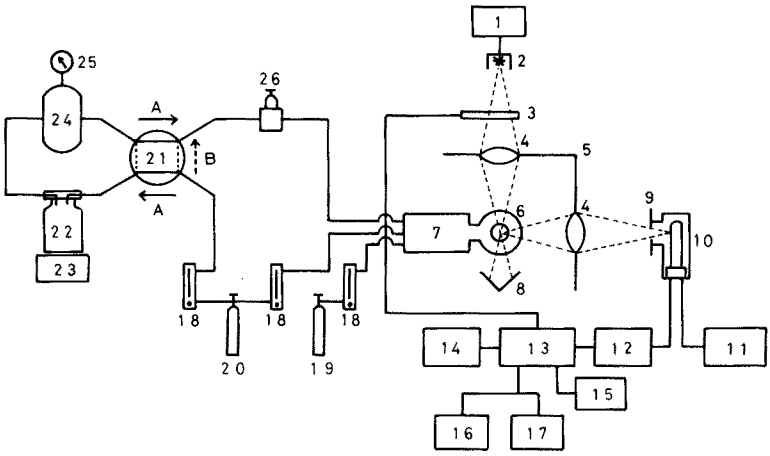

Fig. 1. Schematic diagram of non-dispersive atomic fluorescence instrument. (1) Microwave generator; (2) electrodeless discharge lamp and resonant cavity; (3) light chopper; (4) lenses; (5) panel; (6) burner; (7) nebulizer chamber; (8) light trap; (9) diaphragm; (10) photomultiplier and housing; (11) high-voltage power supply; (12) preamplifier; (13) lock-in amplifier; (14) line-power stabilizer; (15) oscilloscope; (16) pen recorder; (17) digital integrator; (18) flow meters; (19) hydrogen cylinder; (20) argon cylinder; (21) four-way valve; (22) reaction flask; (23) magnetic stirrer; (24) collection vessel; (25) pressure gauge; (26) needle valve; (A) "sweep" gas flow; (B) "by-pass" gas flow.

Hamamatsu TV Co.). The fluorescence radiation was measured at right angles to the axis of the optical path from the light source to the flame. The nitrogen-sheathed, water-cooled burner described previously [26] was used with the Techtron nebulizer (7, Fig. 1). The position of the burner/nebulizer system was adjusted laterally and vertically by a screw clamp (HR-65, Nippon Jarrell-Ash Co.).

General procedure

The experimental conditions are summarized in Table 2. Transfer the sample solution containing antimony to a reaction flask (22, Fig. 1); add an appropriate amount (see below) of concentrated hydrochloric acid and dilute to 20 ml with distilled water. Add a piece of the zinc tablet or a packet of the sodium borohydride, and connect the reaction flask immediately to the apparatus with the valve (21) in the "by-pass" position. Allow the reaction to continue with magnetic stirring for 60—80 s at room temperature. Then turn the valve to the "sweep" position, allowing the argon to sweep the stibine into the flame. Record the fluorescence signal simultaneously (pen recorder for peak-height measurement; digital integrator for peak-area measurement). After recording the signal, turn the valve to the "by-pass" position and remove the reaction flask. Argon was used as carrier gas and as auxiliary gas for the premixed argon (entrained air)—hydrogen flame.

The amount of antimony in the test solutions was 400 ng, corresponding to 20 ppb of antimony, unless otherwise stated.

RESULTS AND DISCUSSION

Effect of flame composition and flame height

To find the optimum flame conditions in the argon (entrained air)—hydroger flame, the fluorescence signal was examined for hydrogen flow-rates of 1.8 to

TABLE 2

Optimum experimental conditions

Microwave power for lamp	18 W (Incident power, 25 W; reflected power, 7 W)
Photomultiplier voltage	700 V
RC time constant	1.0 s
Load resistance	470 kΩ
Modulation frequency	240 Hz
Integration time for peak-area measurement	15 s
Sample volume	20 ml
Reductant	0.6 g Zn (2.0 M HCl) or 0.05 g $NaBH_4$ (0.5 M HCl)
Reaction time	80 s (Zn) or 60 s ($NaBH_4$)
Hydrogen flow-rate	4.0 l min^{-1}
Argon flow-rates	4.0 l min^{-1} for carrier gas and 2.0 l min^{-1} for auxiliary gas
Flame height	5.0 cm from the top of burner head

5.4 l min^{-1}; the total flow-rate of argon and auxiliary gases was kept constant. The results obtained by peak-height measurement for the zinc method were similar to those obtained for the $NaBH_4$ method. As shown in Fig. 2, the fluorescence signal was dependent on variations in the flame composition and flame height. The noise level, not shown in Fig. 2, was also considerably affected by the flame composition and flame height. Taking account of the signal-to-noise ratio, the optimum conditions for the flame were selected (Table 2). The flow-rate of the nitrogen sheath gas was fixed at 1.0 l min^{-1}.

Effect of flow-rate of carrier gas

The fluorescence signal increased with increased carrier gas flow-rate up to 4.0 l min^{-1} when the total flow-rate of argon was kept constant. A flow-rate between 4.0 and 6.0 l min^{-1} gave an almost constant fluorescence signal but below 3.0 l min^{-1}, in which there was no change in the fluorescence signal obtained with peak-area measurement, the peak broadened because of slower introduction of stibine into the flame. The optimum flow-rates of argon are shown in Table 2. Especially for the $NaBH_4$ method, a needle valve (26, Fig. 1) was necessary to prevent blowing-off the flame because of relatively high pressure (0.5—0.6 kg cm^{-2}) in the collection vessel.

Effect of amount of reductant and reaction time

For the zinc method, one small zinc tablet (0.6 g) was enough to reduce antimony to stibine; after a linear rise, the fluorescence signal became independent of the reaction time after 60 s; a reaction time of 80 s was selected.

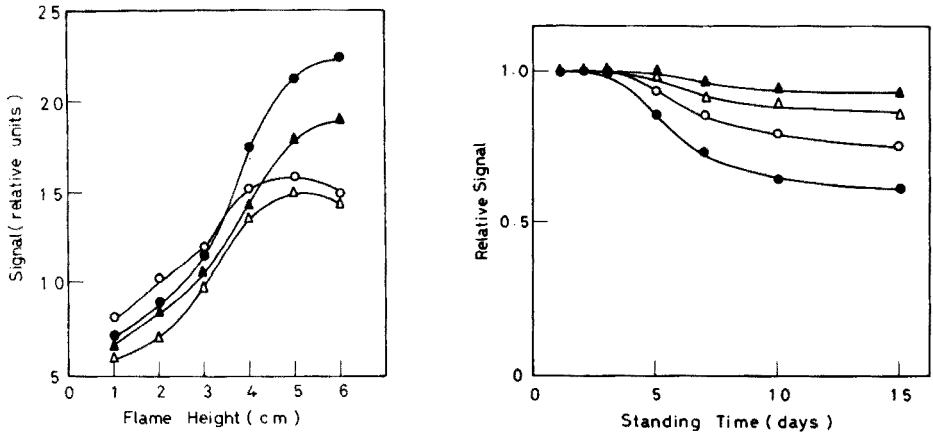

Fig. 2. Effect of flame composition and flame height on the fluorescence signal in an argon (entrained air)—hydrogen flame. Hydrogen flow-rates: (△) 1.8 l min^{-1}; (○) 2.9 l min^{-1}; (●) 4.0 l min^{-1}; (▲) 5.4 l min^{-1}. Argon flow-rates: 4.0 l min^{-1} for carrier gas and 2.0 l min^{-1} for auxiliary gas.

Fig. 3. Stability of dilute antimony solutions stored in borosilicate glass containers. (▲) 5 ppb Sb in 2 M HCl; (△) 20 ppb Sb in 2 M HCl; (○) 10 ppb Sb in H_2O (acidity is ca. 6×10^{-7} M HCl and ca. 1.5×10^{-6} M HNO_3); (●) 40 ppb Sb in H_2O (acidity is ca. 2.4×10^{-6} M HCl and ca. 6×10^{-6} M HNO_3).

For the borohydride method, the effect of weights of sodium borohydride ranging from 0.03 to 0.1 g was examined; the maximum fluorescence signal was given by ca. 0.05 g of sodium borohydride. A reaction time of 60 s was sufficient for complete generation of stibine.

Effect of acidity

All samples and blanks were acidified with hydrochloric acid. The effect of acidity on the fluorescence signal of antimony was examined; the optimum ranges were 1.8—4.0 M for the zinc method and 0.5 ± 0.1 M for the borohydride method. The acidities used are given in Table 2.

Stability of dilute antimony solutions

The stability of dilute antimony solutions is shown in Fig. 3; the results were obtained by the zinc method with peak-height measurement. The relative fluorescence signal is the ratio of the signal for an antimony solution stored in a borosilicate glass container to the signal given by a freshly prepared solution. The loss after 5—15 days can be attributed to adsorption by the container wall and/or volatilization as $SbCl_3$ [27].

Analytical working curve, sensitivity and precision

Under the optimum conditions shown in Table 2, analytical working curves (Fig. 4) were obtained for freshly-prepared antimony standard solutions by the zinc and borohydride methods. Peak-area measurement gave a slightly larger range of linearity than peak-height measurement. This may result from insufficiently rapid response of the recorder.

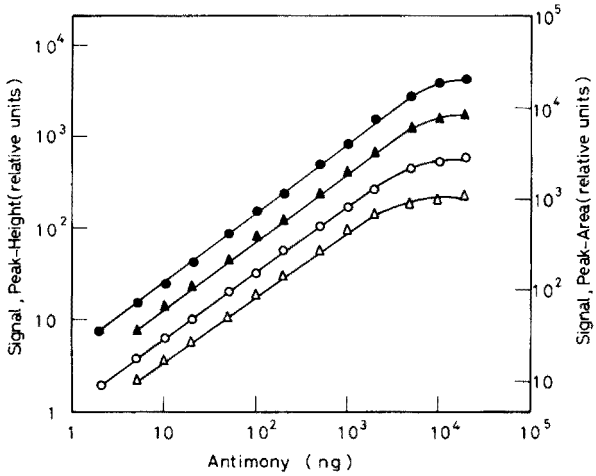

Fig. 4. Analytical working curves for antimony. (•) Zn method, peak-area measurement; (▲) $NaBH_4$ method, peak-area measurement, (○) Zn method, peak-height measurement; (△) $NaBH_4$ method, peak-height measurement.

The detection limits, calculated on the basis of a signal-to-noise ratio of 3:1 as recommended by IUPAC [28], were 0.5 (corresponding to 0.025 ppb) and 1.0 ng (corresponding to 0.05 ppb) of antimony by the zinc and borohydride methods, respectively. The reagent blank had a value of ca. 5 ng of antimony in 20 ml of sample by both methods. In a.a.s., the reagent blank by the zinc method is ca. 3 times greater than that by the borohydride method [13].

The fluorescence signal for antimony was measured 10 times for three antimony concentrations. The results are given in Table 3. Peak-area measurement was the more reproducible but there was little significant difference in precision between the two reduction methods.

Effect of nitric, perchloric, phosphoric and sulfuric acids

The effect of nitric, perchloric, phosphoric and sulfuric acids in the range 0.1—2.0 M was examined with antimony solutions acidified with hydrochloric acid as previously mentioned. The presence of perchloric, phosphoric and sulfuric acids did not affect the fluorescence signal in either of the reduction methods. Nitric acid at concentrations down to 0.001 M caused interference in the zinc method; for example, the presence of 0.001 M nitric acid in the antimony solution gave a signal that was 12% lower than that obtained in the absence of nitric acid (actually 3×10^{-6} M HNO_3 derived from the antimony stock solution). No fluorescence signal was obtained if the nitric acid concentration exceeded 0.1 M in the zinc method, but no significant interference was observed in the borohydride method. It was found that the phosphoric acid contained a significant amount (at the ppm level) of antimony as an impurity.

Effect of diverse elements

No study of the interferences that arise in the a.f.s. of antimony with a hydride generation technique has been published. Most of the interferences in the present method can be considered to be related to the reduction of

TABLE 3

Precision of measurement of atomic fluorescence signal

Antimony (ng)	Relative standard deviation (%)[a]			
	Zn method		$NaBH_4$ method	
	Peak height	Peak area	Peak height	Peak area
2000	4.3	2.7	3.3	2.7
200	4.1	2.4	4.7	3.1
20	3.9	2.8	5.7	3.4

[a] $n = 10$.

antimony to stibine as previously described for the a.a.s. of antimony [13, 20]. The effect of various other elements in 1000-fold excess was examined for the two reduction methods. The compounds added were the same as in previous studies [29, 30]. The results obtained by peak-height measurement are shown in Table 4; peak-area measurements gave no significant differences. An element was considered to interfere when it produced a fluorescence signal differing by over ± 10% from that obtained for antimony alone. The following did not interfere: Al, B, Ba, Be, Ca, Cd, Ce, Cs, Fe, Ga, In, K, La, Li, Mg, Mn, Na, Pb, Rb, Si, Sr, Th, Tl, V, Y, Zn and Zr. Several elements, including other hydride-forming elements, caused a pronounced interference (Table 4). The considerable enhancement caused by bismuth in the borohydride method arises from the spectral overlap of the latter with the iodine line at 206.2 nm radiated from the electrodeless discharge lamp. It has been shown elsewhere [31] that bismuth fluorescence at 206.2, 269.7, and 302.5 nm is stimulated strongly by iodine-containing spectral line sources. The fluorescence signal in the zinc method was independent of the presence of bismuth in 1—1000-fold excess; in the borohydride method, the enhancement by bismuth increased proportionally with the amount of bismuth. Thus bismuth hydride might be much more efficiently produced by the borohydride

TABLE 4

Interference from 1000-fold amounts of diverse elements

Element	Compound added	Relative fluorescence signal[a]	
		Zn method	$NaBH_4$ method
As	As_2O_3	0.39 (100[b])	0.79 (100[b])
Bi	$Bi(NO_3)_3$	1.04	3.29 (0.01[b])
Se	SeO_2	0.61 (100[b])	0.96
Sn	metal in HCl	1.04	0.60 (100[b])
Te	metal in HCl	0.50 (100[b])	0.48 (50[b])
Au	$HAuCl_4$	0.13 (20[b])	0.09 (10[b])
Ni	$NiCl_2$	0.02 (1[b])	0.08 (5[b])
Pd	$PdCl_2$	0.00 (0.5[b])	0.02 (1[b])
Pt	H_2PtCl_6	0.04 (10[b])	0.02 (2[b])
Ag	$AgNO_3$	0.29 (50[b])	0.96
Cr	$CrCl_3$	0 13 (10[b])	1.00
Cu	$Cu(NO_3)_2$	0.08 (10[b])	0.97
W	$NaWO_4$	0.71 (500[b])	1.03
Co	$CoCl_2$	0.98	0.48 (100[b])
Hg	$HgCl_2$	0.98	0.53 (200[b])

[a]Ratio of the fluorescence signal of antimony in the presence of a diverse element to the fluorescence signal of antimony alone.
[b]Ratio of the amount of a diverse element to the amount of antimony which gave no interference in the measurement of fluorescence signal.

method than by the zinc method, and the borohydride method appears to be preferable with respect to interference.

Application to the determination of antimony in waste waters and lead

A sample, taken at the inlet of the Wastewater Treatment Facility, University of Osaka Prefecture, was acidified with hydrochloric acid to give the appropriate acidity (Table 2) and 50 ng of antimony was added. The fluorescence signal was measured under the optimum conditions (Table 2). The results obtained with both the reduction methods are shown in Table 5.

A sample (0.4 g) of lead metal was dissolved in 20 ml of 6 M nitric acid by heating slowly on a hot plate. After cooling, the sample solution was transferred to a 250-ml volumetric flask, diluted to volume with distilled water, and finally diluted by a factor of 500 with 0.5 M hydrochloric acid. A 20-ml aliquot was taken and the fluorescence signal was measured under the conditions given in Table 2. As nitric acid interferes in the zinc method, the borohydride method was used. Values in good agreement with that (1.18% Sb) given by flame a.a.s. were obtained; for 6 determinations, peak-height and peak-area measurements gave average values of 1.17% (r.s.d. 1.7%) and 1.19% (r.s.d. 1.4%), respectively.

Conclusion

Non-dispersive a.f.s. is sensitive and reliable for the determination of antimony at the nanogram level. The sensitivity of the system described is comparable with that of other authors [23, 24]. The zinc method is slightly more sensitive than the borohydride method, which is, however, superior with respect to interference.

An improvement in sensitivity and linear dynamic range for antimony by the non-dispersive system could be made with a non-flame heated quartz cell and a chlorine filter to reduce flame background noise [32, 33]. Work is currently under way to investigate this possibility.

TABLE 5

Determination of antimony (50 ng) added to a waste water

	Zn method		$NaBH_4$ method	
	Peak height	Peak area	Peak height	Peak area
Range	44—54	48—52	45—52	48—52
Average (n = 6), ng	49	50	49	49.5
R.s.d. (%)	6.58	3.35	4.83	3.06

REFERENCES

1 R. M. Dagnall, K. C. Thompson and T. S. West, Talanta, 14 (1967) 1151.
2 K. E. Zacha, M. P. Bratzel, Jr., J. D. Winefordner and J. M. Mansfield, Jr., Anal. Chem., 40 (1968) 1733.
3 R. M. Dagnall, M. R. G. Taylor and T. S. West, Spectrosc. Lett., 1 (1968) 397.
4 D. C. Manning and P. Heneage, At. Absorpt. Newsl., 7 (1968) 80.
5 J. M. Mansfield, Jr., M. P. Bratzel, Jr., H. O. Nordordon, D. O. Knapp, K. E. Zacha and J. D. Winefordner, Spectrochim. Acta, Part B, 23 (1968) 389.
6 A. Fulton, K. C. Thompson and T. S. West, Anal. Chim. Acta, 51 (1970) 373.
7 K. C. Thompson and P. C. Wildy, Analyst, 95 (1970) 776.
8 P. L. Larkins, Spectrochim. Acta, Part B, 26 (1971) 477.
9 D. Kolihová and V. Sychra, Anal. Chim. Acta, 59 (1972) 477.
10 G. E. Bentley and M. L. Parsons, Anal. Chem., 49 (1977) 551.
11 M. P. Bratzel, Jr., R. M. Dagnall and J. D. Winefordner, Anal. Chim. Acta, 52 (1970) 157
12 Y. Yamamoto, T. Kumamaru, Y. Hayashi and R. Tsujino, Anal. Lett., 5 (1972) 419.
13 Y. Yamamoto and T. Kumamaru, Fresenius Z. Anal. Chem., 281 (1976) 353.
14 F. J. Fernandez, At. Absorpt. Newsl., 12 (1973) 93.
15 F. J. Schmidt and J. L. Royer, Anal. Lett., 6 (1973) 17.
16 K.-T. Kan, Anal. Lett., 6 (1973) 603.
17 E. J. Knudson and G. D. Christian, Anal. Lett., 6 (1973) 1039.
18 J. C. Van Loon and E. J. Brooker, Anal. Lett., 7 (1974) 505.
19 K. C. Thompson and D. R. Thomerson, Analyst, 99 (1974) 595.
20 A. E. Smith, Analyst, 100 (1975) 300.
21 J. A. Ferino, J. W. Jones and S. G. Capar, Anal. Chem., 48 (1976) 120.
22 E. N. Pollock and S. J. West, At. Absorpt, Newsl., 11 (1972) 104.
23 K. C. Thompson, Analyst, 100 (1975) 307.
24 K. Tsujii, K. Kuga and I. Sugaya, Chem. Lett., (1975) 695.
25 T. Nakahara, T. Tanaka and S. Musha, Bull. Chem. Soc. Jpn., 51 (1978) 2020.
26 T. Nakahara, T. Tanaka and S. Musha, Bull. Chem. Soc. Jpn., 51 (1978) 2046.
27 M. Zief and J. M. Mitchell, Contamination Control in Trace Element Analysis, Wiley-Interscience, New York, 1976, p. 27.
28 IUPAC, Nomenclature, Symbols, Units and their Usage in Spectrochemical Analysis, Part II, Section 4.1, Revision 1975 [Pure Appl. Chem., 45 (1976) 99].
29 T. Nakahara and S. Musha, Anal. Chim. Acta, 75 (1975) 305.
30 T. Nakahara and S. Musha, Anal. Chim. Acta, 80 (1975) 47.
31 R. M. Dagnall, K. C. Thompson and T. S. West, Talanta, 14 (1967) 1467.
32 T. J. Vickers, P. J. Slevin, V. I. Muscat and L. T. Farias, Anal. Chem., 44 (1972) 930.
33 W. K. Fowler and J. D. Winefordner, Anal. Chem., 49 (1977) 944.

Analytica Chimica Acta, 101 (1978) 385—391

DOSAGE DE L'ALUMINIUM DANS LES LIQUIDES BIOLOGIQUES PAR ABSORPTION ATOMIQUE SANS FLAMME

YVES PEGON

Département de Chimie Analytique, Faculté de Pharmacie, 8, Avenue Rockefeller 69373 Lyon Cedex 2, et Laboratoire de Biochimie, Hôpital Neurologique, 69394 Lyon Cedex 3 (France)

(Reçu le 2 mai 1978)

RESUME

Une nouvelle méthode de dosage de l'aluminium dans les liquides biologiques par absorption atomique sans flamme est décrite. Dans cette méthode, pour diminuer la durée des phases de séchage et de minéralisation et augmenter la reproductibilité, on ajoute à l'échantillon un agent mouillant (Teepol). Pour éviter la formation de chlorures volatils, l'aluminium est transformé en aluminate par addition d'ammoniaque concentrée. Il est ainsi possible d'obtenir un coefficient de variation de 2,5% pour le dosage dans un sérum. Les taux d'aluminium du sérum et du liquide céphalo-rachidien de 20 sujets normaux ont également été déterminés par cette méthode (valeur moyenne pour le sérum: 34,1 $\mu g\ l^{-1}$; valeur moyenne pour le LCR: 19,8 $\mu g\ l^{-1}$).

SUMMARY

Determination of aluminium in biological fluids by atomic absorption spectrometry with electrothermal atomization

A new method for the determination of aluminium in biological fluids by flameless atomic absorption spectrometry is described. A wetting agent (Teepol) is added to shorten the time of drying and ashing steps and to improve reproducibility. Aluminium is converted to aluminate with ammonia liquor to prevent volatile chloride formation. Application of the method to a serum gave results with a relative standard deviation of 2.5%. This method was also applied to the determination of aluminium in serum and cerebrospinal fluid of 20 normal persons: the mean value for the sera was 34.1 $\mu g\ l^{-1}$ and the mean value for the CSF was 19.8 $\mu g\ l^{-1}$ with relative standard deviations of 3.5% and 2.5%, respectively.

Pour établir une corrélation entre les variations du taux d'aluminium dans le sérum ou dans le liquide céphalorachidien (LCR) et certaines affections neurologiques, nous avons dû doser ce métal dans un grand nombre d'échantillons par absorption atomique sans flamme (a.a.s.). Cette méthode a été précédemment utilisée pour le dosage de l'aluminium dans le sérum [1] et dans le sang total [2]. Dans la technique proposée par Fuchs et al. [1], 25 μl de sérum sont injectés dans le four. La programmation en température comporte les phases suivantes: séchage de 60 s à 100°C, minéralisation de 60 s à 300°C, minéralisation de 120 s avec montée de la température jusqu'à 1550°C et atomisation avec interruption du courant d'argon.

Pour améliorer cette technique, nous avons cherché à diminuer la durée de l'analyse, à augmenter la reproductibilité et à minimiser les interférences chimiques ou physiques dues à la matrice. Afin de diminuer le temps d'analyse, nous avons utilisé une phase de séchage à 120°C, suivie d'une seule phase de minéralisation à température fixe. Pour que dans ces conditions le séchage et la minéralisation de la matrice soient suffisants et ne provoquent pas d'interférences physiques sur le dosage, il est nécessaire d'ajouter un agent mouillant à l'échantillon. Pour diminuer les interférences chimiques, il faut modifier l'environnement chimique de l'échantillon car les liquides biologiques contiennent le plus souvent une quantité importante d'ions chlorure, qui peuvent provoquer une perte d'aluminium pendant la phase de séchage et la phase de minéralisation par formation de Al_2Cl_6 volatil.

Ces considérations nous ont amenés à étudier l'influence de différents agents mouillants et de différents composés chimiques sur le signal obtenu en a.a.s. avec l'aluminium, afin de trouver les meilleurs conditions de dosage dans les liquides biologiques.

PARTIE EXPERIMENTALE

Appareillage

Nous avons utilisé un spectrophotomètre d'absorption atomique (Unicam SP 1900) équipé d'un four graphite Massmann (Beckman) et d'un système de correction de l'absorption non spécifique par lampe au deutérium (Unicam SP 1960). Le spectrophotomètre est connecté à un enregistreur Servotrace Sefram.

Les paramètres instrumentaux sont: longueur d'onde 309,3 nm, largeur de fente 0,44 nm, sensibilité enregistreur 10 mV, vitesse papier enregistreur 25 mm min^{-1}. Le débit d'argon est de 1,2 l min^{-1}. La phase d'atomisation a lieu avec ce même débit d'argon. La programmation de température est: phase de séchage de 40 s à 120°C, phase de minéralisation de 40 s, phase d'atomisation de 5 s à 2800°C. Pour l'étude de la variation de l'absorbance en fonction de la température de minéralisation, le programme est arrêté pendant 30 s entre les phases de minéralisation et d'atomisation pour que, au début de la phase d'atomisation, la température du four ne dépende pas de la température de minéralisation.

Le volume d'échantillon injecté dans le four est de 25 μl. L'injection est faite avec une seringue SGE de 50 μl traitée avec une solution de silicone avant chaque série d'expériences [3]. Les liquides biologiques sont prélevés et conservés uniquement dans des tubes en polyéthylène de 10 ml: des essais systématiques, avec soit conservation à + 4°C, soit congélation et décongélation répétées de sérums et de LCR, nous ont montré que seul ce type de tube ne conduit pas à des variations du taux d'aluminium dans le temps.

Réactifs et solutions

Les solutions sont préparées à partir de réactifs Normapur Prolabo et d'eau désionisée avec du matériel lavé avec de l'acide chlorhydrique M et rincé plusieurs fois avec de l'eau désionisée. Les solutions sont conservées dans des flacons en polyéthylène. Les dilutions des liquides biologiques sont faites dans des tubes en polyéthylène.

Les mouillants qui ont été testés sont: Tween 20 (Technicon), Brij 35 en solution à 30% (Technicon), Triton-X100 (Rohm et Haas), Teepol 710 en solution à 40% (Serva).

Les solutions d'aluminium sont obtenues par dilution d'une solution mère (1 g l^{-1}) préparée par dissolution de 1 g d'aluminium métallique dans 10 ml d'acide chlorhydrique (d = 1,18), le volume étant ensuite complété à 1 l avec de l'eau désionisée. Les solutions utilisées pour étudier l'effet des agents mouillants ou de l'environnement chimique sont préparées en ajoutant 50 μl de la solution mère d'aluminium à 1 l de solution d'un acide à la concentration 3×10^{-2} M ou d'hydroxyde de sodium à la concentration 3×10^{-2} M ou d'ammoniac à la concentration 3 M.

Mesure de l'absorbance et dosage

Les valeurs données sont proportionnelles à l'absorbance et sont égales à la hauteur des pics mesurée en centimètres sur l'enregistrement graphique.

Pour réaliser une série de dosages sur des liquides biologiques, la teneur de l'un des échantillons est déterminée par la méthode des ajouts dosés en utilisant deux valeurs d'ajouts [4]. Le taux d'aluminium des autres échantillons est calculé directement sur la courbe ainsi tracée.

RESULTATS ET DISCUSSION

Utilisation d'un agent mouillant

L'adjonction d'un agent mouillant aux échantillons à analyser en a.a.s. est un procédé peu utilisé. Cependant le Triton-X100 à concentration élevée a été employé pour le dosage du plomb dans le sang total [5, 6].

Nous avons étudié l'influence de quatre agents mouillants: Triton-X100, Brij, Tween et Teepol sur la valeur de l'absorbance donnée par une solution à 50 μg Al l^{-1}. Pour cela nous avons réalisé des séries de dix mesures sur des solutions préparées par dilution de la solution mère d'aluminium dans des solutions d'acide nitrique ou d'ammoniac, contenant des quantités variables d'agent mouillant. La température de minéralisation est de 1600°C avec la solution nitrique et de 1700°C avec la solution d'ammoniac. Sur chaque série de mesures nous avons calculé la moyenne et le coefficient de variation (Tableau 1).

Les résultats montrent que l'absorbance est diminuée en présence d'un agent mouillant. Cette diminution dépend de l'agent mouillant utilisé et de l'environnement chimique. Elle est faible avec le Teepol. Le coefficient de variation varie fortement avec la concentration en agent mouillant ce qui

TABLEAU 1

Moyenne ($\overline{m}$) et coefficient de variation (c.v.) pour une solution d'aluminium en milieu nitrique ou en milieu ammoniacal en fonction de la concentration en agent mouillant ($ml\ l^{-1}$)

Concentration agent mouillant	Triton-X100		Brij 35		Tween 20		Teepol	
	$\overline{m}$	c.v.	$\overline{m}$	c.v.	$\overline{m}$	c.v.	$\overline{m}$	c.v.
Milieu nitrique[a]								
0,1	17,5	2,6	17,5	2,5	17,2	2,4	17,8	2,4
0,5	12,0	5,7	17,3	2,1	15,8	4,8	17,6	2,2
1	10,4	10,3	16,2	5,1	13,8	5,9	17,2	2,0
2	9,3	11,2	15,8	7,2	12,0	6,7	17,1	2,1
Milieu ammoniacal[b]								
0,1	15,2	3,1	13,0	1,6	15,4	2,4	17,7	3,2
0,5	11,2	5,8	12,8	4,7	14,7	3,8	17,4	2,6
1	11,2	6,7	9,4	7,2	13,5	8,7	17,3	1,6
2	10,9	7,2	8,5	8,5	12,9	9,1	17,3	1,6

[a]En l'absence d'agent mouillant: $\overline{m}$ = 18,1 et c.v. = 3,6.
[b]En l'absence d'agent mouillant: $\overline{m}$ = 17,9 et c.v. = 4,2.

fait que cette concentration doit être ajustée avec précision dans les échantillons sauf avec le Teepol pour lequel on observe un faible coefficient de variation avec des quantités voisines de 1 ml par litre de solution. C'est pour quoi nous avons choisi d'utiliser ce mouillant.

Environnement chimique

Etant donné les valeurs des produits de solubilité relatifs à la formation de l'hydroxyde, l'aluminium n'est soluble en solution aqueuse qu'à pH acide, sous forme de cations Al^{3+}, ou à pH alcalin, sous forme d'anions aluminate.

Aussi pour connaître l'influence de différents composés chimiques sur les mesures d'absorbance, nous avons préparé des dilutions à 50 $\mu g\ l^{-1}$ de la solution mère d'aluminium, soit dans des solutions d'acide chlorhydrique, d'acide sulfurique, d'acide phosphorique ou d'acide nitrique, soit dans des solutions d'hydroxyde de sodium ou d'ammoniac. L'ammoniaque étant une base faible, la concentration utilisée est élevée afin d'amener le pH à 12,5. A chaque solution nous avons ajouté 1 ml de Teepol par litre. Pour chaque solution nous avons mesuré l'absorbance en fonction de la température de minéralisation (Fig. 1). Les courbes ainsi tracées montrent que l'absorbance est fonction de la température de minéralisation, surtout en milieu chlorhydrique comme l'avaient indiqué Persson et al. [7] et à un degré moindre, en milieu sulfurique.

Sur chaque courbe nous avons déterminé la température qui, tout en étant la plus élevée possible pour faciliter la destruction de la matrice dans le cas d'un milieu complex, donne l'absorbance la plus forte. En utilisant

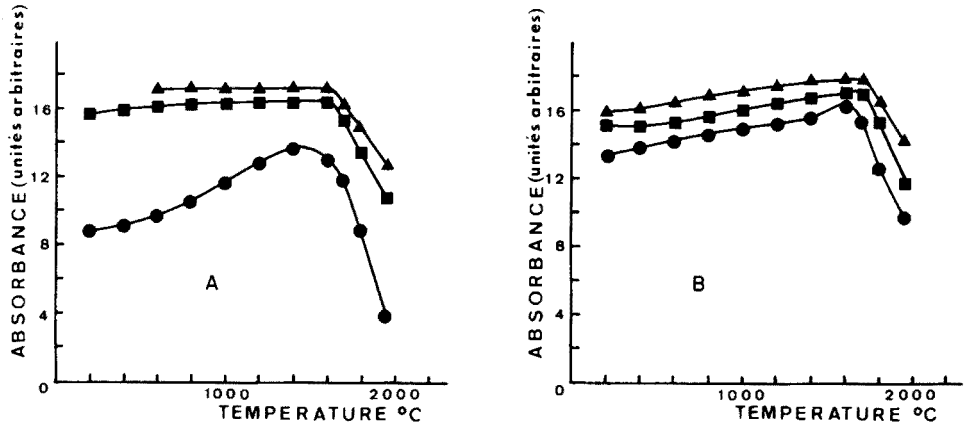

Fig. 1. Variation de l'absorbance donnée par une solution à 50 $\mu g\ l^{-1}$ d'aluminium: (A) en milieu HCl 3×10^{-2} M (•), HNO_3 3×10^{-2} M (▪), H_3PO_4 3×10^{-2} M (▲) en fonction de la température de minéralisation; (B) en milieu H_2SO_4 3×10^{-2} M (•), NaOH 3×10^{-2} M (▪), NH_4OH 3 M (▲) en fonction de la température de minéralisation. H_3PO_4 n'étant pas évaporé pour une température de minéralisation de 200°C ou de 400°C, la mesure de l'absorbance est impossible.

ces températures de minéralisation, nous avons effectué dix mesures sur chaque solution. A partir de ces mesures nous avons calculé les coefficients de variation (Tableau 2). Le coefficient de variation dépend de l'environnement chimique. Il est élevé avec les solutions d'hydroxyde de sodium qui donnent par séchage une matrice qui est source d'interférences physiques en cours de mesure. Il est le plus faible avec les solutions d'ammoniac.

Ceci nous a conduit à choisir l'ammoniaque comme composé à ajouter aux liquides biologiques. L'ammoniaque présente d'autres avantages puisqu'elle permet d'employer une température de minéralisation plus haute que les acides, puisqu'on peut l'utiliser à concentration importante, l'excès étant éliminé dès la phase de séchage et puisque l'anion aluminate formé ne peut pas, contrairement au cation Al^{3+}, donner des chlorures volatils à basse température.

TABLEAU 2

Coefficient de variation (c.v.) en fonction de l'environnement chimique

Milieu	Température minéralisation (°C)	c.v.	Milieu	Température minéralisation (°C)	c.v.
HCl	1400	2,3	HNO_3	1600	2,0
H_2SO_4	1600	2,9	NaOH	1700	4,1
H_3PO_4	1600	2,5	NH_4OH	1700	1,6

Application aux liquides biologiques

Compte tenu des résultats précédents, pour doser l'aluminium dans les liquides biologiques, nous diluons au demi les échantillons dans l'ammoniaque concentrée (d = 0,92) et nous ajoutons environ 1 pour 1000 de Teepol. La température de minéralisation est de 1700°C.

Pour mettre en évidence l'amélioration de la reproductibilité obtenue par l'emploi de Teepol et de l'ammoniaque, nous avons réalisé dix injections avec un sérum dilué au demi dans l'eau, avec et sans Teepol, et avec un sérum dilué au demi dans l'ammoniaque, avec et sans Teepol. Le coefficient de variation calculé dans chaque cas est donné dans le Tableau 3.

Le pouvoir mouillant du Teepol permet à la goutte de s'étaler sur la paroi du tube de graphite, ce qui évite qu'il y ait pendant les phases de séchage et de minéralisation des projections se traduisant par un coefficient de variation très élevé. Il est ainsi possible de diminuer la durée des phases de séchage et de minéralisation, même avec les liquides riches en matière organique. Puisque le temps d'analyse est court: 90 s et que le courant d'argon n'est pas interrompu pendant la phase d'atomisation, un même tube de graphite peut servir à plusieurs centaines de mesures. De plus, la variation de l'absorbance avec le vieillissement du tube de graphite est très lente et une même courbe d'étalonnage peut être utilisée pour une série importante de dosages.

Avec cette méthode nous avons dosé l'aluminium dans le sérum et dans le LCR de vingt sujets normaux. Les résultats sont donnés dans le Tableau 4. Pour le sérum, les valeurs extrêmes: 28 et 40 $\mu g\ l^{-1}$, sont plus proches l'une de l'autre que celles données par d'autres auteurs [1, 8]. Nous pensons que ceci est dû aux soins pris pour le prélèvement et la conservation des liquides biologiques ainsi qu'à l'excellente reproductibilité de la technique utilisée.

TABLEAU 3

Coefficient de variation (c.v.) en fonction du réactif servant à diluer le sérum

Réactif diluant	c.v.	Réactif diluant	c.v.
Eau	16,9	NH_4OH	15,3
Eau + Teepol	8,4	NH_4OH + Teepol	2,5

TABLEAU 4

Taux d'aluminium ($\mu g\ l^{-1}$) dans le sérum et le LCR de 20 sujets normaux

	$\bar{m}$	Ecart type	Valeurs extrêmes
Sérum	34,1	3,5	28—40
LCR	19,8	2,5	16,5—25,5

BIBLIOGRAPHIE

1 C. Fuchs, M. Brasche, K. Paschen, H. Nordbeck et E. Quelhorst, Clin. Chim. Acta, 52 (1974) 71.
2 F. J. Langmyhr et D. L. Tsalev, Anal. Chim. Acta, 92 (1977) 79.
3 R. G. Anderson, I. S. Maines et T. S. West, Anal. Chim. Acta, 51 (1970) 355.
4 G. D. Christian, Anal. Chem., 41 (1969) 24 A.
5 N. P. Kubasik, M. T. Volosin et M. H. Murray, Clin. Chem., 18 (1972) 410.
6 M. A. Evenson et D. D. Pendergast, Clin. Chem., 20 (1974) 163.
7 J. Persson, W. Frech et A. Cedergren, Anal. Chim. Acta, 92 (1977) 95.
8 M. Boukari, J. Rottembourg, M. C. Jaudon, J. P. Clavel, M. Legrain et A. Galli, Nouv. Presse Med., 7 (1978) 85.

Analytica Chimica Acta, 101 (1978) 393—399

DETERMINATION OF DIOCTYLTIN STABILIZERS IN FOOD-SIMULATING SOLVENTS BY ATOMIC ABSORPTION SPECTROMETRY WITH ELECTROTHERMAL ATOMIZATION

A. W. VARNES and V. FRAN GAYLOR

The Standard Oil Company (Ohio), 4440 Warrensville Center Rd., Cleveland, Ohio 44128 (U.S.A.)

(Received 21st March 1978)

SUMMARY

A method is described for estimating the concentration of di(n-octyltin) bis-maleate in five food-simulating solvents recommended by the United States Food and Drug Administration for migration studies on food containers. Atomic absorption spectrometry with electrothermal atomization provides a detection limit of 0.01 ppm tin stabilizer in the food simulators. Both calibration curve and standard addition methods were employed to check for possible matrix effects. Analysis time was less than 90 s per sample. Ethanol solutions were difficult to analyze because of residual inorganic tin blanks, presumably arising from the ethanol container. Water, acetic acid and heptane were free of residual tin blanks. Amounts of tin stabilizer extracted from several different resins ranged from 0.01 to 0.18 ppm.

Di(n-octyltin) bis-maleate is a well-known stabilizer for certain polymers, some of which are used for fabricating food-packaging containers. The U.S. Food and Drug Administration requires that food packaged in poly(vinyl chloride) or vinyl chloride copolymers must contain less than 1 ppm tin stabilizer [1]. Four food-simulating solvents and several sets of time-and-temperature test conditions are specified for evaluating the resistance of plastic containers to extraction of the additives by foods. This paper describes a method for determining the tin stabilizer in such solvents at the sub-ppm level. The method determines total tin; thus if total tin, expressed as tin maleate, is below 1 ppm, then the organotin compound concentration must be smaller.

Atomic absorption spectrometric (a.a.s.) techniques are rapid, almost free of spectral interferences and extremely sensitive, and so were selected for investigation. Sensitivity and selectivity of flame a.a.s. for metals giving rise to volatile hydrides may be enhanced by venting the hydride into the flame, rather than nebulizing the solution. Thomson and Thomerson [2] applied this technique to the determination of tin. Sodium borohydride was added to the sample and the stannane produced was passed into a 17-cm long silica tube heated in an air—acetylene flame. The tube served to atomize the tin and to exclude flame components, which cause spectral interference, from the optical path.

Sensitivity was 0.44 ppb for 1% absorption with 1-ml samples. Precision was ± 4% at the 20-ppb level. Schmidt et al. [3] have devoloped an automated system for determining several metals by hydride generation.

Another generation technique is to react the sample solution containing tin with a mercury compound to liberate mercury vapor. Umland and Schumacher [4] acidified the samples, and then passed the solution through a reductor containing amalgamated lead in a potassium sodium tartrate—sodium hydrogen carbonate mixture to convert all tin to tin(II). The reduced solution was added to an aerated solution of mercury(II) chloride. Mercury was measured at 253.65 nm. Precision was ± 5% at 100 ppb. Christmann and Ingle [5] used a similar approach to detect sub-ppb quantities of tin(II). While such techniques appeared to provide the sensitivity and selectivity needed, the methods seemed to be too time-consuming and preparation and maintenance of generation equipment too demanding for the present purpose.

The fastest a.a.s. technique is direct aspiration into a flame. Several samples per min can be analyzed by such a process. Engberg [6], Sato et al. [7] and Zook [8] have applied flame a.a.s. to the determination of tin in canned foods. Williams [9] used flame a.a.s. to determine bis(tri-n-butyltin) oxide and di-n-butyltin oxide in preserved softwoods by extraction with HCl—ethanol mixtures. A range of 2—50 ppm Sn in solution was obtained. George et al. [10] determined dibutyltin dilaureate in amine feeds by extraction with chloroform and concentration of the extract by heating, followed by addition of methanol. Good recoveries of added organotin compound were obtained. Unfortunately, these methods would all need some sample pre-treatment, and a concentration step would be needed to determine less than 1 ppm of tin.

Barnett and McLaughlin [11] demonstrated that a heated graphite atomizer could be used to determine tin in iron, copper and zinc alloys. Good correlation was obtained with certificate values and the sensitivity was 35 times better than that for flame a.a.s. Since the present matrix would be essentially pure solvent, the fact that good results could be obtained in a 1% alloy solution was encouraging. Meranger [12] applied a method similar to the one reported here to the determination of tin stabilizers in alcoholic beverages. His method included a benzene extraction to separate the organic tin stabilizer from inorganic tin; the detection limit was 0.04 ppm of tin. Thus, the method with the graphite atomizer was investigated for the measurement of tin stabilizers leached from food containers.

An independent study, similar to that reported here, but unknown to the present authors during the investigation, was recently reported [13]. The major differences are that the 286.3 nm tin line is used (the present study shows the 224.6 nm line to give greater sensitivity), and a 30-s ashing period is recommended (considered to be superfluous herein).

EXPERIMENTAL

Apparatus

A Perkin-Elmer model 403 spectrophotometer, equipped with a Perkin-Elmer HGA 2100 heated graphite atomizer, was used with a Perkin-Elmer model 165 strip-chart recorder.

The instrumental variables employed in analyzing for di(n-octyltin)bis-maleate are listed in Table 1. The wavelength chosen is the most sensitive for tin. The drying temperature is slightly above the boiling point of all the solvent systems employed. No charring (ashing) step was used, because little or no residue other than analyte would be left after drying, and charring presents the possibility of tin loss prior to atomization. Background correction was used (see below) and would compensate for traces of other residual material.

The drying time was selected by observing a drop of sample in the tube. Water, 8% ethanol and 3% acetic acid formed drops which did not wet the graphite; 20 s was more than adequate to evaporate the solvent. Heptane and 50% ethanol tended to soak into the graphite so a longer drying time, 30 s, was needed to volatilize these solvents. The atomizing time, 5 s, was chosen so that no residual signal (memory effect) was observed from an aliquot of pure solvent analyzed right after a sample containing 1 ppm of tin stabilizer.

Background correction employed a deuterium arc continuum coincident with hollow-cathode lamp beam, the continuum absorbance being subtracted from the resonance line absorbance to compensate for light scattering and molecular absorption. The 0.7-nm band-pass was necessary to match the intensities of the two beams since the tin lamp was not very intense. Functioning of the background correction was monitored by a "d'Arsonal-type" needle meter. The background correction made it unnecessary to char the sample. No gross needle deflection was noted during atomization. If excessive residue had been present after drying any sample, a large deflection would have been observed, showing that the scattering and/or molecular absorbance was too great for accurate compensation by the background correction system.

TABLE 1

Perkin-Elmer model 403—HGA-2100 settings with background correction

Variable	Value
Wavelength	224.6 nm
Drying cycle	110°C for 20 s (water, 8% ethanol, 3% acetic acid) or 30 s (50% ethanol, heptane)
Atomization cycle	2500°C for 5 s
Gas flow, rotameter	40
Gas mode	Interrupt
Recorder sensitivity	0.25 Absorbance unit f.s.d.; f.s.d., 0.25
Bandpass	0.7 nm
Sample size	50 μl (25 μl for heptane)

A sample size of 50 μl was usually chosen to give the greatest absorbance possible without causing the sample to be dispersed over too large an area of tube. The temperature can vary along the tube, so that too large a sample spreads to the cool ends, and some organic material may remain after drying, which will give rise to molecular absorption too great for satisfactory background compensation. This effect was very pronounced with heptane, so that only 25-μl portions of heptane extracts could be analyzed.

Calibration solutions

Calibration data for all solutions are given in Table 2. All calibration graphs were linear.

Aqueous solutions. Although the method responds only to tin atoms, the efficiency of atom production may vary with the chemical form of the tin. For this reason, di(n-octyltin) bis-maleate was used to prepare standard solutions for calibration. The material used here was found to contain 26.3% tin by flame a.a.s.; 0.100 g was dissolved in acetone (reagent grade) and diluted to 100.0 ml in a volumetric flask to yield a 1000-ppm stock solution. Because the stabilizer is not water-soluble, a further dilution was made with acetone to yield a 50 ppm di(n-octyltin) bis-maleate solution. Further dilutions were made with double-distilled deionized water.

3% Acetic acid. Di(n-octyltin) bis-maleate in acetone (50 ppm) was used to prepare calibration solutions in 3% acetic acid (reagent grade in deionized water).

8% and 50% ethanol. The ethanol used was found to contain 0.5 ppm of tin, so that it was unsuitable for preparing standards in the sub-ppm range. For 8% ethanol, however, a calibration curve could be obtained by subtracting the sample blank signal from that obtained from 8% ethanol solutions containing various concentrations of di(n-octyltin) bis-maleate. To apply the

TABLE 2

Data used in constructing calibration curves for di(n-octyltin) bis-maleate

Organo tin (ppm)	H_2O	Chart divisions[a]		
		8% EtOH	3% HAc	Heptane
0.00	0	40	1	0
0.01	3	50	2	—
0.03	7.7	58	5	—
0.06	19.5	65	10	—
0.08	—	—	—	5
0.125	42.5	87	22	—
0.16	—	—	—	10
0.24	—	—	—	14
0.40	—	—	—	23

[a]Average of two or more injections.

curve to sample extracts, it was necessary to assume that all tin originally present in the ethanol had been absorbed irreversibly by the container, and that tin in the extracts came only from di(n-octyltin) bis-maleate leached into the solvent. Any error arising from these assumptions will lead to high rather than low results.

For 50% ethanol, the tin content of the pure solvent blank was so high that a calibration curve could not be constructed. Extracts were tested solely by standard addition, as described below.

Heptane. Although di(n-octyltin) bis-maleate is soluble in heptane, there was no advantage in preparing a solution directly, rather than from the 50-ppm working solution in acetone. Spectroscopically-pure heptane was used to prepare solutions.

Standard addition method

It was considered possible that some material might be extracted from food containers which could combine with tin, and the resulting species could behave differently from di(n-octyltin) bis-maleate. To guard against erroneous results from such an interaction, a standard addition procedure was employed. For water, 5 μl of an aqueous solution containing di(n-octyltin) bis-maleate was added to the 50-μl sample directly in the graphite tube prior to drying. This approach was used because no tin signals were found from the extracts, but a qualitative verification of the presence of a tin signal of the expected magnitude was required, and was obtained. Furthermore, the traditional approach of preparing solutions by transferring aliquots of sample to other containers, then adding analyte standard solution is more prone to contamination from pipets and containers. "In-tube" addition was also used for the 8% ethanol and 3% acetic acid solution.

For heptane, however, the conventional approach was required, because the heptane drop soaked into the graphite tube and rendered the application of two solutions of sample open to serious question. This consideration also applied to 50% ethanol. In that case, since no direct comparison with a calibration curve was possible (because of the high tin blank) standard addition gave the only data. Because the 50% ethanol blank was excessive, standard additions were made with di(n-octyltin) bis-maleate in double-distilled water. For 8% ethanol, adding 5 ml of water to the 40-ml sample reduced the alcohol content to 7.2%. For 50% ethanol, two solutions were prepared, 5 ml of sample + 0.100 ml of 2.1 ppm di(n-octyltin) bis-maleate and 5 ml + 0.3% ml of that solution. Thus, the alcohol contents were 49% and 47%, respectively. These small changes in ethanol content should not significantly alter the atomization efficiency of tin present in the sample.

RESULTS

Six different types of resin were used to fabricate food-packaging containers, which were extracted with food-simulating solvents under a variety

TABLE 3

Tin stabilizer concentrations (ppm) in food-simulating solvents extracted from various resins[a]

Solvent	Resin/treatment[b]								
	1A	1B	2A	3A	4A	5C	5B	6D	6A
H_2O - Direct	<0.01	<0.01	<0.01	<0.01	<0.01	<0.01	<0.01	<0.01	<0.01
- S.A.	<0.01	<0.01	<0.01	<0.01	<0.01	<0.01	<0.01	<0.01	<0.01
3% HAc - Direct	0.01	0.02	0.03	0.03	<0.01	0.02	0.03	0.01	0.03
- S.A.	<0.01	<0.01	0.02	0.02	<0.01	0.01	0.03	0.01	0.01
8% EtOH - Direct	0.07	0.12	<0.01	<0.01	<0.01	0.01	<0.01	0.01	0.06
- S.A.	0.08	0.18	0.07	0.03	0.02	0.03	0.03	0.04	0.08
50% EtOH - S.A.	0.05	—	—	—	0.14	<0.01	—	0.03	—
Heptane - Direct	0.07	0.06	<0.01	0.01	< 0.01	0.01	0.05	0.01	<0.01
- S.A.	0.06	0.06	0.01	0.01	<0.01	0.03	<0.01	<0.01	<0.01

[a]Results were obtained by the direct and standard addition (S.A.) methods. Dashes indicate that extraction was not done.
[b]Extractions were (A) 30 days, filled at ambient temp. (B) 30 days, filled at ca. 90°C; (C) 6 months, filled at ambient temp.; (D) 2 months, filled at ambient temp. All samples were stored at 51.6°C.

of time-and-temperature conditions. Apparent tin stabilizer levels in each of the extracts tested are recorded in Table 3. "Direct" values were obtained by comparing results from sample extracts to calibration curves constructed from the data in Table 2; standard addition results were obtained in the usual manner.

The values found in this study are probably higher than the actual level of tin stabilizer in the extracts. The signals measured by flameless a.a.s. arise from the total content of tin atoms, not from di(n-octyltin) bis-maleate per se; thus, if tin is extracted as a simple aquated ion or a hydroxyl complex, rather than as the dioctyltin maleate monomer, the tin signal would be larger than that expected if the tin stabilizer were the only tin species present. The method measures total tin, with di(n-octyltin) bis-maleate as the tin source for calibration curves and standard addition.

Recorder tracings generally showed a baseline fluctuation corresponding to ± 0.0013 absorbance unit. The tin signal varied with changes in the solvent system. Water gave the largest tin signal, a 0.01 ppm di(n-octyltin) bis-maleate solution yielding 0.0075 absorbance unit. Acetic acid and heptane were each about a factor of two less sensitive. But even with those two solvents, the analytical signal arising from a 0.01 ppm di(n-octyltin) bis-maleate solution was more than twice the standard deviation of the baseline, a commonly accepted criterion for detection limit. Duplicate measurements gave values differing by $\leqslant 5\%$ of the mean peak height. No meaningful data relating to detection limits could be obtained for ethanolic solutions because of the high blank.

The results recorded in Table 3 indicate that solvents stored in tested resins all contained less than 1 ppm of extracted stabilizer. The direct data are probably more precise, because the calibration curves were constructed from five points, whereas most standard addition results were deduced from only two points. The standard addition results are to be interpreted as showing that no gross differences between "pure" solvent and solvent extracts were depressing tin absorbance. Acetic acid results were generally lower by standard addition, whereas ethanol results were usually higher. Heptane results agreed within the limits of experimental error.

REFERENCES

1 U.S. FDA Regulation 121.2602, Federal Register 39 (1974) 28899; Updated in Regulation 178.2650.
2 K. C. Thomson and D. R. Thomerson, Analyst, 99 (1974) 595.
3 F. J. Schmidt, J. L. Royer and S. M. Muir, Anal. Lett., 8 (1975) 123.
4 F. Umland and E. Schumacher, Fresenius Z. Anal. Chem., 269 (1974) 367.
5 D. R. Christmann and J. D. Ingle, Anal. Chim. Acta, 86 (1975) 285.
6 A. Engberg, Analyst, 98 (1973) 137.
7 N. Sato, K. Tsurata, I. Kamada, S. Narita and H. Abjkawa, J. Food Hygiene Soc. Jpn., 14 (1973) 245.
8 E. G. Zook, Cereal Chem., 47 (1970) 720.
9 A. I. Williams, Analyst, 98 (1973) 233.
10 G. M. George, M. A. Albrecht, L. J. Frahm and J. P. McDonald, J. Ass. Offic. Anal. Chem., 56 (1973) 1480.
11 W. B. Barnett and E. A. McLaughlin, Anal. Chim. Acta, 80 (1975) 285.
12 J. C. Meranger, J. Ass. Offic. Anal. Chem., 58 (1975) 1143.
13 H. L. Trachman, A. J. Tyberg and P. D. Branigan, Anal. Chem., 49 (1977) 1090.

Analytica Chimica Acta, 101 (1978) 401—407

THE DETERMINATION OF IRON IN AQUEOUS PERCHLORATE SOLUTIONS BY ATOMIC ABSORPTION SPECTROMETRY WITH ELECTROTHERMAL ATOMIZATION

P. D. ALLEN, N. A. HAMPSON*, D. C. A. MOORE and M. J. WILLARS
Department of Chemistry, Loughborough University of Technology, Leicestershire, LE11 3TU (Gt. Britain)

(Received 5th May 1978)

SUMMARY

A study of the dissolution rate of magnetite electrodes required a reasonably precise method for the determination of iron in aqueous solutions containing 1 mol kg^{-1} sodium perchlorate. Atomic absorption spectrometry with electrothermal atomization in the wavelength range 248—392 nm with ashing at 1600°C proved to be the most satisfactory method. Iron concentrations in the range 0.1—100 $\mu g\ ml^{-1}$ were determined with 1-μl samples. The addition of low flow rates of acetylene to the nitrogen purge gas improved the reproducibility and increased the carbon rod lifetime.

During the last 20 years the dissolution of ionic crystals has received relatively little attention. Engell [1] has advanced a theory for the dissolution rate in which the rates of ion transfer depend exponentially on the electrochemical potential of the ion in question. Vermilyea [2] later improved the theory by removing the assumption for the chemical potential part of this dependency and also by avoiding Engell's requirement for a deviation from normal crystal stoichiometry. Vermilyea's equations were of the form: rate of ion transfer = $2\ r_f \exp [\alpha\ ZF\ \phi/RT]$, where r_f is the rate of free dissolution of the crystal and ϕ is the potential between the crystal and the Helmholtz layer, i.e. the thermodynamic potential in a fairly concentrated (1 mol kg^{-1}) solution. The theory was tested by Lee and Yeager [3] for the case of a nickel oxide crystal, and it was reported that the potential dependence of the dissolution rate was in satisfactory agreement with theory.

The control of magnetite scales on boiler tubes is a logical and extremely important extension of this subject. The determination of dissolution rates, however, causes problems, for in addition to changing the dissolution rate the potential changes the surface stoichiometry of the magnetite. Also, it is necessary to have a well-defined mass transport process, in order to avoid control of the processes by the electrolyte solution. This has been achieved with a rotating disc electrode (at which the diffusion layer thickness is well defined) under potentiostatic control. The current through the disc is the faradaic contribution to the process, and the changes in the solution ion

concentration with time $dC(Fe)/dt$ reflect the overall rate of dissolution. Even with a large electrode (1.3-cm diam.), the rate of increase of iron species in solution is quite small (1 ppm is typical). The analytical requirement is for a method of determining iron in aqueous solution with an accuracy of 10^{-2} ppm at levels of 1—10 ppm.

Many methods are available for the determination of trace quantities of iron, and several reviews are available [4—14]. Special mention should be made of photometric [15—30], flame spectrometric [31—41], flameless atomic absorption spectrometric [45—47], x-ray fluorescence spectrometric [48, 49] and radio-activation [50, 51] methods, as these appear to have been used to the greatest extent. However, polarography [52], atomic fluorescence [53], mass spectrography [54] and chemiluminescence [55] have also been mentioned as providing useful methods.

A detailed review of this literature indicated that, from the points of view of sensitivity, rapidity and versatility, flameless atomic absorption spectrometry was the most attractive method. Determinations by this method are simple, fast and precise. Low levels of iron can be determined directly: ca. 0.06 $\mu g\ l^{-1}$ can be determined in 0.1-ml samples.

EXPERIMENTAL

Apparatus and reagents

A flameless atomizer (Shandon Southern Ltd., type A3470) was used in conjunction with an atomic absorption spectrometer (Baird Atomic Ltd., type A3400). Spectrographic carbon rods (Ringsdorff-Werke G.M.B.H., type 2) were used throughout. All measurements were made under nitrogen (B.O.C. white-spot grade) with provision for the admixture of hydrocarbon gases. Temperature measurements were made on the graphite rod head assembly with a thermocouple, the data being continuously monitored (Telemax BT 20—100). The criterion for stability and reproducibility was a rod head temperature of 60°C.

All chemicals were of AnalaR grade.

Procedure

Samples (1 μl) were withdrawn from the reaction vessel from time to time. They were transferred to the cavity in the carbon rod when the rod head was at a temperature of 60°C, and the solvent water was removed by evaporation at a setting of 4 V for 20 s. Ashing was carried out in one stage at 9 V (ca. 1600°C) for 20 s; the second stage was available but proved unnecessary for the solutions tested. Immediately ashing was completed, the atomization voltage was applied for 1 s at a setting of 4.5 V, and the resulting signal from atomic and molecular absorption was recorded on a chart recorder. A slit width of 0.025 mm (0.18 mm band pass) was used throughout.

RESULTS AND DISCUSSION

Figure 1 shows typical traces corresponding to a range of ashing temperatures (i.e. a range of voltages applied to the carbon electrodes) for samples containing 1 ppm iron in sodium perchlorate solution (1 mol dm^{-3}). It can be seen that after ashing at the lower temperature twin peaks were obtained, one of these peaks being due to molecular absorption by products of the oxidation of carbon by residual perchlorate. The optimum rod voltage was found to be 9 V. Determinations could readily be made at higher ashing temperatures, but the use of these higher voltages resulted in very short rod lifetimes of the order of 50 cycles of operation. It then became necessary to replace the graphite rod during the analysis of a large number of samples and to restandardize. A subsidiary point is that the cost per analysis is very much increased by operating at these high temperatures.

A typical calibration curve is shown in Fig. 2. The lack of linearity is probably due to the porous nature of the graphite rod allowing some absorption of the sample. An alternative explanation is that small amounts of iron pentacarbonyl are produced during atomization; there is no chemical evidence for this, but thermodynamically it is quite likely under the experimental conditions. It was found to be necessary to repeat standards at intervals of 5 cycles of operation, during the analytical runs, in order to compensate for changes in the rod emission characteristics caused by oxidation of the carbon rod.

To reduce the time-dependent character of the rod emission characteristics, small flow rates of acetylene were bled into the nitrogen purge gas. This type of treatment was first reported by L'vov [56] and has been devel-

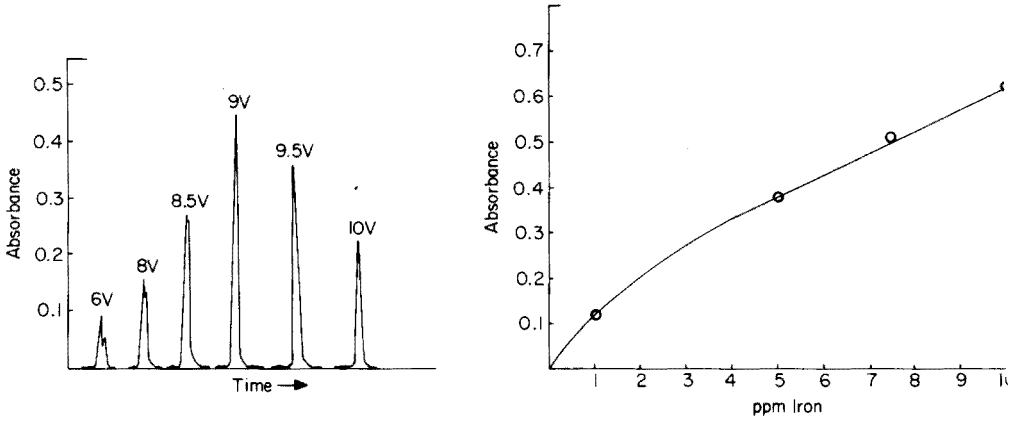

Fig. 1. Atomic absorption traces of a 1-μl sample containing 5-ppm iron in a 1 mol dm^{-3} sodium perchlorate solution analysed at 372 nm. Ashing voltages are shown on the traces. Nitrogen flow rate, 2.5 l min^{-1}. (6 V ≈ 800°C; 8 V ≈ 1350°C; 8.5 V ≈ 1500°C; 9 V ≈ 1600°C; 9.5 V ≈ 1650°C; 10 V ≈ 1700°C)

Fig. 2. Typical calibration curve for 0—10 ppm iron in 1 mol dm^{-3} sodium perchlorate analysed at 372 nm. The purge gas round the carbon rod was nitrogen 2.5 l min^{-1}.

oped by others [57—59]. In the present study, acetylene was admitted to the nitrogen at a rate of 40 ml min^{-1} to produce an initial pyrolytic coating, and was then maintained at 10 ml min^{-1} to repair any damage to the pyrolytic layer during the determinations. This was, however, unsatisfactory as a permanent solution to the damage, and it was necessary to recoat the graphite completely with carbon after about 40 runs. This was a consequence of the extremely oxidizing nature of the perchlorate ion at the experimental temperatures, which engendered considerable porosity on the carbon and gave rise to "memory effects" during analysis.

It was not possible to improve coating life by increasing the bleed rate, for rates above 10 ml min^{-1} produced a subsidiary peak on the absorption trace (Fig. 3); this was due entirely to the increased hydrocarbon flow.

The introduction of hydrocarbon increased the rod lifetimes by a factor of 10, and enhanced the sensitivity. Table 1 shows the sensitivity of the method for some of the spectral lines conventionally used in analyses for iron. These values were quite adequate, allowing the measurement of iron in the range 0.1—100 ppm without undue difficulty.

Figure 4 shows photographs of a used carbon rod, demonstrating the different physical natures of the base carbon and the pyrolytic coating. The carbon

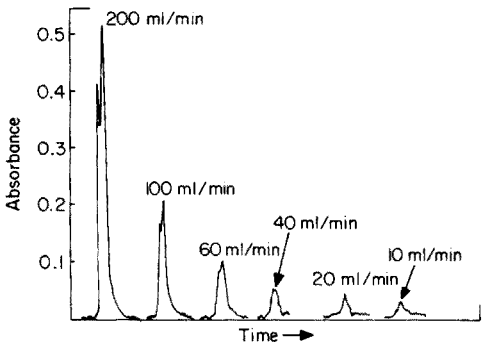

Fig. 3. Traces of blank runs showing the effect of acetylene flow rate. Acetylene flow rates are shown on the peaks; the purge gas was nitrogen at 2.5 l min^{-1}.

TABLE 1

Sensitivity of the method for iron in 1 mol dm^{-3} sodium perchlorate, expressed as concentration for 1% absorption with a 1-μl sample (Nitrogen, 2.5 l min^{-1}; acetylene, 10 ml min^{-1})

Wavelength (nm)	Sensitivity (ppm)	Wavelength (nm)	Sensitivity (ppm)
248.3	0.018	344.1	0.28
252	0.032	386	1
271.9	0.05	392	2.5
372	0.01		

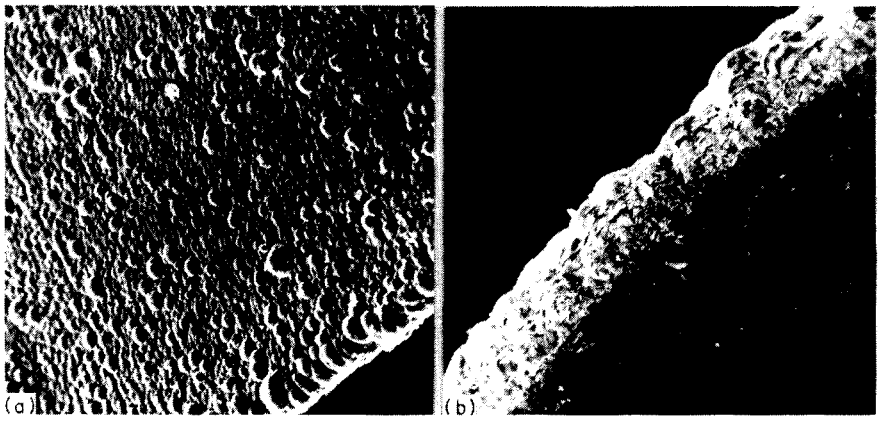

Fig. 4. Photographs of (a) the surface and (b) a section through the pyrolytic coating produced on the graphite rods during an experimental run.

rod itself is seen to be amorphous and coarse-grained. In this state, attack is rapid at grain boundaries producing a highly porous structure. The overlying layer of lamellar pyrolytic graphite is quite fine-grained. In this state the material is relatively resistant to oxidative attack.

Conclusions

The analysis of small samples (1 μl) for iron (0.1—100 ppm) in waters containing a high concentration (1 mol dm^{-3}) of sodium perchlorate is conveniently performed by atomic absorption spectrometry with electrothermal atomization. Careful choice of the ashing temperature removes the excess of supporting salt and allows the iron peak to be measured in isolation.

The use of low flow rates of acetylene increases rod lifetimes and improves the reproducibility of determinations by coating the amorphous carbon rod with a finer-grained pyrolytic carbon material. The destructive effect of the highly oxidizing perchlorate ion on the carbon rod can be controlled by addition of acetylene to the nitrogen purge gas, allowing routine analysis for iron in such solutions.

We are grateful to CERL (P.D.A.), CIBA-GEIGY (D.C.A.M.), Shell Research (M.J.W.) and SRC for financial support.

REFERENCES

1 H. J. Engell, Z. Phys. Chem., N.F., 7 (1956) 158.
2 D. A. Vermilyea, J. Electrochem. Soc., 113 (1966) 1067.
3 Chin-Ho Lee and E. Yeager, Tech. Rep. No. 5, Case Western Reserve University, Ohio, Project NR 359-451, Office of Naval Research (U.S.A.) 1973.
4 U.S. Dept. of Interior, Report of the Committee on Water, Quality Criteria, F.W.P.C.A. 1968.
5 M. J. Fishmann and D. E. Erdmann, Anal. Chem., 47 (1975) 334R.

6 M. J. Fishmann and D. E. Erdmann, Anal. Chem., 45 (1973) 361R.
7 M. S. Shuman and W. W. Fogleman, J. Water Pollut. Control Fed., 48 (1976) 998.
8 I. Kolthoff and P. Elving, Treatise on Analytical Chemistry, Part II, Vol. 2, Wiley-Interscience, New York, 1962, pp. 272—310.
9 A. L. Wilson, The Chemical Analysis of Water, Society for Analytical Chemistry, London, 1974.
10 A.S.T.M., 1969 Book of A.S.T.M. Standards, Part 23, A.S.T.M., Philadelphia, 1969, pp. 893—903.
11 British Standards Institution, B.S. 2690 Part 1, The Institution, London.
12 J. W. McCoy, Chemical Analysis of Industrial Water, MacDonald, London, 1969.
13 C.E.G.B. Research & Development Dept., Methods of Sampling and Analysis, Vol. 1, Steam and Water, C.E.G.B., Leatherhead, Surrey, 1966.
14 A. L. Wilson, Effluent Water Treat. J., 6 (1966) 75, 125.
15 W. B. Fortune and M. G. Mellon, Ind. Eng. Chem. Anal. Ed., 10 (1938) 60.
16 F. D. Snell and L. S. Ettre, Encycl. of Ind. Chem. Anal., Vol. 15, Wiley-Interscience, New York, 1972, p. 50.
17 G. F. Smith, W. J. McCurdy and H. Diehl, Analyst, 77 (1952) 418.
18 H. Diehl and G. F. Smith, The Iron Reagents, G. Frederick Smith Chemical Company, Columbus, Ohio, 1960.
19 C. Hammerton, Proc. Soc. Water Treat. Exam., 16 (1967) 293.
20 F. Nakashima and K. Sakai, Bunseki Kagaku, 11 (1962) 73.
21 W. K. Dougan and A. L. Wilson, Water Treat. Exam., 22 (1973) 100.
22 E. Cerrai and G. Ghersini, Analyst, 91 (1966) 662.
23 E. B. Sandell, Colorimetric Determination of Trace Metals, 3rd edn., Interscience, New York, 1959.
24 F. Schoeller, Gas, Wasser, Waerme, 23 (1969) 79.
25 J. A. Tetlow and A. L. Wilson, Analyst, 89 (1964) 442.
26 E. Cerrai and G. Ghersini, Analyst, 93 (1968) 606.
27 V. Kotelyanskaya, A. Kish and I. Pogoida, Zh. Anal. Khim., 27 (1972) 1128.
28 T. Korenaga, S. Motomizu and K. Tôei, Anal. Chim. Acta, 65 (1973) 335.
29 R. A. Dolmanova, V. I. Rychkova and A. Peshkova, Zh. Anal. Khim., 28 (1973) 1763.
30 V. I. Rychkova and A. A. Rychkov, Zavod. Lab., 39 (1973) 1053.
31 V. A. Fassel and D. V. Golightly, Anal. Chem., 39 (1967) 466.
32 J. A. Platte and V. M. Marcy, Proc. Am. Power Conf., 27 (1965) 851.
33 H. Kaiyama and S. Yasuda, Kogyo Yosui, 154 (1971) 21.
34 C. E. Mulford, At. Absorpt. Newsl., 5 (1966) 88.
35 J. Nix and T. Goodwin, At. Absorpt. Newsl., 9 (1970) 119.
36 S. L. Sachdev and P. W. West, Environ. Sci. Technol., 4 (1970) 749.
37 R. Herrmann and C. T. J. Alkemade, Chemical Analysis by Flame Photometry, Wiley-Interscience, New York, 1963.
38 G. H. Osborn and H. Johns, Analyst, 76 (1951) 410.
39 J. L. Jones and R. D. Eddy, Anal. Chim. Acta, 43 (1968) 165.
40 J. A. Platte, Trace Inorganics in Water, Proc. Miami Beach Symposium (1967), American Chem. Soc., 1968.
41 C. G. Farnsworth, Water Sewage Works, 119 (1972) 52.
42 R. C. P. Sinha, K. C. Singhal and A. C. Banerji, Technology, 5 (1968) 121.
43 H. James, Analyst, 98 (1973) 274.
44 D. G. Biechler, Anal. Chem., 37 (1965) 1054.
45 C. R. Parker, Water Analysis by A.A.S., Varian Techtron, Springvale, Australia, 1968.
46 C. J. Pickford and G. Rossi, Analyst, 97 (1972) 647.
47 F. M. Farnham, Analusis, 2 (1973) 49.
48 H. Watanabe, J. Berman and D. S. Russell, Talanta, 19 (1972) 1363.
49 C. W. Fuchs and R. W. Ryon, Rep. Atom. Ener. Comm. U.S., UCID 16658 (1974).
50 K. H. Lieser and V. Neitzert, J. Radioanal. Chem., 31 (1976) 397.

51 G. Pinte, N. Lefol, S. May and R. Darros, Analusis, 3 (1975) 480.
52 R. C. Rooney and P. J. McIver, Analyst, 87 (1962) 895.
53 D. W. Ellis and D. R. Demers, Trace Inorganics in Water (Adv. in Chem. 73), p. 332.
54 A. Mykytiuk, D. S. Russell and V. Boyko, Anal. Chem., 48 (1976) 1462.
55 R. W. Seitz and D. M. Hercules, Anal. Chem., 44 (1972) 2143.
56 B. V. L'vov, Spectrochimica Acta, Part B, 24 (1970) 53.
57 K. I. Aspila, C. L. Chakrabarti and M. P. Bratzel, Anal. Chem., 44 (1972) 1718.
58 R. W. Morrow and R. J. McElhaney, At. Absorpt. Newsl., 13 (1974) 45.
59 D. R. Thomerson and K. C. Thompson, Am. Lab., 6 (1974) 53.

Analytica Chimica Acta, 101 (1978) 409—412

THE THERMAL DECOMPOSITION OF PLATINUM TETRAMMINE CHLORIDE

J. PAULIK and F. PAULIK*

Institute for General and Analytical Chemistry, Technical University, Budapest (Hungary)

E. CZÁRÁN

Central Research Institute for Chemistry, Hungarian Academy of Sciences, Budapest (Hungary)

(Received 13th March 1978)

SUMMARY

The thermal decomposition of $Pt(NH_3)_4Cl_2 \cdot H_2O$ can be followed by means of the Derivatograph with simultaneous t.g., d.t.g., d.t.a. and e.g.a. The decomposition in a nitrogen atmosphere involves three stages, with maximum rates at 100, 250 and 315°C. Possible reaction pathways release chlorine or nitrogen. A simultaneous evolved gas analysis showed that chlorine is not developed. By direct and indirect methods, it was proved that the gases released during the decomposition to platinum are water, ammonia, hydrogen chloride and nitrogen.

Platinum catalysts are now prepared mainly by the thermal decomposition of platinum tetrammine chloride and a knowledge of every detail of this process is of technological importance. The decomposition involves the possibility of many partly or completely overlapping partial processes and may take place in two fundamentally different ways. One possibility is that in the formation of platinum metal an equivalent amount of chlorine is evolved simultaneously; alternatively, nitrogen is released and further gaseous products may also be formed.

$$Pt(NH_3)_4Cl_2 \cdot H_2O \begin{cases} \nearrow Cl_2, H_2O, NH_3, Pt \\ \searrow N_2, H_2O, NH_3, HCl, Pt \end{cases}$$

The Derivatograph seemed to be suitable for the study of this problem. This thermoanalytical equipment simultaneously performs thermogravimetry (t.g.), derivative thermogravimetry (d.t.g.), differential thermoanalysis (d.t.a) and "evolved gas analysis" (e.g.a), or more precisely, a special modification of e.g.a., namely thermal gas titrimetry (t.g.t) [1—3]. The results of these investigations are described in this paper.

The course of the thermal decomposition of the $Pt(NH_3)_4Cl_2 \cdot H_2O$ complex (Fig. 1) was studied by measuring the weight changes of the sample (curves 5,

6), the rate of these changes (curves 3, 4) and the rate of the enthalpy changes (curves 1, 2). Curves 1, 3 and 5 were obtained in a nitrogen atmosphere and curves 2, 4 and 6 in a mixture of nitrogen with 20% hydrogen. Examinations were also made in the presence of air; the curves so obtained were identical with those obtained in nitrogen.

According to the curves in Fig. 1, the decomposition is a three-stage process. Only the step at 90°C can be identified; on the basis of the temperature and the magnitude of the weight change, water of crystallization was probably evolved. In nitrogen, decomposition of the anhydrous complex started at 200°C and ended at 330°C. In the presence of hydrogen, the decomposition shifted toward lower temperatures. This complex has been examined thermoanalytically by other authors [4—7], who obtained similar results. It therefore became evident that with simultaneous t.g., d.t.g. and d.t.a. examinations alone, further information regarding the mechanism of the decomposition could not be obtained. The experiments were therefore repeated with the help of t.g.t.; qualitative and quantitative analyses of the gaseous products evolved were also carried out.

The essence of the t.g.t. method [2, 3] is that the gaseous products liberated are collected quantitatively with a carrier gas and absorbed in water in an absorption vessel. The gases react with the water and the amount of the compounds formed can be followed automatically by potentiometric titration. The changes in the amount of titrant consumed, recorded as a function of the temperature, are shown by the t.g.t. curve (Fig. 2, curves 2, 4, 6, 7) which reveals the gaseous evolution process.

To distinguish between the alternatives outlined above, the following experiments were carried out in a nitrogen atmosphere. The results are shown in Fig. 2.

The gases evolved during the simultaneous t.g., d.t.g., and d.t.a. experiments were absorbed in solutions containing KI and H_2SO_4. Any iodine released by chlorine could be titrated with thiosulphate solution, but no iodine was released (curve 2); nitrogen, not chlorine, was released in amounts equivalent to the platinum. This basically determined which of the thermal decomposition pathways mentioned above was followed.

By repeating the experiment the amount of the ammonia liberated was also measured. By keeping the absorbent solution permanently at pH 5, the titration was performed with hydrochloric acid solution and glass—calomel electrodes. This gave curve 4 which as Fig. 2 shows, coincides with the second step of the t.g. curve, demonstrating that, in the first period of the decomposition in the range 200—280°C, only ammonia is evolved.

During the ammonia titration, it was observed that at a given point in the decomposition, at ca. 290°C the titrator ceased to add further amounts of hydrochloric acid solution; nevertheless, the pH of the solution began to decrease rapidly. This indicated that, from this point of the decomposition onwards, hydrogen chloride was being liberated.

The experiment was repeated, but the volume of hydrochloric acid con-

sumed in the course of the earlier ammonia titration was added to the absorbant solution at the outset to neutralize the ammonia liberated in the first period of the decomposition. At 290°C, i.e. the temperature at which evolution of ammonia ceased, the automatic burette immediately began to add sodium hydroxide solution to the absorption solution when pH 5 was reached. This allowed the liberation of hydrogen chloride to be followed (curve 5). The conclusion was reached that these compounds evolved simultaneously and entered the absorption solution in the form of NH_4Cl. The total chloride content was therefore determined with silver—calomel electrodes and silver nitrate solution as titrant. In calculating the results, the results of the hydrogen chloride titration were also taken into account. From temperature to temperature, by difference, the amount of titrant corresponding solely to NH_4Cl was calculated (curve 6). It was assumed that one mole of water of crystallization was evolved up to ca. 90°C (curve 2). This suggestion is supported by the magnitude of the weight change indicated by the first step of the t.g. curve, and by the course of the subsequent t.g.t. curves.

Finally, the amount of nitrogen liberated was calculated from the differences in the t.g. and t.g.t. curves (curve 7). For the reduction of platinum, the oxidation of two moles of ammonia to nitrogen is necessary, and this releases the protons required for the formation of HCl and NH_4Cl. Stoichio-

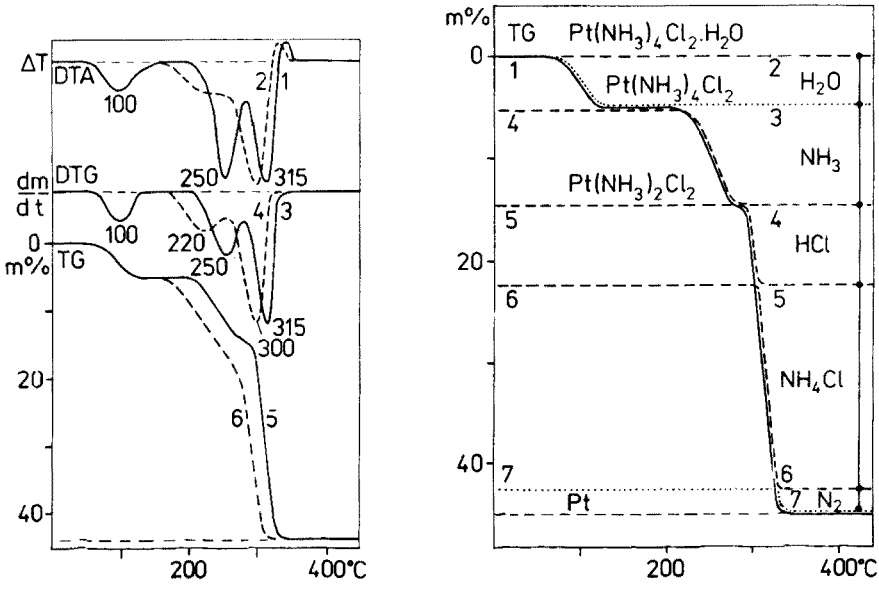

Fig. 1. Decomposition of $Pt(NH_3)_4Cl_2 \cdot H_2O$. In N_2 (curves 1, 3, 5); in N_2 + 20% H_2 (curves 2, 4, 6).

Fig. 2. Decomposition of $Pt(NH_3)_4Cl_2 \cdot H_2O$. Weight change (curve 1); evolution of I_2, H_2O, NH_3, HCl, NH_4Cl and N_2 in nitrogen atmosphere (curves 2—7).

metric calculations made on this basis, and difference calculations from the t.g.—t.g.t. curves, gave surprisingly good agreement for the amount of nitrogen released.

It must be emphasized that, of the gaseous products, only 1 mole of water and 2 moles of ammonia split off separately; the production of nitrogen, HCl and the additional ammonia occurs simultaneously. The quantitative relationships are shown by the respective curves in Fig. 2.

The mechanism of the thermal decomposition of $Pt(NH_3)_4Cl_2 \cdot H_2O$ can therefore be represented schematically as follows:

$$Pt(NH_3)_4Cl_2 \cdot H_2O = Pt(NH_3)_4Cl_2 + H_2O$$
$$Pt(NH_3)_4Cl_2 = Pt(NH_3)_2Cl_2 + 2NH_3$$
$$3Pt(NH_3)_2Cl_2 = 3Pt + N_2 + 4NH_3 + 6HCl$$

The titration curves of experiments carried out in a N_2—20% H_2 mixture [8] showed only negligible differences from Fig. 2, in the relative amounts of NH_3, HCl and NH_4Cl.

The authors thank Prof. E. Pungor for interest in this work and M. Arnold for assistance.

REFERENCES

1 F. Paulik, J. Paulik and L. Erdey, Talanta, 13 (1966) 1405.
2 J. Paulik and F. Paulik, Talanta, 17 (1970) 1224.
3 J. Paulik and F. Paulik, Thermochim. Acta, 3 (1971) 13.
4 See, e.g. W. W. Wendlant and J. P. Smith, The Thermal Properties of Transition Metal Ammine Complexes, Elsevier, Amsterdam, 1967.
5 K. Kinoshita, K. Routsis and A. S. Bett, Thermochim. Acta, 10 (1974) 109.
6 J. N. Kukuskin and F. S. Postnikova, Zh. Prikl. Kim., 44 (1971) 6.
7 J. N. Kukuskin, Kem. Kozl., 37 (1972) 389.
8 E. Czárán, Dissertation, Humboldt University, Berlin, 1973.

Analytica Chimica Acta, 101 (1978) 413—418

THE USE OF CERIUM(IV) PHOSPHATE FOR THE GRAVIMETRIC DETERMINATION AND SEPARATION OF CERIUM

VLADIMÍR MAŠÍN and JAN DOLEŽAL

Department of Analytical Chemistry, Charles University, Albertov 2030, 128 40 Prague 2 (Czechoslovakia)

(Received 16th February 1978)

SUMMARY

A method for the gravimetric determination of cerium as $Ce_3(PO_4)_4$ is described. Cerium can be separated from many metals in this form, as well as from permanganate and dichromate; the cerium separated can then be titrated with iron(II) solution. The method was verified for the determination of cerium in a rare earth concentrate.

The high redox potential of the Ce(IV)/Ce(III) system is often used for titrimetric determinations of cerium with various reductants, usually iron(II); the selectivity is good, the only interferences being oxidants with redox potentials similar to that of cerium, e.g. $Cr_2O_7^{2-}$ or MnO_4^-. In contrast, gravimetric determinations of cerium are inselective. Cerium(IV) is usually precipitated as $Ce(OH)_4$ [1], but all elements yielding insoluble hydroxides interfere. The use of organic reagents is limited by the oxidizing properties of cerium(IV) [2]. Cerium(IV) orthophosphate is very insoluble with a possible pK_{SO} value of 90.1 [3]. It precipitates even below pH 1, along with the orthophosphates of Zr, Ti, Bi, Sn and Th. In this paper, the orthophosphate is used for a gravimetric determination of cerium and for separation of cerium before titration.

The precipitation and composition of cerium(IV) phosphate have been studied for chemical technology [4, 5]. Cerium(IV) phosphate is precipitated in a hydrated form and assumes the composition, $Ce_3(PO_4)_4 \cdot 11H_2O$: after drying at 110°C, this light yellow compound is converted to the pentahydrate at 200°C, and to the very pale yellow anhydrous $Ce_3(PO_4)_4$ at 500—600°C.

EXPERIMENTAL

Reagents

A 0.1 M solution of $Ce(SO_4)_2$ (Merck) was prepared in 0.5 M H_2SO_4, and standardized by potentiometric titration with potassium hexacyanoferrate(II) or iron(II) ammonium sulphate [6, 7]. A 0.1 M solution of iron(II) ammonium sulphate in 0.05 M H_2SO_4 was prepared and standardized by potentiometric titration with potassium dichromate. All the chemicals used were of p.a. grade (Merck or Lachema).

Apparatus

An OP205 pH meter (Radelkis, Hungary) and an LP 7 polarograph (Laboratorní Přístroje, Czechoslovakia) were employed.

Gravimetric procedure

To about 100 ml of ca. 5×10^{-3} M Ce^{4+} solution in 0.1 M H_2SO_4 add 1 M H_3PO_4 to give a final precipitant concentration of about 0.05 M. Allow the precipitate to settle, and after 10—15 min filter on medium-porosity paper. Wash the precipitate with water until the washings are free from sulphate, and ignite to constant weight at a temperature above 900°C. The theoretical conversion factor, 0.5253, is applicable.

Separation and titrimetric procedure

To about 100 ml of ca. 5×10^{-3} M cerium(IV) solution which is up to 1 M in HNO_3 or $HClO_4$, add at least 20 ml of 1 M H_3PO_4 (see below). Filter the $Ce_3(PO_4)_4$ precipitate on a medium-porosity paper and wash thoroughly with water. Tear the filter, and transfer the precipitate to an Erlenmeyer flask. Then wash the filter with water, (1 + 4) H_2SO_4, and again with water. The final volume of the solution is 100—150 ml, containing about 12 ml of 18 M H_2SO_4. The precipitate must not be dissolved on the filter, as Ce^{4+} would react with the paper giving negative errors. The precipitate must be dissolved completely, if necessary, by heating. Titrate the cooled solution with 0.1 M $Fe(NH_4)_2(SO_4)_2$ solution to a ferroin end-point.

As much as 1 M HNO_3 and $HClO_4$ may be present but at least 20 ml of 1 M H_3PO_4 must be added per 100 ml of solution to ensure complete precipitation. The final H_3PO_4 concentration can be as high as 1 M, but the precipitate formed is then very fine and a dense filter must be used. The H_2SO_4 concentration should not exceed 0.6 M to avoid dissolution of the precipitate.

RESULTS AND DISCUSSION

Gravimetric method

Some typical results are given in Table 1. The recoveries are satisfactory, considering the level of concentration of cerium. The concentration of H_2SO_4 must be between 0.1 and 0.3 M; at lower concentrations, negative errors are caused by hydrolysis, and at higher concentrations the precipitate becomes more soluble. The H_3PO_4 concentration must be 0.04—0.08 M in the final solution; higher concentrations lead to positive errors, which appear to be caused by adsorption of phosphate on the precipitate, the error being +10% with 0.3 M H_3PO_4. Nitric acid can be used instead of sulphuric acid, the permissible range then being 0.2—1 M HNO_3.

Tests made with starting solution volumes of 50—300 ml showed that the optimum volume was 100—300 ml (for 0.1 M H_2SO_4—0.05 M H_3PO_4 medium containing the equivalent of 0.1334 g of cerium(IV) phosphate). As the precipitate is voluminous, its weight should not exceed 0.2 g. Washing of larger

TABLE 1

Gravimetric determination of cerium(IV)

Ce^{4+} taken (g)	Theor. equiv. of $Ce_3(PO_4)_4$ (g)	$Ce_3(PO_4)_4$ $\bar{x}$ (g)	Found[a] n	Range (g)	H_2SO_4 (M)
0.0683	0.1301	0.1303[b]	12	0.1293—0.1322	0.1
0.0699	0.1331	0.1324	6	0.1290—0.1347	0.1
0.0341	0.0650	0.0644	6	0.0638—0.0651	0.1
0.1366	0.2600	0.2619	3	0.2611—0.2631	0.1
0.0683	0.1301	0.1304	6	0.1295—0.1321	0.05
0.0683	0.1301	0.1278	6	0.1265—0.1290	0.025
0.0683	0.1301	0.1296	6	0.1290—0.1303	0.2

[a]Mean ($\bar{x}$), number of determinations (n) and range.
[b]Standard deviation, 0.0012 g.

amounts is time-consuming and not every efficient. As the precipitate tends to adsorb ions easily, acidified water or solutions of ammonium nitrate or chloride were not suitable for washing the precipitates. It is best to wash with water until the filtrate is sulphate-free, but prolonged washing causes hydrolysis and therefore low results. Temperatures up to boiling have no effect on the determination, but prolonged standing (more than 8 h) must be avoided because of post-precipitation effects which gave errors of about +5%.

The precipitation conditions were checked by using amperometric titration with a dropping mercury electrode (Fig. 1). It can be seen that precipitation is incomplete at the theoretical consumption of KH_2PO_4 (curve II); this was

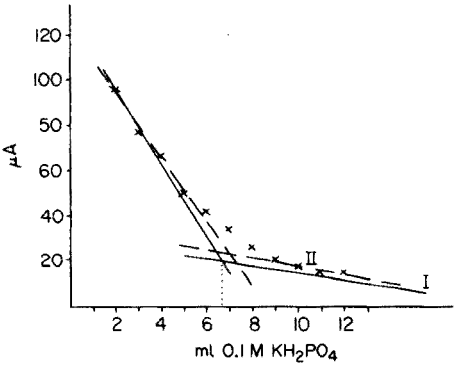

Fig. 1. Amperometric titration. A volume (100 ml) of a solution containing 5×10^{-3} M Ce^{4+}, 0.1 M H_2SO_4, 0.5 M Na_2SO_4 was titrated with 0.1 M KH_2PO_4. The theoretical consumption is 6.65 ml. A dropping mercury electrode (drop time, 4 s) was used at a potential of —0.3 V vs. SCE. The solution was deaerated with argon. (I) Theoretical titration curve; (II) experimental curve.

also indicated by the weak yellow colour of the solution, which disappeared only on further addition of KH_2PO_4.

In the gravimetric method, there is no interference from alkali metals or from large amounts of Zn^{2+}, Mg^{2+}, Ca^{2+}, La^{3+}, Ce^{3+}, $Cr_2O_7^{2-}$ and MnO_4^-, Ba^{2+} and Sr^{2+}; however, washing must be done carefully. Elements forming insoluble phosphates interfere. Thus the concentrations of Fe^{3+}, Al^{3+} and Ag^+ must not exceed one third of that of Ce^{4+} for their effects to be statistically insignificant.

It can be concluded that the gravimetric determination of Ce^{4+} as $Ce_3(PO_4)_4$ is much more selective than precipitation as $Ce(OH)_4$ which is commonly used. Disadvantages of the new method are the necessity of rigorously maintaining the precipitation conditions and the time-consuming washing of the precipitate. Therefore it is likely that the method will find wider use as a separation procedure.

Separation of cerium(IV) as $Ce_3(PO_4)_4$ and its titrimetric determination

Cerium(IV) is commonly titrated with an iron(II) salt [7]. In the presence of permanganate and dichromate, cerium(IV) can be determined by precipitation as $Ce_3(PO_4)_4$, filtration on a paper filter, washing, dissolution in sulphuric acid and titration. Filtering crucibles are unsuitable, as the precipitate is difficult to wash and dissolve. The titrimetric determination is considerably simpler than the gravimetric one, as partial hydrolysis at low acidities and adsorption phenomena caused by excess of phosphoric acid are without effect. The only condition is that the H_3PO_4 concentration must be sufficiently high to permit complete precipitation.

Interferences. If manganese and chromium are present as MnO_4^- and $Cr_2O_7^{2-}$, they do not interfere, but increased attention must be paid to washing of the precipitate. If Ce^{3+}, Mn^{2+} and Cr^{3+} ions are present, they must be oxidized. The oxidation of Ce^{3+} and Cr^{3+} with ammonium peroxodisulphate catalyzed by Ag^+ ions presents no complications, but high concentrations of Mn^{2+} may not be completely oxidized [6] and the fine precipitate of MnO_2 formed contaminates the $Ce_3(PO_4)_4$ precipitate. The manganese concentration should therefore not exceed 8—10 mg/100 ml.

Experience showed that this formation of MnO_2 depends on the oxidation conditions. The following requirements should be observed. The manganese(II) concentration should be as low as possible; the formation of MnO_2 is prevented by the presence of H_3PO_4 and high concentrations of H_2SO_4 but is enhanced by high temperatures and by the presence of Ca^{2+} and Ce^{3+}. For example, when the Ce^{3+} concentration is 70 mg/100 ml, the Mn^{2+} concentration must not exceed 4 mg/100 ml to ensure complete oxidation. The formation of MnO_2 begins only in boiling solution during decomposition of last traces of peroxodisulphate.

If the $Ce_3(PO_4)_4$ precipitate is separated by filtration, it is unnecessary to decompose ammonium peroxodisulphate by boiling. The manganese concentration may then be higher, but washing of the precipitate is rather difficult.

High concentrations of alkali metals and a three-fold amount of Ag^+, Zn^{2+} Ni^{2+} or Co^{2+} do not interfere. Because of the final titration, elements that form sparingly soluble phosphates (e.g. Th and Bi) do not interfere, provided that their amounts are not too high. Iron(III) and aluminium(III) interfere, but their interferences can be partially suppressed by increasing the concentration of phosphoric acid.

Verification of the method

A solution (100 ml) containing known amounts of Ce^{3+}, Mn^{2+} and Cr^{3+}, with sulphuric or nitric acid up to 0.3 M and 3—4 ml of 85% H_3PO_4, was oxidized with 10 ml of a saturated solution of ammonium peroxodisulphate in the presence of 5 ml of 0.1 M $AgNO_3$, by heating for 10 min on a water bath. The peroxodisulphate was not removed. The $Ce_3(PO_4)_4$ precipitate was then filtered off, washed, dissolved and titrated as described under Experimental. The results (Table 2) were quite satisfactory.

The method was applied to a rare earth concentrate, which contained phosphates of rare earths, calcium and magnesium and low concentrations of Fe, Al, Mn, Zn, Cr, Ti, F, etc. The rare earth contents were 20—35%, those of Fe and Al up to 2% and those of Mn and Cr of the order of tenths per cent.

For dissolution, the sample (in an amount depending on the cerium content) was treated with 10 ml of water, 10 ml of concentrated HNO_3 and 30 ml of concentrated H_2SO_4. After evaporation to a paste, 100 ml of about 0.3 M H_2SO_4 or HNO_3 and several drops of hydrogen peroxide (to reduce and dissolve any Ce^{4+} present) were added and the solution was evaporated to one third of its original volume. The solution was then transferred to a 100-ml volumetric flask and diluted with water to the mark. A 10—25-ml aliquot of the supernatant liquid was transferred to a beaker containing about 80 ml of 0.1 M H_2SO_4, 20 ml of 1 M H_3PO_4 , 10 ml of saturated ammonium peroxodisulphate and 5 ml of 0.1 M $AgNO_3$. After heating for 10 min on a water bath, the precipitate was allowed to settle, filtered, and washed with water. The precipitate was then dissolved and titrated as described under Experimental.

TABLE 2

Determination of cerium in the presence of manganese and chromium

Ce	Taken (mg)		Ce found (mg)[a]
	Mn	Cr	
71.0	—	—	70.7
35.4	—	—	35.5
71.0	2	5.2	71.2
71.0	5	5.2	71.3
71.0	11	5.2	71.5
71.0	—	52.0	71.1

[a]Average of three determinations.

TABLE 3

Determination of cerium in a rare earth concentrate, and comparison with the oxalate method

Sample No.	Cerium found (%)[a]	
	Oxalate method	Proposed method
1	11.93	12.10
2	12.55	12.70
3	13.10	13.25
4	15.25	15.33
5	15.55	15.60

[a] Average of duplicate determinations.

The results obtained for real samples are given in Table 3, along with the results obtained by the oxalate method. For the latter method, the rare earth elements were precipitated as the oxalates [1] and ignited to the oxides, which were dissolved in sulphuric acid in the presence of peroxide. The cerium was finally determined after oxidation with ammonium peroxodisulphate by titration with iron(II) to a ferroin end-point [7]. The differences in the results are statistically insignificant.

In conclusion, the proposed gravimetric determination is more selective than the current precipitation as the hydroxide. However, the precipitation reaction is particularly suitable for separation of cerium(IV), chiefly from permanganate and dichromate, which interfere in the commonly used titrations. For analysis of rare earth concentrations, the proposed method is faster and gives slightly higher results than the time-consuming oxalate method.

REFERENCES

1 L. Erdey, Theorie und Praxis der Gravimetrischen Analyse, Band II, Akademiai Kiado, Budapest, 1964, p. 494.
2 H. L. Kapoor, Y. K. Agrawal and P. C. Verma, Talanta, 22 (1975) 193.
3 L. G. Sillén and A. E. Martell, Stability Constants of Metal Ion Complexes, Vol. I, Chemical Society, London, 1964, p. 183.
4 I. A. Atanasiu and M. Babor, Bull. Sect. Sci. Acad. Roumaine, 20 (1938) 27, 32.
5 J. Sedláček, Scientific Papers of the Institute of Chemical Technology, Part I, CSAV, Prague 1959, p. 71.
6 J. Číhalík, Potentiometry, CSAV, Prague, 1961, pp. 356, 679.
7 G. Charlot, Metody Anal. Khim., Mir, Moscow, 1965, pp. 453, 915.

Analytica Chimica Acta, 101 (1978) 419—422

Short Communication

CONSTRUCTION AND BEHAVIOUR OF A MICRO FLOWTHROUGH COPPER(II)-SELECTIVE ELECTRODE

W. E. VAN DER LINDEN* and R. OOSTERVINK

Laboratory for Analytical Chemistry, University of Amsterdam, Nieuwe Achtergracht 166, Amsterdam (The Netherlands)

(Received 28th February 1978)

Ion-selective flowthrough electrodes are of interest for continuous monitoring. Such devices can be used for direct monitoring of the ion concerned, as well as for monitoring any other compound which will participate in a stoichiometric reaction that changes the concentration of the ion detected by the electrode. Another interesting application of flowthrough electrodes is in flow-injection analysis [1].

The characteristics of the copper(II)-selective membranes prepared in earlier work [2] were such that these membranes were considered suitable for the construction of flowthrough electrodes. The construction of similar electrodes has been reported by Thompson and Rechnitz [3], and by Blaedel and Dinwiddie [4]. Two types of electrode are described here. Under certain conditions the electrodes can also be used for the direct monitoring of complexing agents.

Experimental

Figures 1 and 2 show the two flowthrough electrodes used. In both electrodes, pellets of 13 mm diameter are employed. In the dismountable electrode (Fig. 1) made of perspex, the pellets are about 0.4-mm thick; in the other electrode, the pellets are about 1-mm thick. This latter electrode was very simply constructed as suggested by Thompson and Rechnitz [3]. The pellet is embedded in the polymer Polypol PS 230 (Polyservice, Amsterdam) by using a polyethylene mould, and the polymer is hardened at 60°C. The flowthrough channel in the body and the pellet is made by careful drilling.

Potentials were recorded with an Orion digital mV-meter, model 801 A, connected to a Philips recorder PM 8100. To adjust the desirable offset a potentiostat (Knick S 16) was used. For the flow-injection analysis, an Altex sample injection valve made of Kel-F and Teflon was employed.

As can be seen from the flow diagram (Fig. 3), the experimental set-up consisted of two tubes, one for the introduction of the continuous sample flow or the injection of samples (A), and the other for the buffer solution to which some copper is added (B). For flow injection, buffer solution is pumped through tube A. Adequate mixing of the two flows is ensured by inserting a tube (D) of 5-cm length (2-mm i.d.) filled with small glass beads (0.5-mm diam.).

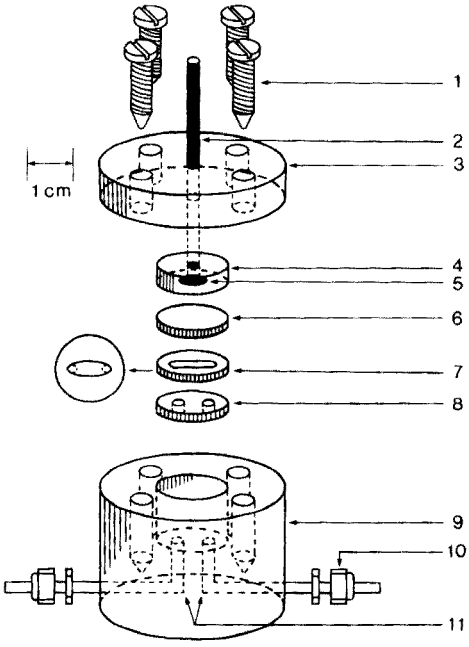

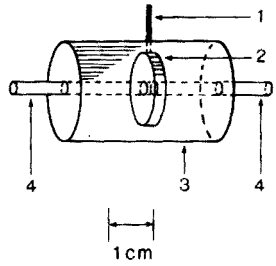

Fig. 1 (left). Dismountable flowthrough electrode. (1) Screws; (2) silver wire; (3) perspex lid; (4) silicone rubber plug; (5) silver disc; (6) copper sulfide pellet; (7) spacer; (8) silicone rubber disc; (9) perspex body; (10) Swagelock connection; (11) inlet/outlet.

Fig. 2. (right). Disposable flowthrough electrode. (1) Silver wire; (2) copper sulfide—silver sulfide pellet; (3) Polypol polymer body; (4) inlet/outlet.

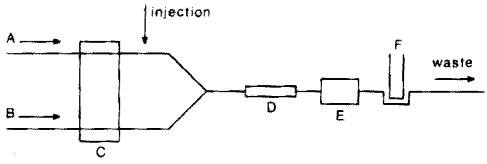

Fig. 3. Flow diagram. (A) and (B) Tubing, 0.5-mm i.d.; (C) pump; (D) mixing tube reactor; (E) flowthrough electrode; (F) reference electrode.

Three different pumps were tested: an Ismatec PMP Duo plunger pump; a Gilson Minipulse 2 peristaltic pump; and a LKB type 4912 A peristaltic pump. When the same solution was pumped through tubes A and B a constant signal was recorded, the noise level being less than 0.1 mV (Fig. 4, line a). When a continuous flow of a dilute copper solution was pumped in tube B, a regular pattern with variations of about 0.5—1.0 mV was observed when the Ismatec pump was used (Fig. 4, line b). The LKB pump showed some variations of the order of 0.2 mV (Fig. 4, line c). The best results were obtained with the Gilson pump (Fig. 4, line d). The variations cannot be attributed to electrostatic influences introduced by the pump, as no variations were observed whe

the same solution was pumped through tubes A and B. The variations observed must be due to unequal delivery by the two tubes during one cycle, thus causing a pulsating concentration level at the detector. With peristaltic pumps, there is an inevitable but slight pulsation, which is visible in Fig. 4 (line c), and also appeared as a small variation of higher frequency superimposed on the variations discussed above. Throughout further experiments, the Gilson pump was used. To avoid the influence of static electricity, the whole set-up must be electrically shielded.

All chemicals used were of analytical-reagent grade. The buffer solutions were pH 4.75 (0.05 M acetate buffer) and pH 6.25 (0.05 M maleate buffer). Ionic strength was maintained at 0.1 with KNO_3.

Results and discussion

The dismountable electrode shows a fast response (90% of the maximal response value in 6 s) provided that the spacer is the proper size; three thicknesses of the spacer were tested (3, 1.2 and 0.3 mm), and the thinnest gave the best results.

The "disposable" electrode has a much slower response (90% of the maximal response in about 50 s). The great advantage of this electode is that it is simple and cheap to prepare, so that it can be regarded as disposable. For both electrodes, the signal was remarkably constant for several days provided that a continuous flow through the electrode was maintained.

The disposable electrode was subsequently used for continuous monitoring of the copper content in tap water, which arises from copper pipes; Fig. 5 shows a run of 22 h. The level indicated by A is the potential obtained when channel A was fed with deionized water. The run was started at the end of the day; during the night little tap water is used and an increase of the copper concentration is observed, but in the morning, from point B, there is a decrease because of the much higher water consumption in the laboratory. The irregularities in the recording are due to air bubbles in the water supply passing the electrode, after which the electrode needs some time before the correct potential is restored.

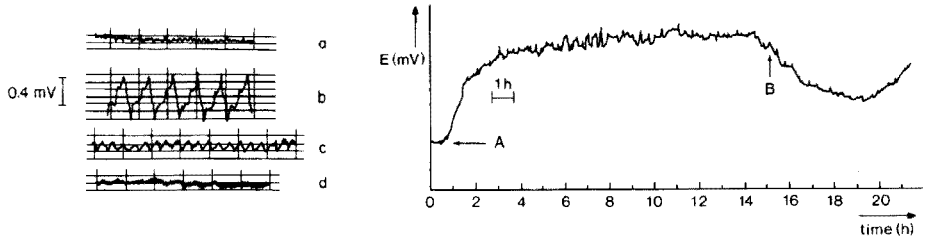

Fig. 4. Potential recordings for different pumps. (a) Ismatec PMP Duo with the same solution in tubes A and B. (b) Ismatec PMP Duo with acetate buffer in tube A and acetate buffer + 10^{-4} M Cu^{2+} in tube B. (c) LKB peristaltic pump with solutions as in (b). (d) Gilson peristaltic pump with solutions as in (b).

Fig. 5. Variation of copper content in tap water during a 22-h run.

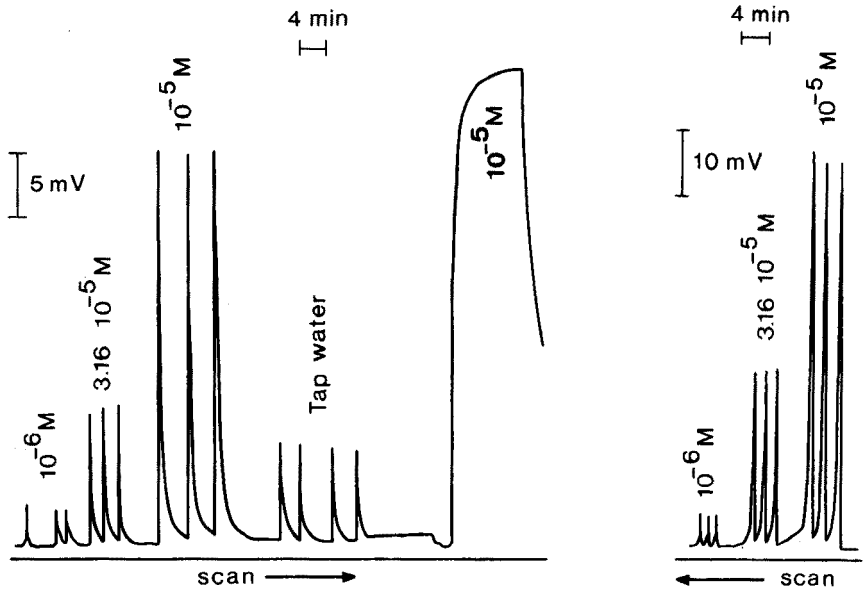

Fig. 6. Flow-injection analysis of Cu^{2+}. pH 6.25; flow 30 $\mu l\,s^{-1}$; channel A, buffer + injection of Cu^{2+} as indicated; channel B, buffer + 10^{-6} M Cu^{2+}.

Fig. 7. Flow-injection analysis of Trien. pH 6.25; flow 30 $\mu l\,s^{-1}$; channel A, buffer + injection of Trien as indicated; channel B, buffer + 10^{-6} M Cu^{2+}.

Figure 6 shows some results of flow-injection experiments with the disposable electrode. Copper concentrations in the range 10^{-5}—10^{-6} M were injected by means of the injection valve and a loop of 0.13 ml. It appeared to be useful to introduce a constant copper concentration level as background, so that the potential was fixed at a well-defined value in between the different injection peaks. A drawback of this procedure is that the calibration curve is no longer strictly linear. The determination of 10^{-5} M Cu^{2+} was not affected by the presence of 10^{-4} M Co^{2+}, Ni^{2+}, Zn^{2+}, Pb^{2+} and Cd^{2+}. Even the presence of 10^{-4} M Fe^{3+} showed an interference of less than 10%.

As can be seen from Fig. 7, reproducible peaks are observed if a complexing agent is injected. The direction of the potential changes is now opposite. Here again, tailing of the peaks is largely reduced by maintaining a constant low copper concentration level.

These three examples illustrate the applicability of two simple flowthrough electrodes.

REFERENCES

1 J. Růžička, E. H. Hansen and E. A. Zagatto, Anal. Chim. Acta, 88 (1977) 1.
2 G. J. M. Heijne, W. E. van der Linden and G. den Boef, Anal. Chim. Acta, 89 (1977) 287.
3 H. Thompson and G. A. Rechnitz, Chem. Instrum., 4 (1972) 239.
4 W. J. Blaedel and D. E. Dinwiddie, Anal. Chem., 47 (1975) 1070.

Analytica Chimica Acta, 101 (1978) 423—427

Short Communication

SPECTROPHOTOMETRIC DETERMINATION OF ULTRAMICRO AMOUNTS OF COPPER WITH α,β,γ,δ-TETRAPHENYLPORPHINE IN THE PRESENCE OF A SURFACTANT

HAJIME ISHII, HIDEMASA KOH and TADAAKI MIZOGUCHI

Chemical Research Institute of Non-Aqueous Solutions, Tohoku University, Katahira, Sendai-shi, 980 (Japan)

(Received 22nd February 1978)

Recently, water-soluble porphyrins such as α,β,γ,δ-tetraphenylporphine trisulphonate [1, 2], α,β,γ,δ-tetra(3-*N*-methylpyridyl)porphine [3], α,β,γ,δ-tetra(4-sulphophenyl)porphine [4] and α,β,γ,δ-tetra(4-carboxyphenyl)-porphine [5] have been examined as extremely sensitive spectrophotometric reagents for metals. Water-insoluble porphyrins, however, have not been studied, except for α,β,γ,δ-tetraphenylporphine (TPP or H_2L) which has been used for the determination of submicro amounts of zinc in glacial acetic acid [6]. If a water-insoluble porphyrin could be used to form a complex with metal ions in aqueous solution, many types of porphyrin which can be synthesized easily and purified with relatively high yield, could probably be used as sensitive spectrophotometric reagents for metals. It is well known that water-insoluble organic materials can often be solubilized in surfactant micelles, and this has been utilized analytically [7]. In the present work, TPP (I) and sodium lauryl sulphate (SLS) were examined as the water-insoluble porphyrin and the surfactant, respectively, for the spectrophotometric determination of copper(II). A practical method suitable for copper at μg l^{-1} levels can be based on the Soret band of the complex formed.

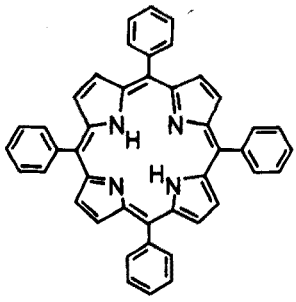

(I)

Experimental

Apparatus and reagents. Absorption spectra were obtained with a Hitachi 556 automatic recording spectrophotometer and absorbances were measured

with a Hitachi 139 spectrophotometer, with 10-mm glass cells. A Hitachi M-7 glass electrode pH meter was used for pH measurements.

TPP solution (5×10^{-5} M) was prepared by dissolving 15.4 mg of TPP in 50 ml of dioxane and diluting the solution to 500 ml with aqueous 10% SLS solution. TPP was synthesized by refluxing pyrrole and benzaldehyde in propionic acid [8]. Other reagents and the water used were prepared as described earlier [3].

Recommended procedure. Place the sample solution containing less than 3.5 μg of copper(II) in a 25-ml volumetric flask. Add 1 ml of 0.2% hydroxylammonium chloride solution, 3 ml of 5×10^{-5} M TPP solution and 1 ml of acetate buffer (pH 4.7), and dilute to ca. 20 ml with water. Heat for 3 min in a boiling water-bath and allow to cool to room temperature in running water. Add 2 ml of 0.5 M sulphuric acid and dilute to the mark with water. Measure the absorbance at 414 nm against a reagent blank as reference.

Results and discussion

Selection of surfactant. As TPP and its copper(II) complex are insoluble in water, their solubilization with various surfactants was examined. SLS, cetyltrimethylammonium bromide (CMAB) and Triton X-100 were tested as anionic, cationic and non-ionic surfactants, respectively. SLS and Triton X-100 proved to be superior to CMAB both in dissolution power for TPP and the complex, and in the stability of the resulting solution. SLS was preferable to Triton X-100 because the latter has a cloud point around 70°C; as described below, this creates problems in heating the solution to accelerate the complexation of TPP with copper(II). Accordingly, SLS was employed as the surfactant.

Absorption spectra. The Soret band of TPP and its copper(II) complex in 1% SLS solution are shown in Fig. 1. Above pH 4.7, the Soret band of TPP lies at 418 nm (this corresponds to the free base form, H_2L) and below pH 2.7, it shifts to 438 nm as a result of formation of the diprotonated form, H_4L^{2+} (Fig. 1A). The absorption spectrum of the H_2L form of TPP in the region 500—700 nm (not shown) was typical of the etio-type porphyrin. However, the Soret band of the complex (Fig. 1B), lies at 414 nm without regard to pH and is very close to that of the H_2L form of TPP. Therefore, when the Soret band of the complex is used to obtain high sensitivity in the determination of copper, the absorbance measurements must be carried out in acidic media, where excess of TPP exists in the H_4L^{2+} form and its Soret band is clearly distinguished from that of the complex. However, as the complex formation reaction of TPP with copper(II) is very slow and incomplete in such acidic media even at elevated temperatures, it is preferable to form the complex at somewhat higher pH and to measure the absorbance of the complex at 414 nm against the reagent blank after acidification, e.g., with sulphuric acid.

Reaction rate of complex formation. Although the formation of the copper(II)—TPP complex proceeds very slowly at room temperature, it is

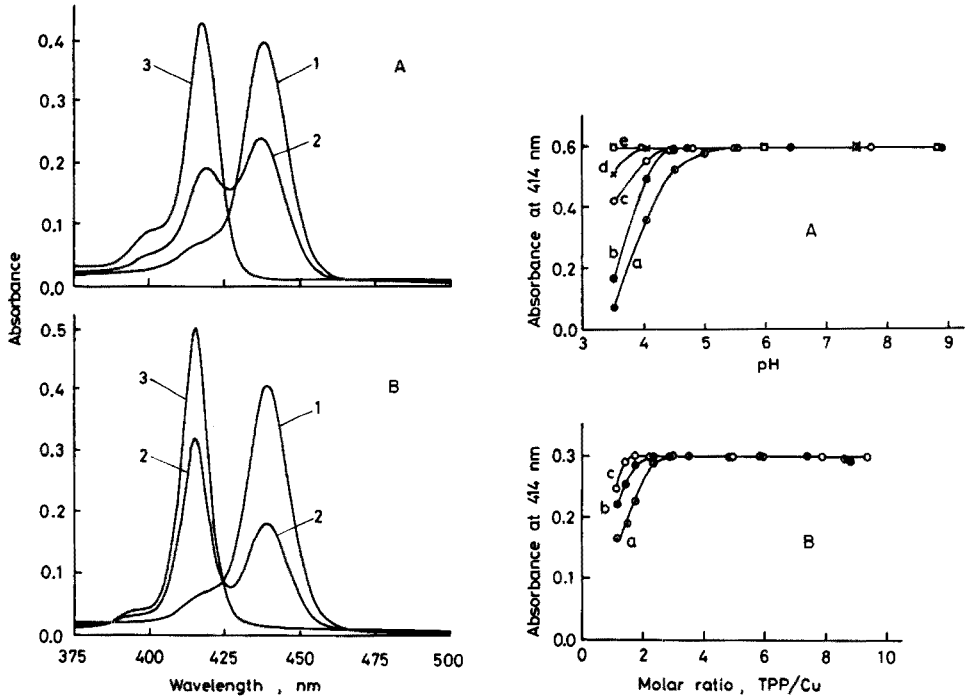

Fig. 1. (left) Absorption spectra of TPP (A) and its copper(II) complex (B) in 1% SLS solution. Concentration of TPP, 9.4×10^{-7} M; reference, water. (A) Curve 1, pH <2.7; curve 2, pH 4.1; curve 3, pH > 4.7. (B) Curve 1, [Cu]/[TPP] 0; curve 2, [Cu]/[TPP] 0.6; curve 3, [Cu]/[TPP] 2.5.

Fig. 2. (right) Influence of (A) pH and (B) TPP concentration on the complex formation at 100°C. (A) Concentration of copper, 79.0 $\mu g\ l^{-1}$; TPP, 5.5×10^{-6} M; SLS, 1.1%; reference, reagent blank; heating time, (a) 2 min; (b) 3 min; (c) 5 min; (d) 10 min; (e) 30 min. (B) Concentration of copper, 40.2 $\mu g\ l^{-1}$; SLS, 1.1%; pH 4.7; reference, reagent blank; heating time, (a) 3 min; (b) 5 min; (c) 10 min.

accelerated by increasing temperature, pH and concentrations of TPP and copper(II). The addition of a reagent such as hydroxylamine or pyridine was also effective in accelerating the complex formation, hydroxylamine being somewhat more effective. In this work, therefore, complex formation was accelerated by heating the solution at about 100°C in the presence of hydroxylammonium chloride.

pH and heating time. The influence of pH on the complex formation for various heating times at 100°C is shown in Fig. 2A, which clearly indicates the following aspects: (i) the lower limit of pH, above which a constant absorbance is obtained, is closely related to heating time; (ii) the complex is formed quantitatively even at pH 3.5, when the solution is heated for 30 min; and (iii) to shorten the heating time, the pH must be raised.

Concentration of TPP. The influence of TPP concentration on the complex formation was investigated at pH 4.7 with varying heating time at 100°C (Fig. 2B). It can be seen that the TPP concentration necessary to obtain constant

absorbance increases with decreasing heating time, and that in the case of heating for 3 min, more than a 3-fold excess of TPP to copper(II) is necessary.

Concentration of SLS. To solubilize TPP and its copper(II) complex and obtain a constant absorbance, the SLS concentration must be kept above 0.8%. (Conductimetric titrations showed that the critical micelle concentration (c.m.c.) of SLS was about 0.24%.) At the c.m.c., the absorbance was about two-thirds of that found for SLS concentrations exceeding 0.8%.

Concentration of hydroxylamine. As the complex formation is accelerated remarkably by adding hydroxylamine, the effect of its concentration was examined. The results showed that the complex was formed quantitatively within 3 min under the recommended conditions to give a constant absorbance, when more than 0.5 ml of 0.1% hydroxylammonium chloride solution was added.

Amount of sulphuric acid for acidification. Although the rate of complex formation increases with increasing pH, above about pH 3.5, (Fig. 2A), the Soret band of the complex cannot be distinguished from that of TPP (Fig. 1). Accordingly, the complex formation is taken to completion at a suitable pH above 3.5, followed by acidification to distinguish the Soret bands clearly from each other. In the recommended procedure, sulphuric acid is used for this purpose. The complex, once formed, is very stable even in acidic solution. Thus, constant absorbances are obtained when 0.3—1.5 ml of 1 M sulphuric acid is added (the pH of the final solution is between 0.6 and 1.2.). Further addition of sulphuric acid causes turbidity in the solution because of destruction of SLS micelles.

Calibration curve. A plot of the absorbance vs. the concentration of copper conforms to Beer's law in the range of 0.1—3.5 μg of copper. The equation for the calibration curve is Cu ($\mu g\ l^{-1}$) = $134 \times A$ where A is the absorbance of the sample at 414 nm measured against the reagent blank. The apparent molar absorptivity and the sensitivity for 0.001 absorbance are $4.7_3 \times 10^5$ l mol^{-1} cm^{-1} and 0.13_4 ng cm^{-2}, respectively.

Twelve standard solutions containing 960 ng of copper were determined by the recommended procedure. The results gave a relative standard deviation of 0.9%.

Interference studies. Solutions containing 960 ng of copper(II) and various amounts of each ion or salt to be tested were prepared. The copper was then determined by the recommended procedure. The maximum permissible amounts of foreign ions or salts in determinations with an error of 3% are summarized in Table 1, from which it can be seen that there are remarkably few interferences with the determination, although the limiting value for palladium(II) is not very large.

Composition of the complex. A continuous variations plot showed that the ratio of TPP to copper in the complex formed under the recommended conditions is 1:1.

TABLE 1

Influence of ions and salts on the determination of 960 ng Cu(II)

Ions or salts	Tolerance limit
Al(III), Ca(II), Cd(II), Co(II), Mg(II), Mn(II), Pb(II)	> 1000 μg
Cr(III), Fe(II), Fe(III), Ni(II), V(IV), V(V)	100 μg
Ag(I)[a], Hg(II)[a], Zn(II)	10 μg
Pd(II)	5 μg
$NaNO_3$, KNO_3, $NaClO_4$, Na_2SO_4	> 0.04 M
NaCl, KCl, NH_4Cl, NaBr, KBr, NaI, KI, K_2SO_4, Na-tartrate	0.004 M
NaSCN, KSCN, Na-citrate	0.0004 M

[a]Instead of 1 ml of 0.2% hydroxylammonium chloride solution, 0.4 ml of 0.5% hydroxylammonium sulphate solution was added.

This work was supported financially in part by a scientific research grant from the Ministry of Education and a grant of the Asahi Glass Foundation for the Contribution to Industrial Technology, to which our thanks are due.

REFERENCES

1 J. Itoh, T. Yotsuyanagi and K. Aomura, Anal. Chim. Acta, 74 (1975) 53.
2 J. Itoh, M. Yamahira, T. Yotsuyanagi and K. Aomura, Bunseki Kagaku, 25 (1976) 781.
3 H. Ishii and H. Koh, Talanta, 24 (1977) 417.
4 H. Ishii and H. Koh, Nippon Kagaku Kaishi, (1978) 390.
5 H. Ishii, H. Koh and Y. Okuda, Nippon Kagaku Kaishi, in press.
6 C. V. Banks and R. E. Bisque, Anal. Chem., 29 (1957) 522.
7 For example, M. Kodama, H. Matushita and T. Tominaga, Nippon Kagaku Kaishi, (1976) 614; H. Watanabe and H. Matsunaga, Bunseki Kagaku, 25 (1976) 35, etc.
8 A. D. Adler, F. R. Longo, J. D. Finarelli, J. Goldmacher, J. Assour and L. Korsakoff, J. Org. Chem., 32 (1967) 476.

Analytica Chimica Acta, 101 (1978) 429—432

Short Communication

RADIOTRACER INVESTIGATION OF THE COLD-VAPOUR ATOMIC ABSORPTION METHOD OF ANALYSIS FOR TRACE MERCURY

D. C. STUART*

Nuclear Research Building, McMaster University, Hamilton, Ontario (Canada)

(Received 27th February 1978)

Trace analysis for mercury in environmental samples, and especially in foodstuffs, has become of great interest because of the highly toxic nature of this element and its compounds. The analytical technique most commonly employed is atomic absorption [1], because it is widely available and relatively straightforward. Normal atomic absorption spectrometers can be converted for cold-vapour mercury analysis by commercially available kits [2]. Many devices have been reported in the literature, but all such systems are basically the same, following the methods of Hatch and Ott [3] and Poluetkov et al. [4, 5].

Because of certain problems found in application of this method, a careful check of the procedures used was undertaken, with radiotracer mercury to facilitate the investigation. The results obtained in conjunction with those of sample ashing procedures [6], indicate that the method is less straightforward than its simplicity suggests.

Experimental

Apparatus and reagents. A schematic diagram of the set-up used, based on the Jarrell-Ash kit, is shown in Fig. 1. Radioactivities were measured with a 7.6 × 7.6-cm sodium iodide well-type scintillation detector connected to a Canberra model 8100 multichannel pulse-height analyzer.

All chemicals used were of reagent-grade purity. ^{197}Hg was produced in the McMaster Nuclear Reactor by irradiating known amounts of mercury(II) chloride sealed in quartz capsules; the capsules were then frozen in liquid nitrogen and broken open, and solutions were prepared for use as standards.

Procedures. Each step in the recommended Jarrell-Ash procedure [2] was followed carefully by means of the radiotracer mercury standards. The test sample must contain the mercury to be analyzed as Hg(II) in solution, neither organically bound nor strongly complexed. An aliquot of tin(II) chloride solution is added to the test sample to reduce the mercury present, and the reaction vessel is attached to the aeration apparatus at point A

*Present Address: SLOWPOKE Nuclear Reactor, Trace Analysis Research Centre, Dalhousie University, Halifax, N.S., Canada B3H 4J1.

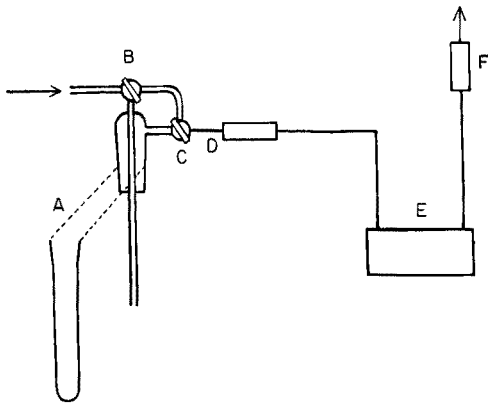

Fig. 1. Mercury accessory kit. (A) Reaction vessel (13 ml); (B) tubing and stopcock (6.5 ml); (D) drying tube and plastic tubing (10 ml); (E) absorption cell (29 ml); (F) flowmeter.

(Fig. 1). Stopcocks B and C are turned to bubble air through the test solution. This sweeps the reduced mercury into the absorption cell, E, where the atomic absorption at 253.7 nm is monitored.

Stability of mercury solutions

Standards containing 1.8×10^{-7} g of radiotracer mercury were placed in the reaction vessels. While standing, no loss of mercury was observed, but after addition of the tin(II) chloride, immediate loss occurred followed by a continuous slow loss. If the reaction vessel was shaken to promote mixing, immediate losses of about 10% were measured. Figure 2 shows typical data. This demonstrates the necessity of ensuring that the sample be connected to the apparatus the instant that reductant is added; better still, reductant should be added to the already connected apparatus.

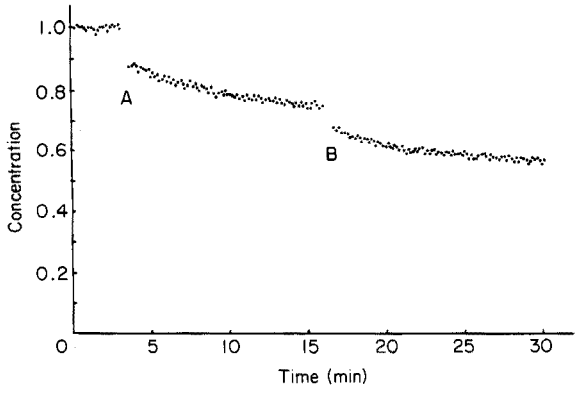

Fig. 2. Stability of mercury solution. (A) Addition of tin(II) chloride; (B) solution shaken briefly.

Trapping of mercury in the system

When radiotracer mercury standards were aerated through the flow-through system, it was found that significant quantities of mercury were trapped. The drying agent was especially bad. In particular, calcium chloride, when it became slightly moist, trapped all the radiotracer mercury. Magnesium perchlorate was considerably better, typically trapping only several per cent of a 1.8×10^{-7} g standard. During these experiments, water vapour was tested and not observed to cause significant absorption at the mercury wavelength. A drying agent is, therefore, not required. It is necessary, however, to prevent the aerosol which is formed by the action of the aeration bubbler from being carried into the system, because this results in a transfer of the test solution which may cause a spurious absorption signal and slowly coats the walls with solute. Careful insertion of filter paper discs in place of the drying agent (point D in Fig. 1) was effective in removing the aerosol.

Glass wool plugs were found to trap about 10% of the activity. The latter mercury is "exchangeable", as shown by the fact that running a non-radioactive mercury standard through the system displaced the originally trapped radioactive mercury. Metal fittings (such as the brass parts of the flowmeter) also act as effective traps for the mercury vapour, as evidenced by the build-up of radioactivity during the experiments.

After the method had been modified as suggested by the above results, the trapping of mercury in the flow system was further investigated. Starting with a freshly cleaned and assembled system, six radiotracer mercury standards of 2.9×10^{-8} g were run consecutively through the system, and the amount recovered in a trap at the exhaust end was measured. The system was then flushed with two non-radioactive standards of 1.0×10^{-7} g each, and the recovery of activity in a fresh trap was measured. The data (Table 1) show that 1.5×10^{-8} g of radiotracer mercury was lost to the system during the first six runs. This amount was subsequently recovered in the seventh and eighth runs, demonstrating the exchangeable nature of the trapping. The mercury was not localized in any one spot, but was rather spread over the whole system. Long periods of aeration did not remove the trapped mercury.

These results show that everything the mercury vapour contacts in the system presents a potential problem of trapping which should be checked. It is very desirable to have the minimum possible surface area exposed. Even with

TABLE 1

Trapping of mercury in the system

Sample number[a]	1	2	3	4	5	6	7	8
Radiotracer recovered (%)	90 ± 4	80 ± 4	88 ± 4	94 ± 4	98 ± 4	99 ± 4	48 ± 3	2 ± 1

[a]Samples 1—6 each contained 2.9×10^{-8} g of radiotracer mercury. Samples 7 and 8 contained 1.0×10^{-7} g of non-active mercury.

all precautions, some mercury is retained in the system, and this is exchanged during successive runs. These observations cast doubt on the reliability of the absorption signals obtained during the analytical procedure, particularly if the mercury content of successive samples varies widely, or if samples are run which contain less than the amount of mercury which is exchangeably trapped in the system. The first few samples run through a newly cleaned system always yield low values.

The financial support of the National Research Council of Canada is gratefully acknowledged. This research was carried out in the laboratories of Professor K. Fritze, McMaster University, whose advice and encouragement are deeply appreciated.

REFERENCES

1 See e.g., A. M. Ure, Anal. Chim. Acta, 76 (1975) 1.
2 See e. g., Jarrell-Ash Atomic Absorption Application Laboratory, No. Hg-1, Aug. 1970; H. L. Kahn, At. Absorpt. Newsl., 10 (1971) 58; H. M. Mittelhauser, At. Absorpt. Newsl., 9 (1970) 34.
3 W. R. Hatch and W. L. Ott, Anal. Chem., 40 (1968) 2085.
4 N. S. Poluektov and R. A. Vitkun, Zh. Anal. Khim., 18 (1963) 33.
5 N. S. Poluektov, R. A. Vitkun and Y. V. Zelyukova, Zh. Anal. Khim., 19 (1964) 937.
6 D. C. Stuart, Anal. Chim. Acta., 96 (1978) 83.

Analytica Chimica Acta, 101 (1978) 433—436

Short Communication

L'INFLUENCE DE TRACES D'OR(III) SUR LES PHENOMENES D'ADSORPTION EN VUE DE LA CONSERVATION DE SOLUTIONS DILUEES DE MERCURE(II) DANS DES RECIPIENTS EN VERRE

(The effect of low concentrations of gold(III) on adsorption phenomena in the storage of dilute mercury(II) solutions in glass containers)

S. DOGAN et W. HAERDI*

Département de chimie minérale, analytique et appliquée de l'Université de Genève (Suisse)

(Reçu le 24 avril 1978)

Le mercure(II) à l'état de traces est très facilement adsorbé sur les parois des récipients, ceci dans un temps relativement court. Divers auteurs ont déjà étudié ce phénomène dans différents milieux. Ainsi, Rosain et Wai [1], Coyne et Collins [2], Litman et al. [3] ont effectué des déterminations en présence de différents acides; Watling [4], Omang [5] et Feldman [6] en milieu acide et acide-permanganate ou en milieu acide-dichromate [6]. Récemment Lo et Wai [7] et Christmann et Ingle [8] ont obtenu des résultats satisfaisants en présence d'or(III) en milieu acide nitrique.

Dans ce travail, l'adjonction de traces d'or(III) dans des solutions diluées de mercure(II), en milieu aqueux, a été étudiée afin d'éviter l'adsorption de cet ion sur les parois des récipients pendant le stockage, lorsqu'on veut par la suite effectuer un dosage quantitatif.

Dans une série d'essais préliminaires, nous avons étudié l'adsorption de Hg(II) en présence de Au(III) et celle de Au(III) en présence de Hg(II) sur microbilles de verre (0,1-mm diam.), utilisées comme agent d'extraction des ions métalliques [9, 10]. Malgré la grande surface réactionnelle des microbilles (2 g), nous avons constaté l'influence importante de Au(III) sur l'adsorption de Hg(II) et l'adsorption sélective de Au(III) en présence de ce dernier pour des pH proches de la neutralité.

Pour contrôler la variation de la concentration de Hg(II), au sein de la solution contenue dans des ballons jaugés en verre (Jena borosilicate), nous avons utilisé deux techniques différentes: contrôle par spectrométrie d'absorption atomique sans flamme (s.a.a.s.f.) et par traceur radioactif ^{203}Hg. D'autre part, nous avons, dans une certaine mesure, confirmé l'adsorption sélective de Au(III) sur les parois des récipients en présence de Hg(II) au moyen du contrôle de la concentration de Au(III) par traceur radioactif ^{195}Au.

Contrôle de la variation de concentration du mercure(II) par s.a.a.s.f.

Pour cette étude, nous avons travaillé à deux pH différents: 2,2 et 6,3. A chacun de ces pH, nous avons préparé deux séries de solutions de mercure(II) dans des ballons de 100 ml. La première série ne contenait que le mercure tandis que la deuxième contenait en plus Au(III) ($6{,}6 \times 10^{-8}$ M sous forme de $AuCl_4^-$). Les ballons sont préalablement lavés avec HNO_3 (1 + 1), rincés à l'eau bidistillée et remplis avec une même solution de mercure, $[Hg]_t = 2 \times 10^{-8}$ M (mercure absolu 4 ng ml^{-1}, sous forme de $Hg(NO_3)_2$, p.a. Merck), après ajustement du pH au moyen de HNO_3 (p.a. Merck). Les mesures ont été effectuées sur 5 ml de solution, selon la technique de séparation du mercure(II) sur cuivre métallique et son dosage par s.a.a.s.f. [11]. La Fig. 1 représente les résultats obtenus, en %, en fonction du temps de stockage.

Nous constatons qu'en présence de Au(III), l'adsorption de Hg(II) est presque négligeable aux deux pH étudiés (courbes b). Par contre, en absence de Au(III), l'adsorption du mercure est importante, notamment à pH 6,3 où le complexe dominant $Hg(OH)_2$ est plus facilement adsorbé que la forme libre, Hg^{2+}.

Contrôle de la variation de concentration du mercure(II) et de l'or(III) au moyen de traceurs radioactifs

Nous avons également vérifié l'adsorption de Hg(II) et de Au(III) au moyen des traceurs radioactifs ^{203}Hg ($t_{1/2}$ = 47 j) et ^{195}Au ($t_{1/2}$ = 187 j) à deux pH différents (2,0 et 5,5) pour $[Hg]_t = 9{,}2 \times 10^{-7}$ M et $[Au]_t = 6{,}6 \times 10^{-8}$ M. La radioactivité des solutions a été mesurée sur 1 ml de solution dans des tubes en polystyrène. Les résultats obtenus en fonction du temps de stockage sont représentés sur les Figs. 2 et 3.

On remarque, tout d'abord, une faible adsorption de Hg(II) en présence et en absence de Au(III), à pH 2,0, étant donné la concentration relativement élevée du mercure. Par contre, à ce même pH, Au(III) est très facilement adsorbé en présence et en absence de Hg(II) (Fig. 3.).

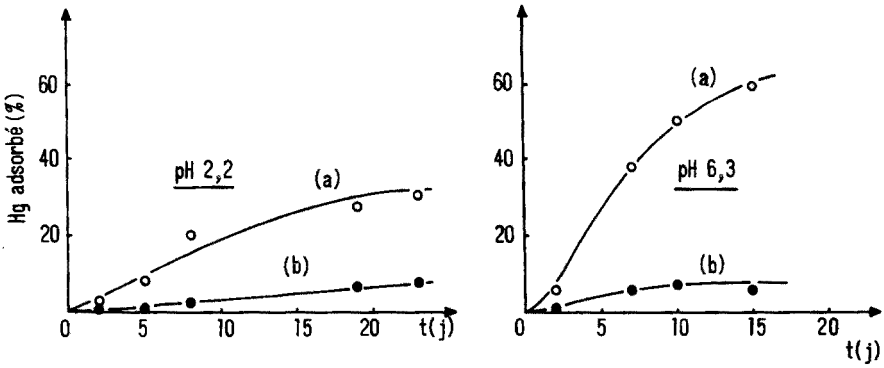

Fig. 1. Adsorption de Hg(II) sur les parois des ballons en fonction du temps de stockage (contrôle par s.a.a.s.f.). $[Hg]_t = 2 \times 10^{-8}$ M. (a) En absence de Au(III); (b) en présence de $[Au(III)]_t = 6.6 \times 10^{-8}$ M.

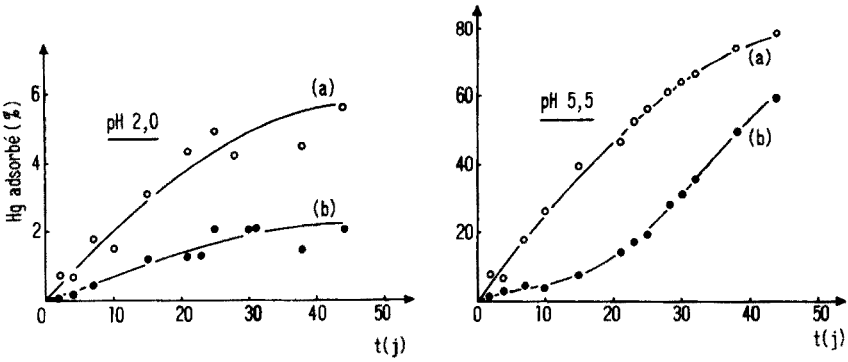

Fig. 2. Adsorption de Hg(II) sur les parois des ballons en fonction du temps de stockage (contrôle par traceur radioactif), $[Hg]_t = 9{,}2 \times 10^{-7}$ M. (a) En absence de Au(III); (b) en présence de $[Au(III)]_t = 6{,}6 \times 10^{-8}$ M.

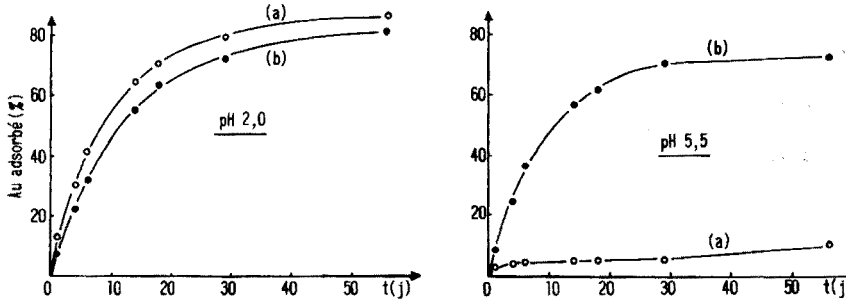

Fig. 3. Adsorption de Au(III) sur les parois des ballons en fonction du temps de stockage (contrôle par traceur radioactif), $[Au]_t = 6{,}6 \times 10^{-8}$ M. (a) En absence de Hg(II); (b) en présence de $[Hg(II)]_t = 9{,}2 \times 10^{-7}$ M.

Au pH 5,5, pour la même concentration de mercure, les courbes montrent bien que la présence de Au(III) abaisse nettement l'adsorption du mercure. Celle-ci est en effet d'environ 10—15% après une vingtaine de jours (Fig. 2, courbe b), tandis qu'en absence de Au(III), elle atteint 50% environ pour le même temps de stockage (courbe a). A partir du vingtième jour, nous constatons une augmentation rapide de l'adsorption en présence de Au(III); on pourrait donc penser qu'après l'adsorption de l'or(III) en solution, le mercure commence lui à s'adsorber. En effet, à ce pH 5,5, l'adsorption de Au(III) est très significative. Nous constatons qu'il y a, d'une part, une adsorption sélective de Au(III) en présence de Hg(II) (Fig. 3, courbe b), et, d'autre part une confirmation du commencement de l'adsorption de Hg(II) en présence de Au(III) (Fig. 2, courbe b) au moment où l'adsorption de Au(III) en présence de Hg(II) atteint le palier.

Influence des traces de Au(III) sur la détermination de Hg(II) par absorption atomique sans flamme

Nous avons pu constater que l'adjonction de traces de Au(III), dans des eaux naturelles afin d'éviter l'adsorption du mercure sur les parois des récipients n'a aucun effet gênant sur la détermination du mercure au moyen de notre technique de préconcentration sur poudre de cuivre métallique suivie de son dosage par spectrométrie d'absorption atomique sans flamme [12].

BIBLIOGRAPHIE

1 R. M. Rosain et C. M. Wai, Anal. Chim. Acta, 65 (1973) 279.
2 R. V. Coyne et J. A. Collins, Anal. Chem., 44 (1972) 1093.
3 R. Litman, H. L. Finston et E. T. Williams, Anal. Chem., 47 (1975) 2364.
4 R. J. Watling, Anal. Chim. Acta, 75 (1975) 281.
5 S. H. Omang, Anal. Chim. Acta, 53 (1971) 415.
6 C. Feldman, Anal. Chem., 46 (1974) 99.
7 J. M. Lo et C. M. Wai, Anal. Chem., 47 (1975) 1869.
8 D. R. Christmann et J. D. Ingle, Anal. Chim. Acta, 86 (1976) 53.
9 N. Lakhoua et W. Haerdi, Chimia, 25 (1971) 125.
10 S. Dogan, Thèse, Université de Genève, No. 1795 (1977).
11 S. Dogan et W. Haerdi, Anal. Chim. Acta, 76 (1975) 345.
12 S. Dogan et W. Haerdi, Anal. Chim. Acta, 84 (1976) 89.

Analytica Chimica Acta, 101 (1978) 437—440

Short Communication

IRON INTERFERENCE ON THE ULTRATRACE DETERMINATION OF COPPER IN NATURAL WATERS BY DIFFERENTIAL PULSE ANODIC STRIPPING VOLTAMMETRY

J. E. BONELLI*, R. K. SKOGERBOE* and H. E. TAYLOR

U.S. Geological Survey, Mail Stop 407, Denver Federal Center, Denver, Colorado 80225 (U.S.A.)

(Received 23rd May 1978)

Differential pulse anodic stripping voltammetry (d.p.a.s.v.) offers substantial capability for the ultratrace determination of certain metal ions in aqueous solutions. During a development program on analytical methods, it was noted that natural water samples subjected to d.p.a.s.v. for copper showed anomalously high values relative to the results obtained by atomic absorption and plasma emission spectrometry [1, 2] when significant quantities of iron were present.

The d.p.a.s.v. method involves wet ashing of the sample followed by the simultaneous reduction of metal ions to a mixed mercury amalgam in an ammonium citrate supporting electrolyte/buffer (0.2 M citrate, pH 5) medium, and subsequent analysis with a Princeton Applied Research Model 374 Polarographic** Analyzer and a Model 302 Universal Mercury Electrode. Similar methods in various media have been widely reported [e.g. 3—7]. Interference effects of significance noted in these methods include the formation of intermetallic compounds in the mercury amalgam, suppression of stripping peaks by substances adsorbed on the working electrode, unresolved stripping peaks, and chemical oxidation of amalgamated metals out of the working electrode.

The iron interference was positive in nature, directly proportional to the iron concentration in the range 0—10 $mg\,l^{-1}$, and operative on the anodic stripping determination of copper in either the single or multielement analysis mode. The observed interference was shown to result from a diffusion-controlled current attributable to iron in the sample.

D.p.a.s.v. of synthetic samples containing iron(III) only, copper only, and mixtures of copper and iron(III) revealed that the apparent copper stripping peak contained a substantial contribution from iron (Fig. 1). Furthermore, within experimental error, the composite peak current was the algebraic sum of the currents from both iron and copper when determined separately. Although the current peaks for copper and iron occur at slightly different

*Department of Chemistry, Colorado State University, Ft. Collins, Colorado 80523 (U.S.A.).
**The use of trade names does not imply endorsement by the U.S. Geological Survey.

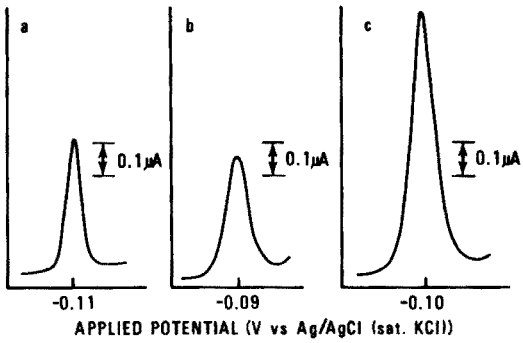

Fig. 1. D.p.a.s. voltammograms of synthetic samples. (a) 10.0 μg Cu l^{-1} ; (b) 1.0 mg Fe l^{-1}; (c) 10.0 μg Cu l^{-1} in the presence of 1.0 mg Fe l^{-1} . 60-s deposition at —1.3 V.

applied potentials (—0.11 and —0.09 V, respectively, vs. Ag/AgCl (sat. KCl)), they are not resolved by d.p.a.s.v.

Several experiments were performed to determine the nature of the iron peak. The peak current was independent of deposition potential within the range —0.15 to —1.30 V vs. Ag/AgCl (sat. KCl), and independent of the deposition from 0 to 300 s. Added iron(II) produced a similar peak at the same applied potential. Differential pulse voltammograms obtained in both anodic and cathodic potential scan directions produced similar peaks at the same applied potentials. In the context of the present investigations, the iron peak was identified as a differential pulse voltammetric curve resulting from the oxidation of iron(II) to iron(III) at the working electrode.

Attempts to eliminate or mask the interference effect chemically were unsuccessful. Although a change of medium between the deposition and stripping steps would eliminate the interference, it is not a practical alternative on the PAR 374 automated system.

The interference effect is small per unit iron concentration; however, it can lead to substantial errors when low levels of copper are determined in the presence of large amounts of iron (Table 1). Clearly a standard additions procedure will not compensate for the interference. The relative error introduced by the interference, however, can be decreased by increasing the deposition time.

A direct experimental method of correction that minimized the required analysis time was finally chosen. Since the peak current from iron is independent of deposition time, a zero deposition time voltammogram was obtained and algebraically subtracted from a normal stripping voltammogram for samples and standards alike. Thus i_p (net) = i_p (60 s dep.) — i_p (0 s dep.), and i_p (net) ∝ [Cu]. This method compensated for the current contribution from iron and also for the limited copper deposition during the rest and potential scan periods (see Fig. 2).

TABLE 1

Results obtained for copper (in $\mu g\ l^{-1}$) on river water sample (Error estimate is based on triplicate analyses.)

Sample	D.p.a.s.v.	D.p.a.s.v. corrected	I.c.a.p.
River water	11.2 ± 0.9	10.7 ± 1.3	9.7 ± 1.0
River water + iron[a]	21.0 ± 2.4	8.5 ± 1.3	—
River water + copper[b]	16.4 ± 1.0	15.8 ± 0.9	14.4 ± 1.5
River water + iron[a] + copper[b]	25.5 ± 1.5	15.5 ± 1.8	—

[a] 1.0 mg l^{-1} added. [b] 5.0 $\mu g\ l^{-1}$ added.

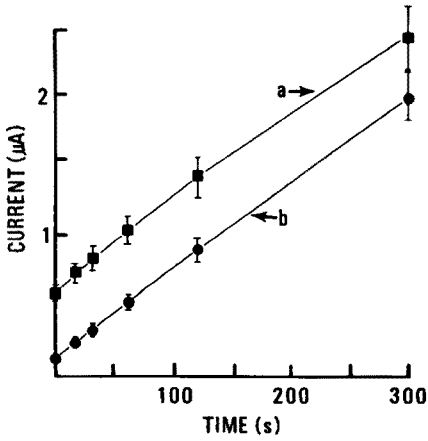

Fig. 2. Observed peak current as a function of deposition time. (a) 10.0 μg Cu l^{-1} in the presence of 1.0 mg Fe l^{-1}; (b) 10.0 μg Cu l^{-1}. Deposition at −1.30 V.

A river water sample estimated [1] to contain approximately 10 μg Cu l^{-1} and no detectable iron was analyzed for copper by the above d.p.a.s.v. technique with this correction method and by direct aspiration into an inductively-coupled argon plasma emission spectrometer [2]. The sample was then spiked with iron (1.0 mg l^{-1}) and analyzed again. A portion of the original river water sample was spiked with copper (5.0 $\mu g\ l^{-1}$) and subjected to the same scheme by the two techniques with and without an iron spike (1.0 mg l^{-1}). The data (Table 1) clearly show that the presence of 1 mg Fe l^{-1} (a typical concentration in natural waters) leads to an error for copper of over 100% at the 10 $\mu g\ l^{-1}$ level. Furthermore, the correction method gives results indistinguishable from those obtained before the iron spike addition within experimental error for both copper concentration levels. The copper spike recovery (ca. 100%) is not affected by the d.p.a.s.v. technique or the interference correction.

Other empirical or theoretical methods could possibly be used to correct for the interference. For example, mathematical means which have been employed to interpret overlapping stationary electrode polarographic curves ([8] and references therein) may have application.

It has been suggested that large concentrations of iron interfere with the d.p.a.s.v. determinations of certain metals including copper in citrate medium at pH 3 by oxidizing amalgamated metals out of the mercury working electrode [4]. Experiments in this laboratory at pH 5 and pH 3 have contradicted this observation. It should also be pointed out that the circumstance of the nearly complete superimposition of the iron and the copper peaks is unusual. Limited data obtained in pH 4—5 acetate media imply, however, that this interference effect is still operative to a small, but detectable extent.

To our present knowledge, the possible role of interference effects of this nature on stripping determinations has only been explicitly recognized in the earlier work of Ariel et al. [9] who reported the interference of manganese on the stripping determination of copper in steels. Clearly in cases where complex matrices are involved (as in environmental samples), the potential for such interferences is large.

REFERENCES

1 E. Brown, M. W. Skougstad and M. J. Fishman, Techniques of Water Resources Investigations of the U.S. Geological Survey, Methods for Collection and Analysis of Water Samples for Dissolved Minerals and Gases, U.S. Government Printing Office, Washington, DC, 1970, p. 83.
2 J. R. Garbarino and H. E. Taylor, Abstract of the Fourth Annual FACSS Meeting, Detroit, MI, 1977.
3 Proposed Test Method for Cadmium and Lead in Water by Differential Pulse Anodic Stripping Voltammetry, 1977 Annual Book of ASTM Standards, Part 31 (Water), American Society for Testing and Materials, Philadelphia, 1977, p. 1052.
4 Differential Pulse Stripping Voltammetry of Water and Wastewater, Application Brief W-1, Princeton Applied Research Corporation, Princeton, NJ 08540, 1976.
5 T. M. Florence and G. E. Batley, J. Electroanal Chem., 75 (1977) 791.
6 Y. K. Chau and K. Lum-Shue-Chan, Water Res., 8 (1974) 383.
7 T. R. Copeland, J. H. Christie, R. A. Osteryoung and R. K. Skogerboe, Anal. Chem., 45 (1973) 2171.
8 Q. V. Thomas and S. P. Perone, Anal. Chem., 49 (1977) 1369.
9 M. Ariel, U. Eisner and S. Gottesfeld, J. Electroanal. Chem., 7 (1964) 307.

Analytica Chimica Acta, 101 (1978) 441—444

Book Reviews

T. M. S. Chang (Ed.), *Biomedical Applications of Immobilized Enzymes and Proteins, Volume 2*, Plenum, New York, 1977, xx + 359 pp., price $47.40.

The analytical applications of immobilized enzymes continue to expand rapidly. This is amply illustrated by the present volume, which is concerned to a large extent with analytical processes, mainly, but by no means exclusively, in the clinical field. The first part of the book contains valuable reviews of subjects such as the use of immobilized enzymes in automated analysis, urinalysis and enzyme electrodes, as well as of the thermal enzyme probe and the monitoring of volatile products of enzymatic reactions with a low-resolution mass spectrometer. Enzyme-linked immunoabsorbent assay and radio-immunoassay with gel-entrapped antibodies are also described in some detail. Outside the clinical field, the automatic detection and monitoring of pesticides with immobilized cholinesterases is particularly timely. The second part is more prophetic, dealing with desirable goals and likely developments in fields such as multi-step enzyme systems, immobilized enzymes with pyridine nucleotide coenzyme requirements, plasminogen activators and enzymes attached to nylon tubes. The predicted extension of mechano-sensitive enzyme systems to amplification of sound is particularly intriguing.

To the reader already involved with enzymes, this book will provide a wealth of clearly presented information about current (and future) developments concerning immobilized enzymes. To the analytical chemist who shies away from enzymes, reading of selected chapters could well impress upon him the often unrecognised applicability and potential of immobilized enzymes.

A. Townshend

A. Wiseman (Ed.), *Topics in Enzyme and Fermentation Biotechnology, Vol. 1*, Ellis Horwood, Chichester, 1977, 191 pp., price £10.50 ($19.95).

This is the first of a series of collected reviews, which can be regarded as extensions of the *Handbook of Enzyme Biotechnology* (1975), also edited by Dr. Wiseman, and reviewed earlier in this journal. This first volume deals with seven topics, none of which is concerned with the analytical aspects of enzyme technology. However, the discussion of both flotation and foam fractionation as a means of separating a large range of biological molecules and microorganisms will be greeted with interest by a wide spectrum of chemists. There are also fascinating accounts of the problems of patents regarding microorganisms and their products, and of the search for a commercially viable enzymatic conversion of glucose to fructose. Other chapters

deal with the regulation of enzyme synthesis in continuous culture, aeration of culture fluids, enzymatic alterations of penicillins and cephalosporins, and drug applications of microbial cytochromes P-450. The book concludes with a subject index.

The overall impression is of a competently written, balanced selection of articles, which, although aimed mainly at the specialist, is produced in such a way that a much wider audience can appreciate the developments described, and enjoy reading about them.

A. Townshend

E. F. Mooney (Ed.), *Annual Reports on NMR Spectroscopy, Vol. 6C*, Academic Press, London, 1977, xiii + 658 pp., price £33.50.

This bulky volume is devoted entirely to tables of n.m.r. data on organic metal carbonyl complexes compiled by P. W. Hickmott, M. Cais and A. Modiano. Chemical shifts and coupling constants are listed for ca. 3000 compounds. The data are tabulated according to the metal atom and subdivided corresponding to the hapto system; thus it proves reasonably simple to locate particular compounds. This is not a review in the customary sense in that there is no discussion, though some explanatory remarks are provided in the tables. Most of the data given refer to protons or fluorine-19 though there are occasional entries for carbon-13 and other nuclei. This presumably reflects the period of literature coverage (1965—1971) which is largely prior to the advent of routine Fourier-transform n.m.r. spectrometers.

The authors should be commended for undertaking this very considerable work which should be a standard reference source for those working with metal carbonyl complexes. Regrettably, the gap between the end of literature coverage (1971) and publication seems excessive, and the price is rather high.

W. B. Jennings

G. A. Webb (Ed.), *Annual Reports on NMR Spectroscopy, Vol. 7*, Academic Press, London, 1977, ix + 300 pp., price £16.00.

Volume 7 of Annual Reports heralds a change of Editor from E. F. Mooney to G. A. Webb. The new Editor has in fact been a regular contributor to this series. According to the preface, emphasis will be given to nuclei other than protons and general reviews will be discontinued. Furthermore we are informed that the intention is to publish volumes annually, which is entirely reasonable given the title!

By comparison with Volume 6, which appeared in three parts, the present

volume is of modest size and contains three reviews. In the first of these, R. Fields surveys the literature on the fluorine-19 n.m.r. spectra of fluoroalkyl and fluoroaryl derivatives of the transition metals published between 1972 and 1975. Fluorine-n.m.r. has featured regularly in this series, and this review provides a large amount of useful chemical shift and coupling constant data in the customary format of annotated structural formulae rather than tables. Chapter 2 by M. Witanowski, L. Stefaniak and G. A. Webb is concerned with nitrogen-n.m.r. and updates earlier reviews on this subject. Topics considered include the theory of nitrogen screening constants and their correlation with molecular structure, experimental techniques for obtaining and calibrating spectra, J coupling between ^{15}N and other nuclei, and ^{14}N and ^{15}N relaxation. These topics are well described and considerable tabulated data are provided. The final chapter by R. E. Wasylishen is concerned with spin—spin coupling between carbon-13 and nuclei in the first row of the periodic table. A considerable quantity of experimental and calculated coupling constant data published between 1974 and mid-1976 is given in tabulated form.

All of the reviews are authoritative and well presented. The review on nitrogen-n.m.r. is particularly timely in that ^{15}N spectra can now be obtained relatively routinely on commercial FT instruments. It is commendable that in contrast to some previous reviews in this series, the literature coverage is reasonably up to date. This volume will provide an invaluable reference work for spectroscopists active in the areas of fluorine, nitrogen or carbon n.m.r., and for synthetic chemists who have recourse to these spectra for structural information.

W. B. Jennings

T. G. Dzubay (Ed.), *X-Ray Fluorescence Analysis of Environmental Samples*, Ann Arbor Science Publishers, Ann Arbor, Michigan, 1977, pp. 325, price £18.50.

This volume contains 25 contributions from various groups of workers who describe developments in quantitative analysis of environmental samples by x-ray fluorescence. Each contribution is presented in the form of a research publication. Instrumental aspects are described in the first group of six papers and these are followed by three papers on aerosol sampling. Dichotomous and cascade samplers are described, while one paper is concerned with the widely used technique of filtration and in particular discusses the results of tests on the filtration efficiency of thirteen filter media. Two subsequent papers outline sample preparation for water analysis by x-ray fluorescence. The remaining papers describe calibration techniques followed by problems and correction techniques applicable to spectral analysis. Most of the papers contain a reasonable list of up-to-date references and there is a good general index.

The text is unlikely to be useful to those seeking an introduction to x-ray fluorescence techniques in general, or as applied to environmental samples in particular. However, those working in the field may find various items of interest.

R. S. Barratt

Erratum

M. Hanif, M. A. Chaudry and S. Hamdani, A Rapid Method for the Determination of Palladium by the ring-oven technique. *Anal. Chim. Acta*, 98 (1978) 145—146.

The amounts in Table 1 should be read as nonograms (ng) instead of micrograms (μg).

ANALYTICA CHIMICA ACTA, Vol. 101 (1978)

AUTHOR INDEX

(continued from outside of cover)

Short Communications

Printed in The Netherlands.

VOL. 101 No. 2 ANALYTICA CHIMICA ACTA NOVEMBER 1, 1978

CONTENTS

(continued on inside page of the cover)